CANADIAN THESES

THÈSES CANADIENNES

NOTICE

The quality of this microfiche is heavily dependent upon the quality of the original thesis submitted for microfilming. Every effort has been made to ensure the highest quality of reproduction possible.

If pages are missing, contact the university which granted the degree.

Some pages may have indistinct print especially if the original pages were typed with a poor typewriter ribbon or if the university sent us an inferior photocopy.

Previously copyrighted materials (journal articles, published tests, etc.) are not filmed.

Reproduction in full or in part of this film is governed by the Canadian Copyright Act, R.S.C. 1970, c. C-30.

AVIS

La qualité de cette microfiche dépend grandement de la qualité de la thèse soumise au microfilmage. Nous avons tout fait pour assurer une qualité supérieure de reproduction.

S'il manque des pages, veuillez communiquer avec l'université qui a conféré le grade.

La qualité d'impression de certaines pages peut laisser à désirer, surtout si les pages originales ont été dactylographiées à l'aide d'un ruban usé ou si l'université nous a fait parvenir une photocopie de qualité inférieure.

Les documents qui font déjà l'objet d'un droit d'auteur (articles de revue, examens publiés, etc.) ne sont pas microfilmés.

La reproduction, même partielle, de ce microfilm est soumise à la Loi canadienne sur le droit d'auteur, SRC 1970, c. C-30.

THIS DISSERTATION
HAS BEEN MICROFILMED
EXACTLY AS RECEIVED

LA THÈSE A ÉTÉ
MICROFILMÉE TELLE QUE
NOUS L'AVONS REÇUE

NL-339 (r.86/06)

Canada

ISBN 0-315-33295-6

ACKNOWLEDGEMENTS

I wish to express my sincere thanks to my supervisor, Dr. Martha Salcudean, for her advice, guidance and encouragement during this work.

The financial support received from the Natural Sciences and Engineering Research Council of Canada and the Department of Energy, Mines and Resources is gratefully acknowledged.

My gratitude also to Dr. Ashok Malhotra and Dr. Peri Sabhapathy for their valuable discussions and suggestions.

Finally, a special thanks to my wife, Monique for her support, both moral and financial, throughout this study.

ABSTRACT

The work presents an analysis and comparative evaluation of different methods used for the numerical solution of heat conduction problems with phase change. Many techniques have been published to solve solidification or melting problems, but much of this work has focussed on ice-water problems. The specific case of solidifying metals has been mostly a beneficiary of these techniques. The present work compares the performance of various numerical techniques applied to an infinite plate and a square ingot of infinite length. Both solidifying liquid metal as well as ice-water test cases are considered.

The present work examines a number of different techniques ranging from the well-known enthalpy method, apparent capacity method and post-iterative (elementary) method to more recently published techniques which employ the freezing index or other more involved methods. Both finite difference and finite-element formulations are considered. Emphasis is placed on weak formulations as it is felt that these tend to be simple to program and they are generally easily implemented in existing single phase codes. Both these attributes render the weak formulation very attractive to the practicing engineer.

The different techniques were applied to a number of test cases and the results analysed for accuracy, cost of implementation and sensitivity to various parameters. The relative merits and limitations of each method are discussed. It is shown that some methods which perform well for ice-water problems perform poorly for metals and the opposite appears true as well. Improvements to the techniques are suggested for some

methods. In particular, the apparent capacity method proved to be unacceptable in terms of accuracy when applied to the test cases. A novel approach using the apparent capacity profile and an integration through the nodal volume to find an effective capacity for the volume was implemented and large gains in accuracy were achieved. The modified apparent capacity method now appears to be one of the best methods for modelling solidifying metal castings.

TABLE OF CONTENTS

TABLE OF CONTENTS (Continued)

LIST OF TABLES

LIST OF FIGURES

LIST OF FIGURES (Continued)

LIST OF FIGURES (Continued)

NOMENCLATURE

C	specific heat (J/kg K)
e	specific energy (J/kg)
E	energy (J)
f_C	function to calculate apparent capacity from temperature
f_L	function to calculate latent heat released from temperature
f_T	function to calculate temperature from enthalpy
f_H	function to calculate enthalpy from temperature
Fo	Fourier moduli $k\Delta t/\rho C(\Delta x)^2$
H	enthalpy (J)
ΔH	heat in enthalpy budget of post iterative method (J)
I	number of points used in standard deviation calculation
k	thermal conductivity (W/m k)
K	constant in homographic approximation
ℓ	characteristic length in test problems (m)
L	latent heat of fusion (J/kg)
$N(\xi,\eta)$	basis or interpolation functions in finite element method
N	number of time steps used in standard deviation calculation
q	heat flux density (W/m^2)
Q	heat entering into nodal volume (W)
r	fraction of time step during which phase front is in element
s	standard deviation (°C)
$S(t)$	position of phase front at time "t"
t	time (s)
T	temperature (°C)
ΔT	mushy range (°C)
TT	analytical or converged temperature (°C)
u	freezing index = $k \int_o^t T\, dt$ (J/m)
V	volume (m^3)
x,y	cartesian coordinates (m)

Δ	increment
ξ	local coordinate in finite element method
η	local coordinate in finite element method
μ	liquid water content
ρ	density (kg/m^3)
Ω	estimate for fraction solid
$\theta(x,y)$	approximate temperature profile [°C]

Subscripts

1	solidus
2	liquidus
app	apparent
eff	effective
f	phase change or phase front
i-1,i,i+1	grid points (x direction)
i-1/2	position of left element boundary
i+1/2	position of right element boundary
j-1,j,j+1	grid points (y direction)
L	liquid
S	solid
t,x,y	derivative with respect to time, x or y

Superscripts

*	second order approximation
n-1,n,n+1	time steps
r	denotes the fraction of the time step during which the phase front is in the element
Δt	denotes "in time Δt"

CHAPTER I

INTRODUCTION

Numerical methods are gaining in applications in a number of different industries and are contributing extensively to the solution of complex problems at reasonable cost. The procedures generally followed when developing a numerical simulation include the following steps:

- develop a physical model of the problem
- write the characteristic differential equations along with the appropriate boundary conditions
- select a method to discretize the differential equations and transform them into algebraic equations
- write a computer program to solve the system of algebraic equations
- test the numerical results against existing analytical solutions for some simple cases relevant to the problem to be investigated
- compare the numerical results with experimental results.

Even if excellent agreement is achieved between the numerical results and the experimental results, for the test cases investigated, numerical methods should never completely replace experimental methods since numerical solutions can be no better than the physical model on which they are based. A combination of numerical and experimental investigations which compliment each other, however, can lead to significant improvement in problem simulation compared to solely experimental or only numerical investigation.

Recent advancements in numerical modelling of phenomena encountered in permanent mold casting indicate the possibility of developing a general purpose program to simulate this process. Permanent mold casting

is characterized by the use of hardened steel or iron molds, into which liquid metal is introduced by the action of gravity or low pressure air. The process has a wide range of applications. A major user of the process is the automotive industry which uses permanent molds to cast components such as wheels, brake drums and cylinder heads.

Designing permanent molds is a complex process. The mold designer must decide upon the best cooling pattern within the mold in order to obtain the desired cooling rates and solidification front advancement in the casting. The cooling medium is generally water or air. In some cases, gas or electric heaters are also used to heat parts of the mold. Besides the type and pattern of cooling or heating to be used, the mold designer must account for radiation effects and the effects of filling times and techniques. If the temperature gradients in the mold or casting are large, thermal stresses occur which can result in deterioration or cracking. If the rate of cooling in the casting is slow, segregation of the alloying elements in the casting can occur which greatly affects the quality of the casting. If solidification in the casting is not directional (i.e. the phase front advances primarily in one direction), shrinkage voids can be formed. The mold designer wishes to avoid these shrinkage voids or, if that is not possible, have them occur in a part of the casting which will be machined off at a later time. Obviously, designing an effective mold is not an easy task. Mold design has commonly been done by a trial and error process. A mold design is conceived, constructed and implemented and the quality of the resulting casting is examined. If the casting is not acceptable, the mold design is modified and this process is repeated. Constructing and testing molds is costly and time consuming. If a numerical simulation of the process

can be developed, the trial and error process can be greatly reduced resulting in substantial savings.

Recently, considerable effort (Salcudean and Abdullah [1] and Erickson [2]) has been directed toward developing a general purpose metal casting program which can be used by mold designers.

Numerical modelling of the permanent mold process is a complex task. As the casting solidifies, it shrinks, which at a certain point in time may result in the formation of a gap between the casting and the mold. This gap greatly affects the heat transfer from the casting to the mold. The gap formation is a very complex phenomenon and therefore difficult to simulate mathematically. Gap formation has generally been modelled by assuming a gap formation time and setting an artificial gap heat transfer coefficient. Sully [3] and Srinivasan [4] have both investigated the casting-mold heat transfer. Another difficult aspect of the process to model is the liberation of latent heat as the liquid metal in the casting solidifies. This thesis deals with the numerical simulation of this latent heat release.

Many techniques have been developed to mathematically simulate the liberation of latent heat in solidification problems. Much of the testing of these techniques has dealt with modelling ice-water problems. The specific case of solidifying metals has primarily been a beneficiary of the techniques developed for ice-water problems. An in-depth examination of the various techniques available for mathematically modelling solidification, applied to solidifying metals, is required. The need for research to compare the relative performances of the various methods of simulating the latent heat effect has been mentioned in the literature by Fox [5] and Furzeland [6].

1.1 Objective of Present Investigation

The objective of this thesis is to review existing techniques of mathematically modelling phase change and to suggest the technique or techniques (be it an already existing technique, a modified existing technique or a completely new technique) most suited for implementation in a general purpose metal casting algorithm. The criteria for comparing the different techniques are:

1) Ease of implementation;
2) Accuracy of solution;
3) Ability to account for physical phenoma common in metal casting problems (eg. "mushy region");
4) Cost (CPU time and virtual memory storage) of using the technique.

1.2 Defining the Problem

Considering only the casting and assuming that appropriate boundary conditions can be defined for its surface, the problem to be solved is that of a liquid metal at a known initial temperature distribution cooling and solidifying with time. This solidification is characterized by material properties which are temperature dependent. Heat transfer is by conduction in the solid portion and a combination of conduction and convection in the liquid portion of the casting. If the variation in material properties is not large, this variation can be modelled easily by numerical methods. Convection in the liquid phase can be significant in some cases, but in this study it is ignored in order to isolate the errors associated with modelling the latent heat effect. Once the best techniques of modelling phase change in liquid metals are found, they can be added to an algorithm which accounts for variable material properties

and convection in the liquid region among other phenomena. The goal of this thesis is to isolate the phase change phenomenon and examine the performance of a number of different methods of numerically simulating it.

With these assumptions, the problem reduces to the one illustrated in Figure 1. This problem is known as the Stefan or moving boundary problem. Essentially, there are two regions (note that isothermal solidification has been assumed which is not always the case for metal alloys) a solid region and a liquid region. The two regions are separated by a boundary which is termed the phase front. In order to illustrate the problem, a one-dimensional formulation is shown. The transient heat equation can be written for the liquid and solid regions as:

$$\frac{\partial}{\partial x} k_L \frac{\partial T_L}{\partial x} = \rho_L C_L \frac{\partial T_L}{\partial t} \qquad \text{(liquid region)} \qquad (1.1)$$

$$\frac{\partial}{\partial x} k_S \frac{\partial T_S}{\partial x} = \rho_S C_S \frac{\partial T_S}{\partial t} \qquad \text{(solid region)} \qquad (1.2)$$

At the interface boundary, the following conditions exist:

$$T = T_f$$

and

$$k_S \frac{\partial T_S}{\partial x} - k_L \frac{\partial T_L}{\partial x} = \rho L \frac{\partial S(t)}{\partial t} \qquad (1.3)$$

where "L" is the latent heat.

The difficulty in numerically modelling the Stefan problem is that the phase front moves with time and its position is not known a priori.

Many methods of modelling phase change attempt to replace Equations 1.1 to 1.3 by a single equation. These are known as weak methods.

In the case of solidifying alloys, the problem is complicated due to the possible existence of a mushy region. Examining the $Fe-Fe_3C$ phase diagram given in Figure 2, it is evident that if approximately 4.3% of carbon exists, such that cooling follows line A, solidification occurs isothermally at 1148°C. If, however, the percentage of carbon is such that path B is followed, solidification does not occur isothermally. There is a region between approximately 1250°C and 1148°C where both solid and liquid co-exist. This is known as the "mushy region". Such a region is common in alloys and hence it is imperative that a general purpose metal casting algorithm is capable of accounting for it.

1.3 Layout of the Thesis

The main body of the thesis consists of six chapters. A review of the literature on numerical modelling of phase change problems is presented in Chapter 2. Chapter 3 presents a brief description of both the finite difference, and the finite element methods. In Chapter 4, a more detailed description is given of those methods which have been investigated in this thesis. The fifth chapter presents the test cases used in order to investigate the performance of the various methods. Chapter 6 presents and discusses the results and the last chapter summarizes the conclusions and suggests future work to be done.

CHAPTER II

LITERATURE SURVEY

There exist numerous methods for solving moving boundary problems. The investigators who have made contributions in this field are far too numerous to completely list here. The pioneer in this field is Stefan [8] who formulated a mathematical model of the phenomena of freezing soils and hence solidification (melting) problems are often referred to as Stefan problems. Later, Neumann [9] presented an analytical solution to a one-dimensional Stefan problem. Neumann's solution is still used today to test the accuracy of different numerical schemes. Unfortunately, unless the problem geometry is extremely simple, analytical solutions are not available and hence most techniques for solving Stefan problems rely on some numerical scheme, usually based on finite difference or finite element methods.

One of the simplest techniques of accounting for the liberation of latent heat in solidification problems, is to set up an energy budget at each node of a finite difference or finite element grid. The nodal temperature is then set back to the phase change temperature after each time step until enough heat has been accumulated to account for the latent heat associated with that node. The finite difference formulation of the technique was described by Dusinberre [10] and later by Doherty [11]. Rolph and Bathe [12] later implemented a similar technique into a finite element formulation of the Stefan problem.

A commonly used technique of accounting for the latent heat in a fixed spatial grid is to artificially increase the heat capacity near the phase change temperature. Some of the early work developing this

technique was done by Hashemi and Sliepcevich [13] who used an implicit finite difference formulation of the problem. Later, Comini et al. [14] implemented the method with a finite element formulation. Recently, Pham [15] presented an innovative approach to the technique using a three-level finite difference formulation.

Many of the more recent works have dealt with methods which formulate the governing equations in terms of enthalpy. Crowley [16] used the enthalpy formulation with a finite difference scheme to solve two-dimensional problems. Bell et al. [17] tested the explicit finite difference formulation of the enthalpy method in the region of a singularity. Recently, Tacke [18] presented an innovative formulation of the explicit enthalpy method for one-dimensional problems, which is based on an enthalpy balance to locate the phase front within the element which contains it. He tested his technique on both test cases of ice-water and solidifying steel. If an implicit scheme is used, the enthalpy method requires the solution of a system of nonlinear equations. Meyer [19] Shamsunder and Sparrow [20] and Jerome [21] have all presented formulations of the implicit enthalpy method.

Some researchers have transformed the governing equations to use the freezing index as the state variable. Kikuchi and Ichikawa [22] used this method to solve two-dimensional ice-water problems. Later, Blanchard and Fremond [23] introduced the homographic approximation [24] along with the freezing index to solve two-dimensional freezing of soil around buried pipes.

A technique which attempts to track the phase front using the method of lines was presented by Meyer [25]. The technique can run into difficulties if the moving boundary shape is not a single valued function of

the base coordinates. Also, the method is not suitable for problems where a mushy range exists.

Lazaridis [26] presented a method which solves for the front location and solves the finite difference equations based on this location. His method is capable of handling multi-dimensional problems but is extremely complex. He tested his method on solidifying metal test cases and found satisfactory agreement with existing solutions.

Duda et al. [27] presented a technique which transforms the governing partial differential equations into a coordinate system where the phase boundaries correspond to fixed coordinate surfaces. The technique involves an iterative solving scheme and is not easily added to existing single phase codes. Sparrow et al. [28] have also applied the concept to the melting of a solid about a cylinder. An implicit scheme was used.

Crank and Gupta [29] have used a technique which examines the position of an isotherm as a function of time. The technique requires a small time solution and is difficult to apply to complex problems where the value of the isotherm position is multi-valued. Crank and Crawley [30] have also used this method.

Several researchers have presented techniques, usually with a finite element formulation which deform the spatial grid in order to track the phase front. Some recent work using this technique has been done by Lynch et al. [31] and Lynch [32]. Lynch [32] tested his method on freezing water test cases.

Some researchers have presented techniques specially for one-dimensional solidification problems. Goodrich's method [33] and the "dual grid" method of Voller and Cross [34] fall into this category.

Other researchers have presented fairly in-depth reviews of existing methods, but few actually carry out a comparison of the performance of various methods when applied to specific problems. An extensive review of the literature is given by Lunardini [35]. Due to the interest in this field, however, a number of important papers have been written since his review.

Finally, it should be mentioned that the majority of researchers have tested their methods on ice-water test cases, and the problem of solidifying metal has been primarily a beneficiary of the former.

CHAPTER III

PROCEDURES FOR SOLVING THE TRANSIENT HEAT FLOW EQUATION

Numerical methods transform the governing differential equations of a problem into algebraic equations which can be solved using computers. The two main classes of numerical methods are the finite difference and the finite element methods. Both methods are introduced in this section. In order to simplify the discussion, the description is restricted to two dimensions and material properties such as density, thermal conductivity and heat capacity are assumed constant and isotropic. The transient heat conduction equation to be solved is:

$$\rho c \frac{dT}{dt} = k \frac{d^2T}{dx^2} + k \frac{d^2T}{dy^2} \qquad (3.1)$$

where internal heat generation has been assumed to be zero. The following section is meant as an introduction to the two methods in order to identify the differences between the two formulations.

3.1 Finite Difference Method

A number of books exist which describe finite difference methods. An introduction to the method is given by Holman [36]. Shih [37] gives a more detailed description of the method.

The finite difference method of solving a differential equation can be formulated in different ways. One way of setting up the finite difference equation is based on a truncated Taylor series as follows:

$$T(x_0+\Delta x,y_0) = T(x_0,y_0) + \Delta x \left.\frac{dT}{dx}\right|_0 + \frac{\Delta x^2}{2}\left.\frac{d^2T}{dx^2}\right|_0 + \frac{\Delta x^3}{6}\left.\frac{d^3T}{dx^3}\right|_0 + \ldots \quad (3.2)$$

Dividing by Δx and truncating the right hand side after the second order term gives:

$$\left.\frac{dT}{dx}\right|_0 = \frac{T(x_0+\Delta x,y_0) - T(x_0,y_0)}{\Delta x} \; 0\Delta x \quad (3.3)$$

where $0\Delta x$ means that the truncation error is $|TE| \ll k(\Delta x)$ where k is a constant. As the spatial increment (Δx) is decreased, the truncation error also decreases. Equation 3.3 is the forward difference expression of the first derivative in "x" since it depends on the value of "T" at x_0,y_0 and at "$x_0+\Delta x,y_0$".

When variable properties or unusual boundaries exist however, it is often preferable to obtain the finite difference equation from an energy balance formulation which is based on the physics of the problem.

Consider a node in a two-dimensional discretized space as illustrated in Figure 3. Associated with this node is a volume which is enclosed by dashed lines in the figure. Considering heat to conduct in from the left and bottom faces and heat to conduct out from the right and top faces and assuming a unit depth, the heat entering the faces in time "Δt" can be defined as:

$$Q_{i-1,j} = -k\,\Delta t\,\Delta y_{i,j}\,\frac{(T_{i,j} - T_{i-1,j})}{\left(\frac{\Delta x_{i,j}}{2} + \frac{\Delta x_{i-1,j}}{2}\right)} \quad (3.4)$$

$$Q_{i+1,j} = -k\,\Delta t\,\Delta y_{i,j}\,\frac{(T_{i+1,j} - T_{i,j})}{\frac{\Delta x_{i+1,j}}{2} + \frac{\Delta x_{i,j}}{2}} \quad (3.5)$$

$$Q_{i,j+1} = - k \Delta t \Delta x_{i,j} \frac{(T_{i,j+1} - T_{i,j})}{(\frac{\Delta y_{i,j+1}}{2} + \frac{\Delta y_{i,j}}{2})} \quad (3.6)$$

$$Q_{i,j-1} = - k \Delta t \Delta x_{i,j} \frac{(T_{i,j} - T_{i,j-1})}{(\frac{\Delta y_{i,j}}{2} + \frac{\Delta y_{i,j-1}}{2})} \quad (3.7)$$

If heat is generated within the volume it can be defined as:

$$Q_g = \Delta x_{i,j} \Delta y_{i,j} \Delta t \, q \quad (3.8)$$

where q is in "W/m^3", but this is neglected for this discussion.

The enthalpy change for time "Δt" can be defined as:

$$\Delta H = (\Delta x_{i,j})(\Delta y_{i,j}) \rho C (T^{n+1}_{i,j} - T^{n}_{i,j}) \quad (3.9)$$

The first law of thermodynamics states that the net heat entering the volume associated with the node must equal the change in enthalpy of the volume if no heat is generated internally. Assuming a uniform grid, with $\Delta x = \Delta y$, Equations 3.4 to 3.7 and 3.9 can be combined to give

$$\rho C \Delta x^2 (T^{n+1}_{i,j} - T^{n}_{i,j}) = M k \Delta t (T^{n}_{i+1,j} + T^{n}_{i-1,j} + T^{n}_{i,j+1} + T^{n}_{i,j-1} - 4T^{n}_{i,j})$$

$$+ (1 - M) k \Delta t (T^{n+1}_{i+1,j} + T^{n+1}_{i-1,j} + T^{n+1}_{i,j+1} + T^{n+1}_{i,j-1} - 4T^{n+1}_{i,j}) \quad (3.10)$$

If "M" in Equation 3.10 is set equal to "1", the temperature $T^{n+1}_{i,j}$ is known in terms of temperatures at the previous time step. This is known

as an explicit formulation. The advantage of this formulation is that no system of simultaneous equations need be solved. Rewriting the explicit formulation of the problem, it follows

$$T_{i,j}^{n+1} = (1 - 4Fo)\, T_{i,j}^{n} + Fo(T_{i-1,j}^{n} + T_{i+1,j}^{n} + T_{i,j-1}^{n} + T_{i,j+1}^{n}) \quad (3.11)$$

where $Fo = \dfrac{k\,\Delta t}{\rho G\,\Delta x^2}$.

Examination of Equation 3.11 reveals that if "$Fo > 1/4$", the coefficient of "$T_{i,j}^{n}$" becomes negative. Physically this implies that an increase in "$T_{i,j}^{n}$" results in a decrease of "$T_{i,j}^{n+1}$" for the same surrounding temperatures at time "n". Obviously, this is impossible and hence for the explicit formulation, "Fo" is restricted to "$Fo < 1/4$" for two-dimensional prblems. The same one-dimensional formulation results in the restriction "$Fo < 1/2$".

If "M" in Equation 3.10 is set to "0", the temperature "$T_{i,j}^{n+1}$" is defined in terms of temperatures at time "n+1". This means that a system of simultaneous equations must be solved in order to find the updated temperatures "T^{n+1}". This is known as the fully implicit formulation of the problem. Rewriting the implicit formulation of the problem gives:

$$(1 + 4Fo)\, T_{i,j}^{n+1} = T_{i,j}^{n} + Fo(T_{i+1,j}^{n+1} + T_{i-1,j}^{n+1} + T_{i,j+1}^{n+1} + T_{i,j-1}^{n+1}) \quad (3.12)$$

Obviously, the coefficient of $T_{i,j}^{n+1}$ cannot be negative. The implict formulation of the problem can be shown to be unconditionally stable (the errors are always bounded) and hence there are no restrictions on the time step.

Although it is not discussed here in detail, "M" from Equation 3.10 can be set to any number between "0" and "1". For example, setting "M=1/2" results in the well known Crank-Nicolson Method. These formulations are known as semi-implicit since they require a system of simultaneous equations to be solved.

Considering the one-dimensional implicit formulation of the problem, it is apparent that although systems of simultaneous equations must be solved, the matrices are very sparse. In fact, if the nodes are numbered properly (sequentially) tridiagonal matrices results. There exist very efficient algorithms for solving tridiagonal matrices. Carnahan et al. [38] describe an algorithm for solving a tridiagonal matrix and a description is given in Appendix A of this thesis.

However, implicit finite difference formulations of two and three-dimensional problems do not yield tridiagonal matrices. It is desirable to make use of the efficiency of the tridiagonal matrix solver in multi-dimensional problems. The Alternating Direction Implicit method (ADI) presented by Peaceman and Rachford [39] is a scheme which succeeds in doing this. The method consists of dividing each time step into three time levels for three-dimensional problems or two time levels for two-dimensional problems. Considering the two-dimensional case, in the first time level, the "x" derivatives are in the implicit form and "y" derivatives are in the explicit form. This results in a tridiagonal matrix. During the second time level, the order is reversed. Assuming "$\Delta x=\Delta y$" this can be expressed as:

$$\rho C\, \Delta x^2 (T_{i,j}^{n+1/2} - T_{i,j}^{n}) = k\,\frac{\Delta t}{2}\,(T_{i+1,j}^{n+1/2} + T_{i-1,j}^{n+1/2} - 2T_{i,j}^{n+1/2}) + k\,\frac{\Delta t}{2}\,(T_{i,j+1}^{n} + T_{i,j-1}^{n} - 2T_{i,j}^{n}) \quad \text{For } n+1/2 \tag{3.13}$$

$$\rho C\,\Delta x^2(T_{i,j}^{n+1} - T_{i,j}^{n+1/2}) = k\,\frac{\Delta t}{2}\,(T_{i+1,j}^{n+1/2} + T_{i-1,j}^{n+1/2} - 2T_{i,j}^{n+1/2})$$

$$+ k\,\frac{\Delta t}{2}\,(T_{i,j+1}^{n+1} + T_{i,j-1}^{n+1} - 2T_{i,j}^{n+1}) \quad \Big\} \text{ For } n+1$$

(3.14)

It can be shown that the Alternative Direction Implicit method is unconditionally stable. It should be noted that only the full time step solutions are valid, not the intermediary steps.

For a further description of finite difference methods, including how to formulate boundary conditions, see Shih [37].

3.2 Finite Element Method

Finite element methods are widely described in the technical literature. A very well known book is by Zienkiwicz [40]. Cook [41] gives a description of the finite element method applied to heat conduction problems.

The finite element method is a numerical procedure for solving a differential equation or a system of differential equations. The fundamental concept of the finite element method is that any continuous quantity such as temperature can be approximated by a discrete model composed of a set of piecewise continuous functions defined over a finite number of subdomains. For illustrative purposes, the two-dimensional problem is formulated using three noded linear elements. The same approach can be used to formulate one or three-dimensional problems or for quadratic or higher order elements. The three noded linear element is the element which is used for the two-dimensional problems in this thesis.

When formulating in-finite elements it is convenient to work in local coordinates, and to later transfer the equations to the global coordinate system.

The three noded "unit" linear triangle is shown in Figure 4. The first step in formulating the method is to define a continuous function over the given subdomain. In order to do this, three basis functions are defined such that the temperature at any point within the subdomain is:

$$T(\xi,\eta) = T_1N_1(\xi,\eta) + T_2N_2(\xi,\eta) + T_3N_3(\xi,\eta) \qquad (3.15)$$

where the subscripts refer to the nodal points as numbered in the local coordinate system. In order to ensure continuity over the element faces, it is evident that the value of $T(\xi,\eta)$ along a face must depend only upon the nodes on that face as they are the only nodes common to the two elements joined at that face. This implies in the three noded triangular element case that the value of the shape function for a given node must be zero along the opposite face. For higher order elements, which have more than two nodes to a side, there is a further stipulation that the value of the basis functions be zero at all other nodes. This is necessary in order for Equation 3.15 to always result in the nodal temperature when it is evaluated at that nodal point. Finally, if all the nodal temperatures of this element are equal, the basis function must give that constant temperature throughout the element. This implies that the basis functions must be unity at their respective nodes. The basis functions which satisfy these criteria for the simple three noded unit triangle illustrated in Figure 4 are:

$$N_1(\xi,\eta) = 1-\xi-\eta$$
$$N_2(\xi,\eta) = \xi \qquad \text{or} \quad [N] = \begin{bmatrix} 1-\xi-\eta \\ \xi \\ \eta \end{bmatrix} \tag{3.16}$$
$$N_3(\xi,\eta) = \eta$$

These basis functions are all linear and hence the term "linear" element. Adding a node to the middle of each side of the triangular element, results in quadratic basis functions and therefore a quadratic element.

Having defined the temperature variations in the local coordinate system, it is necessary to transform the local coordinates "ξ,η" to the global coordinates "x,y". In order to do this, the same basis functions as derived earlier are used. This means:

$$x(\xi,\eta) = x_1N_1(\xi,\eta) + x_2N_2(\xi,\eta) + x_3N_3(\xi,\eta)$$
$$y(\xi,\eta) = y_1N_1(\xi,\eta) + y_2N_2(\xi,\eta) + y_3N_3(\xi,\eta)$$

or

$$\begin{bmatrix} x \\ y \end{bmatrix} = [N]^T \begin{bmatrix} x_1 & y_1 \\ x_2 & y_2 \\ x_3 & y_3 \end{bmatrix} \tag{3.17}$$

When formulating the transient heat equation it is necessary to evaluate partial derivative of "T(x,y)". In order to evaluate these derivatives, the following formulae are used:

$$\frac{\partial T}{\partial \xi} = \frac{\partial T}{\partial x}\frac{\partial x}{\partial \xi} + \frac{\partial T}{\partial y}\frac{\partial y}{\partial \xi}$$

$$\frac{\partial T}{\partial \eta} = \frac{\partial T}{\partial x}\frac{\partial x}{\partial \eta} + \frac{\partial T}{\partial y}\frac{\partial y}{\partial \eta}$$

or rewriting:

$$\begin{bmatrix} T_{,\xi} \\ T_{,\eta} \end{bmatrix} = \begin{bmatrix} x_{,\xi} & y_{,\xi} \\ x_{,\eta} & y_{,\eta} \end{bmatrix} \begin{bmatrix} T_{,x} \\ T_{,y} \end{bmatrix} \tag{3.18}$$

The 2×2 matrix is known as the Jacobian "[J]". In three-dimensions, the Jacobian is a 3×3 matrix.

The entries in [J] can be evaluated for the three noded triangle as:

$$x_{,\xi} = \frac{\partial x(\xi,\eta)}{\partial \xi} = x_1 \frac{\partial N_1(\xi,\eta)}{\partial \xi} + x_2 \frac{\partial N_2(\xi,\eta)}{\partial \xi} + x_3 \frac{\partial N_3(\xi,\eta)}{\partial \xi}$$

$$= x_1(-1) + x_2(1) + x_3(0) \tag{3.19}$$

$$x_{,\eta} = \frac{\partial x(\xi,\eta)}{\partial \eta} = x_1 \frac{\partial N_1(\xi,\eta)}{\partial \eta} + x_2 \frac{\partial N_2(\xi,\eta)}{\partial \eta} + x_3 \frac{\partial N_3(\xi,\eta)}{\partial \eta}$$

$$= x_1(-1) + x_2(0) + x_3(1) \tag{3.20}$$

and similarly for $y_{,\xi}$ and $y_{,\eta}$.

The left hand side vector of Equation 3.18 can be evaluated as;

$$T_{,\xi} = T_1(-1) + T_2(1) + T_3(0)$$
$$T_{,\eta} = T_1(-1) + T_2(0) + T_3(1)$$

Multiplying Equation 3.18 by the inverse $[J]^{-1}$ gives:

$$\begin{bmatrix} T_{,x} \\ T_{,y} \end{bmatrix} = [J]^{-1} \begin{bmatrix} T_{,\xi} \\ T_{,\eta} \end{bmatrix} \tag{3.21}$$

where all terms on the right hand side can be evaluated in terms of the nodal quantities.

As mentioned earlier, the differential equation to be solved in two-dimensions is:

$$k \frac{\partial^2 T}{\partial x^2} + k \frac{\partial^2 T}{\partial y^2} - \rho C \frac{\partial T}{\partial t} = 0 \qquad (3.22)$$

If "$\theta(x,y)$" is an approximate solution to this partial differential equation, evaluating Equation 3.22 with "$\theta(x,y)$" results in

$$k \frac{\partial^2 \theta}{\partial x^2} + k \frac{\partial^2 \theta}{\partial y^2} - \rho C \frac{\partial \theta}{\partial t} = \varepsilon \qquad (3.23)$$

where "ε" is a residual error.

In order to find the best solution "$\theta(x,y)$", the residual error "ε" must be minimized over the solution space. To do this, the well known Galerkin method [42] is used. Galerkin's method requires that the residual error be orthogonal to the basis functions. For one element, the required integral is:

$$\int_0^1 \int_0^1 [N]^T \left(k \frac{\partial^2 \theta}{\partial x^2} + k \frac{\partial^2 \theta}{\partial y^2} - \rho C \frac{\partial \theta}{\partial t}\right) |J| \, d\xi \, d\eta = 0$$

where

$$\theta(\xi,\eta) = \theta_1 N_1(\xi,\eta) + \theta_2 N_2(\xi,\eta) + \theta_3 N_3(\xi,\eta) \qquad (3.24)$$

For a detailed description of how this integral is evaluated, see Segerlind [43]. The result of this integration is of the form:

$$[C][\theta]_{,t} + [K][\theta] = 0 \qquad (3.25)$$

where "[C]" and "[K]" are (3×3) matrices for the three noded triangle and "[θ]" is the vector of unknown nodal temperatures to be determined.

The $[\theta]_{,t}$ term can be formulated in terms of finite differences, and as in the finite difference method, the formulation can be implicit or explicit depending on what time step the vector [θ] is evaluated at.

Once Equation 3.25 is formulated for all the elements in a problem, the element matrices [C] and [K] are joined together to form the global capacity matrix [C] and stiffness matrix [K].

This description only illustrates the approach of the finite element method. For details on how the global matrices are assembled and how to formulate boundary conditions, see Segerlind [43].

CHAPTER IV

METHODS

The first step in analyzing the applicability of the various methods for implementation into a general purpose metal casting algorithm is to set a number of criteria and to evaluate the various methods based on these criteria. Some methods are very specialized and are only capable of handling certain geometries (for example, Goodrich's [33] method can only handle one-dimensional problems) and hence are not applicable for implementation into a "general purpose" algorithm. Others [25] are only for isothermal solidification problems and hence cannot handle a "mushy range" often encountered in metal casting problems. The criteria for choosing the methods to be investigated are;

1) ability to solve multi-dimensional problems,
2) ease of implementation,
3) ability to account for a "mushy" region (latent heat not released at a unique temperature) commonly encountered in metal casting problems.

The so called "weak methods" fulfill these criteria to a great extent. Weak methods replace the moving boundary problem equations (Equations 1.1 to 1.3) with a single equation and do not explicitly make use of the phase boundaries. Because of this, they are often capable of handling problems where the phase change region is a volume (solidification over a mushy range) as well as problems where it is a surface (isothermal solidification). Weak methods, which do not explicitly make use of the phase boundaries, also have significant advantages in multi-dimensional problems where front tracking is complicated. Descriptions of the

methods chosen for investigation are given in the following sections. The discussion is restricted to two-dimensions, however extending the methods to three-dimensions is generally possible.

4.1 Post Iterative (Isothermal)

The post iterative method of accounting for latent heat [10,11] is probably the simplest of all the methods. The method consists of setting up a heat sink at the nodes undergoing phase change by setting the temperature of those nodes which drop from above the phase change temperature in one time step, to below it in the next time step, back to the phase change temperature. This process is continued until an amount of heat equivalent to the latent heat of the volume associated with the node has been accumulated. The nodal temperature is then allowed to fall normally. The latent heat associated with each node can be calculated as follows;

$$E^{L}_{i,j} = L \rho \Delta x \Delta y \qquad (4.1)$$

The basic steps of the procedure may be summarized as follows;

1) The temperatures at time step "n" are known.
2) The temperatures at time step "n+1" are calculated assuming single phase conduction.
3) The nodes which were above the phase change temperature at time step "n" and have fallen below it for time step "n+1" are set back to the phase change temperature. The temperature by which the node was set back is used to calculate heat using the following formula;

$$E^{\Delta t}_{i,j} = (T_f - T^{n+1}_{i,j})\ C\ \rho\ \Delta x\ \Delta y \qquad (4.2)$$

4) The heat accumulated at node "i,j" is added to the heat accumulated at that node in previous time steps to give;

$$E^{n+1}_{i,j} = E^{n}_{i,j} + E^{\Delta t}_{i,j} \qquad (4.3)$$

5) If "$E^{n+1}_{i,j}$" is greater than "$E^{L}_{i,j}$", the nodal temperature is set to;

$$T^{n+1}_{i,j} = (E^{L}_{i,j} - E^{n+1}_{i,j})/(C\ \rho\ \Delta x\ \Delta y) \qquad (4.4)$$

Both explicit and implicit finite difference as well as implicit finite element formulations of this method have been considered in this thesis.

4.2 Post Iterative (Mushy Region)

This method is similar to the isothermal post iterative method, except that a mushy region is to be accounted for. Salcudean and Mashaie [44] and Salcudean and Abdullah [45] have used a finite difference formulation of this method to solve permanent mold casting problems. Rolph and Bathe [12] consider a finite element formulation which is based on accounting for latent heat in a similar manner.

Basically, the steps are the same as for the isothermal post iterative method but the equations for heat accumulation are different. Since latent heat is released over a temperature range, the amount released is a function of temperature in that range. For example, the variation illustrated in Figure 5, is described by the function;

$$f_L(T) = 0 \qquad \text{if } T < T_1$$
$$f_L(T) = L(T-T_1)/(T_2-T_1) \qquad \text{if } T_1 < T < T_2 \qquad (4.5)$$
$$f_L(T) = L \qquad \text{if } T > T_2$$

Any variation in latent heat release with temperature can be formulated in a similar manner. The equations for heat accumulation become;

If $T^{n+1}_{i,j} < T_2 < T^{n}_{i,j}$ then;

$$E^{\Delta t}_{i,j} = (T_1 - T^{n+1}_{i,j})\, C\, \rho\, \Delta x\, \Delta y \qquad (4.6)$$

if $T_1 < T^{n}_{i,j} < T_2$ then;

$$E^{\Delta t}_{i,j} = (T^{n}_{i,j} - T^{n+1}_{i,j})\, C\, \rho\, \Delta x\, \Delta y \qquad (4.7)$$

and, instead of setting the nodal temperature back to the phase change temperature, it is set to the value which satisfies the equation;

$$(f_L(T^{n+1}_{i,j}) - E^{n+1}_{i,j}) = (T^{n+1}_{i,j} - T_1)\, C\, \rho\, \Delta x\, \Delta y \qquad (4.8)$$

As in the previous method, if "$E^{n+1}_{i,j}$" is greater than "$E^{L}_{i,j}$", $T^{n+1}_{i,j}$ is set to;

$$T^{n+1}_{i,j} = (E^{L}_{i,j} - E^{n+1}_{i,j})/(C\, \rho\, \Delta x\, \Delta y) \qquad (4.9)$$

Although this method is intended to account for a mushy region, it is possible to model isothermal solidification by approximating the isothermal phase change to occur over a small temperature range. Such an assumption may have a smoothing effect on the temperature profiles. This possibility has been investigated.

Again, both implicit and explicit finite difference as well as implicit finite element formulations of this method have been considered.

4.3 Apparent Capacity

This is a very commonly used method of accounting for the latent heat effect [13-15]. An advantage of the method is that it is very easily implemented into existing single phase codes. Although a mushy region is necessary in order to implement the technique, isothermal solidification can be modelled by assuming the solidification to take place over a small temperature range.

The technique consists of artificially increasing the value of heat capacity in the mushy range by the appropriate amount in order to account for the latent heat. Figure 6A illustrates a possible apparent capacity variation with temperature. In this figure, the specific heat has been assumed constant throughout the solid and the liquid phases. The value of "C_{app}" in this figure is set such that;

$$C_{app} = [\int_{T_1}^{T_2} C \, dT + L]/(T_2 - T_1) \qquad (4.10)$$

Figure 6B illustrates a smooth curve approximation to the apparent capacity function, where the specific heat is also a function of temperature. This figure illustrates that any variation "$f_C(T)$" can be assumed so long as;

$$L = \int_{T_1}^{T_2} (f_C(T) - C(T)]\, dT \qquad (4.11)$$

There are a number of ways of implementing this method. If an explicit scheme is used, the procedure is as follows;

1) Temperatures are known at time "n".
2) Using these temperatures, and the assumed apparent capacity variation, evaluate the apparent capacity for each node.
3) Calculate the temperatures at time "n+1" using the capacities found in step "2".

When an implicit scheme is used however, the problem becomes nonlinear since the apparent capacity should be calculated based on the unknown temperatures of time "n+1". This necessitates the use of an iterative solving routine which can be very costly. An alternative approach is to utilize the apparent capacities based on the previous time step as in the explicit case. The accuracy of this approximation has been investigated.

As mentioned earlier, isothermal solidification can be modelled using this method if a small mushy region is assumed. If the assumed mushy region is too large, however, the temperature profiles may be adversely affected. The effect of the size of the assumed mushy range has been investigated.

Both implicit and explicit finite difference formulations of the apparent capacity method have been investigated.

4.4 Enthalpy Method

This has been one of the most popular methods of modelling the latent heat effect in recent years. Many recent publications have dealt with this method [16-21].

The method consists of writing the transient part of the energy equation in terms of enthalpy instead of temperature;

$$\rho \frac{dH}{dt} = k \left(\frac{\partial^2 T}{\partial x^2} + \frac{\partial^2 T}{\partial y^2}\right) \qquad (4.12)$$

An "enthalpy vs temperature" variation is then assumed. For the isothermal solidification case, this variation is as in Figure 7A. The step jump in the value of the enthalpy at "T_f" in this figure is equivalent to the latent heat "L".

A piecewise linear approximation to the case where a mushy region exists is illustrated in Figure 7B. For this variation, the enthalpy function "f_H" is given by;

$$\begin{aligned} f_H &= CT && \text{if} \quad T < T_1 \\ f_H &= CT + L(T-T_1)/(T_2-T_1) && \text{if} \quad T_1 \leq T \leq T_2 \\ f_H &= CT + L && \text{if} \quad T > T_2 \end{aligned} \qquad (4.13)$$

If the actual enthalpy function for a given material is available, it can be used when implementing the enthalpy method.

The steps to be followed when an explicit scheme is used, are;

1) The temperatures, and hence the enthalpies are known at time "n".

2) The enthalpies for time "n+1" are calculated based on;

$$H^{n+1}_{i,j} = H^{n}_{i,j} + \frac{k\ \Delta t}{\rho\ \Delta x^2} (T^{n}_{i+1,j} + T^{n}_{i-1,j} + T^{n}_{i,j-1} + T^{n}_{i,j+1} - 4T^{n}_{i,j}) \tag{4.14}$$

assuming $\Delta x = \Delta y$.

3) The enthalpies of time "n+1" are converted to temperatures based on the assumed "enthalpy vs temperature" variation.

The implicit formulation of this method results in a set of non-linear equations since the "n+1" enthalpies have to be calculated based on the unknown "n+1" temperatures. For this investigation, a Newton iterative solving technique has been used. The equation to be solved is;

$$0 = (H^{n+1}_{i,j} - H^{n}_{i,j}) - \frac{k\ \Delta t}{\rho\ \Delta x^2} (T^{n+1}_{i+1,j} + T^{n+1}_{i-1,j} + T^{n+1}_{i,j+1} + T^{n+1}_{i,j-1} - 4T^{n+1}_{i,j}) \tag{4.15}$$

assuming $\Delta x = \Delta y$.

The solution procedure is as follows;

1) Temperatures and hence enthalpies are known at time "n".

2) An initial guess is made to the "n+1" temperatures (the "n" temperatures have been used as the initial guess).

3) Starting from the first nodal point, a new guess is made to the temperature "$T^{n+1}_{i,j}$" based on a Newton linearization of Equation 4.15 as follows;

$$T^{n+1}_{i,j}(new) = T^{n+1}_{i,j} + (H^{n}_{i,j} - H^{n+1}_{i,j} + \frac{k\ \Delta t}{\rho\ \Delta x^2}(T^{n+1}_{i-1,j} + T^{n+1}_{i+1,j} + T^{n+1}_{i,j-1}$$

$$+ T^{n+1}_{i,j+1} - 4T^{n+1}_{i,j}))/(\frac{dH^{n+1}_{i,j}}{dT} + 4\ \frac{k\ \Delta t}{\rho\ \Delta x}) \qquad (4.16)$$

where all values on the right hand side are the most recent values. Since a piecewise linear approximation to the enthalpy function has been assumed for the purpose of this thesis, "dH/dT" can have only three values depending on whether "H" is in the solid ($dH/dT=C_S$), the mushy ($dH/dT=C+L/\Delta T$) or the liquid ($dH/dT=C_L$) region.

4) If the new guess for "$T^{n+1}_{i,j}$" is not sufficiently close to the previous value of "$T^{n+1}_{i,j}$", step 3 is repeated until a specified degree of convergence has been achieved.

5) Steps 3 to 4 are repeated for all nodal points.

6) Equation 4.16 is evaluated using the newly obtained guesses for the "n+1" temperatures. If the result is not sufficiently close to zero for all the nodal points, steps 3 to 5 are repeated.

At first glance, this method appears to be identical to the apparent capacity method if the same mushy range is assumed. There is, however, a subtle difference in that the apparent capacity method excludes the capacity term from the transient differential where as the enthalpy method includes it to give an enthalpy gradient rather than a temperature gradient. The difference, however subtle, may have significant implications.

Both explicit and implicit formulations of the enthalpy method have been investigated.

4.5 Pham's Method

This recently published technique [15] is actually a hybrid of the enthalpy and apparent capacity methods. The technique uses a three-time level finite difference formulation which should be unconditionally stable and convergent.

The three-time level finite difference approximation to the energy equation is given by;

$$C^n_{i,j}\,(T^{n+1}_{i,j} - T^{n-1}_{i,j}) = \frac{2\,\Delta t\,k}{3\,\rho\,\Delta x^2}\,\big[(T^{n-1}_{i+1,j} + T^{n}_{i+1,j} + T^{n+1}_{i+1,j}) + (T^{n-1}_{i-1,j} + T^{n}_{i-1,j} + T^{n+1}_{i-1,j}) + (T^{n-1}_{i,j+1} + T^{n}_{i,j+1} + T^{n+1}_{i,j+1}) + (T^{n-1}_{i,j-1} + T^{n}_{i,j-1} + T^{n+1}_{i,j-1}) - 4(T^{n-1}_{i,j} + T^{n}_{i,j} + T^{n+1}_{i,j})\big) \qquad (4.17)$$

if $\Delta x = \Delta y$.

The right hand side of Equation 4.17 gives the enthalpy gain due to heat conduction for a time interval of 2 ΔT. This enthalpy gain can be approximated by;

$$\Delta H^{*}_{i,j} = \frac{2\,k\,\Delta t}{\rho\,(\Delta x^2)}\,[T^{n}_{i+1,j} + T^{n}_{i-1,j}\;\; T^{n}_{i,j+1} + T^{n}_{i,j-1} - 4T^{n}_{i,j}] \qquad (4.18)$$

The temperature "$T^{n+1}_{i,j}$" can be approximated by;

$$T^{*}_{i,j} = f_T\,[f_H(T^{n-1}_{i,j}) + \Delta H^{*}_{i,j}] \qquad (4.19)$$

Finally, the apparent capacity "$C^n_{i,j}$" can be approximated by;

$$C^{n}_{i,j} = \frac{\Delta H^{*}}{T^{*} - T^{n-1}_{i,j}} \qquad (4.20)$$

This means that an approximation to "$C^{n}_{i,j}$" can be calculated based completely on quantities known at time "n".

The system of equations generated by using this apparent capacity "$C^{n}_{i,j}$" in Equation 4.17 is then solved to find the temperatures "$T^{n+1}_{i,j}$". As a precaution against jumping the latent heat peak, the temperatures "$T^{n+1}_{i,j}$" are recalculated (after having solved the system of equations) as follows:

$$T^{n+1}_{i,j}(\text{corrected}) = f_T \left[f_H(T^{n-1}_{i,j}) + C^{n}_{i;j}(T^{n+1}_{i,j} - T^{n-1}_{i,j}) \right] \qquad (4.21)$$

The term in the square brackets represents the calculated new enthalpy at node "i". If "$C^{n}_{i,j}$" was underestimated, causing "$T^{n+1}_{i,j}$" to "jump" past the freezing range, Equation 4.21 will reset "$T^{n+1}_{i,j}$" back to the freezing range.

4.6 Effective Capacity

This method, which the author is proposing is a modified approach to the apparent capacity method. With this method, the nodal temperatures are assumed to be correct for the node, and not for the whole volume associated with the node. A temperature profile is assumed between the nodal points, and instead of calculating an apparent capacity based on only the nodal temperature, an effective capacity for the volume associated with the node is found by integrating through the volume with

the assumed temperature profile and apparent capacity function. The integral to be evaluated is the following;

$$C_{eff} = \iint_{element} f_C(T)\, dxdy \Big/ \iint_{element} dxdy \qquad (4.22)$$

This integration may be carried out by means of an exact integration for simple one-dimensional cases with simple apparent capacity functions and temperature profiles. For the two-dimensional runs where an exact integration is not possible, the nodal volume is subdivided into a number of subvolumes, and the integration is performed numerically using the following formula;

$$C_{eff} = \Big[\sum_{m=1}^{ns} f_C(T_m) \Big] / ns \qquad (4.23)$$

where; m - the subvolume at which "T_m" is evaluated.

ns - the total number of equal volume subvolumes.

The number of subvolumes is chosen based on the temperature gradients through the nodal volume in order to insure that the peaks in the apparent capacity profile through the nodal volume are not missed. If the nodal volume does not contain the mushy range, the integration is not performed and the heat capacity of the nodal volume is set to the specific heat of the material.

For the purpose of this work, linear temperature profiles between the nodes have been assumed. Figure 8A illustrates a possible temperature profile for a one-dimensional problem, along with the apparent capacity distribution which results, assuming the apparent capacity

function given by Figure 6A. Since node "i" is not within the mushy range, the apparent capacity method sets the heat capacity of the entire nodal volume "i" to "C", thus neglecting the latent heat effect for that time step. By evaluating the integral in Equation 4.22, the effective capacity method sets the heat capacity of the nodal volume to "$(3/4)C + (1/4)C_{app}$" thus accounting for the latent heat effect.

If, however, the temperature profile and apparent capacity distribution are as in Figure 8B, the apparent capacity method sets the heat capacity of the complete nodal volume "i" to "C_{app}", thereby overemphasizing the latent heat effect for that time step. The proposed effective capacity method again sets the heat capacity to "$(3/4)C + (1/4)C_{app}$". Similar problems occur in multi-dimensional cases.

By evaluating Equation 4.22 at each time step, for those nodal volumes which contain the mushy range, it is ensured that the latent heat effect is properly accounted for at all time steps, even if the mushy range falls between two nodal points. Finally, by evaluating the effective capacity, the latent heat effect starts to be accounted for when the leading edge of the mushy region crosses the element boundary not when it crosses the node as in the apparent capacity method. Implicit and explicit finite difference as well as implicit finite element formulations of the proposed effective capacity method have been investigated.

4.7 Tacke's Method

This method, which is a variation of the enthalpy method, was introduced very recently by Tacke [18]. The technique uses an explicit formulation, and is only applicable to one-dimensional isothermal

solidification problems. Although these limiations are quite restrictive, the approach is innovative enough to merit investigation.

Tacke uses a control volume approach with a linear temperature profile approximation between the nodes. For the control volume undergoing phase change however, he assumes the discontimuity in the temperature gradient to occur at the phase front (as it should be) rather than at the node (where it occurs in a conventional control volume formulation).

Figure 9B illustrates the temperature profile for a control volume undergoing phase change, assuming a linear temperature profile. The discontinuity in the temperature gradient is at the phase front. Figure 9A shows the corresponding enthalpy variation within the control volume.

The total heat content (enthalpy) of the control volume can be calculated as;

$$H = \rho L(1-\Omega)\Delta x + \rho C(T_{i+1/2}-T_f)(1-\Omega)\Delta x/2 - \rho C(T_f-T_{i-1/2})\Omega\Delta x/2 \quad (4.24)$$

total heat content — latent heat (I) — sensible heat (II) — sensible heat (III)

Once "Ω" is known, the heat flux density into and out of the control volume can be calculated as;

$$q_{i-1} = k\,\frac{T_f-T_{i-1}}{x_f-x_{i-1}} \qquad q_i = k\,\frac{T_{i+1}-T_f}{x_{i+1}-x_f} \quad (4.25)$$

The steps of the method can be summarized as;

1) The temperatures, enthalpies and the phase front position are known at time "n".

2) The control volume equations are set up using Equation 4.25 for the control volume undergoing phase change.

3) Enthalpies are calculated for time "n+1" using the following formula;

$$H_i^{n+1} = H_i^n + \frac{\Delta t}{\rho \Delta x} (q_i - q_{i-1}) \qquad (4.26)$$

4) The "n+1" enthalpies are converted to temperatures in the usual manner for the control volumes not containing the phase front. For the volume which contains the phase front however, Equation 4.24 is solved by Newton iterations to find "Ω". Once "Ω" is known, the nodal temperature can be easily determined.

Care must be taken when the phase front passes from one control volume to another in a time step (i.e., $\Omega > 1$). If the front passes from volume "i" to "i+1" in one time step, the fraction of the time step which is spent in "i" can be estimated as;

$$r = (1 - \Omega^t)/(\Omega^{n+1} - \Omega^n) \qquad (4.27)$$

For the fraction of the time step which the phase front was in control volume "i+1", a better estimate for the heat flux density is;

$$q_i^r = \frac{T_f - T_i}{x_f^{t+\Delta t} - x_i} \qquad (4.28)$$

Because of this effect, if "$\Omega > 1$" during a time step, the enthalpy of control volume "i" is corrected by adding

$$\Delta H = \frac{\Delta t}{\rho \Delta x} (1-r) (q_i^r - q_i) \tag{4.29}$$

The enthalpy of control volume "i+1" is corrected by subtracting the same amount.

4.8 Blanchard and Fremond's Method

This is another recently published and innovative method. The technique was presented by Blanchard and Fremond [23]. The technique uses the freezing index in the energy equation and the homographic approximation [24] to estimate the liquid water content at a given temperature. The homographic approximation to the liquid water content "μ" can be expressed as;

$$\mu = \frac{1}{2} \left(\frac{(T-T_f)}{K+|T-T_f|} + 1 \right) \tag{4.30}$$

Figure 10 illustrates the shape of the homographic approximation, along with the actual curve of "μ vs T" for a material which undergoes isothermal solidification. If "T" is greater than "T_f", the approximation to the liquid water content approaches unity, however if "T" is less than T_f, the approximation approaches zero. The smaller the value of the constant "K", in the homographic approximation, the closer the approximation is to the actual curve. This does not necessarily mean that "K" should always be chosen very small as the magnitude of "K" may have other effects on the numerical solution. The effect of the chosen value of this constant on the numerical solution has been investigated.

The specific energy of the solidifying material can be defined as;

$$e = CT + L\mu \tag{4.31}$$

Using this definition, the energy equation becomes;

$$\rho \frac{de}{dt} = k \left[\frac{\partial^2 T}{\partial x^2} + \frac{\partial^2 T}{\partial y^2}\right] \tag{4.32}$$

Integrating Equation 4.32 gives;

$$\rho e^t - \rho e^o = \int_o^t k \left(\frac{\partial^2 T}{\partial x^2} + \frac{\partial^2 T}{\partial y^2}\right) dt \tag{4.33}$$

If the freezing index is defined as;

$$u = k \int_o^t T dt \qquad \text{or} \qquad T = \frac{1}{k} \frac{du}{dt} \tag{4.34}$$

the integrated energy equation can be rewritten as;

$$\rho e^t - \rho e^o = \frac{\partial^2 u}{\partial x^2} + \frac{\partial^2 u}{\partial y^2} \tag{4.35}$$

Equation 4.35 can be formulated in the usual manner, using a finite difference or finite element approach. The finite difference formulation results in;

$$\rho\left(C + \frac{L}{2}\left(\frac{1}{K+|T_{i,j}|}\right)\right) \frac{1}{k}\left(\frac{u_{i,j}^{n+1} - u_{i,j}^{n}}{\Delta t}\right) = \rho\left(CT^o + \frac{L}{2}\left(\frac{T_{i,j}^o}{K+|T_{i,j}^o|}\right)\right.$$

$$\left. + \frac{1}{\Delta x^2}\left(u_{i+1,j}^{n+1} + u_{i-1,j}^{n+1} + u_{i,j+1}^{n+1} + u_{i,j-1}^{n+1} - 4u_{i,j}^{n+1}\right)\right) \tag{4.36}$$

At time "t=0" all values of "u" are zero. After the system of equations has been solved once, values of "$u_{i,j}^{\Delta t}$" are found. In order to convert these values of "$u_{i,j}^{\Delta t}$" to temperatures, the gradient of "u" with respect to time must be evaluated. This can be done using the following formula;

$$\frac{du}{dt} = \frac{u_{i,j}^{n+1} - u_{i,j}^{n}}{\Delta t} \qquad (4.37)$$

For the purpose of this thesis, the temperatures given by Equation 4.37 have been assumed to be representative of the "n+1/2" temperatures. Therefore, after the system of equations has been solved once, temperatures are only known for time "$\Delta t/2$", and hence twice as many matrices must be solved compared to a conventional temperature formulation with the same time step.

Both implicit finite difference as well as implicit finite element formulations have been investigated.

CHAPTER V

TEST PROBLEMS

In order to evaluate the performance of the various numerical methods for modelling phase change problems, it is necessary to set appropriate test problems and compare the actual solution to these problems with the solutions obtained from the different numerical methods. Since the goal of this work is to determine the best method for implementation into a general purpose metal casting algorithm, these test problems should be as close as possible to actual metal casting problems. Unfortunately, this means that phenomena such as variable properties, convection in the liquid region and gap formation between the casting and the mold should be included in the problems. If these phenomena are included, it is very difficult to determine the actual solutions to the test problems. Even if the actual solutions are obtained, it is almost impossible to determine exactly what fractions of the overall errors in the numerical solutions are due to inaccuracies in the latent heat release modelling and what fractions are due to numerical errors in modelling other phenomena such as convection in the liquid phase. Because of this, test problems have been selected which consist only of heat conduction and release of latent heat. By setting such test problems, the latent heat effect is isolated and errors associated with modelling it can be examined. Material properties and boundary conditions have been set to approximate those of typical metals being cast in permanent molds.

The first three test cases are one-dimensional. Figure 11 illustrates the geometry of the problem. The entire domain is assumed to

be at a uniform initial temperature above the phase change temperature, with the leading end (x=0) dropped to some temperature below the phase change temperature at time "t=0". Table 1 gives the material properties and boundary conditions used for the first three test cases. Typical material properties for iron (test case #1), aluminum alloy (test case #2) and water (test case #3) have been assumed. All material properties have been assumed constant in order to avoid possible errors associated with numerical modelling of variable material properties. For information on material properties of metals, see [46-48]. The solidifying water test case has been included in order to examine the differences between the numerical behaviour of water and metal problems. For test cases #1 and #3, the well known Neumann analytical solution was used to compare the computed results with. Although the Neumann solution is for an infinite solid, the assumption of a constant temperature T(l,t) was found to be acceptable as only an advance of the front through a short distance from the boundary is considered in the computations of the test cases.

The other two test cases are two-dimensional. Figure 12 illustrates the geometry of the problem. The problem corresponds to one quarter of a long square cross-section solid initially at some temperature above the phase change temperature, with the surface dropped to some temperature below the phase change temperature at time "t=0". Table 1 gives the material properties for these two-dimensional test cases. Again, typical material properties for iron (test case #4) and an aluminum alloy (test case #5) have been assumed.

CHAPTER VI

RESULTS AND DISCUSSION

The five test cases of Chapter 5, were solved using the techniques described in Chapter 4. The results have been analyzed for accuracy and sensitivity to various parameters such as time step and assumed mushy range. For the two-dimensional test runs, cost of utilization has also been examined. Cost has not been examined for the one-dimensional test runs since the costs of the two-dimensional runs are more significant. A reason for this is that in the one-dimensional test runs, the resulting matrices are always tridiagonal, which is not the case in multiple dimensions. As stated in Chapter 4, for some of the methods, both finite difference and finite element formulations have been investigated. For the one-dimensional finite element runs, three noded quadratic elements were used with a lumped capacity matrix. For the two-dimensional finite element runs, three noded triangular elements were used, again with a lumped capacity matrix. For the finite difference formulations, central differences were used in the spatial domain.

The time steps, spatial increments and mushy ranges used in the computations are given in Tables 2 and 3. The spatial increments in all the test cases were chosen to be reasonable for the scale of the phenomenon investigated. For the ice-water test case, the material properties, time steps and spatial increments were taken similar to those used by Goodrich [33] as his is a commonly used test case for ice-water problems. The time steps investigated for the three one-dimensional test

cases were chosen to represent similar ranges of the Fourier moduli (Fo), as shown in Table 2. For the two-dimensional test cases (test cases #4 and #5), as well as the one-dimensional test cases involving a mushy range (test case #2), no analytical solution exists to compare the calculated results with. Therefore, these three problems were solved by a number of methods on an extremely fine grid. It was shown that all methods converged to the same result if a fine enough grid and small enough time step were used (the time steps and spatial increments used in the calculations are; test case #2 - $\Delta t = 1.5s$, $\Delta x = 0.0125$ m, test case #4 - $\Delta t = 1.0s$, $\Delta x = \Delta y = 0.002$ m, test case #5 = $\Delta t = 0.1s$, $\Delta x = \Delta y = 0.005m$). The converged solutions for test cases #2, 4 and 5 are given in Figures 60, 128 and 138 respectively. The time steps and spatial increments used in these figures were chosen by decreasing their values until a desired accuracy (standard deviation between the results less than 0.5°C for test cases #2 and #5 and less than 1.0°C for test case #4) in the results was obtained. These "converged" results were used when calculating the standard deviations of the various methods.

The standard deviations were calculated as:

$$s = \left[\sum_{n=1}^{N} \left[\sum_{i=1}^{I} (T_i^n - TT_i^n)^2 / I \right]^{0.5} \right] / N$$

where "TT" is the analytical result for nodal point "i" at time "n" if the analytical solution exists or, if the analytical solution does not exist, it is the converged result obtained as mentioned earlier: The value of "N" was chosen such that, "$N\Delta t$" represents a given total time for each problem. This total time is "10000s" for the first test case

(1-D iron), 2000s for the second test case (1-D aluminum), "700000s" for the third test case (1-D water), "1000s" for the fourth test case (2-D iron) and "100s" for the fifth test case (2-D aluminum). For some time steps, the value of "N" is not an integer. In these cases, the calculations were done for a time represented by the closest integer larger than "N", and the appropriate fraction of the final time step standard deviations was used in order to represent the given total time for that test case. The number of nodal points used in the standard deviation calculations varies for the five test cases. For test cases #1 and #3, where the analytical solution exists, all the nodal points of the discretized space were used in the calculations since it is not necessary to read and write the analytical solutions in a data file. In order to reduce the costs associated with reading and writing into a data file, only representative nodal points were used in the standard deviation calculations for test cases #2, 4 and 5. Figure 13 illustrates the discretized space used for the first three one-dimensional test cases. The standard deviations given for test case #2 are based on nodal points 2 to 9, as shown in Figure 13. Figure 14 illustrates the 6×6 mesh used for test cases #4A and #5A. The standard deviations given for test cases #4 and 5, are based on nodal points A,B,C,D, and E as shown in Figure 14. The nodal points used in test cases #4B and #5B, were chosen to represent the same locations as the ones shown in Figure 14.

The (x,y) coordinates of these points are;

A = (0.02,0.02)

B = (0.02,0.04)

C = (0.02,0.08)

D = (0.06,0.08) Note: the spatial domain is 0.1×0.1m

E = (0.08,0.08)

Since the goal of this thesis is to examine the errors due to the numerical simulation of the latent heat release it is desirable to eliminate as many other sources of errors as possible in order to isolate the errors of interest. One source of additional errors is the stepwise initial boundary condition. This is a source of errors in many numerical problems where a stepwise initial boundary condition is approximated with a grid point of finite volume. In order to minimize this error, the calculations were started at a small time after time "t=0" for those problems which have an analytical solution (test cases #1 and #3). The temperature distributions for this starting time were obtained from the analytical solution.

The results of the test runs are given in Figures 15 to 144. The figures are divided into groups based on the five test cases. In some of these plots, the vertical axis label is "Relative Temperature". This label was chosen to indicate that the solidifying temperature (or when a mushy range exists, the middle of the mushy range) is always taken to be zero and hence temperatures given are relative to the freezing point. For the first three test cases, plots are given of calculated nodal temperatures against time for representative nodal points and time steps and plots of standard deviation of the results against size of time step for each of the methods investigated. Since test cases #1 and #3 are isothermal solidification problems, plots of standard deviation of the results against assumed mushy range are also given for those methods which model isothermal solidification by assuming it to occur over a small temperature range. For test cases #4 and #5, plots of calculated nodal temperatures against time are given for representative nodal points and time steps. Standard deviation plots are not given for the two-

dimensional test cases due to the high cost of generating such results. The results are also summarized in tables. Both the tables and the figures are given since figures often reveal information which is impossible to extract from a table of results. The tables of results have been referenced when discussing general trends in the results.

6.1 1-D Iron and 1-D Aluminum

Table 4 gives the standard deviations for the one-dimensional runs. The first two test cases (1-D iron and 1-D aluminum) are discussed first. Referring to the two metal test cases in Table 4, the accuracy of the post iterative method of accounting for the latent heat release, appears acceptable compared to the other methods for smaller time steps, particularly for the explicit cases, but not very good for the larger time steps. Even in the solidifying aluminum alloy test case where the latent heat is spread over a large temperature range (100°C), the standard deviations are large (27.4°C) for the larger time steps. Figures 49 to 51 show the effect of the time step on the standard deviations of the results from the implicit post iterative solutions to the first test case. It is evident from these figures that increasing the time step results in a rapid decrease in the accuracy of the solutions. Figures 15 and 16 give the temperature histories calculated by the explicit post iterative method for the 1-D iron test case. These figures reveal that although the overall errors may be small for the smaller time steps, the errors near the phase front can be large. Figure 65 shows the temperature histories calculated by the implicit post iterative method for the second test case (1-D aluminum). The temperatures are falling unrealistically when the nodal points are within the mushy range. Figure

35 shows the effect of the size of the assumed mushy range on the accuracy of the results for the implicit post iterative solution to the 1-D iron test case (isothermal solidification). There appears to be an optimal mushy range to assume (90°C), but it is very large. It appears then that in order to achieve the best accuracy using the post iterative method, very small time steps and, for isothermal solidification problems, large assumed mushy ranges must be used. Even with these parameters, the errors near the phase front may still be large.

Referring again to Table 4, the accuracy of the apparent capacity solution to the solidifying iron test case is very poor compared to the other methods. The apparent capacity solution to the second test case (1-D aluminum) is better in terms of accuracy, but still not as good as some of the other methods, particularly for the explicit runs with larger time steps. Figure 52 gives the variation of the standard deviation with the size of the time step used in the calculations for the 1-D iron test case. The standard deviations are very large (often above 20°C), and decreasing the time step does not always result in better accuracy. From Figure 52, there is no trend towards better accuracy with decreasing time step. Figure 76 shows the same plot, but for the solidifying aluminum test case. Although the mushy range is much larger in this case than the one assumed in the first test case, the solution shows the same scatter as in the previous case. These large errors in the solutions obtained using the apparent capacity method result because for metals, the probability of the mushy region (whether assumed or actual) falling between two nodal points at a give time is high. When this occurs, the latent heat effect is not taken into account for that time step and hence the temperatures fall unrealistically fast during that time step. Figure 17

gives the predicted nodal temperatures using the apparent capacity method for the solidifying iron test case. As expected, the predicted temperatures are low. Increasing the size of the assumed mushy range in the first test case may help alleviate this problem by decreasing the probability of the mushy range falling between two nodal points. Figure 36 illustrates the effect of the assumed mushy range on the implicit apparent capacity solution to the first test case. As expected, increasing the assumed mushy range results in better accuracy, but an unrealistically large mushy range must be assumed (greater than 80°C for standard deviations consistently below 5°C). It is difficult to predict, for a given problem, what mushy range should be assumed. The performance of the apparent capacity method appears to be very unpredictable when applied to the solidifying metal test cases and an unrealistically large mushy range must be assumed in order to achieve good accuracy for the isothermal solidification test case.

Referring to Table 4, the accuracy of the enthalpy method is good compared to the other methods for the first two test cases. Only for larger time steps in the solidifying aluminum test case, do the results appear to be significantly less accurate than some of the other methods. Figure 18 gives the temperature histories for the first test case (1-D iron) predicted using the explicit enthalpy method. As with the post iterative method, the overall solution is quite good, but the errors near the phase change temperature are large. Figure 37 shows the effect of size of the assumed mushy range on the accuracy of the solution to the 1-D iron test case, solved by the implicit enthalpy method. There appears to be an optimal mushy range to assume, but the error associated with deviating from this value is very small (less than 1°C for the range

considered). Figure 77 shows the effect of the size of time step on the solution of the 1-D aluminum test case using the implicit enthalpy method. The errors are quite small (below 10°C), and decreasing the time step always results in better accuracy. The enthalpy method gives accurate results for the 1-D metal test cases. It is not necessary to search for the optimal size of mushy range to assume, as its effect is small. Decreasing the time step always results in slightly better accuracy, but the effect is not as large as for the post iterative method. It should be mentioned that for the formulation used in this thesis (see Section 4.4) convergence problems were encountered in the iterative solving routine when the updated guesses dropped from above the mushy range to below the mushy range in one iteration. These problems were overcome by setting the updated guess back to a temperature in the mushy range (T=0°C in this case) when this situation occurred.

From Table 4, the accuracy of Tacke's method is very good for the solidifying iron test case. The method was not applied to the second test case since it cannot account for a mushy range (as mentioned earlier, Tacke's method is a modified approach to the enthalpy method for one-dimensional isothermal solidification problems). Figure 20 gives the temperature histories predicted using Tacke's method for the first test case. The results are very accurate even near the phase change temperature. Figure 48 shows the effect of the time step on the accuracy of the results obtained using Tacke's method to solve the first 1-D iron test case. The results are very accurate (less than 3°C standard deviation) for the range of time steps given, except near "t=250s", which represents the limiting value of the time step for an explicit formulation, based on

"Fo<0.5". For its range applicability then Tacke's method gives excellent accuracy.

Referring again to Table 4, Pham's formulation of the apparent capacity method gives improved accuracy compared to the apparent capacity method for the first two test cases for smaller time steps. For larger time steps, however, the problems associated with the apparent capacity method persist and the results in some cases are worse than with the apparent capacity method. Figure 78 shows the effect of time step on the accuracy of the solution to the solidifying aluminum test case using Pham's method. The trend observed in Table 4 is apparent from this figure. The accuracy of the solution decreases slowly with increasing time step size, up to a time step value of "65s". For larger time steps, the standard deviation of the results increases sharply with increasing time step. Figure 68 shows the temperature histories for the solidifying aluminum test case predicted by Pham's method. From this plot, the recalculation of the temperatures, as described in Section 4.5 of this thesis, is causing scatter in the predicted solution about the actual solution. Pham's method succeeds in alleviating the problems associated with the apparent capacity method for lower time steps, but the predicted temperature histories are not smooth with respect to time as expected and the problems persist for larger time steps.

From Table 4, the proposed effective capacity method appears to be very accurate for the first two test cases. The superior accuracy of the effective capacity method compared to the other methods is particularly evident in the solidifying aluminum test case, where for some time steps, the effective capacity standard deviations are less than half of the standard deviations of the next best method. Figure 27 illustrates the

temperature histories for the solidifying iron test case predicted by the implicit effective capacity method. The predicted solution is very accurate, including near the phase change temperature where some of the previously discussed methods performed poorly. Figure 69 illustrates the temperature histories predicted by the effective capacity method for the solidifying aluminum test case. Again, the accuracy is excellent, including the mushy range. Figure 55 illustrates the effect of the size of the time step on the accuracy of the solution predicted by the effective capacity method. The standard deviations are small (below 6°C), including the larger time steps, and there is a trend towards better accuracy with decreasing time step although the curve is not smooth. Figure 79 illustrates the same plot, for the solidifying aluminum test case. Again, the accuracy is good (below 5°C) for all time steps, and there is a trend towards improved accuracy with decreasing time step. Figure 39 illustrates the effect of the size of the assumed mushy range on the solution to the 1-D iron test case using the effective capacity method. There appears to be an optimal value of the assumed mushy range, but the error associated with deviating from this value is very small. Finally, Figure 57 illustrates the effect of the time step on the accuracy of the solution to the 1-D iron test case, predicted by the effective capacity method. The only difference between this figure and Figure 55 is that in this case, a Gaussian distribution of the apparent capacity with respect to temperature has been assumed within the mushy range. Ninety-five percent of the latent heat has been assumed to be released in the temperature range from "-5.0°C" to "+5.0°C". This is the same assumed mushy range as in Figure 55, except that in Figure 55, a linear release of latent heat with temperature has been assumed. Although different apparent capacity profiles have been assumed, the results are identical. This means that the shape of the assumed apparent capacity

profile has no significant influence when modelling isothermal solidification using the effective capacity method. This contradicts the findings of Erickson [2] for the apparent capacity method, who states that the manner in which the heat of fusion is added to the specific heat curve can play an important role in the results. This implies that the importance of the shape of the assumed apparent capacity variation in the apparent capacity method is primarily in changing the probability of missing the apparent capacity peak, since in the effective capacity method where the latent heat effect cannot be missed for any time steps, the shape of the apparent capacity variation has no significant effect on the results. The proposed effective capacity method then appears very accurate in solving the two one-dimensional solidifying metal test cases whether a mushy range exists, or the isothermal solidification case is solved by assuming a small mushy range.

Referring to Table 4, the results using Blanchard and Fremond's method [23] which uses a freezing index formulation with the homographic approximation [24] to the liquid fraction seem very accurate compared to the other methods for the solidifying iron test case. Figure 29 illustrates the temperature histories obtained for the 1-D iron test case using this method. The time steps used for the plots of the results from this method are always twice as large as for the other methods, since for the formulation used in this thesis (see Section 4.8), every time the resulting matrix is solved, the time advances only one-half of the time step due to the hopscotch nature of the technique. From Figure 29, the results are accurate, including the results near the phase change temperature. Figure 58 illustrates the effect of the time step on the accuracy of the solution obtained with Blanchard and Fremond's method. The results are very accurate (standard deviations below 6°C), even for the

larger time steps, and there is a trend towards improved accuracy with decreasing time step. Figure 41 illustrates the effect of the magnitude of the assumed constant (K) in the homographic approximation to the fraction liquid. The effect is quite large (a range of approximately 4°C in the standard deviation for the range of "K" investigated) particularly for the lower magnitudes. It should be mentioned that as Rolph and Bathe [12] state, this method can be difficult to add to existing single phase codes due to the transformation to the freezing index.

6.2 1-D Water

The third test case is the one-dimensional ice-water test case. Examinining the 1-D water results in Table 4, and since the total temperature range of the initial conditions is only 12°C, and hence a standard deviation of 1°C represents 8.3% of the total, the standard deviations are extremely large, except for Tacke's method. The standard deviations of the results obtained with Tacke's method are one order of magnitude smaller than of any other method. This is contrary to the observations from the solidifying metal test cases discussed previously.

Figures 81 and 92 illustrate temperature histories calculated by the explicit post iterative method and the implicit enthalpy method for the ice-water test case. There are large fluctuations in the predicted temperature histories. Figure 94 illustrate the temperature histories predicted by the proposed effective capacity method for the 1-D water test case. Again, the same large fluctuations persist. Examining Figures 81 to 98, reveals that these problems exist for all the methods except for Tacke's method. Figure 127 illustrates results from the effective capacity method using the same grid as shown in Figure 13, and

the same boundary conditions as for the 1-D water test case, except that a spatial increment of 0.05m instead of 0.125m, and a time step of 3000s instead of 20000s have been used. Even with these smaller spatial increments, and smaller time steps, the large fluctuations in the results persist. Evidently an extremely fine grid must be used in order for these fluctuations to be negligible. Figure 105 illustrates the effect of the size of the assumed mushy range on the results from the implicit enthalpy method. Increasing the size of the assumed mushy range does not appear to improve the results. Figure 107 shows the same plot for the implicit effective capacity method. Increasing the size of the assumed mushy range improves the results slightly, but the standard deviations continue to be an order of magnitude greater than with Tacke's method.

It appears then that there are significant differences in the numerical behaviour between the solidifying metal and the ice-water test cases. Examining the ratio of the latent heat to the total sensible heat which is released if the whole domain drops from its initial condition to the boundary temperature gives:

1-D Iron Test Case	$L/[C(150 + 500)] \times 100$	$= 38\%$
1-D Aluminum Test Case	$L/[C(150 + 400)] \times 100$	$= 80\%$
1-D Ice-Water Test Case	$L/[C(2 + 10)] \times 100$	$= 330\%$

The ratio of the latent heat to the sensible heat in the ice-water test case is much higher than in the two metal test cases. This implies that in the ice-water test case, the effect of the latent heat is greater than in the metal test case. The traditional enthalpy method sets the nodal temperature of the volume containing the phase front to a constant

temperature while the phase front is within the nodal volume (assuming isothermal solidification). Tacke's formulation of the enthalpy method allows the nodal temperature to fall more rapidly while the phase front is within the nodal volume by following the front and correcting the nodal temperatures based on the phase front position. With the other methods, once the phase front has passed through the nodal volume, the nodal temperature is unrealistically high and hence for the following few time steps the nodal temperature falls quickly and begins to oscillate about the actual solution as seen in Figure 92. Although Tacke has succeeded in formulating his method for the one-dimensional case, it is extremely difficult to extend it to multiple dimensions. The main difficulty is that the phase front is no longer necessarily parallel to the element boundaries and therefore the heat fluxes at the element boundaries are very difficult to define and the phase front is very difficult to locate. Also, since neighbouring elements may contain the phase front at the same time, it is very difficult to locate the front within a nodal volume.

Besides the ratio of the latent heat to the sensible heat, there are other differences between ice-water problems and solidifying metal problems. These differences arise from the geometries of typical problems in the two cases. Often, ice-water problems consist of solidification (melting) around a buried pipe or some similar phenomena which many times have very simple geometry (sometimes even one-dimensional). Casting in permanent molds however, is characterized by complex geometries and three-dimensional numerical formulations are generally necessary.

6.3 2-D Iron and 2-D Aluminum

Tables 5 and 6 give a summary of the results for the methods which were extended to a two-dimensional formulation and used to solve the final two test cases. All of these formulations use an implicit scheme. The finite difference formulations all use the well known Alternating Direction Implicit (ADI) scheme which solves two tridiagonal matrices at every time step. The finite element formulations use Gaussian elimination, (taking into account the banded nature of the matrices) to solve the resulting matrices. Although this is not the most efficient method of solving the matrices, observations will still be made about the relative costs of the different methods. The runs were done on a 48 megabyte Amdahl 5850 computer with accelerator. The costs which are quoted are based on CPU time and virtual memory usage. It should be noted that only the relative magnitudes are important as costs can vary depending on the computer system used.

From Table 5, the post iterative method is quite accurate, but not as accurate as some of the other methods. Figures 129 to 131 give the temperature histories for test case #4A (solidifying iron) predicted by the various formulations of the post iterative method. As in the one-dimensional test cases, although the overall errors are low (standard deviations between 10°C and 19°C for these conditions), the errors near the phase change temperature are large. There appears to be little difference, in terms of standard deviations, between the isothermal formulation of the post iterative method and the formulation which assumes a small mushy range, although for larger assumed mushy ranges the difference may be more significant. The cost column of Table 5 reveals that the post iterative method is the most inexpensive to implement of

the methods investigated. This is expected due to the relative simplicity of the method. This implies that it is possible to use a very fine grid in order to increase the accuracy of the solution near the phase change temperature and maintain competitive costs.

The apparent capacity runs in Table 5, were done using the parameters given in Table 3 and were redone with a larger assumed mushy range (50°C as shown in Table 5) in order to assess the effect of the magnitude of the assumed mushy range. For the smaller mushy range (10°C), the accuracy is very poor (standard deviations above 35°C); including the results for the finer grid of test case #4B. Figure 132, gives the temperature histories for test case #4A predicted by the apparent capacity method. The large errors are evident from this figure. The results in Table 5 for the apparent capacity method employing a larger mushy range are much improved compared to the apparent capacity method with the smaller assumed mushy range. Figure 133 showing the temperature histories for test case #4A (solidifying iron) predicted by this formulation of the apparent capacity method confirms this observation. Decreasing the spatial increment (test case #4B) however increases the standard deviation from the actual solution for the apparent capacity method with the larger assumed mushy range. This is contrary to what is expected. As in the one-dimensional test cases, the performance of the apparent capacity method is very unpredictable and decreasing the time step (and the spatial increment in this case) does not always increase the accuracy of the solution. The cost of implementing the apparent capacity method is the lowest of the methods investigated (as low as the post iterative method) but the unpredictable nature of the results renders it unattractive.

As with the apparent capacity method, the effective capacity runs in Table 5 were done using the parameters of Table 3, as well as with a larger assumed mushy range. The results using the parameters of Table 3 are fairly accurate (standard deviations from 7 to 17°C), but the costs associated with implementing the method are very high. These high costs are related to the integrating subroutine in the effective capacity algorithm attempting to locate such a small assumed mushy range in the first few time steps, when the boundary condition temperature gradients are very large. Increasing the magnitude of the assumed mushy range facilitates this integration and hence dramatically reduces the costs associated with the effective capacity method and increases the accuracy, as is evident in Table 5. The cost of implementing the effective capacity method with the larger assumed mushy range is higher than for the previously discussed methods, but competitive. If not for the large temperature gradients in the first few time steps, these costs would be much lower. The results from the effective capacity method with the larger assumed mushy range are very accurate (standard deviations from 3° to 10°C). Figure 136 illustrate the temperature histories obtained for the solidifying iron test case #4A using the effective capacity method with an implicit finite difference formulation. The results are accurate overall, as previously seen from Table 5, and this figure reveals that the solution is accurate near the phase change temperature. The performance of the effective capacity method then is good in solving two-dimensional isothermal solidification problems by assuming a small mushy range, but the cost of implementing the method can be high if the mushy range is small and the temperature gradients in the element containing the phase front are large.

Referring again to Table 5, the enthalpy formulation gives good accuracy for the two-dimensional solidifying iron test case. Figure 137 showing the temperature histories predicted by the enthalpy method reveals that the errors are concentrated near the phase change temperature. Referring to Table 5, the cost of implementing the enthalpy method is acceptable for the smaller time steps, but increases at a faster rate than the other methods with decreasing spatial increment.

Table 6 gives the results for the fifth test case (solidifying aluminum alloy) which has a mushy range of "100°C". For this test case the post iterative solution standard deviations from the actual solution are high (above 19°C for the coarse grid). Figures 139 and 140 give the temperature histories predicted by the post iterative method formulations for the solidifying aluminum test case (#4A). The errors are very large, particularly in the mushy range. This corresponds to the observations from the one-dimensional aluminum test case.

The apparent capacity results from Table 6, reveal that the accuracy of the method is poor in predicting the solidifying aluminum test case (standard deviations above 23°C for both grids). Figure 141 illustrates the temperature histories predicted by the apparent capacity method. The method is severely underpredicting the temperatures. This corresponds to the obervations from the one-dimensional test case.

From Table 6, the effective capacity method is very accurate (standard deviations below 11°C for all grids) in solving the solidifying aluminum test case. For both grids, the best results are from the effective capacity method. Figures 142 and 143 give the temperature histories predicted by the effective capacity method formulations for test case #4A. The results are very accurate, even in the mushy range.

Although the cost is slightly greater for the implementation of the effective capacity method than for some of the other methods, this is a very simplified problem. In a practical problem, relatively few of the nodal points in the grid change phase since the grid includes the mold as well as the casting. Having temperature-dependent material properties increases the cost per grid point. If grid size is dominated by the latent heat effect, the effective capacity method may offer substantial savings by reducing the number of nodal points necessary for a given accuracy.

Finally, Table 6 shows that the enthalpy method gives very accurate results for the two-dimensional solidifying aluminum test case (standard deviations below 12°C for all grids). Figure 144, illustrating the temperature histories predicted by the enthalpy method reveals that there may be some inaccuracies in the results near the mushy range, but overall the errors are small. The cost of implementing the enthalpy method is competitive, but increases more rapidly than the other methods with decreasing spatial increment and time step. Since this method uses an iterative solving routine, as the number of grid points increases, the difference between the cost of implementing the enthalpy method and the other methods which solve the matrices using an elimination scheme is expected to increase. Due to the high degree of accuracy achieved with the enthalpy method, however, it must be considered as a competitive method for this type of problem.

6.4 Stability of the Methods

A numerical method is considered to be stable, if the errors of the transient numerical solution are bounded. Because of the nonlinear

nature of the algebraic equations resulting from some of the methods, the usual means of examining the question of stablity (e.g., von Neumann's method) are inapplicable. In this thesis, no rigorous mathematical analysis of stability has been undertaken. A method of investigating stability is to conduct numerical experimentation with various combinations of time steps and spatial increments. In the course of doing the runs for this thesis, many such combinations were investigated and instabilities were never encountered except with the explicit formulations when the time steps were such that the usual limits on the Fourier moduli were exceeded ($Fo < 0.5$ for 1-D problems and $Fo < 0.25$ for 2-D problems).

Another method of estimating the stability limit is to determine whether or not all the coefficients of the discretized equation are positive. This criterion has been proposed by Patankar [49] and can be understood by considering that an increase in the value of the temperature at one grid point should, with other conditions remaining unchanged, lead to an increase in the value of temperature at a neighbouring grid point. In Section 3.1, it was shown that this criterion leads to upper limits on the Fourier moduli for explicit formulations. The methods which increase the heat capacity in order to account for the latent heat, actually result in a decrease in the Fourier moduli for the nodal volumes which contain the phase front, therefore, the limit on the time step is always governed by the nodal points which are not changing phase. It appears then that the size of the time step is governed by accuracy considerations and not stability considerations, except for explicit formulations, where the usual limits on the Fourier moduli apply. A more rigorous analysis must be undertaken however, before definite conclusions can be made.

6.5 Finite Different vs Finite Element

The question has often been posed of which is the better method, finite difference or finite element. As is often the case, there is no simple answer, and the answer depends on what problem is to be solved and what the criteria are for evaluation. Some researchers have published work directed towards answering this question (see Hsu [50]). During the course of this investigation, many of the test cases were solved by both finite difference as well as finite element formulations of the same method. Referring to the results in Tables 4, 5 and 6, and considering only the accuracy of the solutions, reveals no definitive advantage of one formulation over the other. In some cases, the accuracy of the finite difference results appears to be better while in others the finite element results appear better. Tables 5 and 6 showing the results from the two-dimensional runs reveal that the accuracy of the finite element formulation of the post iterative method is inferior to the finite difference formulation of the same method. This is believed to be due to the higher degree of coupling between the elements in the finite element case. It should be mentioned that these trends may be completely different if higher order finite difference approximations to the derivatives are used, or if higher order elements are used in the finite element formulations.

The cost columns of these same tables show that the Alternating Direction Implicit formulation of the finite difference method (which makes use of the efficiency of the tridiagonal matrix solving algorithm) offers substantial savings compared to the finite element formulation. This is one of the most significant advantages of the finite difference method. The savings of the ADI method are expected to be larger for

three-dimensional problems. It should be stressed, however, that the test cases used are very simplified and therefore the observed trends cannot be generalized. Certain advantages and disadvantages can be stated for the two methods by investigating the general formulations of the methods. When the Alternating Direction Implicit or some other similar formulation can be used, this is a definite advantage of the finite difference method. In general, the finite difference method tends to be simpler to formulate than the finite element method, but more difficult to make into a general purpose algorithm. It is easier to concentrate a finite element grid near regions where rapid variations of the dependent variable are expected (such as near the phase front). Also, the finite element formulations tend to handle boundary conditions better than finite difference formulations, particularly curved boundaries. The question of which method is better then is not easily answered, the answer depending on the problem to be solved and the criteria which are important.

CHAPTER VII

CONCLUSIONS AND FUTURE WORK

A number of existing methods for simulating phase change which were found to meet desirable criteria for implementation into a general purpose metal casting algorithm have been programmed. A new method for modelling phase change, based on the apparent capacity method, has been developed and programmed. The performance of the various methods in solving five test cases has been evaluated. It has been shown that:

- the post iterative method of accounting for latent heat gives inaccurate results, particularly near the phase change temperature, for the one-dimensional solidifying metal test cases
- the results from the post iterative method formulations are very sensitive to the magnitude of the time step
- the apparent capacity method underpredicts the solutions to the solidifying metal test cases and generally gives the lowest accuracy
- decreasing the time step when using the apparent capacity method does not necessarily improve the accuracy of the results for the solidifying metal test cases
- in order that the results using the apparent capacity method be close (standard deviation below 5 C) to the actual solution for the 1-D iron test case an unrealistically large mushy range must be assumed (80 C)
- Pham's formulation of the apparent capacity method improves the results for smaller time steps but also underpredicts the actual solution with larger time steps for the solidifying metal test cases
- the enthalpy method results are accurate for the solidifying metal test cases except near the phase change temperature for isothermal solidification problems
- the solutions to the solidifying metal test cases using the enthalpy method are relatively insensitive to the size of the time step and mushy range
- Tacke's formulation of the enthalpy method gives accurate results for the 1-D iron test case but cannot account for a mushy region or multiple dimensions

- the results using Tacke's method are excellent near the phase change temperature
- the solutions to the solidifying metal test cases using the proposed effective capacity method are very accurate including near the phase front
- the results of the effective capacity method for the solidifying metal test cases are relatively insensitive to the size of the time step and mushy range
- the results for the 1-D iron test case using Blanchard and Fremond's method are very sensitive to the parameter in the homographic approximation
- all methods except Tacke's method give very inaccurate solutions to the solidifying water test-case for the grids and time steps considered
- Tacke's method gives accurate solutions to the solidifying water test case including near the phase change temperature
- the primary difference between the numerical behavior of solidifying metal and solidifying water problems is due to the much larger ratio of latent heat to sensible heat for solidifying water problems
- the post iterative and apparent capacity methods are the least expensive to use
- the cost of using the effective capacity method can be large if the temperature gradients are large compared to the mushy range
- the cost of using the implicit enthalpy method is large and increases rapidly with increasing nodal points
- the solutions from the various methods appear to remain stable for the range of parameters tested except when the usual limits on the Fourier moduli are exceeded for the explicit formulations

Finally, some of the relative advantages of the finite difference and finite element methods have been discussed.

Future work should be concentrated on isothermal solidification problems where latent heat is large compared to sensible heat (as in ice-water problems). Some work should also be done to render the integrating subroutine of the effective capacity method more efficient by adding a check for when the temperature gradients are large compared

to the mushy range.. Simplifying assumptions can be made in order to decrease the time taken to perform the integration for this case. This problem is not expected to be significant for metal casting processes, where it has been shown that the effective capacity method performs better than the other methods investigated.

Table 1. Material properties and boundary conditions for the five test cases.

	Test Case #1 1-D Iron	Test Case #2 1-D Aluminum	Test Case #3 1-D Water	Test Case #4 2-D Iron	Test Case #5 2-D Aluminum
Thermal Conductivity (W/mK)	30.0	130.0	2.0	30.0	130.0
Heat Capacity (J/kg K)	800.0	900.0	2,500.0	800.0	900.0
Density (kg/m^3)	7,000.0	2,500.0	1,000.0	7,000.0	2,500.0
Latent Heat (J/kg)	200,000.0	400,000.0	100,000.0	200,000.0	400,000.0
Phase Change Temperature (°C)	0.0	-	0.0	0.0	-
Mushy Range (°C)	-	-50.0 to +50.0	-	-	-50.0 to +50.0
ℓ (m)	1.0	1.0	2.5	0.1	0.1
T(x,o) (°C)	150.0	150.0	2.0	-	-
T(o,t) (°C)	-500.0	-400.0	-10.0	-	-
T(ℓ,t) (°C)	150.0	150.0	2.0	-	-
T(x,y,o) (°C)	-	-	-	150.0	150.0
T(o,y,t) = T(x,o,t) (°C)	-	-	-	-500.0	-400.0

Table 2. Conditions for test cases #1, #2 and #3.

	Test Case #1 1-D Iron Explicit	Test Case #1 1-D Iron Implicit	Test Case #2 1-D Aluminum Explicit	Test Case #2 1-D Aluminum Implicit	Test Case #3 1-D Water Explicit	Test Case #3 1-D Water Implicit
Δx (m)	0.05	0.05	0.05	0.05	0.125	0.125
No. of nodes	21	21	21	21	21	21
Δt "A" (s)	70	200	7	20	2000	10000
Fourier moduli "A"	0.15	0.43	0.16	0.46	0.10	0.50
Δt "B" (s)	140	600	14	60	6000	30000
Fourier moduli "B"	0.30	1.3	0.32	1.4	0.31	1.5
Δt "C" (s)	210	1000	21	100	10000	50000
Fourier moduli "C"	0.45	2.1	0.49	2.3	0.50	2.6
Mushy Range* (°C)	10	10	100	100	0.5	0.5
Constant in Homographic Approximation* (°C)	10	10	-	-	0.5	0.5

* Either assumed or actual where applicable.

Table 3. Conditions for test cases #4 and #5.

	Test Case 4A 2-D Iron	Test Case 4B 2-D Iron	Test Case 5A 2-D Aluminum	Test Case 5B 2-D Aluminum
$\Delta x = \Delta y$ (m)	0.02	0.01	0.02	0.01
Grid	6×6	11×11	6×6	11×11
Δt (s)	20	10	5.0	2.0
Mushy Range* (°C)	10	10	100	100

* Either assumed or actual where applicable.

Table 4. Standard deviations for test cases #1, #2 and #3.

	Test Case #1 1-D Iron (°C)			Test Case #2 1-D Aluminum (°C)			Test Case #3 1-D Water (°C)		
	A	B	C	A	B	C	A	B	C
Explicit Time Step (s)	70	140	210	7	14	21	2000	6000	10000
Post Iterative (isothermal, explicit)	4.3	4.6	5.2	-	-	-	0.17	0.17	0.17
Post Iterative (mushy, explicit)	3.8	4.1	4.7	2.6	2.6	3.0	0.16	0.16	0.17
Apparent Capacity (explicit)	12.5	17.2	19.0	2.8	6.4	9.4	0.32	0.60	0.65
Enthalpy Method (mushy, explicit)	3.8	4.1	4.5	2.4	2.3	2.2	0.17	0.16	0.17
Effective Capacity (explicit)	3.5	4.1	4.8	1.2	1.6	2.7	0.24	0.26	0.33
Tacke Method (explicit)	1.4	1.8	2.3	-	-	-	0.021	0.017	0.03
Implicit Time Step (s)	200	600	1000	20	60	100	10000	30000	50000
Post Iterative (isothermal, implicit)	7.0	11.0	14.0	-	-	-	0.45	0.75	1.0
Post Iterative F.E. (isothermal, implicit)	12.0	19.0	25.0	-	-	-	0.40	0.75	1.0
Post Iterative (mushy, implicit)	7.0	11.0	21.0	9.0	19.0	27.4	0.40	0.75	1.0
Apparent Capacity (implicit)	12.0	15.0	17.0	5.2	5.9	9.7	0.60	1.3	0.65
Enthalpy Method (mushy, implicit)	3.5	4.3	5.8	4.5	6.2	8.3	0.16	0.16	0.17
Pham Method (implicit)	5.5	17.0	32.0	4.0	6.5	>30	0.20	0.60	1.7
Effective Capacity (implicit)	2.3	3.2	5.0	1.5	3.2	4.3	0.18	0.22	0.32
Effective Capacity F.E. (implicit)	2.4	3.0	4.8	1.6	2.5	4.0	0.18	0.22	0.26
Blanchard & Fremond (implicit)	2.2	3.8	6.0	-	-	-	0.29	0.29	0.28
Blanchard & Fremond F.E. (implicit)	3.7	4.0	5.0	-	-	-	0.46	0.46	0.46

Table 5. Costs and standard deviations for test case #4.

	Test Case #4A 2-D Iron Δt = 20s $\Delta X = \Delta Y$ = 0.02m		Test Case #4B 2-D Iron Δt = 10s $\Delta X = \Delta Y$ = 0.01m	
	Cost*	Standard Deviation (°C)	Cost*	Standard Deviation (°C)
Post Iterative (isothermal, F.D.)	0.02	10.9	0.07	7.4
Post Iterative (mushy, F.D.)	0.02	10.3	0.07	6.8
Post Iterative (mushy, F.E.)	0.11	18.6	2.08	12.2
Apparent Capacity (F.D.)	0.02	55.9	0.07	39.8
Apparent Capacity (mushy = -25 to +25, F.D.)	0.02	9.5	0.07	12.5
Effective Capacity (F.D.)	2.64	17.2	4.15	7.7
Effective Capacity (F.E.)	2.95	14.0	10.5	10.4
Effective Capacity (mushy = -25 to +25, F.D.)	0.23	10.5	0.58	3.2
Enthalpy (F.D.)	0.10	9.5	1.03	5.9

*Cost = constant (395 + virtual memory pages) CPU time

Table 6. Costs and standard deviations for test case #5.

	Test Case #5A 2-D Aluminum Δt = 5s $\Delta X = \Delta Y$ = 0.02m		Test Case #5B 2-D Aluminum Δt = 2s $\Delta X = \Delta Y$ = 0.01m	
	Cost*	Standard Deviation (°C)	Cost*	Standard Deviation (°C)
Post Iterative F.D.	0.02	19.2	0.04	9.7
Post Iterative F.E.	0.05	38.7	1.04	19.0
Apparent Capacity F.D.	0.02	42.3	0.04	23.6
Effective Capacity F.D.	0.09	8.6	0.31	3.5
Effective Capacity F.E.	0.19	10.3	3.33	7.2
Enthalpy (F.D.)	0.06	12.0	0.81	5.7

*Cost = constant (395 + virtual memory pages) CPU time

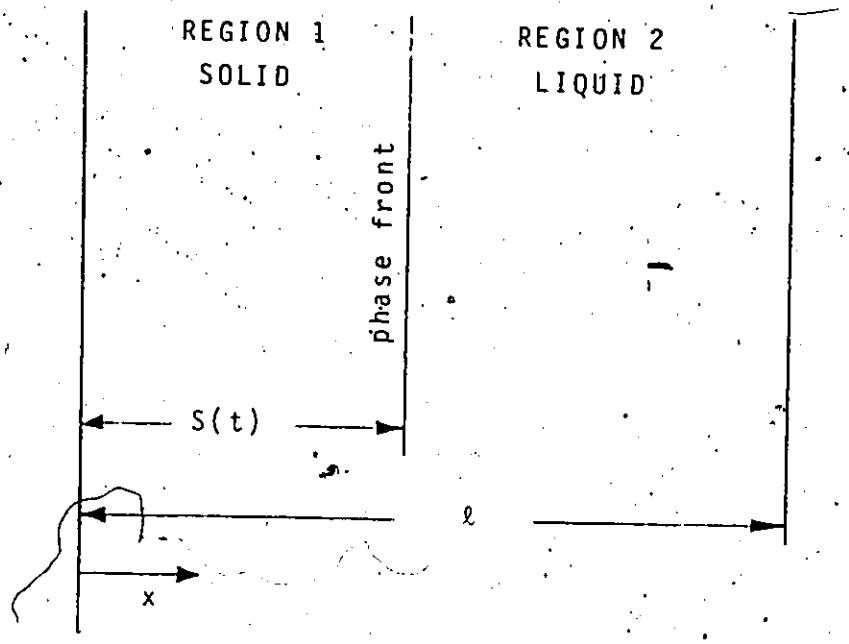

Fig.1 The one-dimensional Stefan problem.

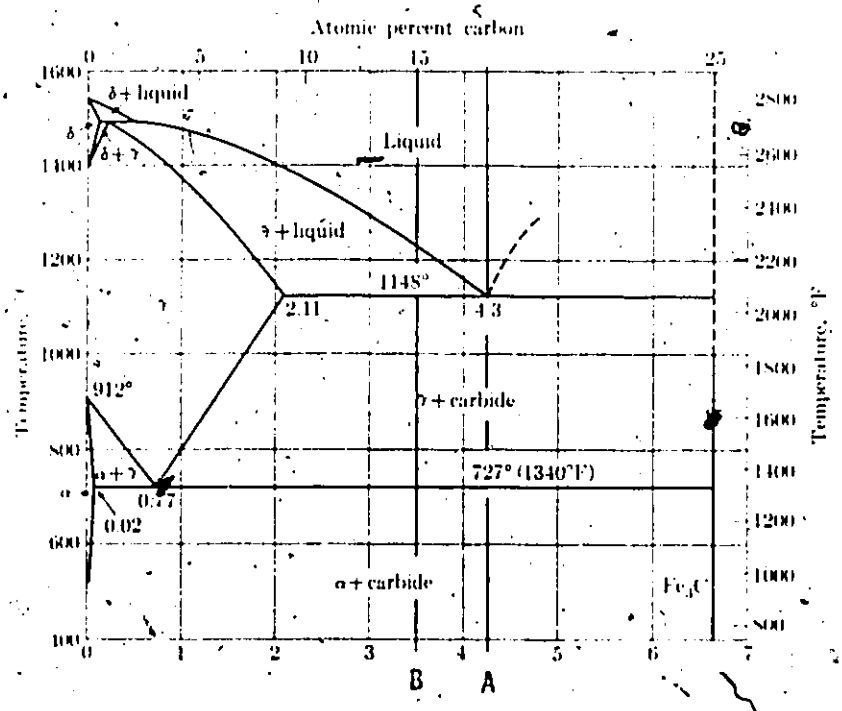

Fig.2 Fe-Fe_3C phase diagram (7).

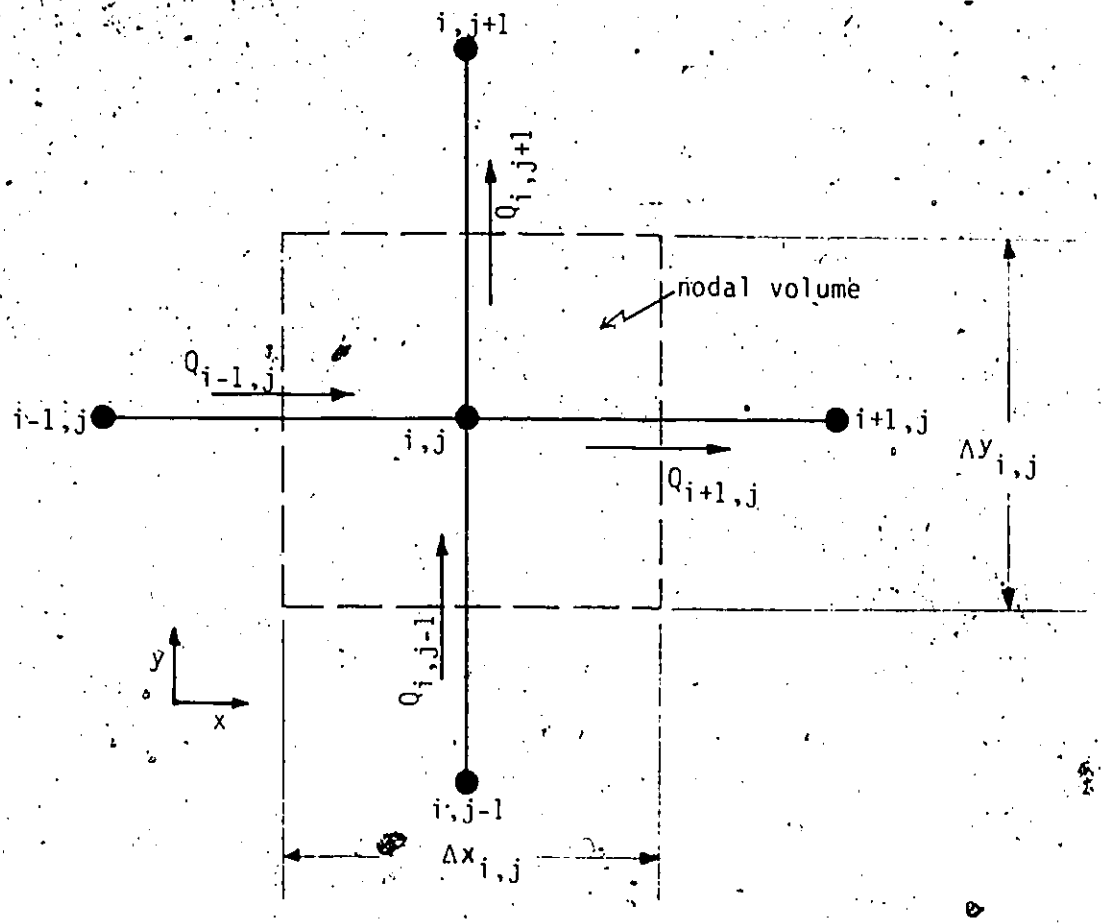

Fig.3 Two-dimensional finite difference node.

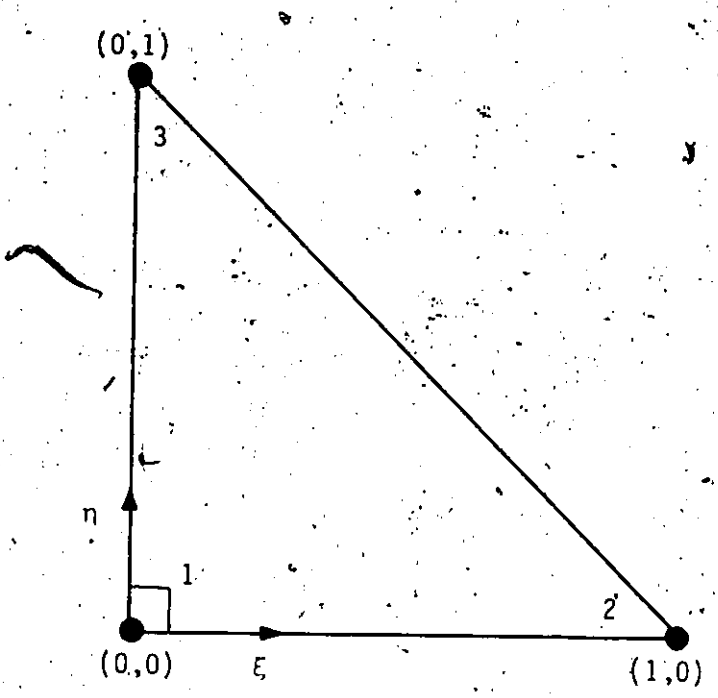

Fig.4 Three noded unit triangular finite element.

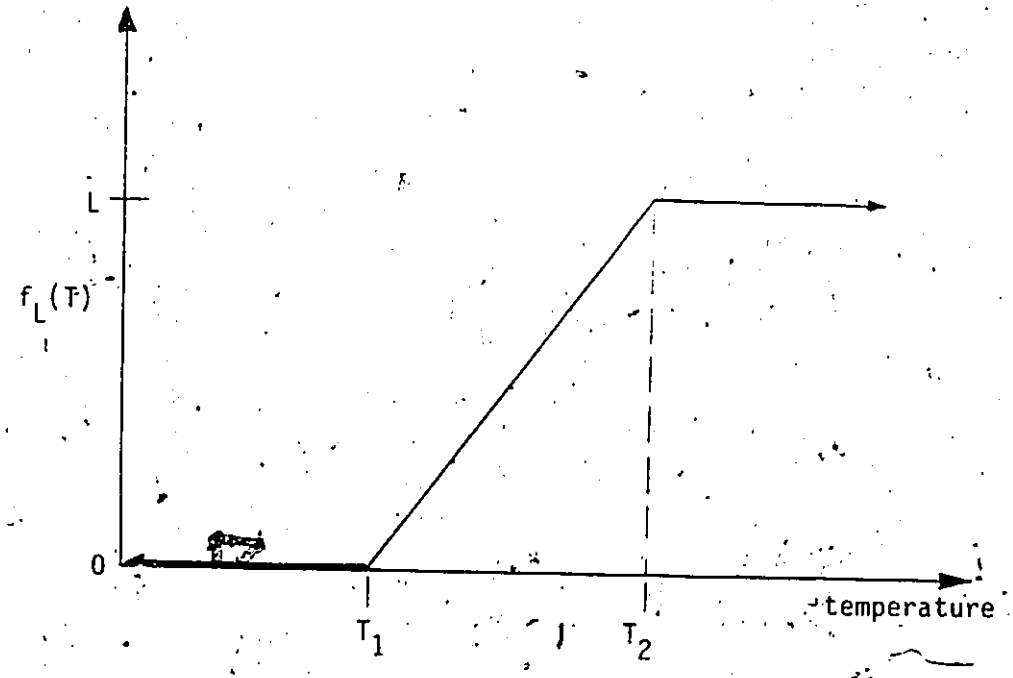

Fig.5 Diagram representing linear release of latent heat.

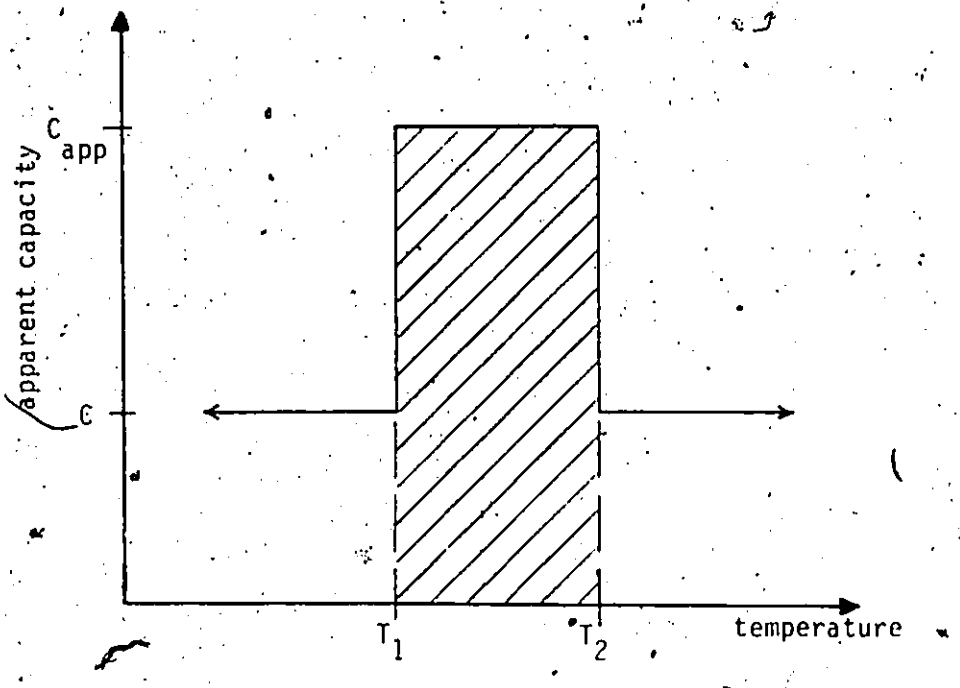

Fig.6a Apparent capacity profile (step changes in heat capacity).

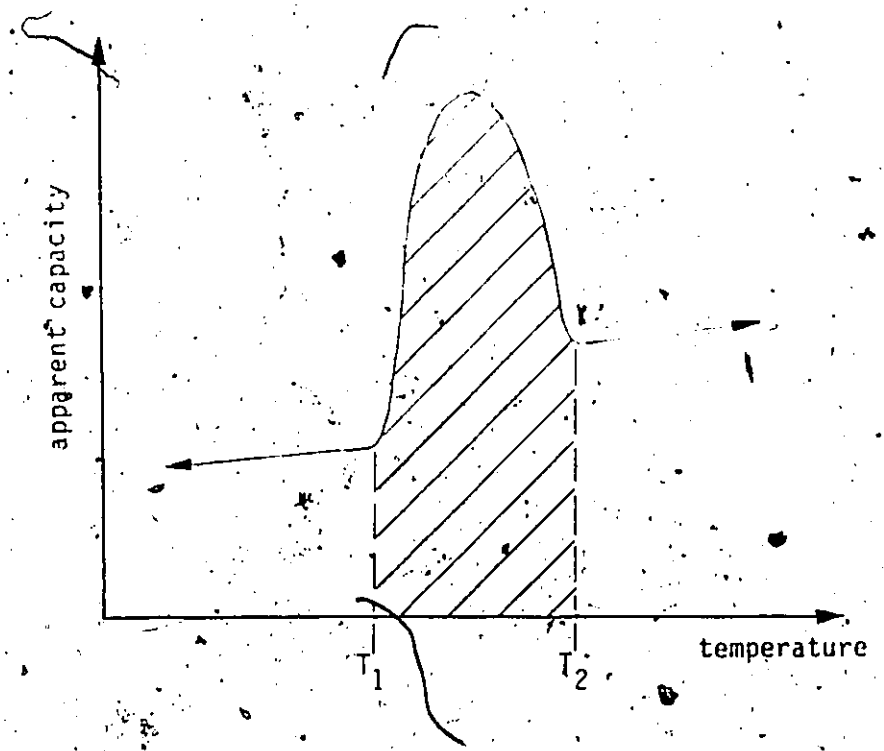

Fig.6b Apparent capacity profile (smooth variation in heat capacity).

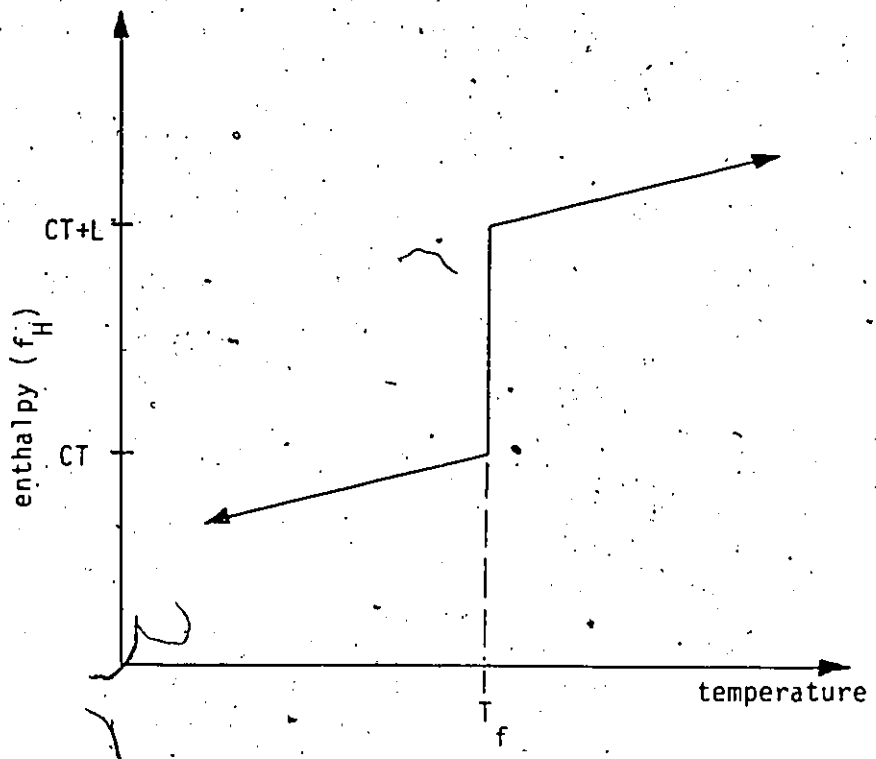

Fig.7a Enthalpy profile for isothermal solidification.

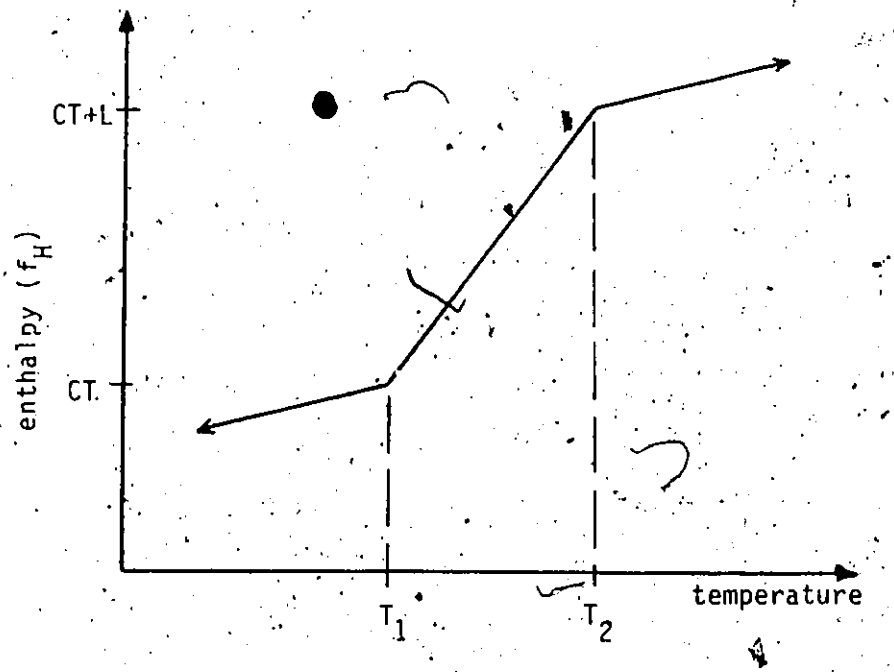

Fig.7b Enthalpy profile for solidification over a temperature range.

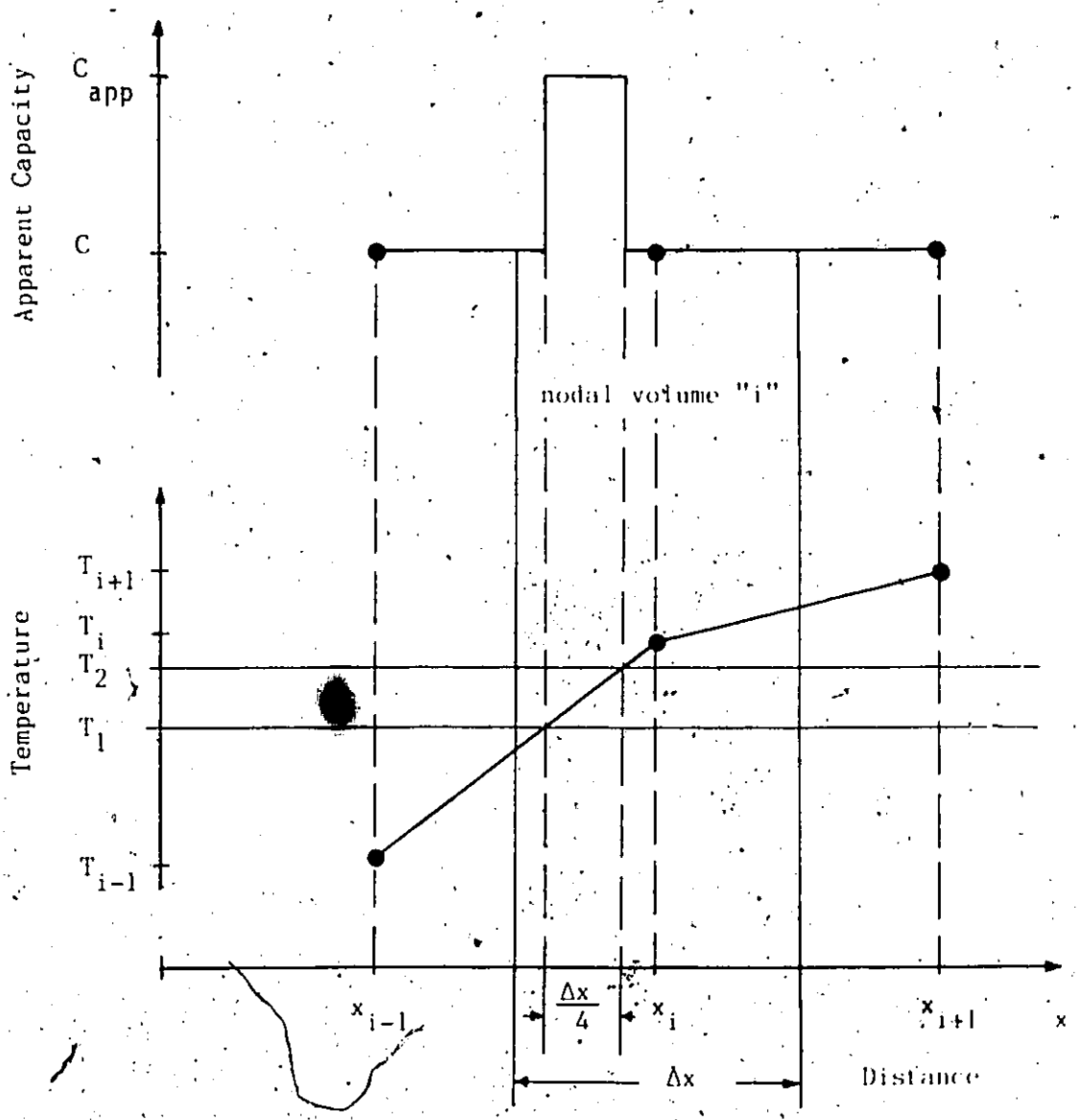

Fig.8a One-dimensional temperature and heat capacity profile in an element.

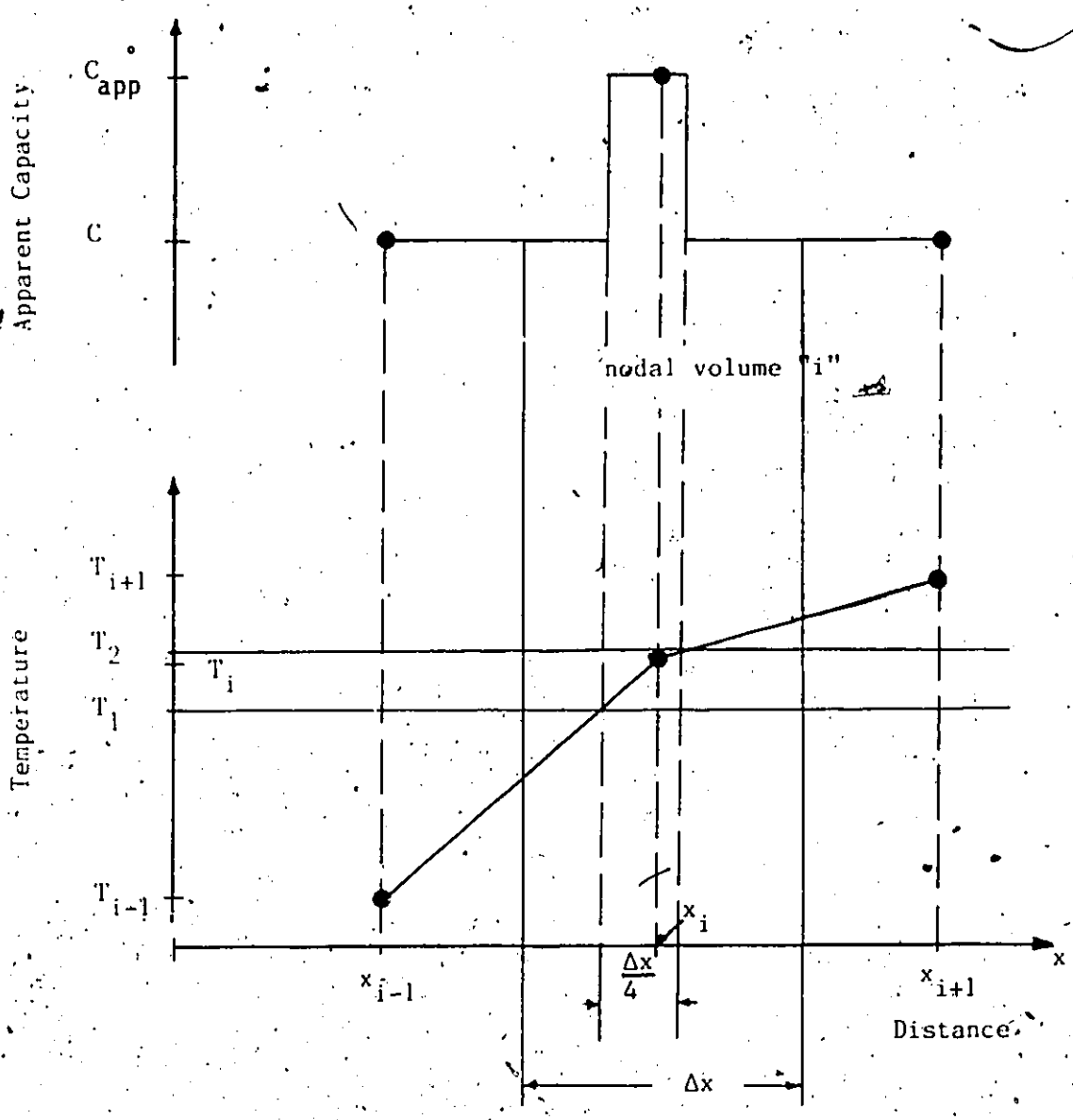

Fig. 8b. One-dimensional temperature and heat capacity profile in an element.

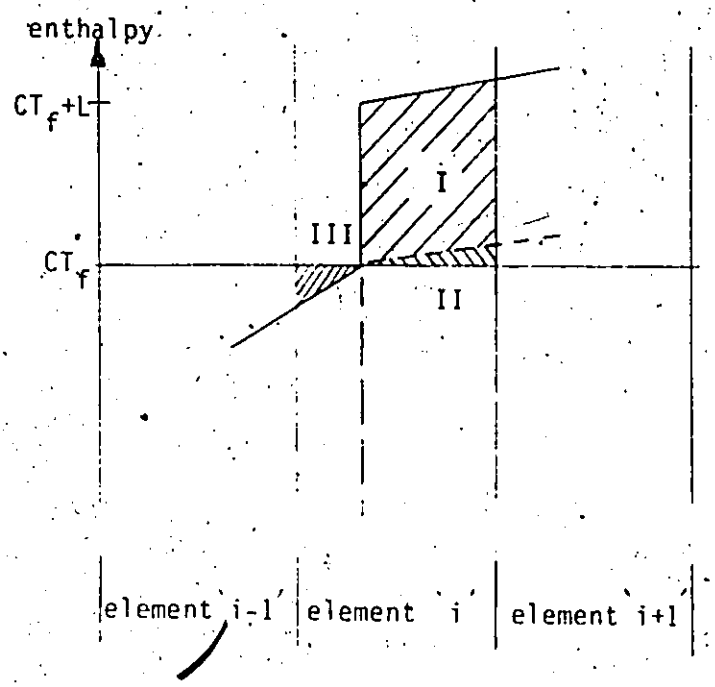

Fig.9a Enthalpy distribution for element containing phase front.

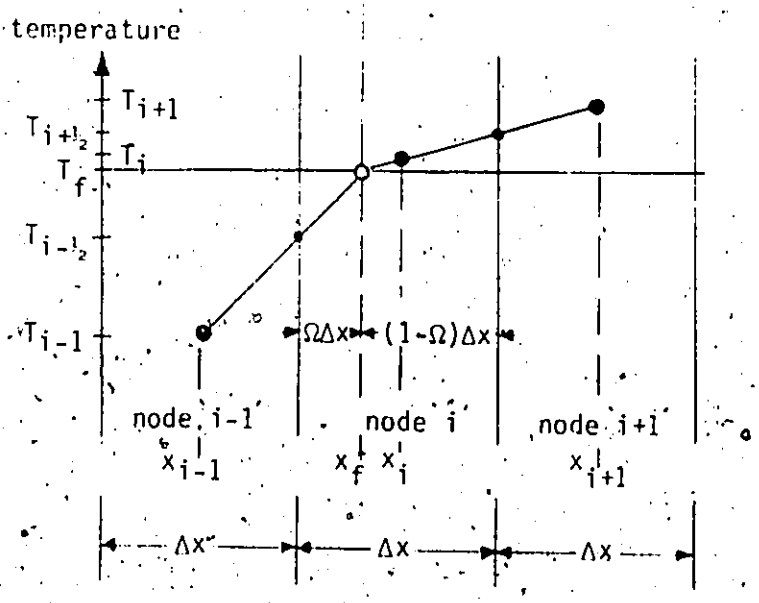

Fig. Temperature distribution for element containing phase front.

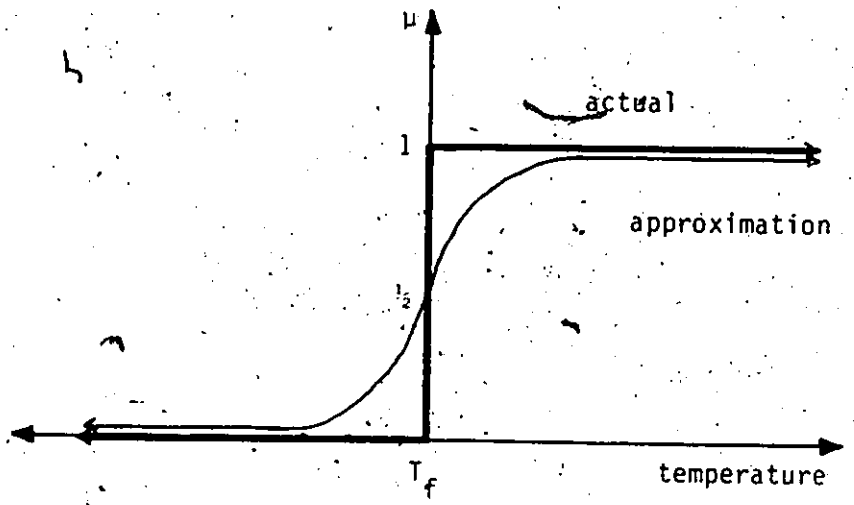

Fig.10 Homographic approximation to liquid water content.

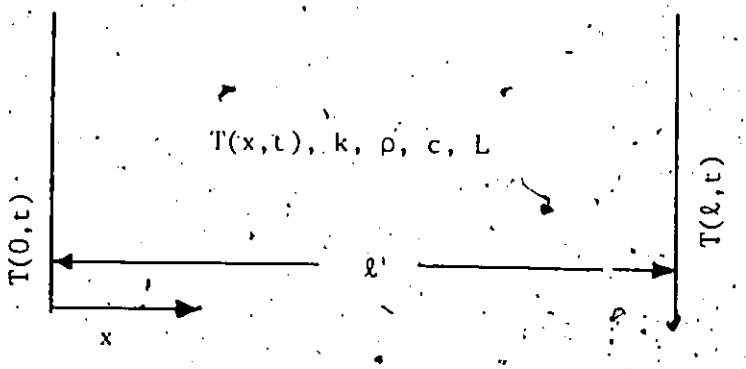

Fig.11 Schematic of one-dimensional test problem.

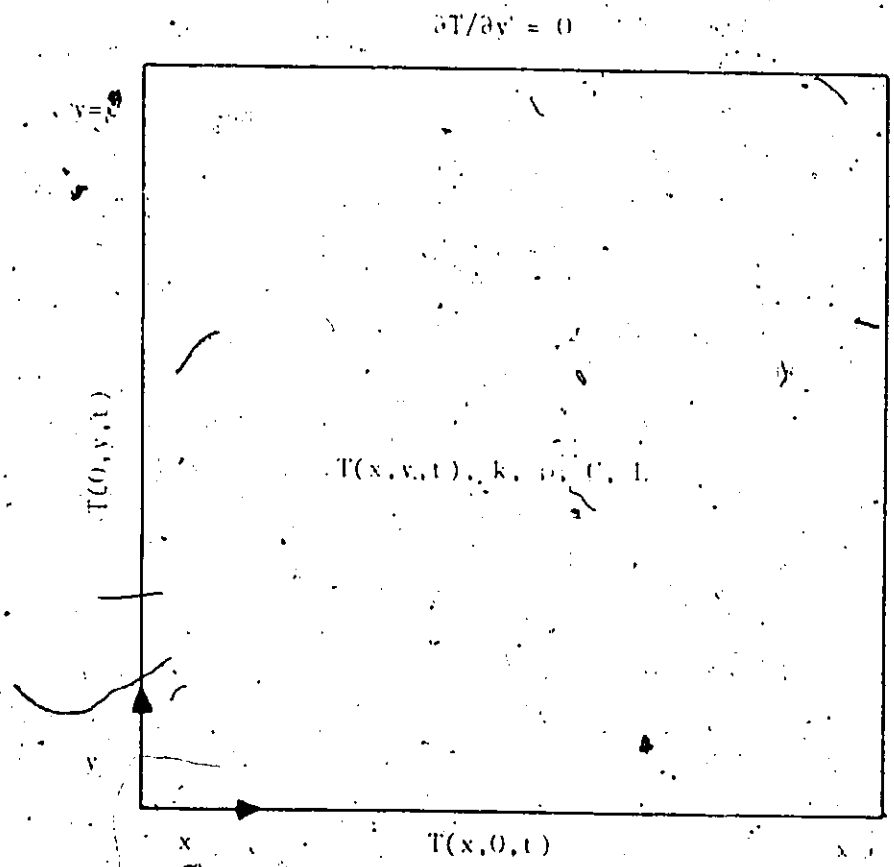

Fig.12 Schematic of two-dimensional test problem.

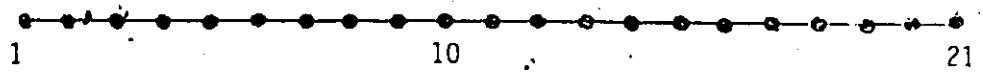

Fig.13 Grid for one-dimensional problems.

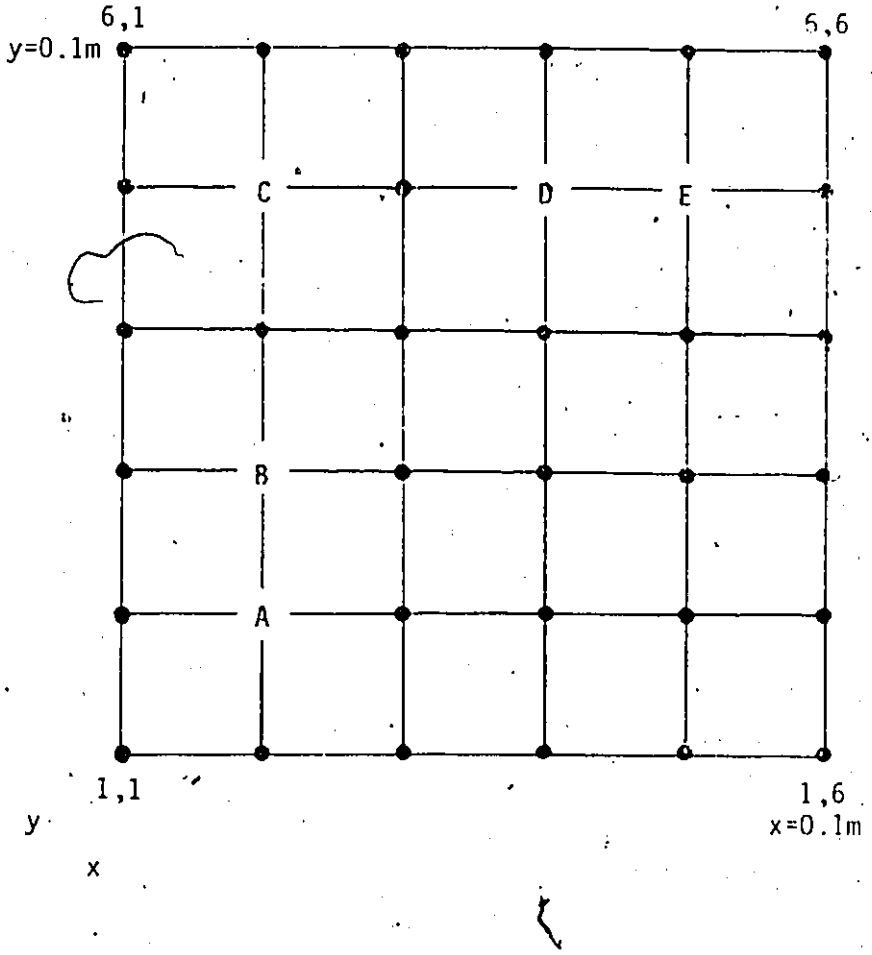

Fig.14 6x6 grid for two-dimensional problems.

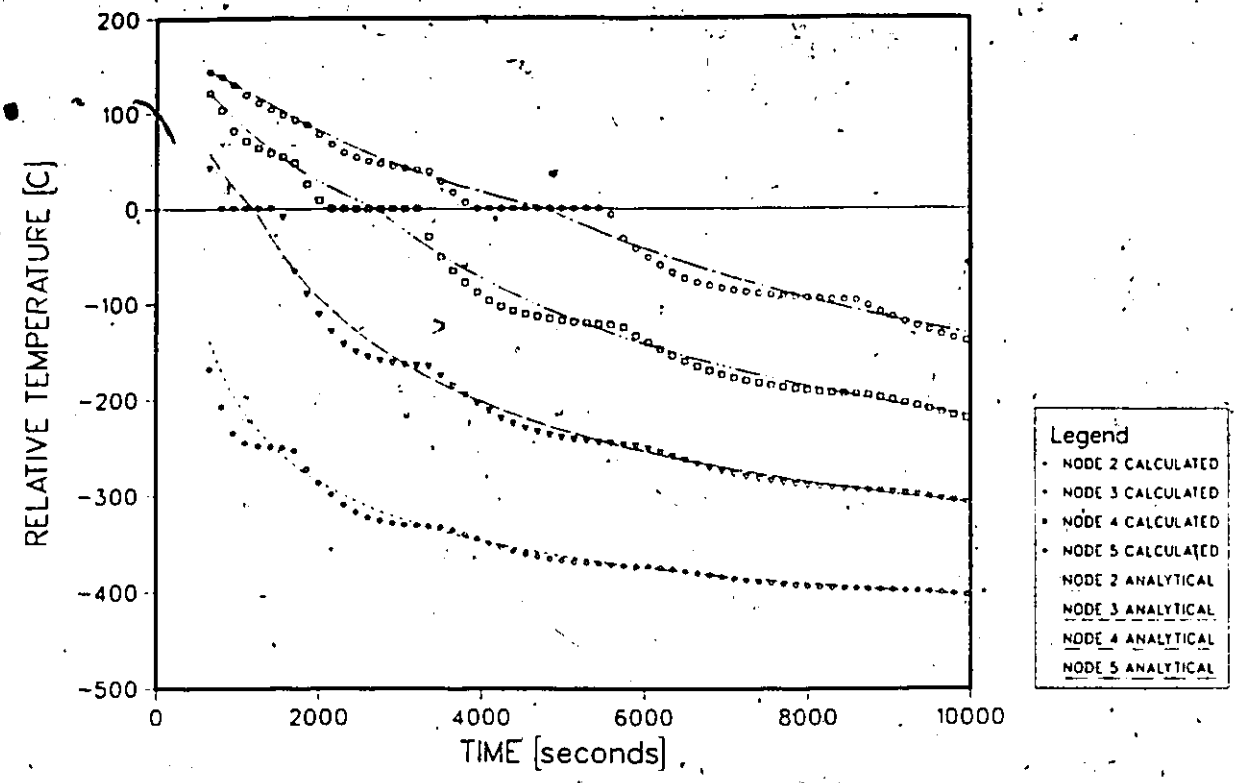

Fig.15 Temperature histories for test case#1 by the post iterative(isothermal) method, explicit finite difference formulation. Time step is 150 s.

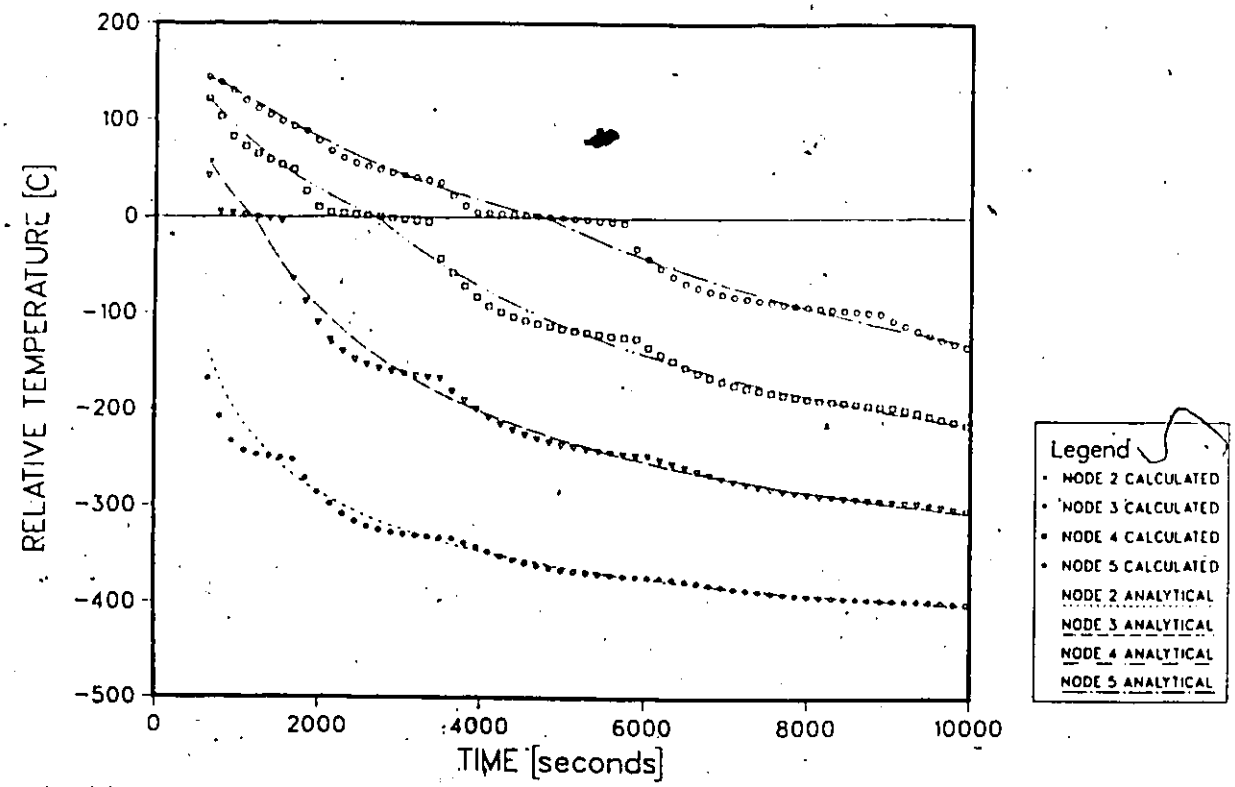

Fig.16 Temperature histories for test case#1 by the post iterative method (mushy=-5.0 to +5.0 C), explicit finite difference. Time step= 150 s.

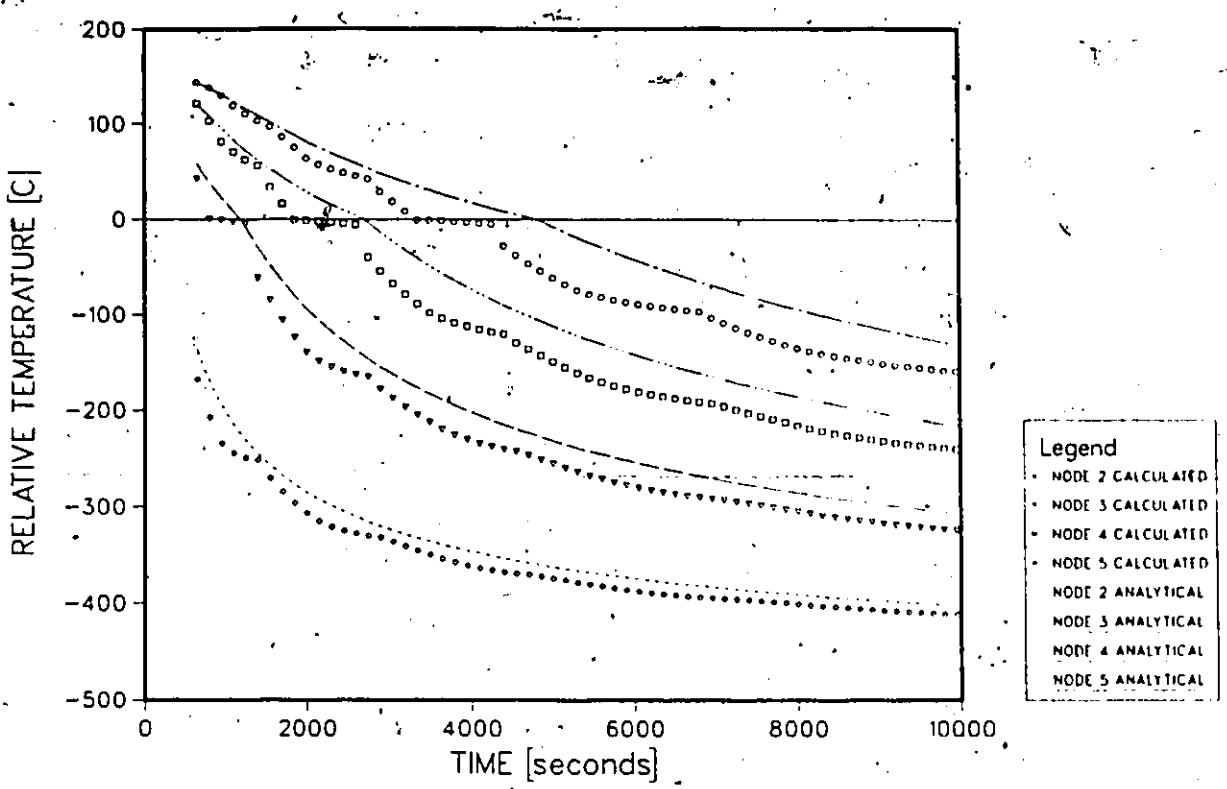

Fig.17 Temperature histories for test case#1 by the apparent capacity method (mushy=-5.0 to +5.0 C), explicit finite difference. Time step is 150s.

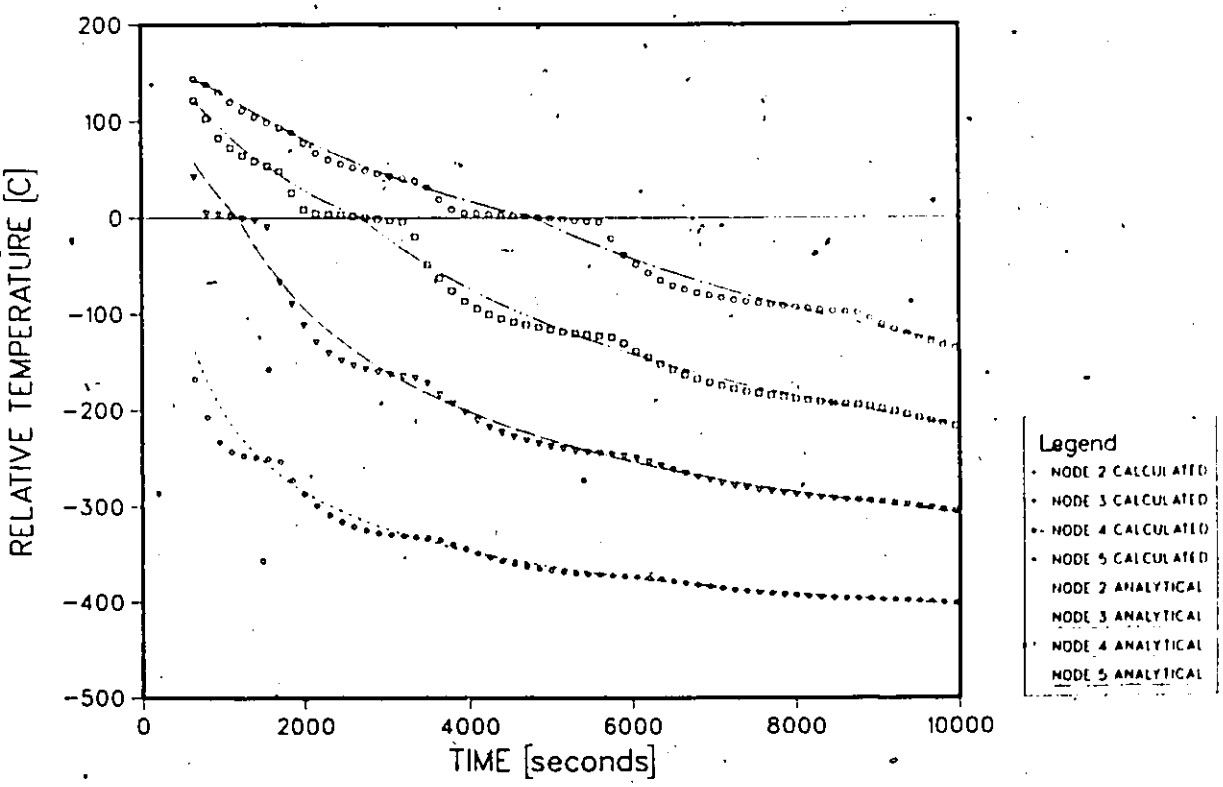

Fig.18 Temperature histories for test case#1 by the enthalpy method (mushy=-5.0 to +5.0 C), explicit finite difference. Time step is 150s.

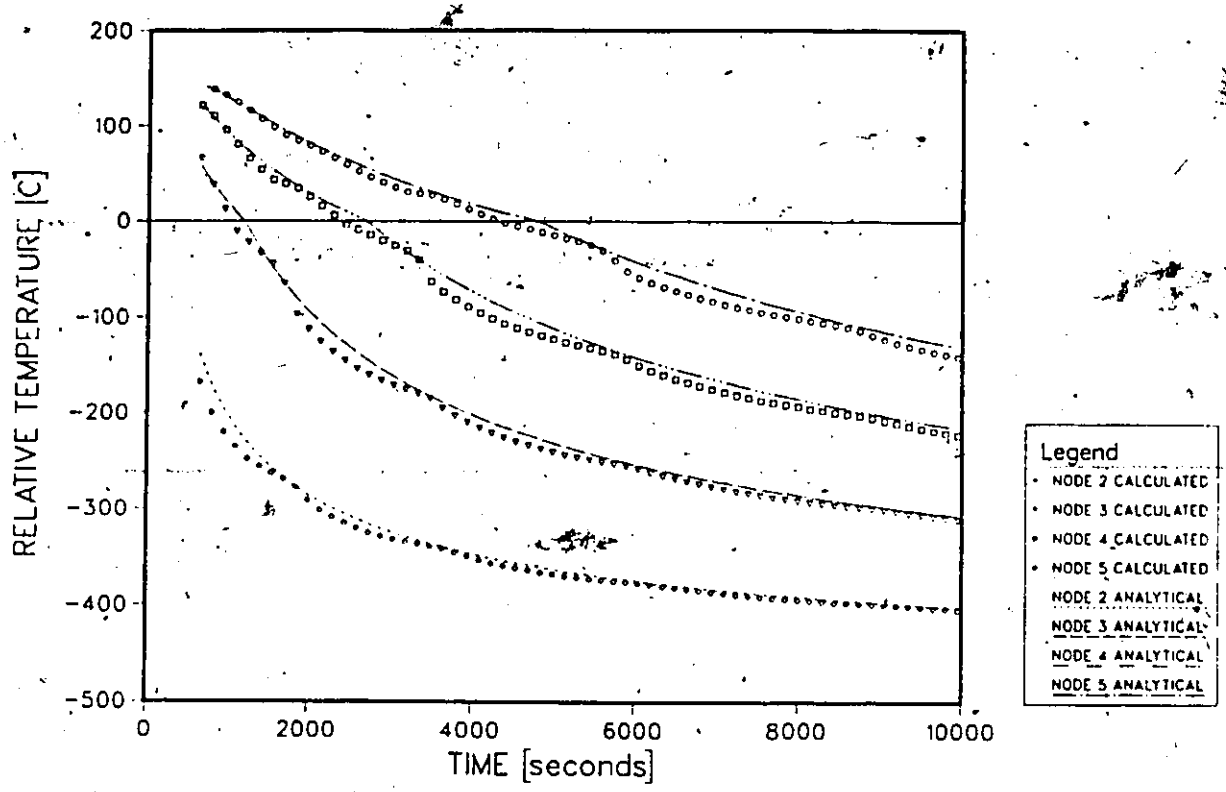

Fig.19 Temperature histories for test case#1 by the effective capacity method (mushy=-5.0 to +5.0 C), explicit finite difference. Time step is 150s.

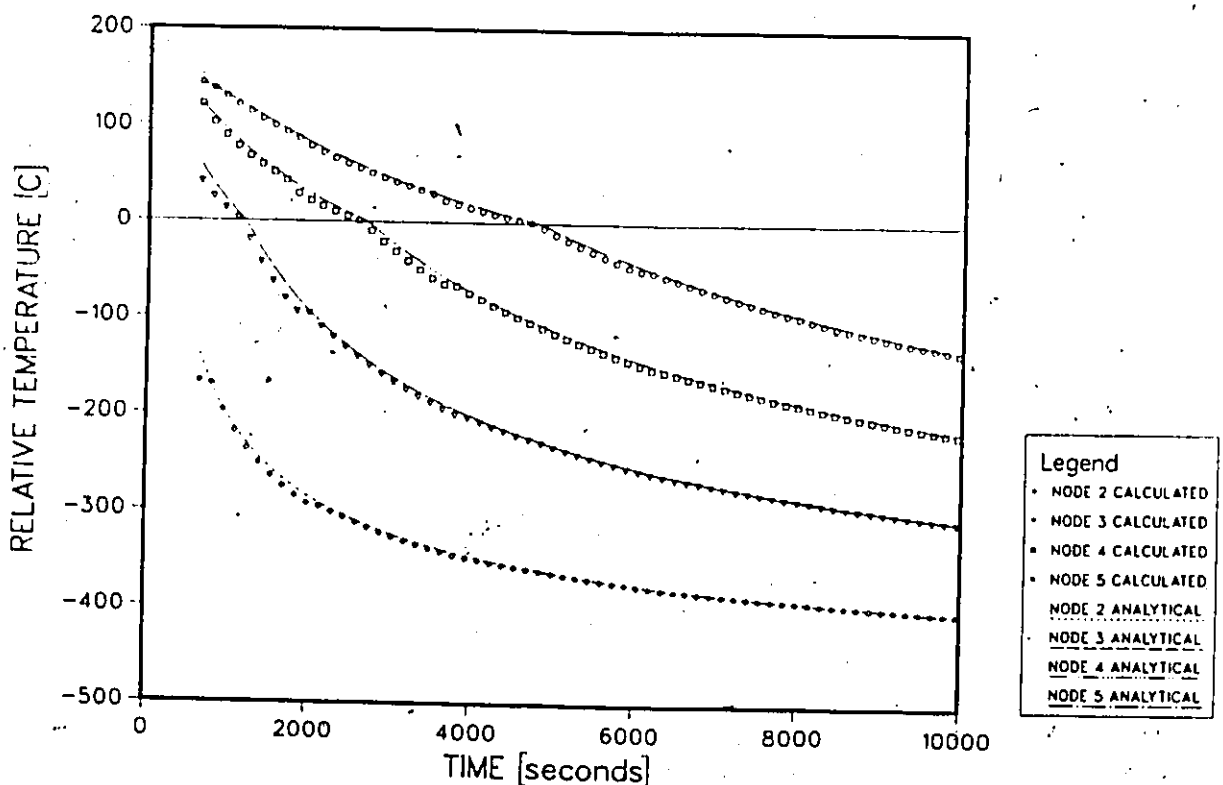

Fig.20 Temperature histories for test case#1 by Tácke's method, explicit finite difference. Time step is 150s.

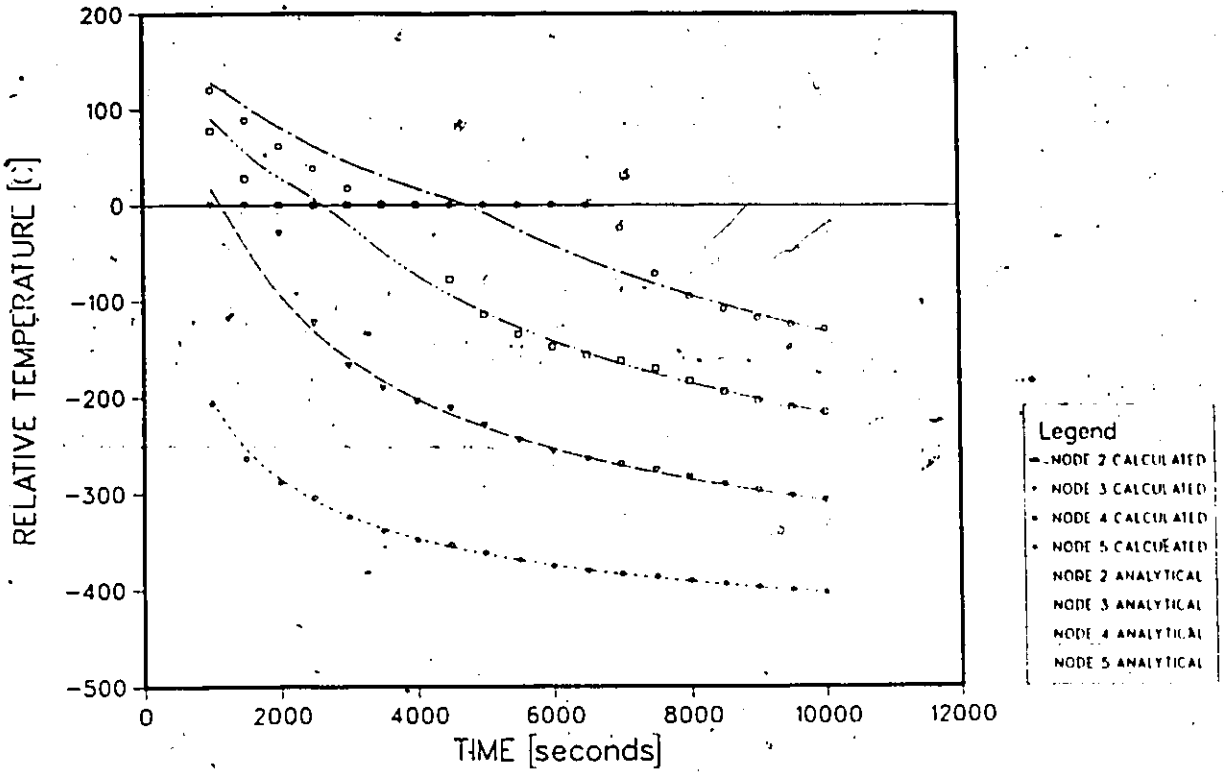

Fig.21 Temperature histories for test case#1 by the post iterative(isothermal) method, implicit finite difference. Time step is 500s.

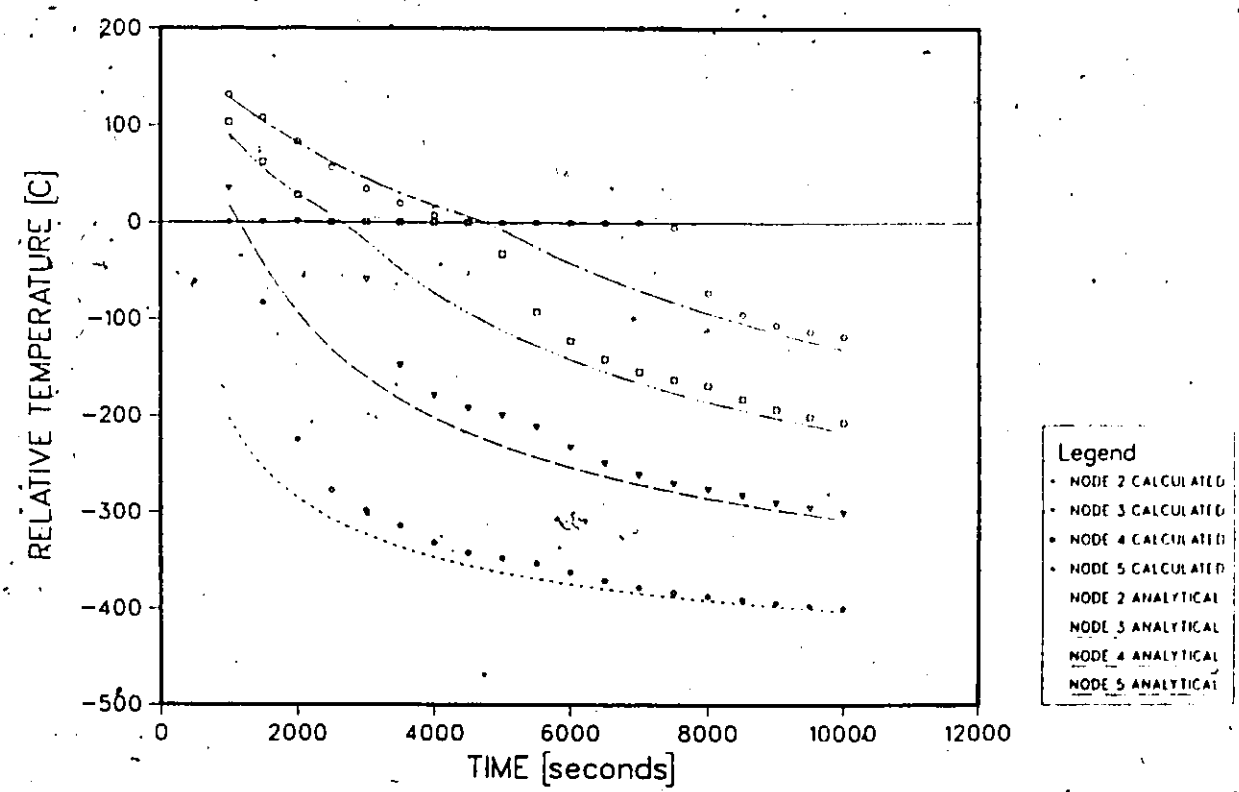

Fig.22 Temperature histories for test case#1 by the post iterative(isothermal) method, implicit finite element. Time step is 500s.

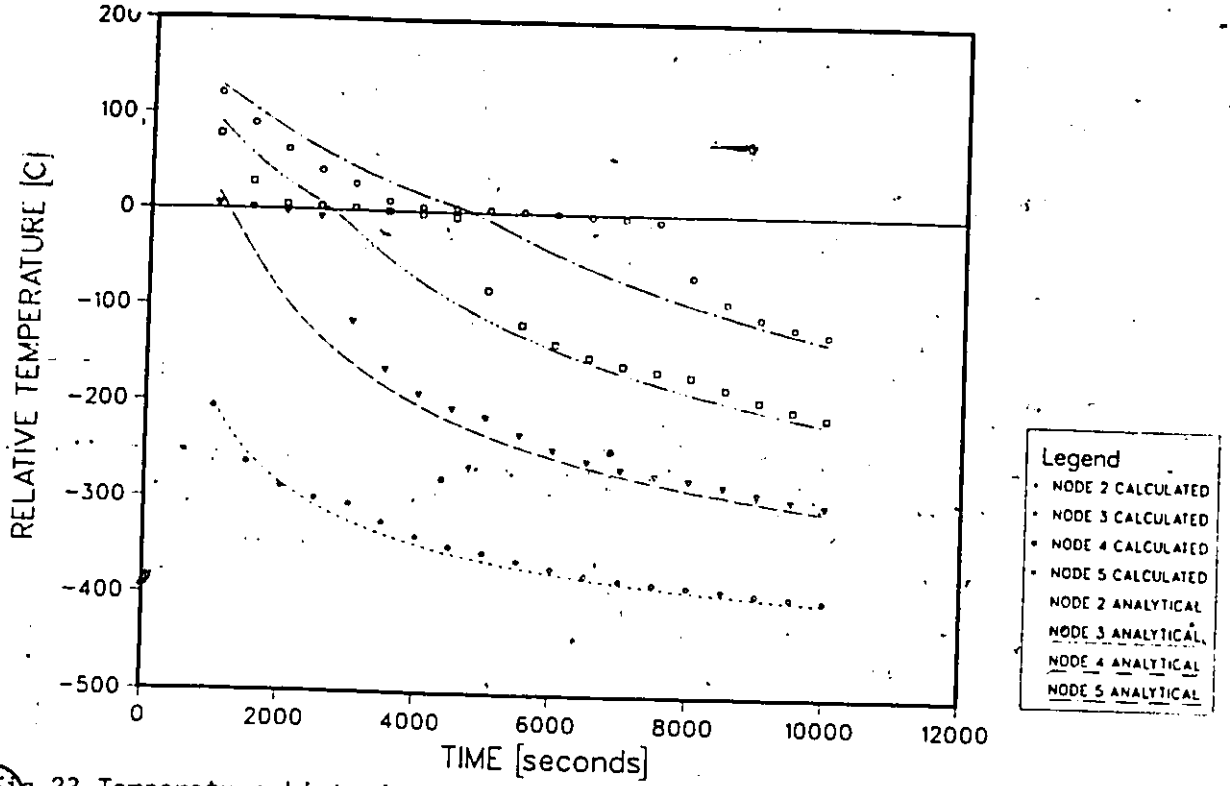

Fig.23 Temperature histories for test case#1 by the post iterative method (mushy=-5.0 to +5.0 C), implicit finite difference. Time step is 500s.

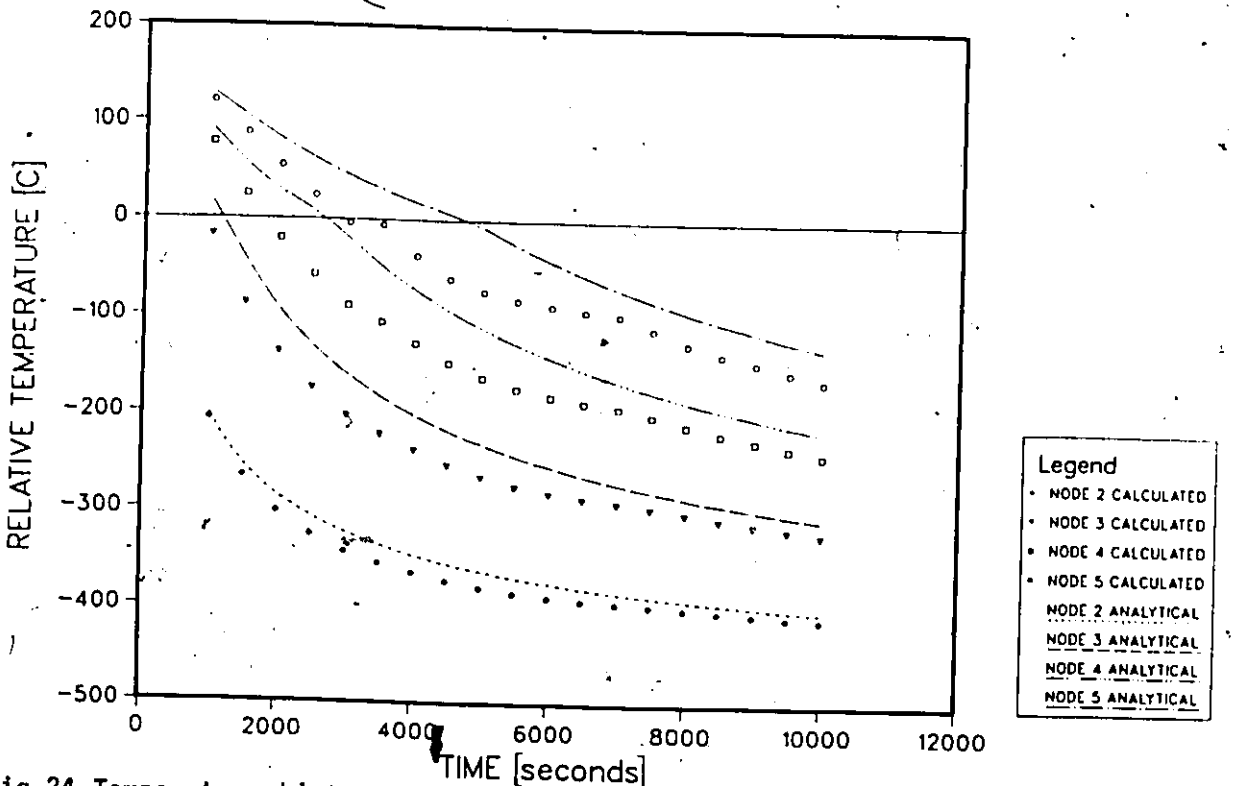

Fig.24 Temperature histories for test case#1 by the apparent capacity method (mushy=-5.0 to +5.0 C), implicit finite difference. Time step is 500s.

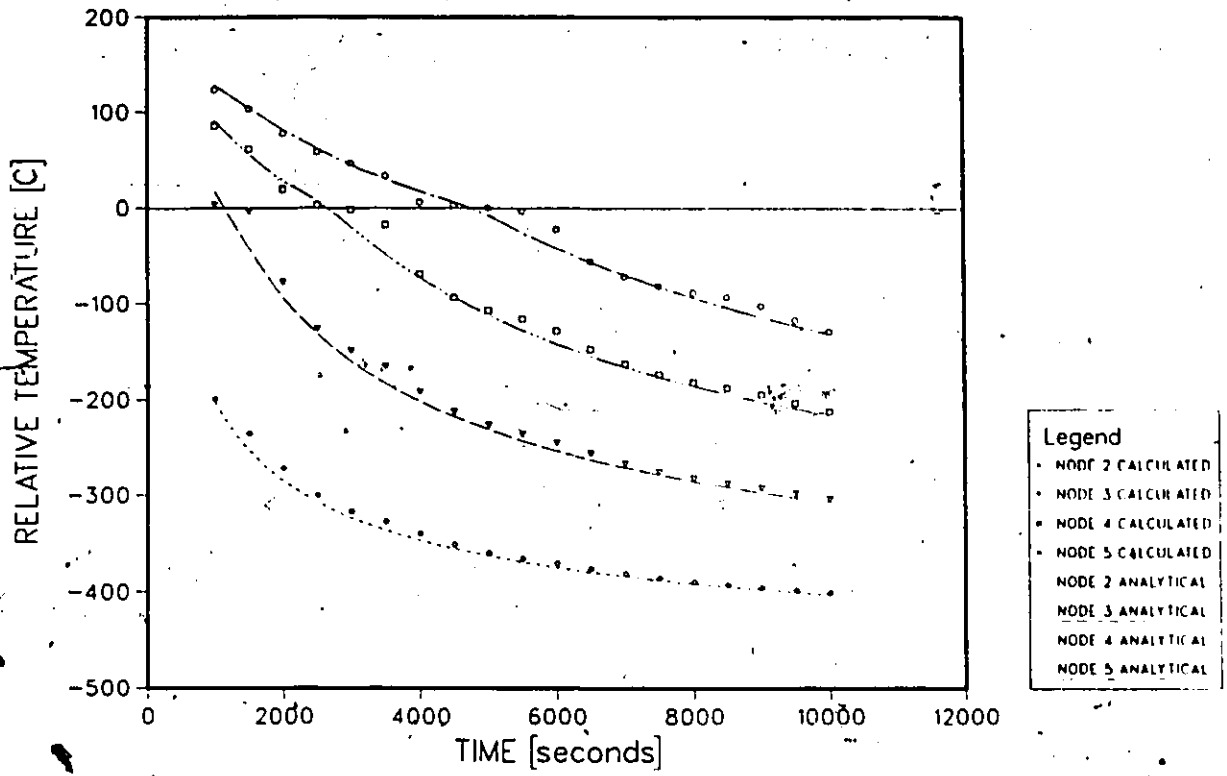

Fig.25 Temperature histories for test case#1 by the enthalpy method (mushy=-5.0 to +5.0 C), implicit finite difference. Time step is 500s.

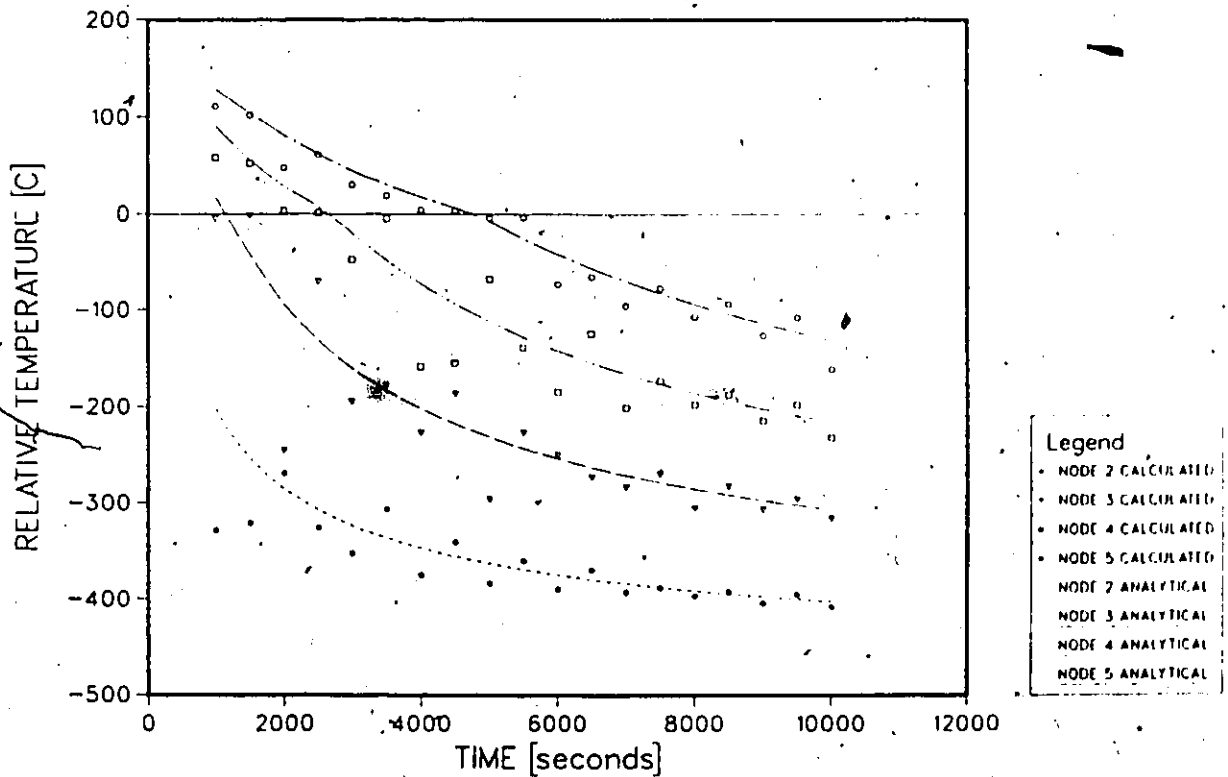

Fig.26 Temperature histories for test case#1 by Pham's method (mushy=-5.0 to +5.0 C), implicit finite difference. Time step is 500s.

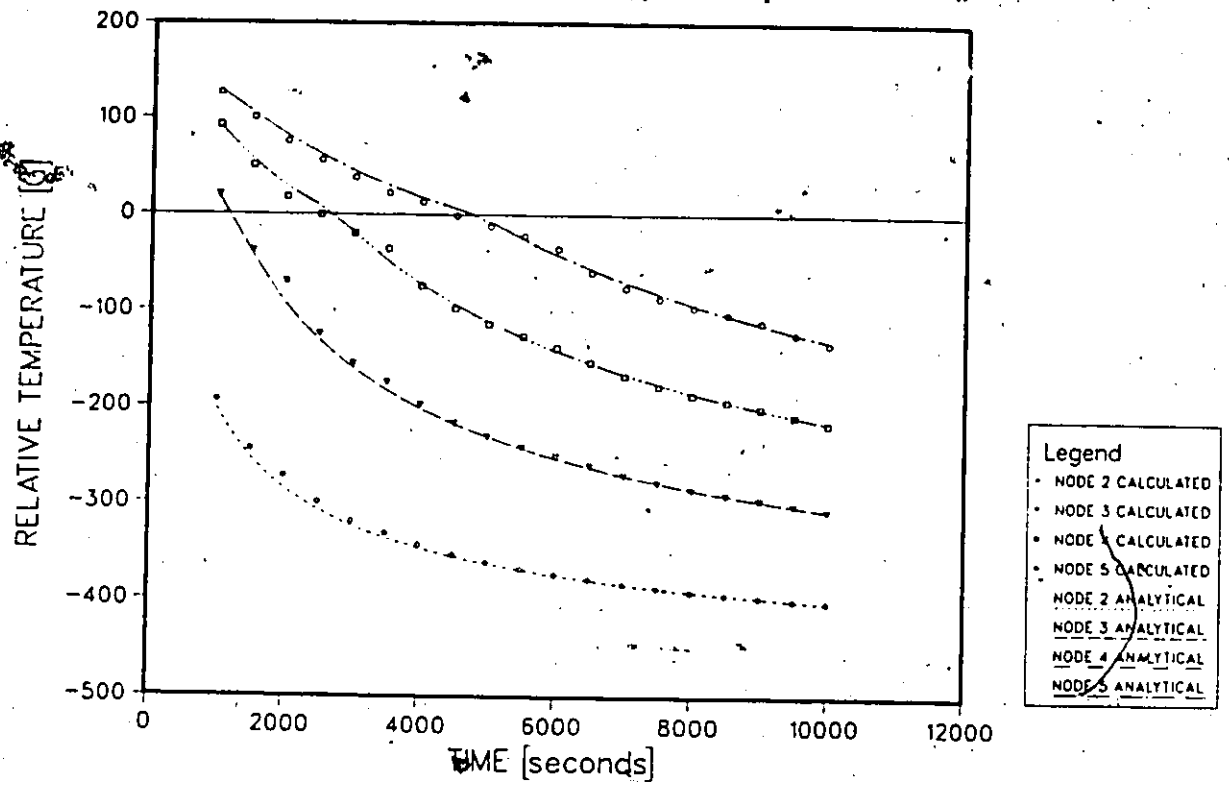

Fig.27 Temperature histories for test case#1 by the effective capacity method (mushy=-5.0 to +5.0 C), implicit finite difference. Time step is 500s.

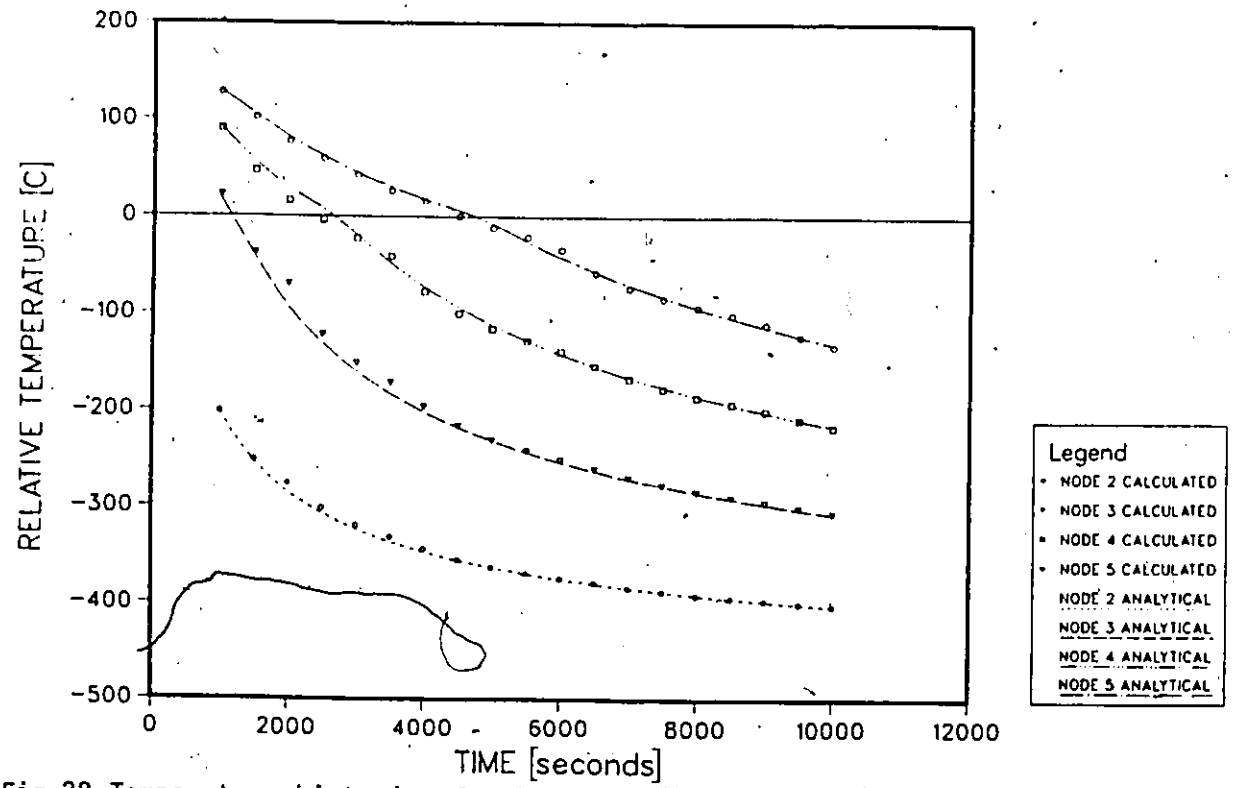

Fig.28 Temperature histories for test case#1 by the effective capacity method (mushy=-5.0 to +5.0 C), implicit finite element. Time step is 500s.

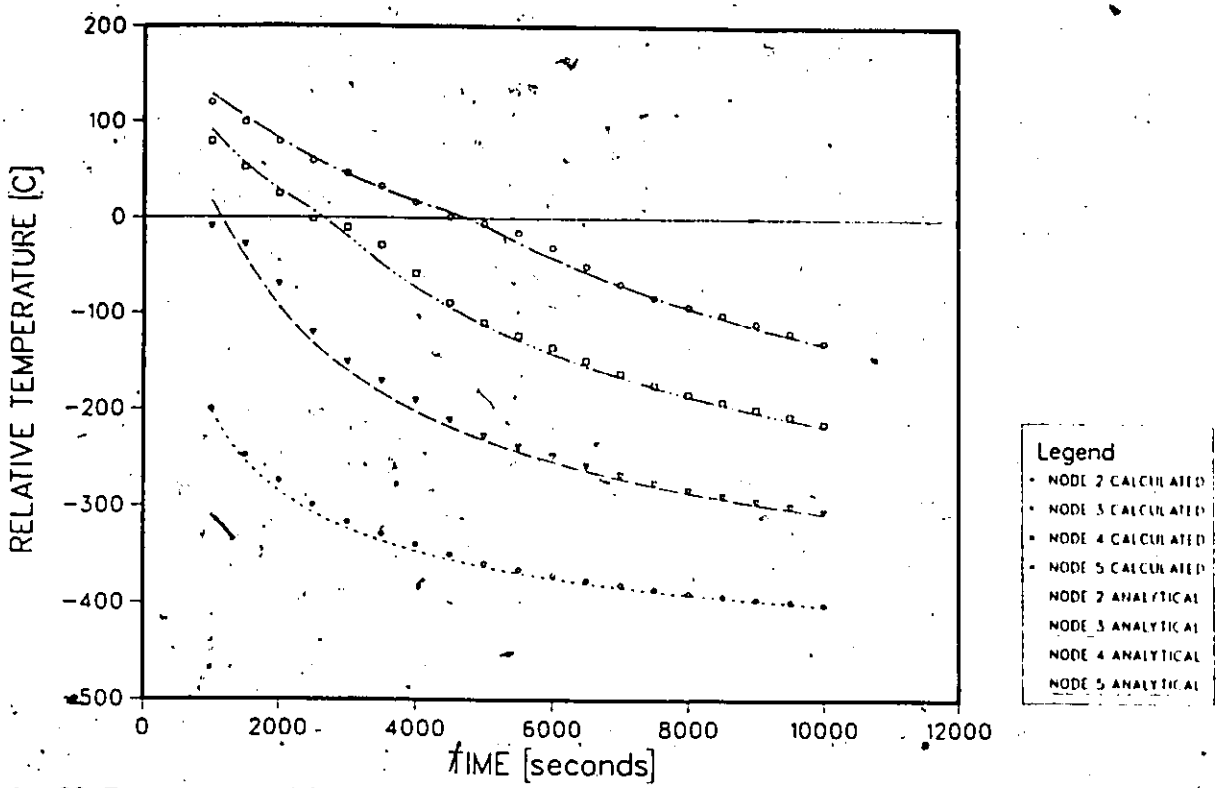

Fig.29 Temperature histories for test case#1 by Blanchard and Fremond's method (parameter= 10.0 C), implicit finite difference. Time step is 1000s.

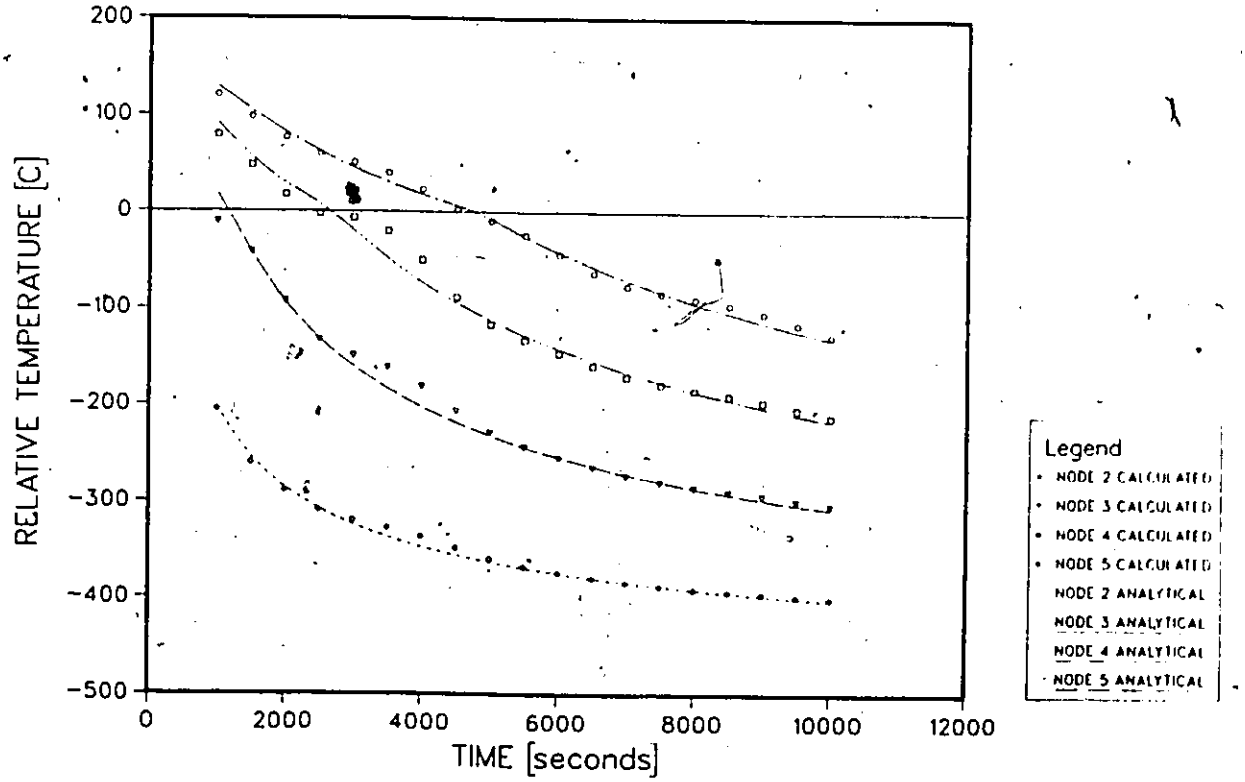

Fig.30 Temperature histories for test case#1 by Blanchard and Fremond's method (parameter= 10.0 C), implicit finite element. Time step is 1000s.

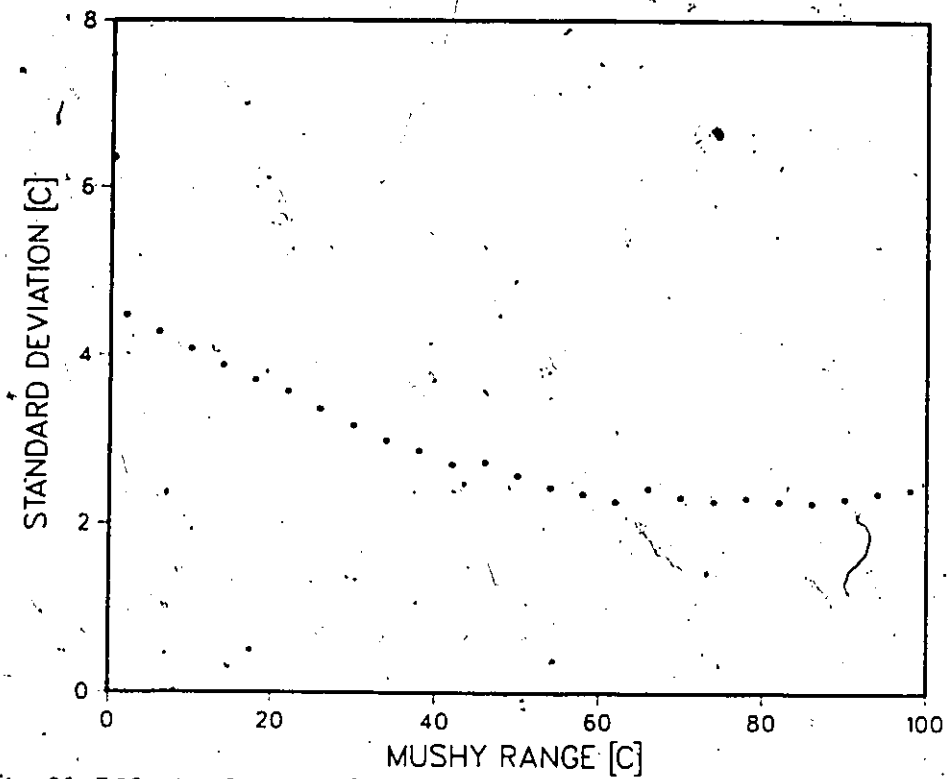

Fig.31 Effect of assumed mushy range on solution to test case#1 by the post iterative method, explicit finite difference. Time step is 150s.

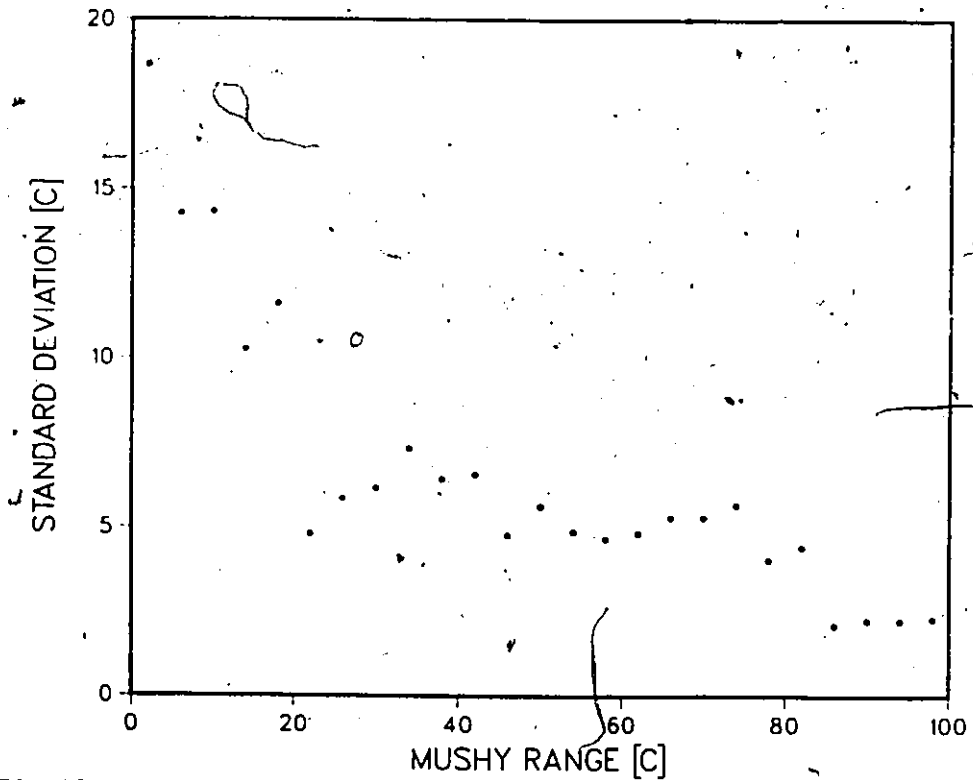

Fig.32 Effect of assumed mushy range on solution to test case#1 by the apparent capacity method, explicit finite difference. Time step is 150s.

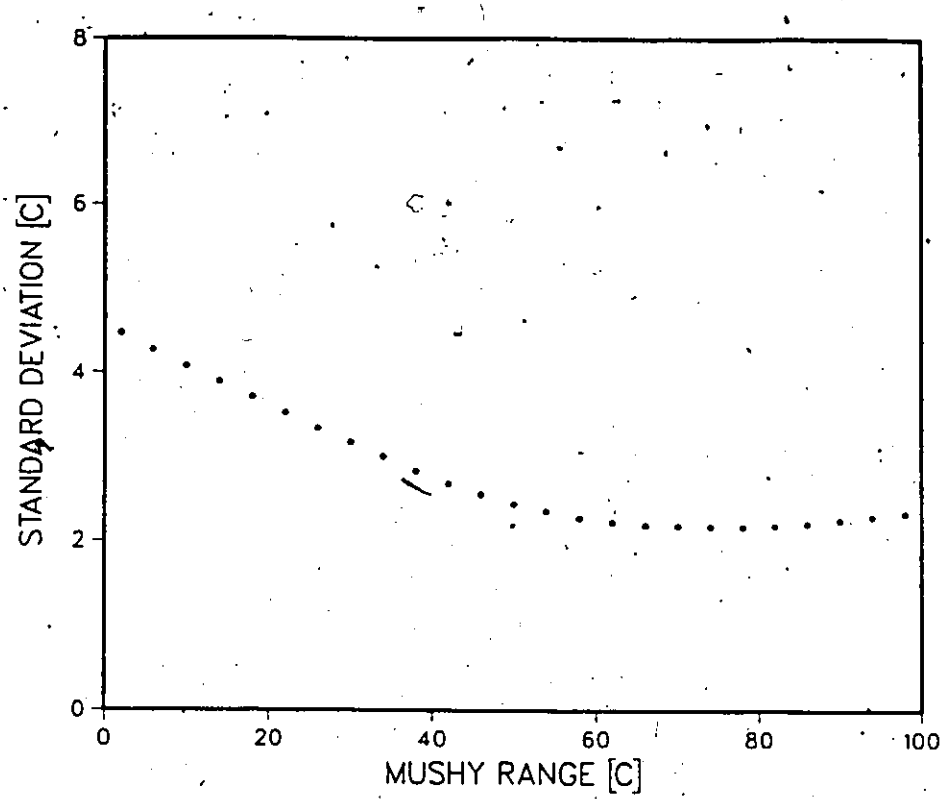

Fig.33 Effect of assumed mushy range on solution to test case#1 by the enthalpy method, explicit finite difference. Time step is 150s.

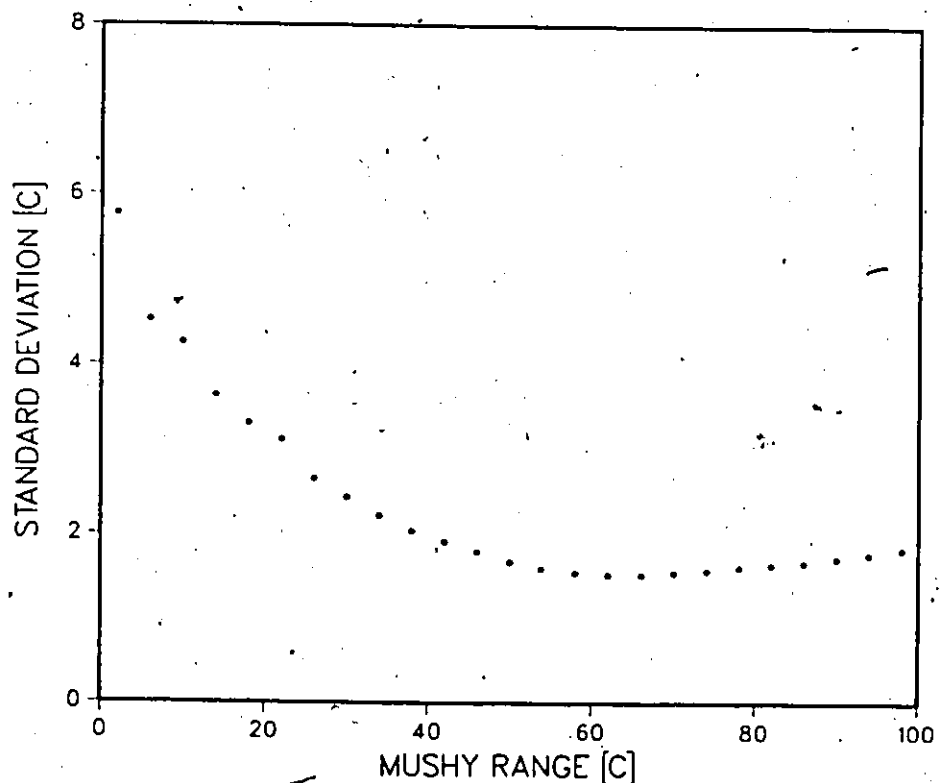

Fig.34 Effect of assumed mushy range on solution to test case#1 by the effective capacity method, explicit finite difference. Time step is 150s.

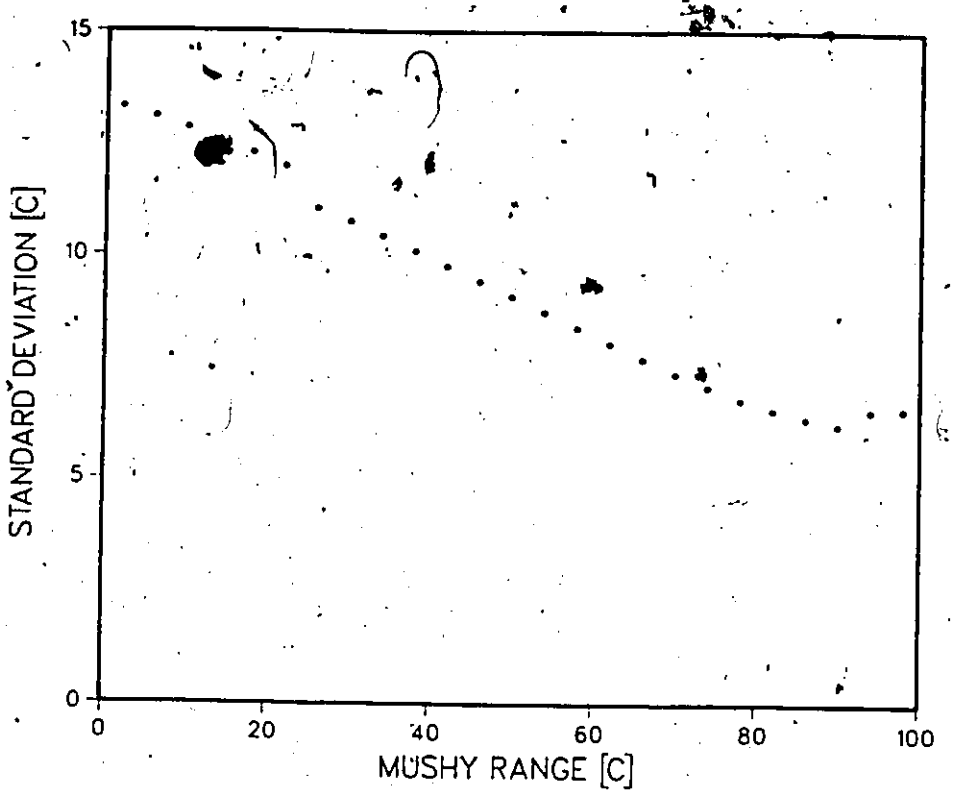

Fig.35 Effect of assumed mushy range on solution to test case#1 by the post iterative method, implicit finite difference. Time step is 500s.

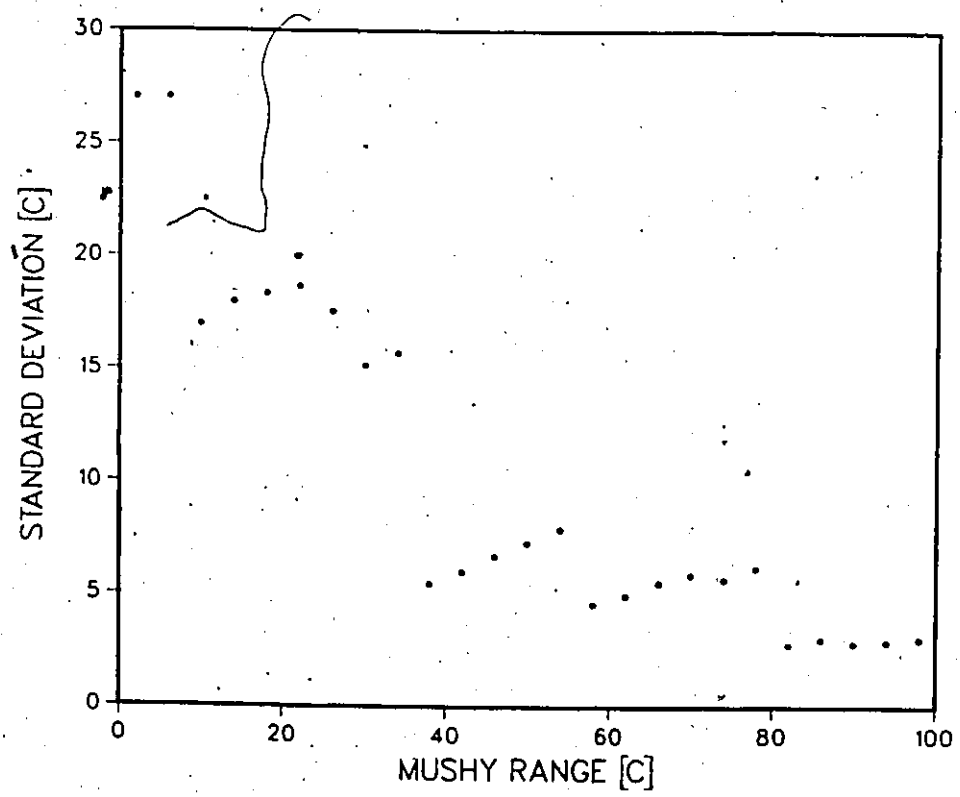

Fig.36 Effect of assumed mushy range on solution to test case#1 by the apparent capacity method, implicit finite difference. Time step is 500s.

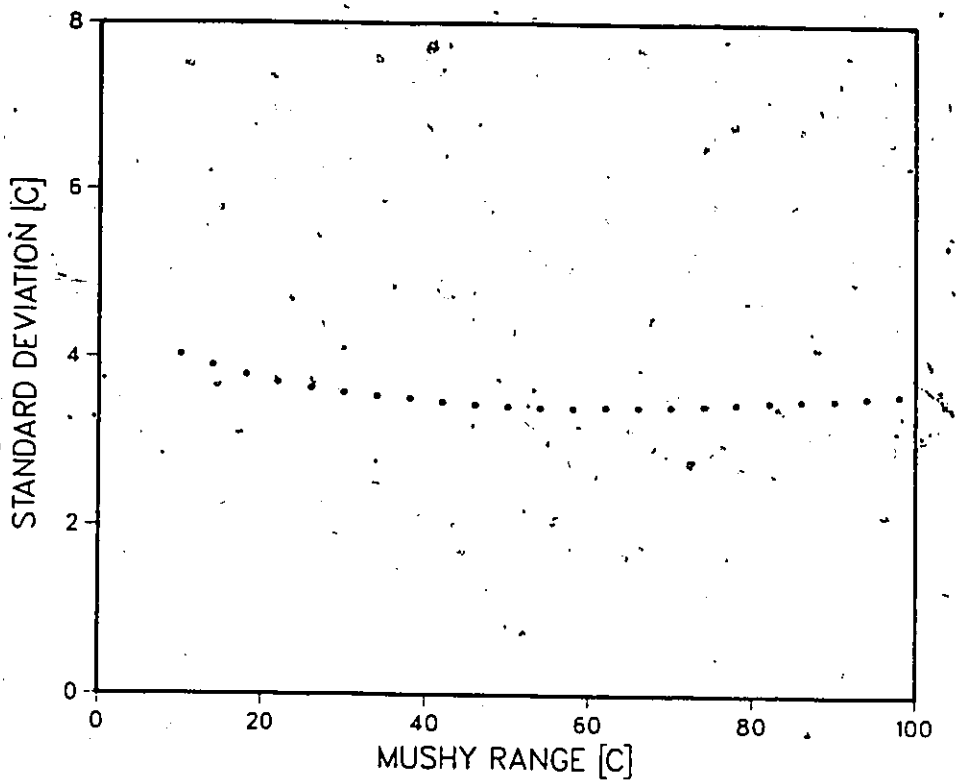

Fig.37 Effect of assumed mushy range on solution to test case#1 by the enthalpy method, implicit finite difference. Time step is 500s.

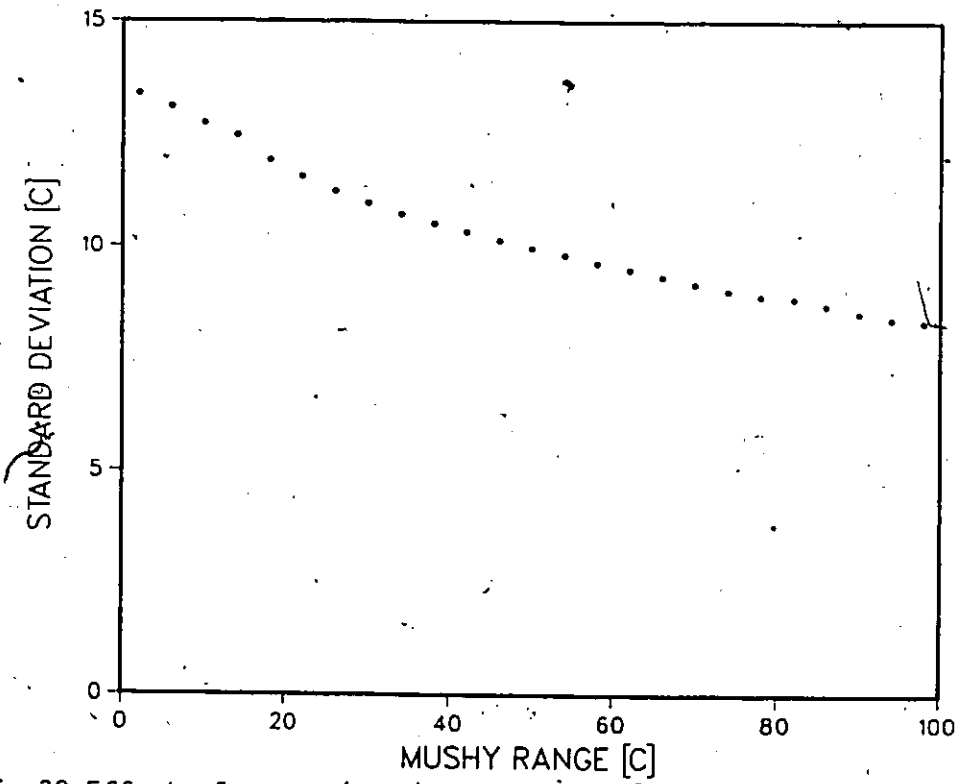

Fig.38 Effect of assumed mushy range on solution to test case#1 by Pham's method, implicit finite difference. Time step is 500s.

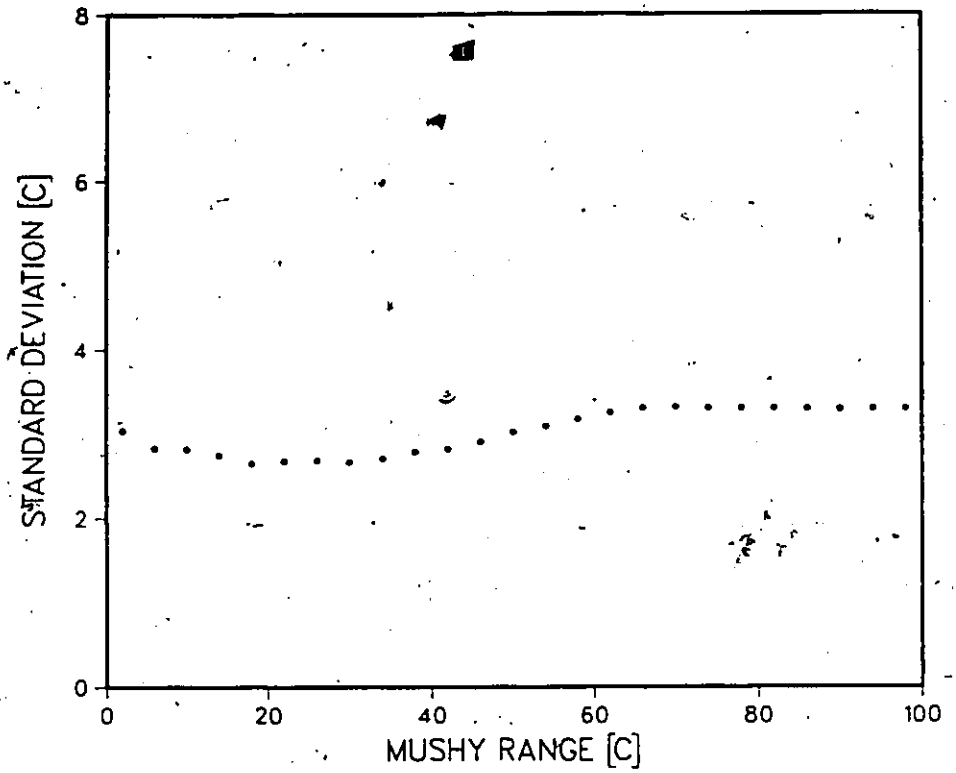

Fig.39 Effect of assumed mushy range on solution to test case#1 by the effective capacity method, implicit finite difference. Time step is 500s.

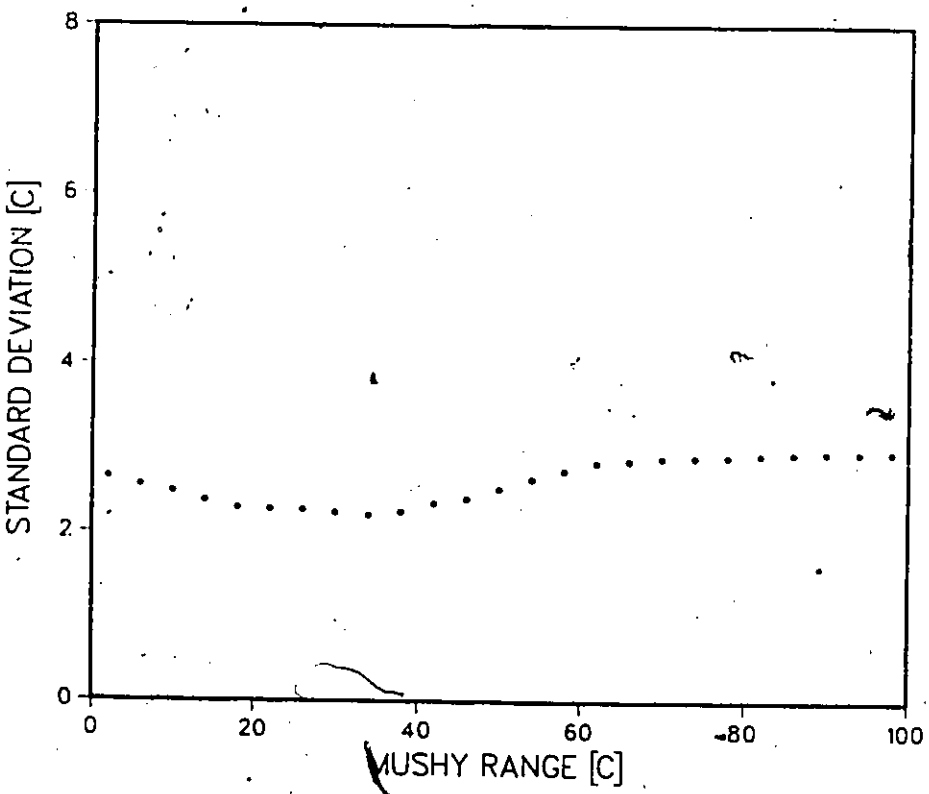

Fig.40 Effect of assumed mushy range on solution to test case#1 by the effective capacity method, implicit finite element. Time step is 500s.

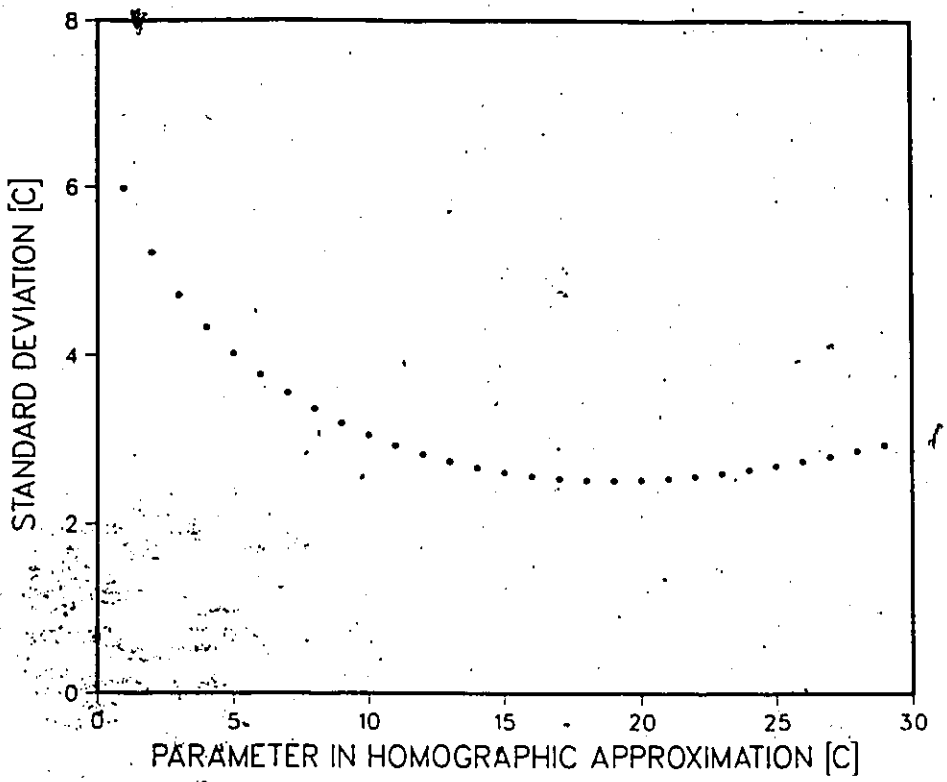

Fig.41 Effect of assumed parameter on solution to test case#1 by Blanchard and Fremond's method. Implicit finite difference. Time step is 1000s.

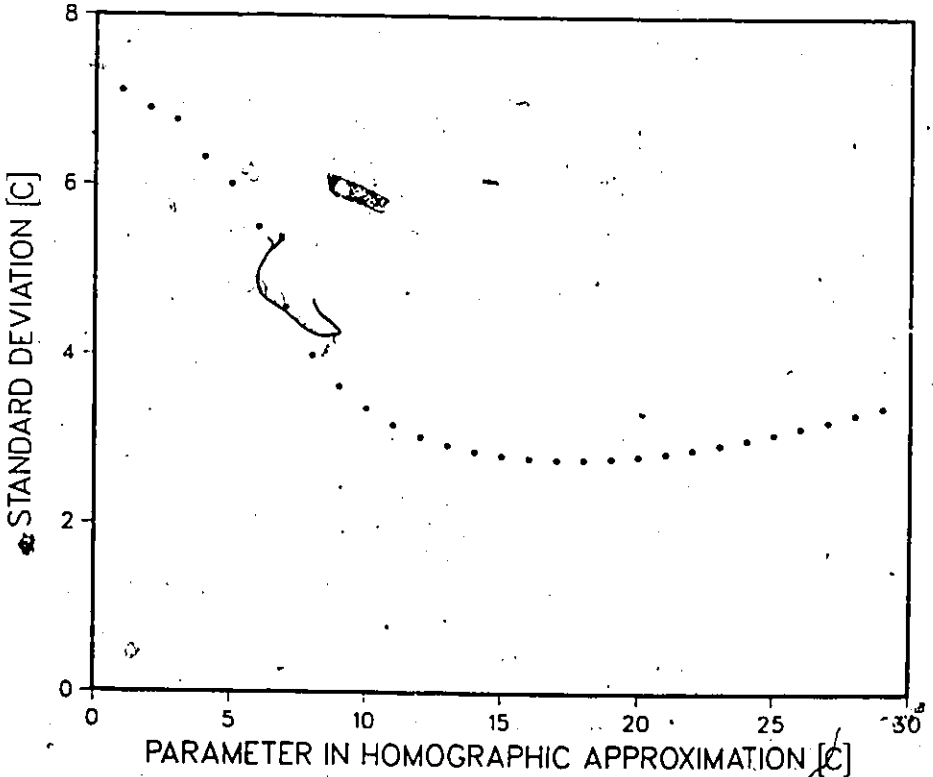

Fig.42 Effect of assumed parameter on solution to test case#1 by Blanchard and Fremond's method, implicit finite element. Time step is 1000s.

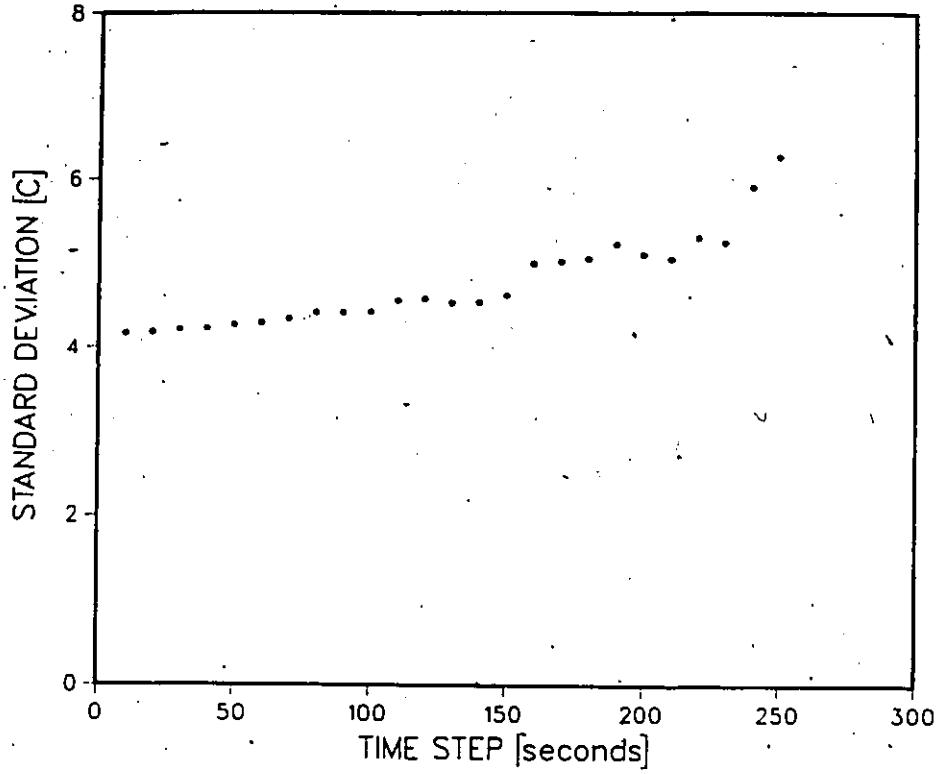

Fig.43 Effect of time step size on solution to test case#1 by the post iterative (isothermal) method, explicit finite difference.

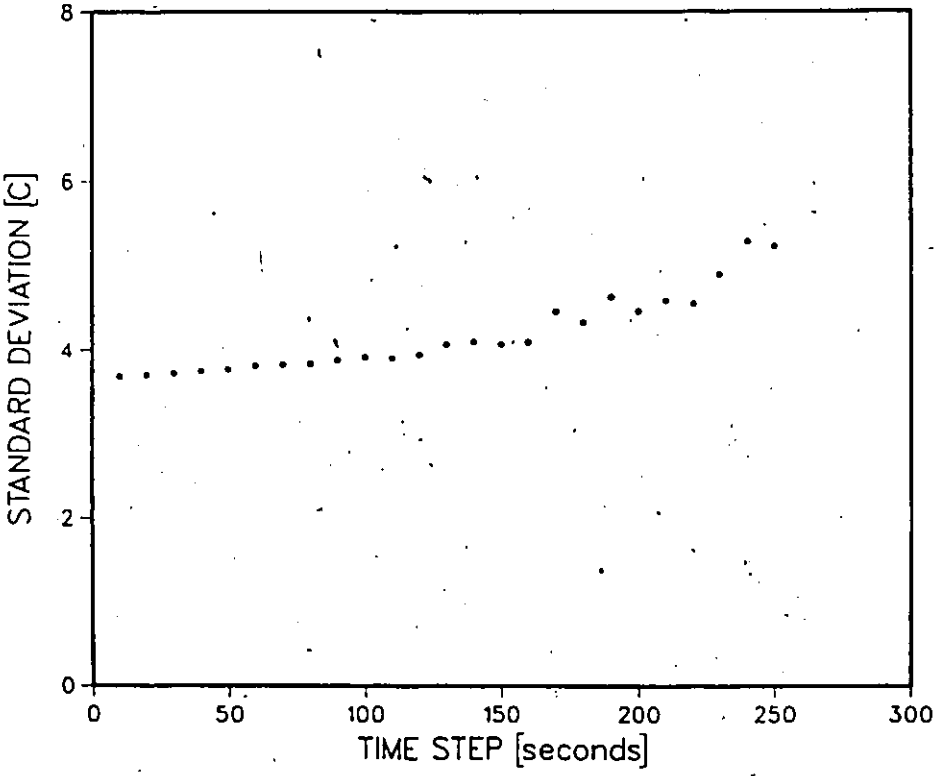

Fig.44 Effect of time step size on solution to test case#1 by the post iterative method, explicit finite difference (mushy=-5.0 to +5.0 C).

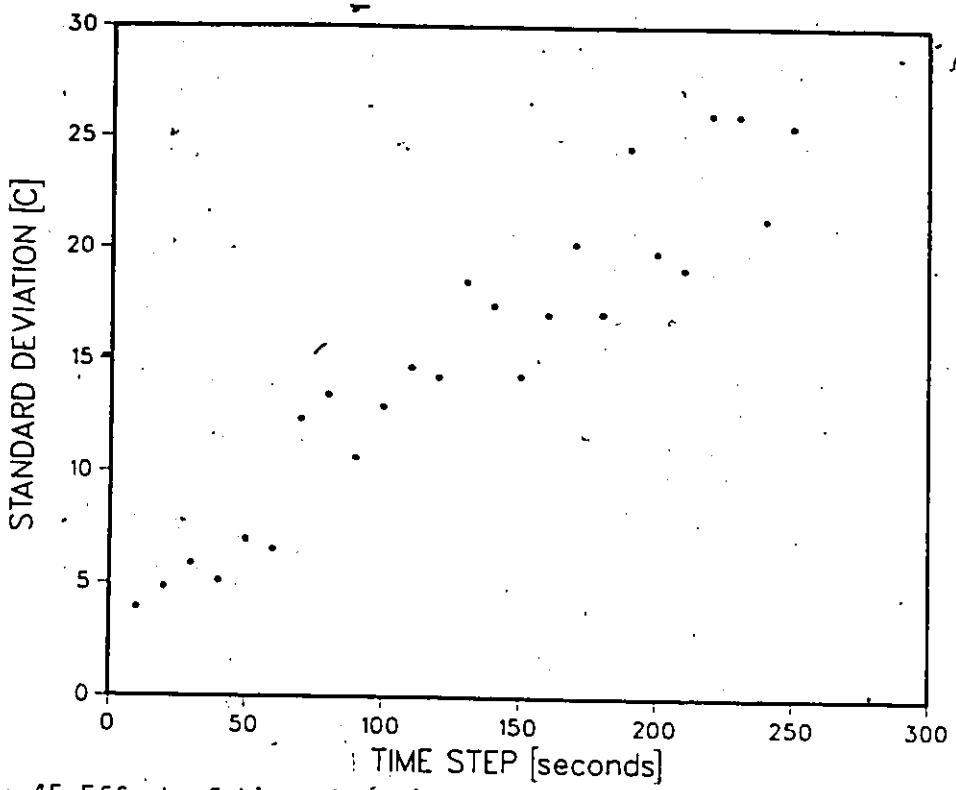

Fig.45 Effect of time step size on solution to test case#1 by the apparent capacity method, explicit finite difference (mushy=-5.0 to +5.0 C).

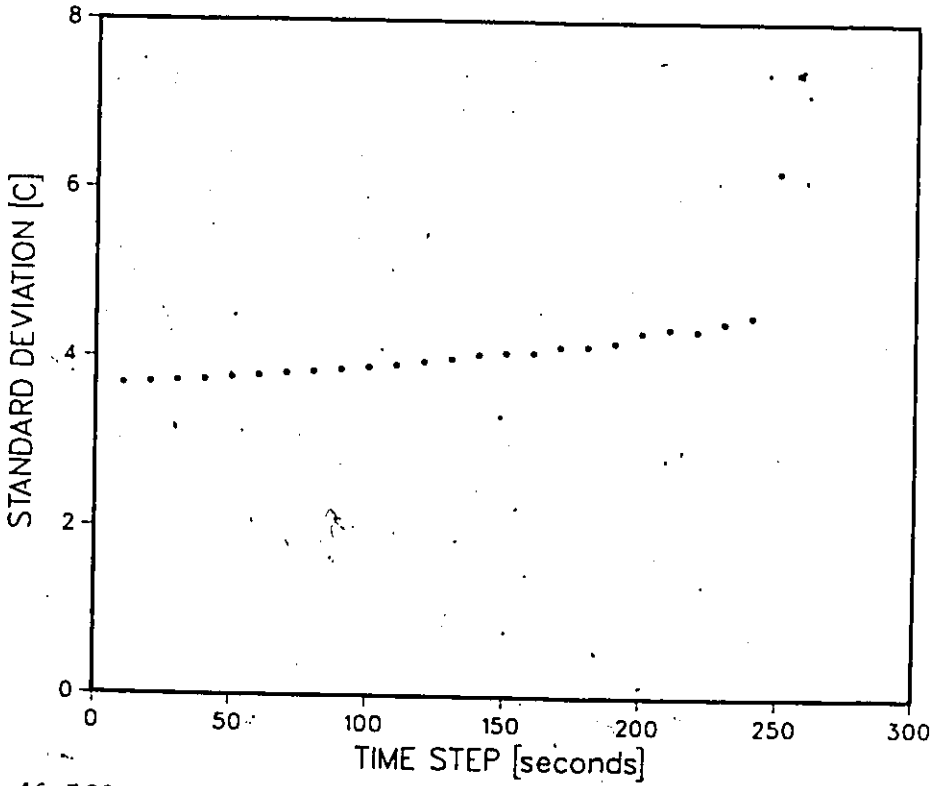

Fig.46 Effect of time step size on solution to test case#1 by the enthalpy method, explicit finite difference (mushy=-5.0 to +5.0 C).

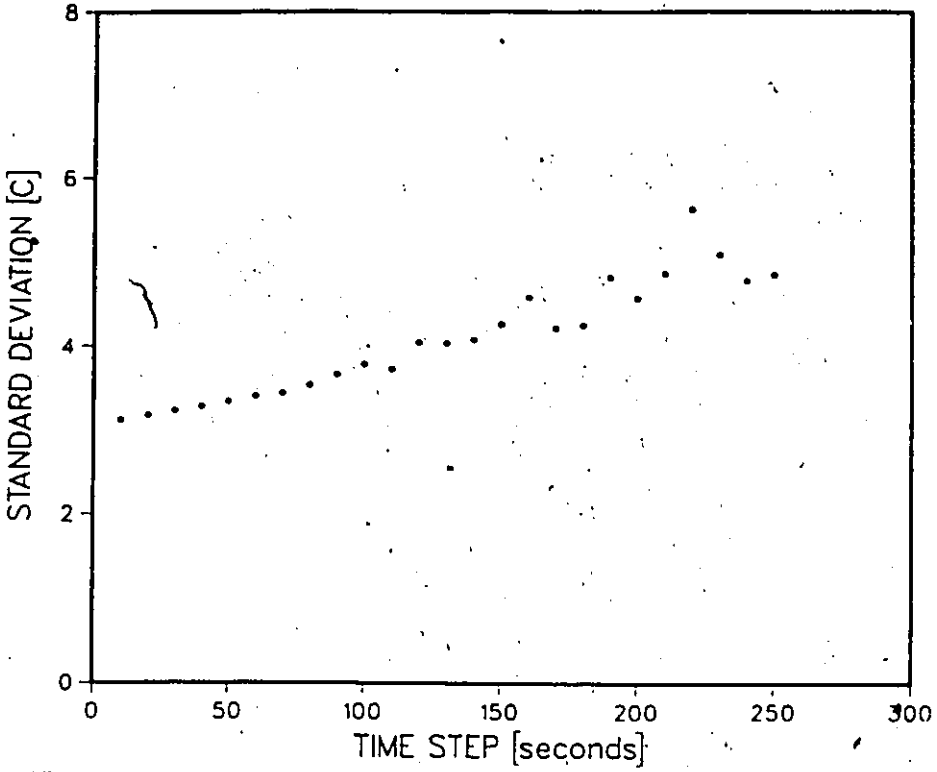

Fig.47 Effect of time step size on solution to test case#1 by the effective capacity method, explicit finite difference (mushy=-5.0 to +5.0 C).

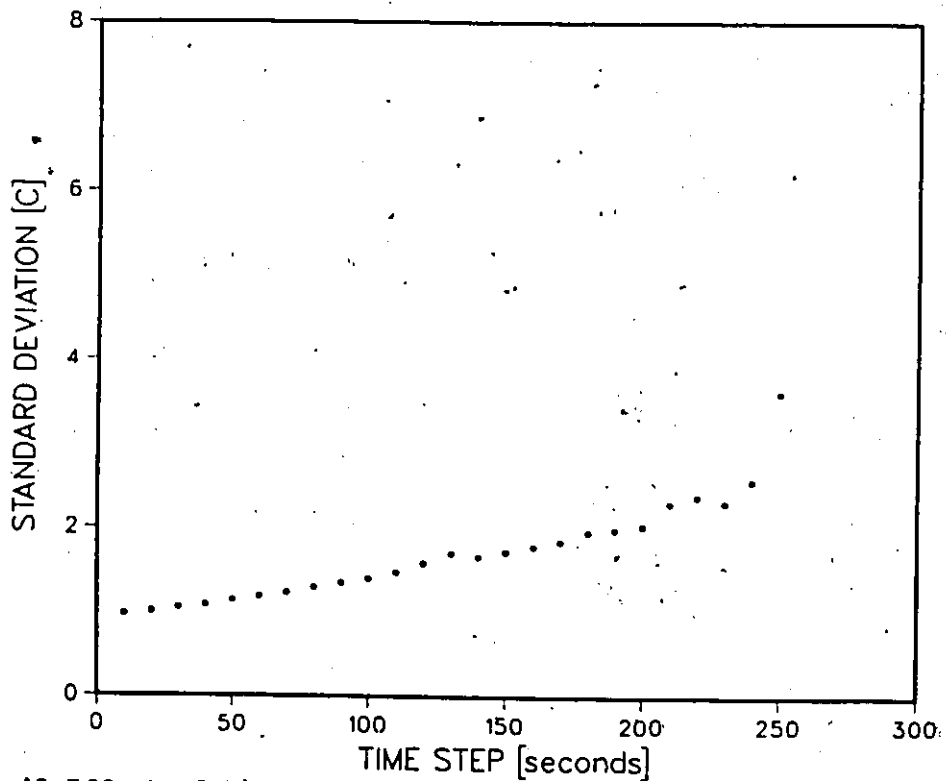

Fig.48 Effect of time step size on solution to test case#1 by Tacke's method, explicit finite difference.

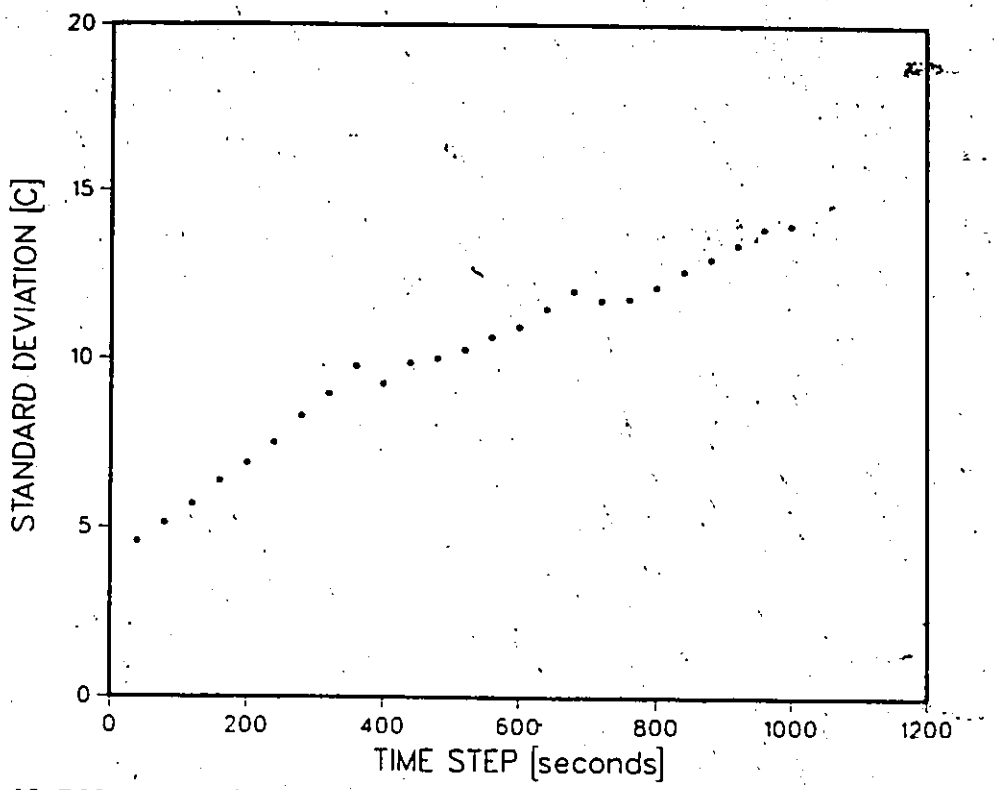

Fig.49 Effect of time step size on solution to test case#1 by the post iterative (isothermal) method, implicit finite difference.

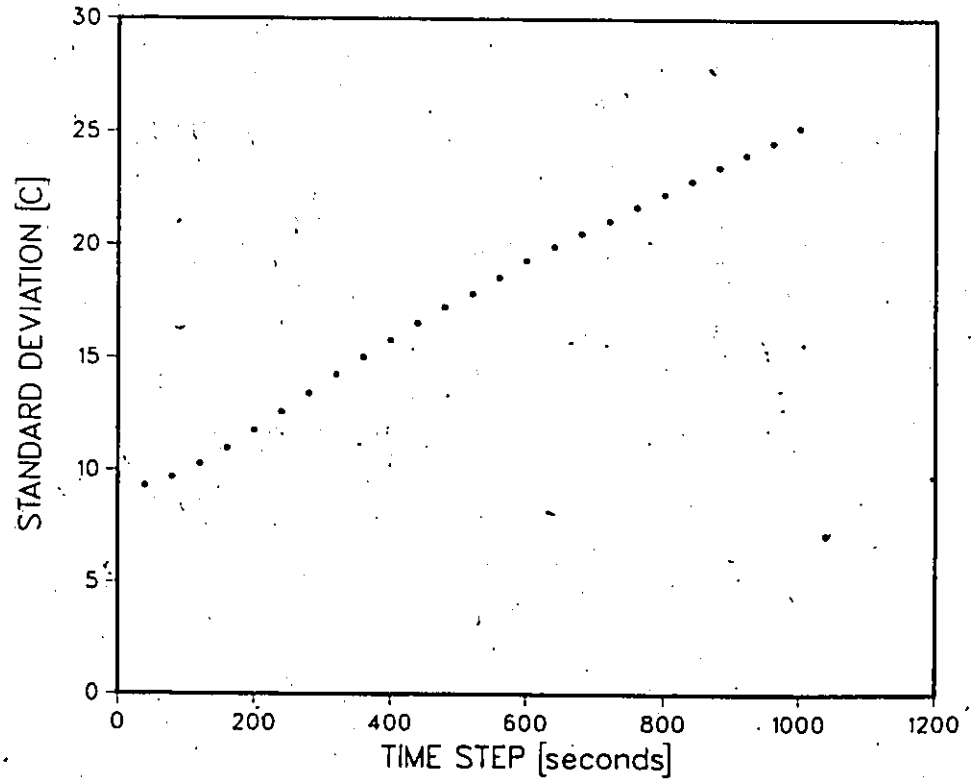

Fig.50 Effect of time step size on solution to test case#1 by the post iterative (isothermal) method, implicit finite element.

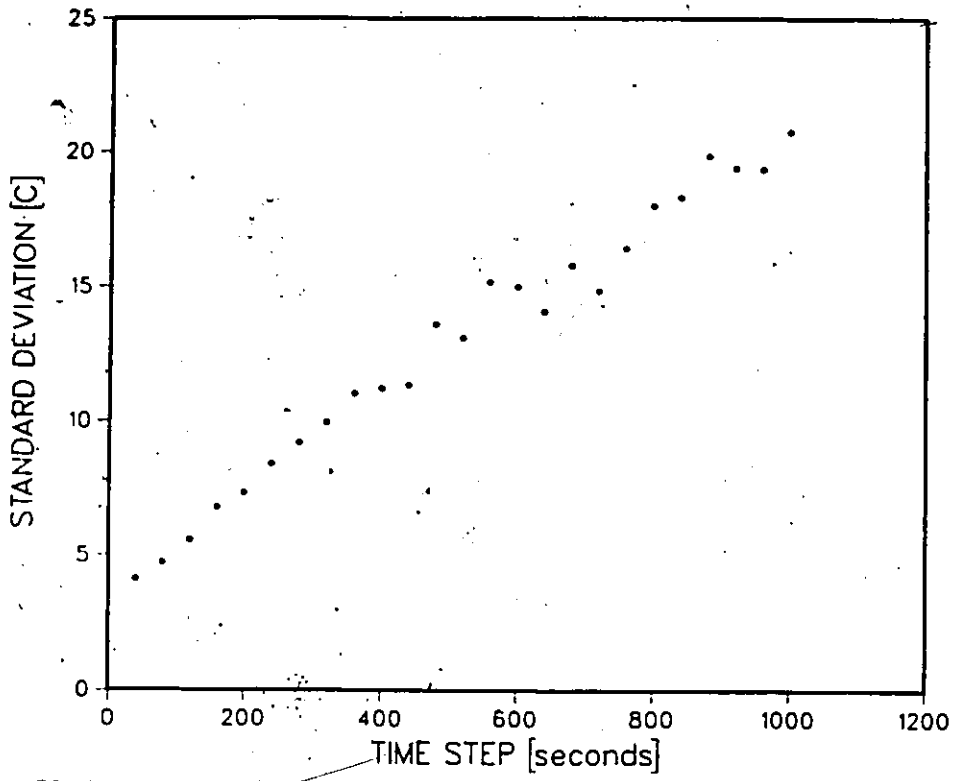

Fig.51 Effect of time step size on solution to test case#1 by the post iterative method, implicit finite difference (mushy=-5.0 to +5.0 C).

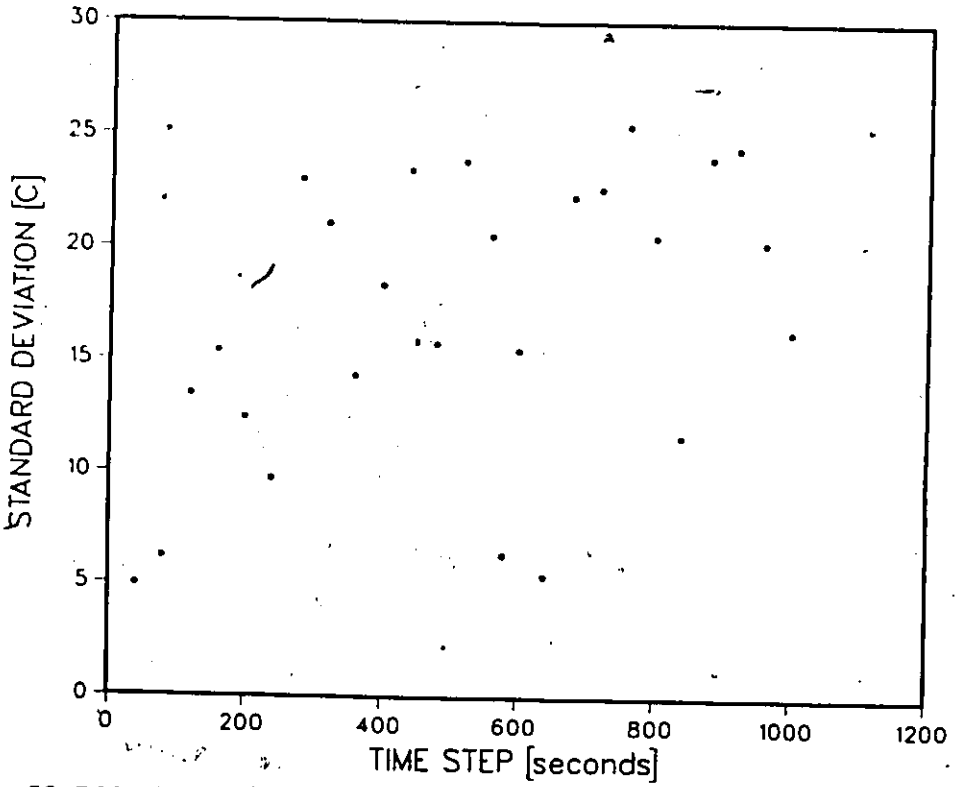

Fig.52 Effect of time step size on solution to test case#1 by the apparent capacity method, implicit finite difference (mushy=-5.0 to +5.0 C).

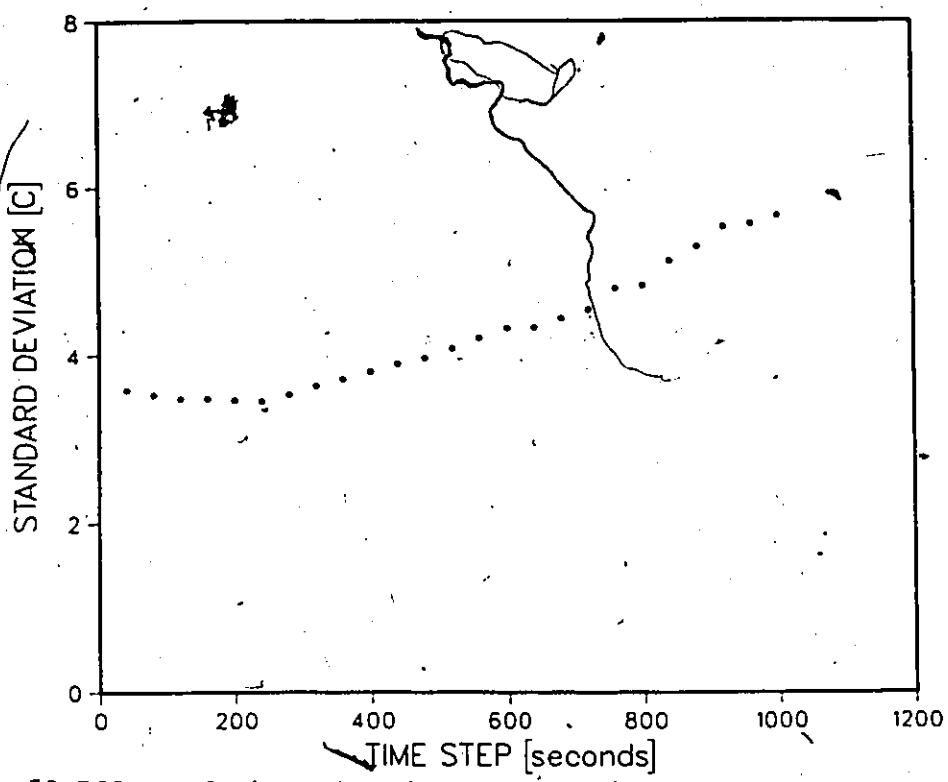

Fig.53 Effect of time step size on solution to test case#1 by the enthalpy method, implicit finite difference (mushy=-5.0 to +5.0 C).

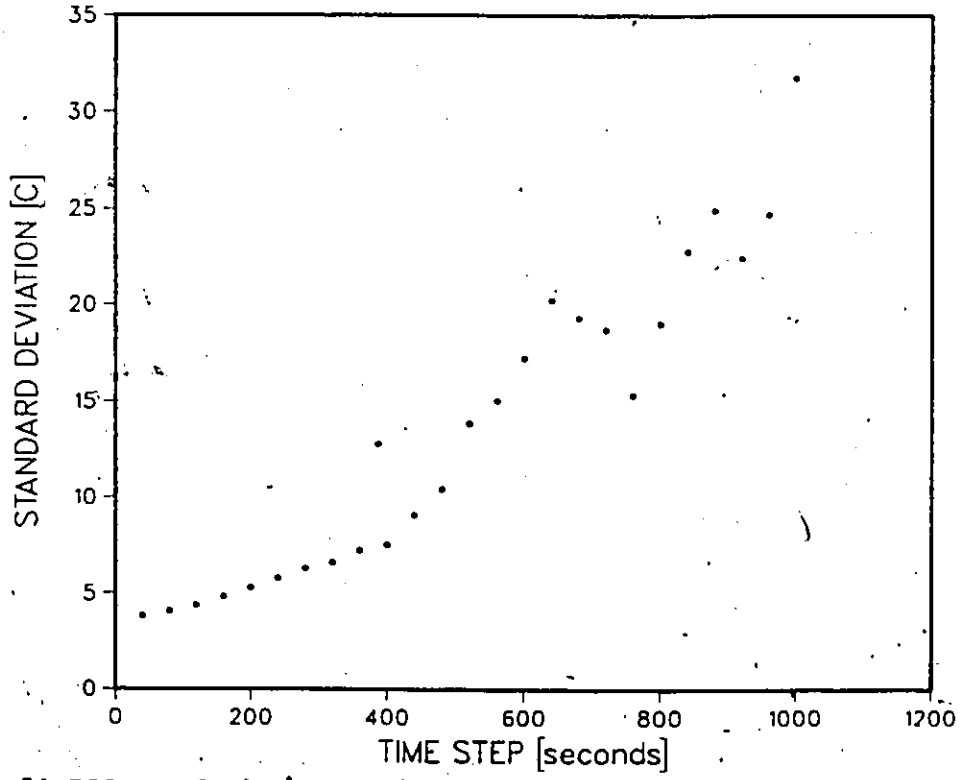

Fig.54 Effect of time step size on solution to test case#1 by Pham's method, implicit finite difference (mushy=-5.0 to +5.0 C).

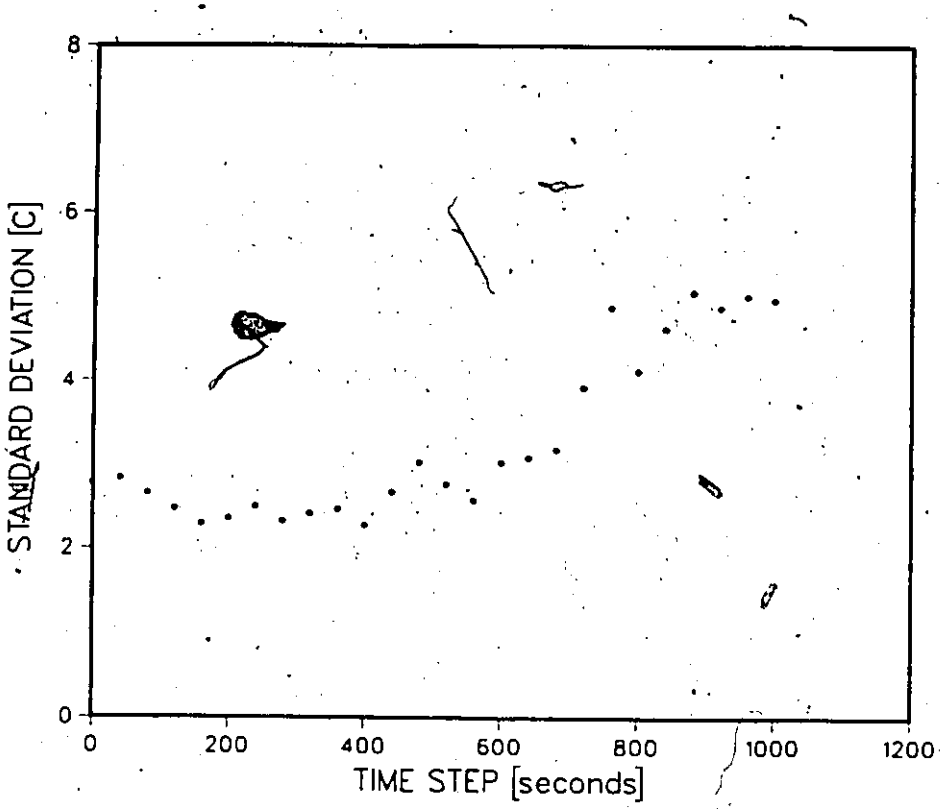

Fig.55 Effect of time step size on solution to test case#1 by the effective capacity method, implicit finite difference (mushy=-5.0 to +5.0 C).

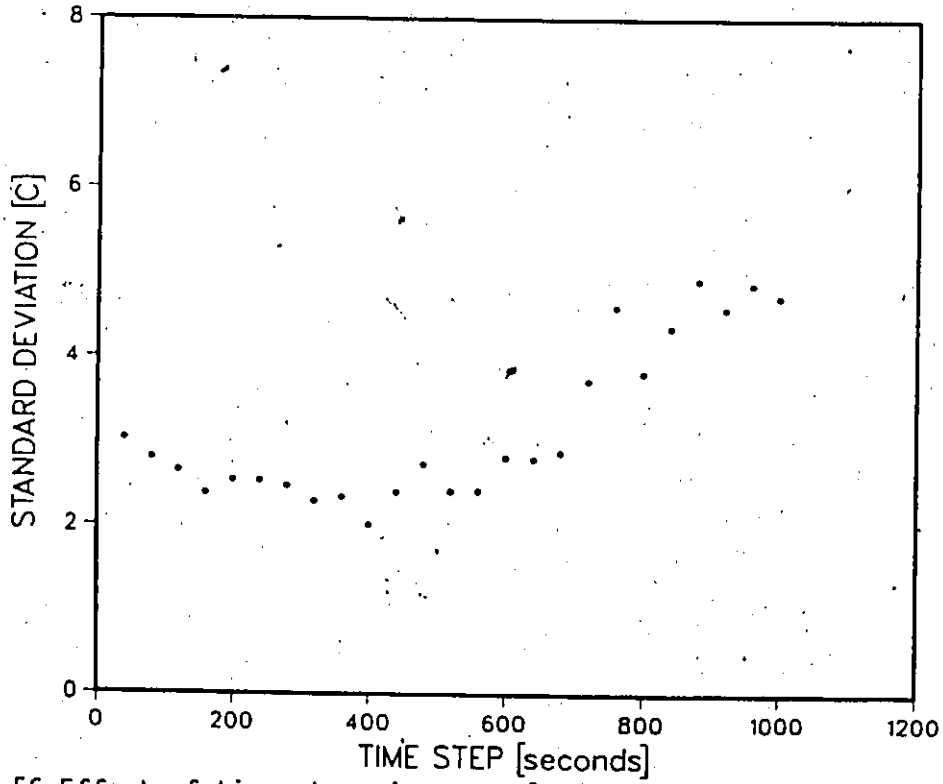

Fig.56 Effect of time step size on solution to test case#1 by the effective capacity method, implicit finite element (mushy=-5.0 to +5.0 C).

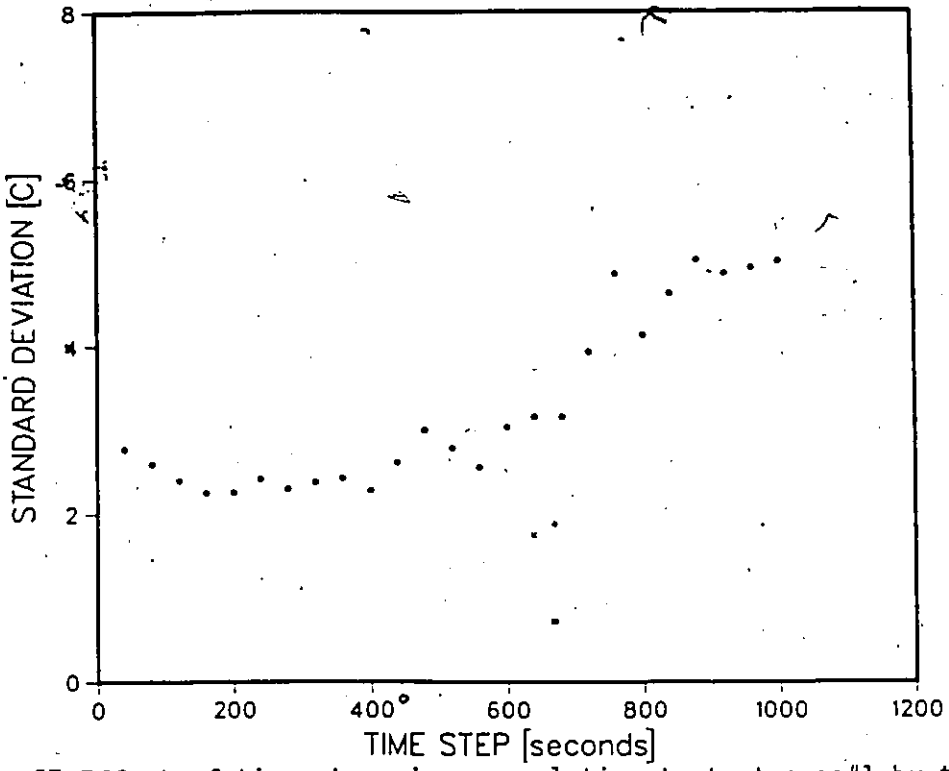

Fig.57 Effect of time step size on solution to test case#1 by the effective capacity method, implicit finite difference (mushy=normal distribution).

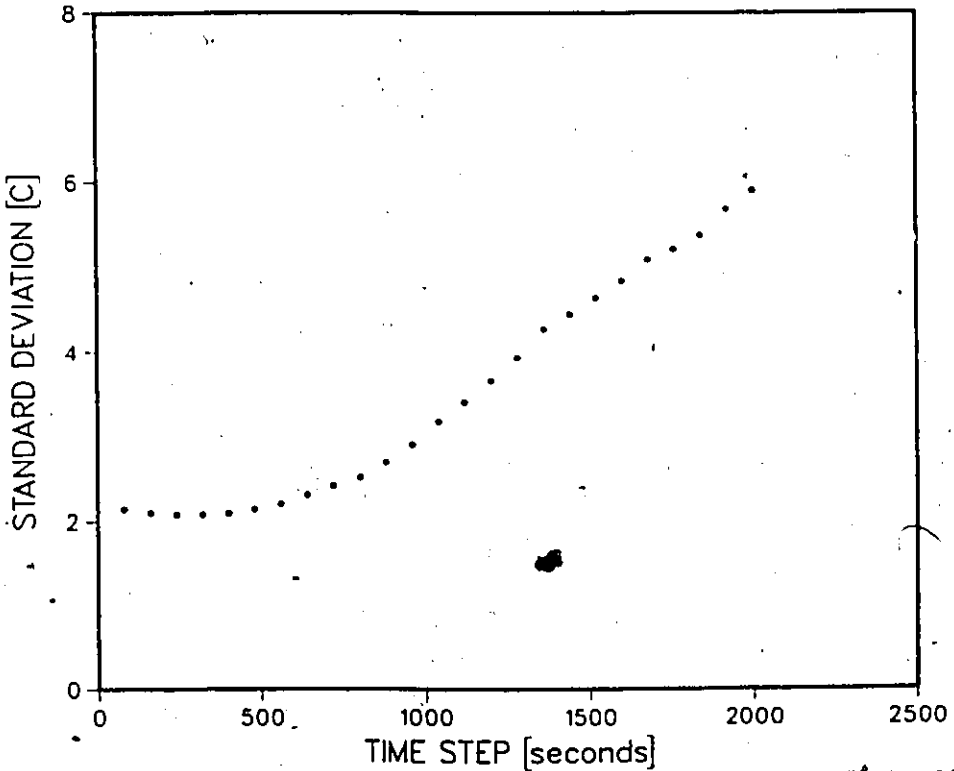

Fig.58 Effect of time step size on solution to test case#1 by Blanchard and Fremond's method, implicit finite difference (parameter= 10.0 C).

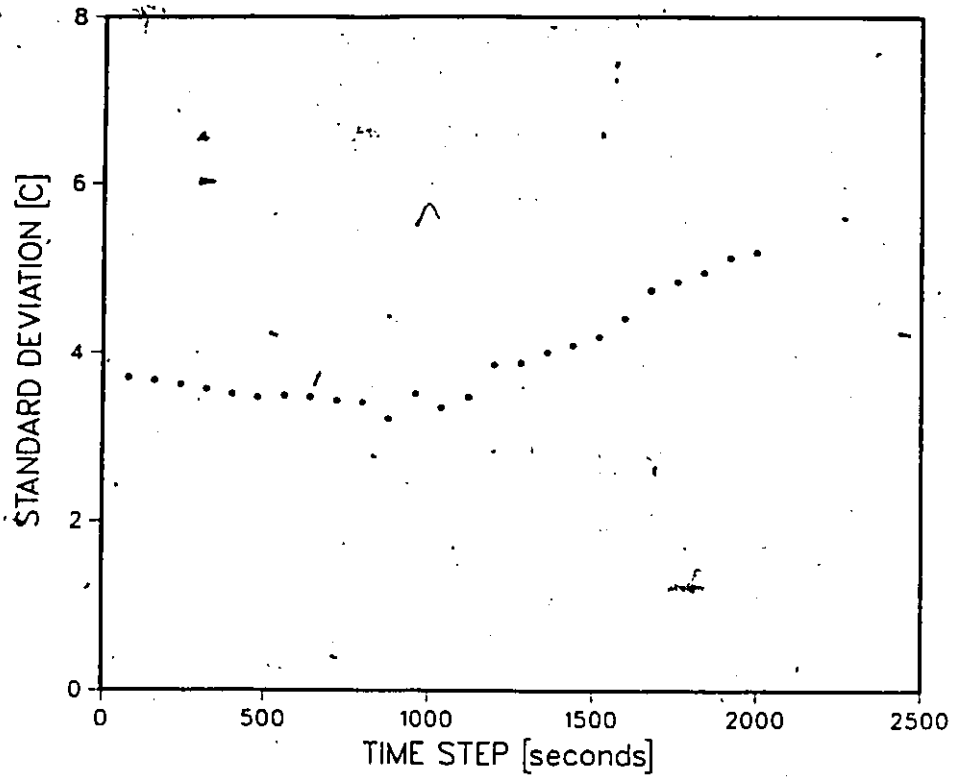

Fig.59 Effect of time step size on solution to test case#1 by Blanchard and Fremond's method, implicit finite element (parameter= 10.0 C).

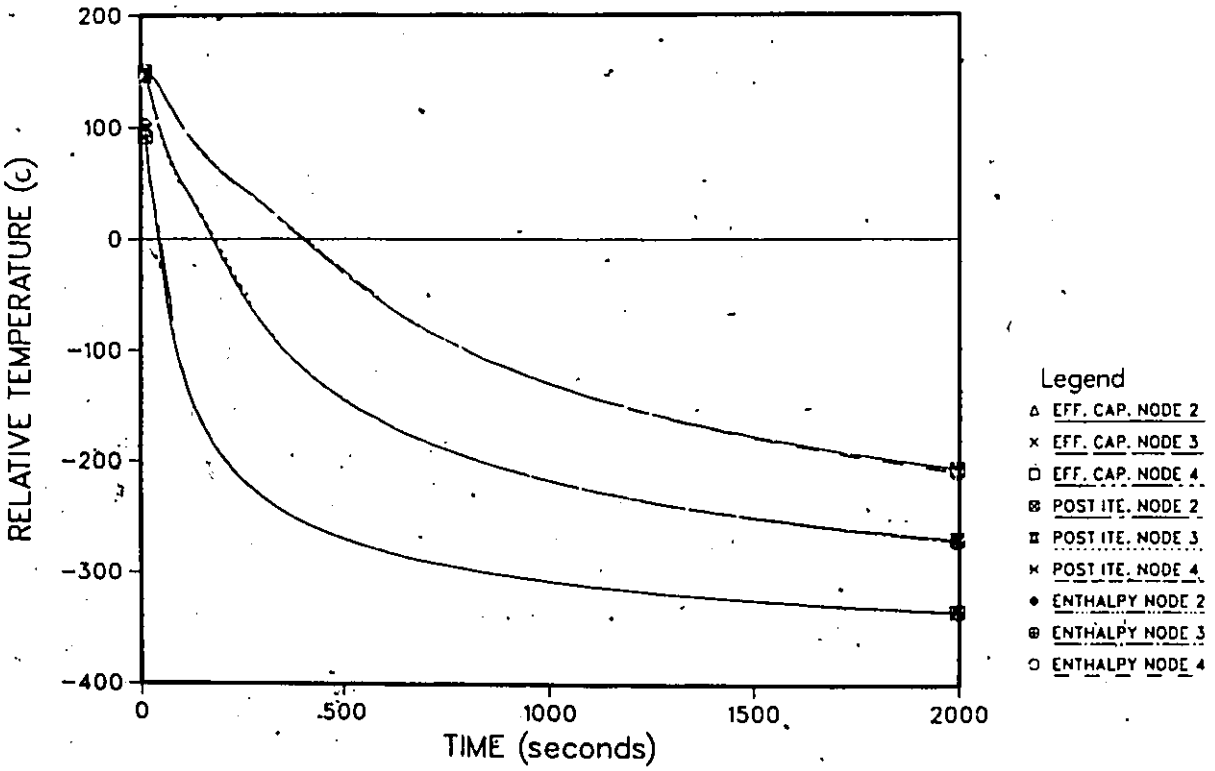

Fig.60 Converged solution for test case#2. Time step is 1.5s and the spatial increment is 0.0125m.

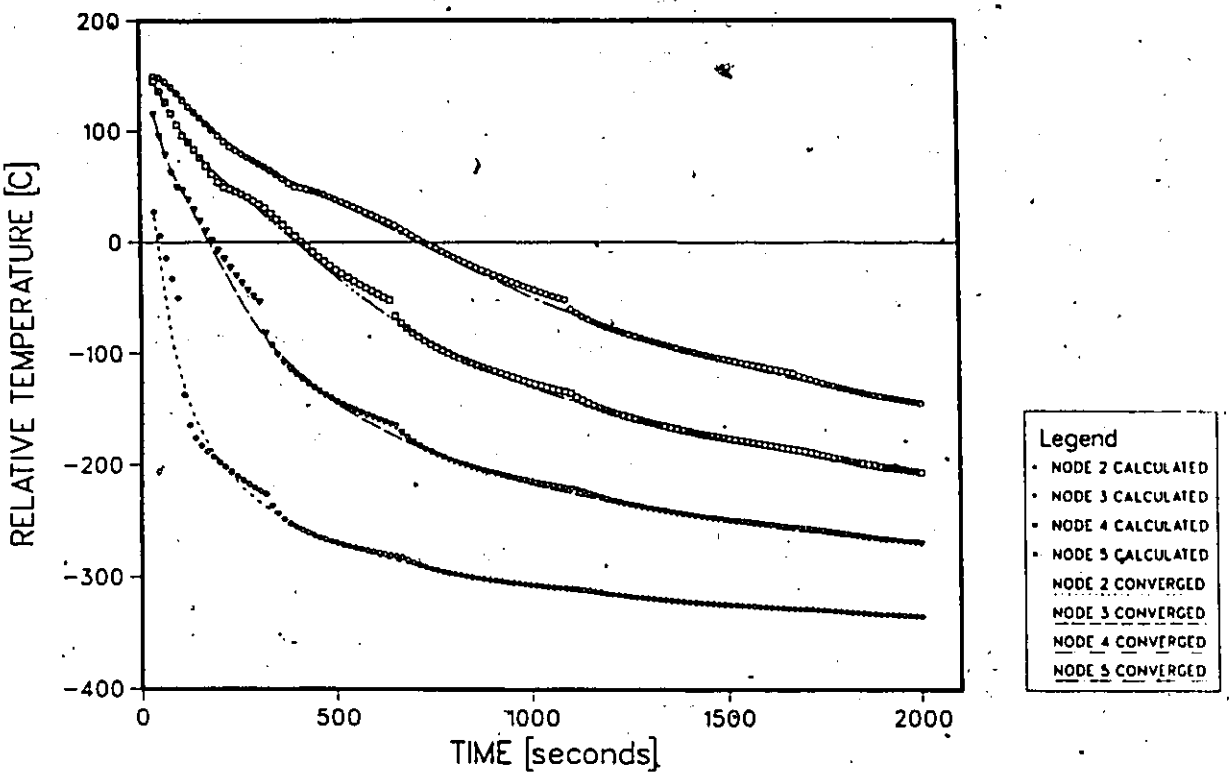

Fig.61 Temperature histories for test case#2 by the post iterative method, explicit finite difference. Time step is 15s.

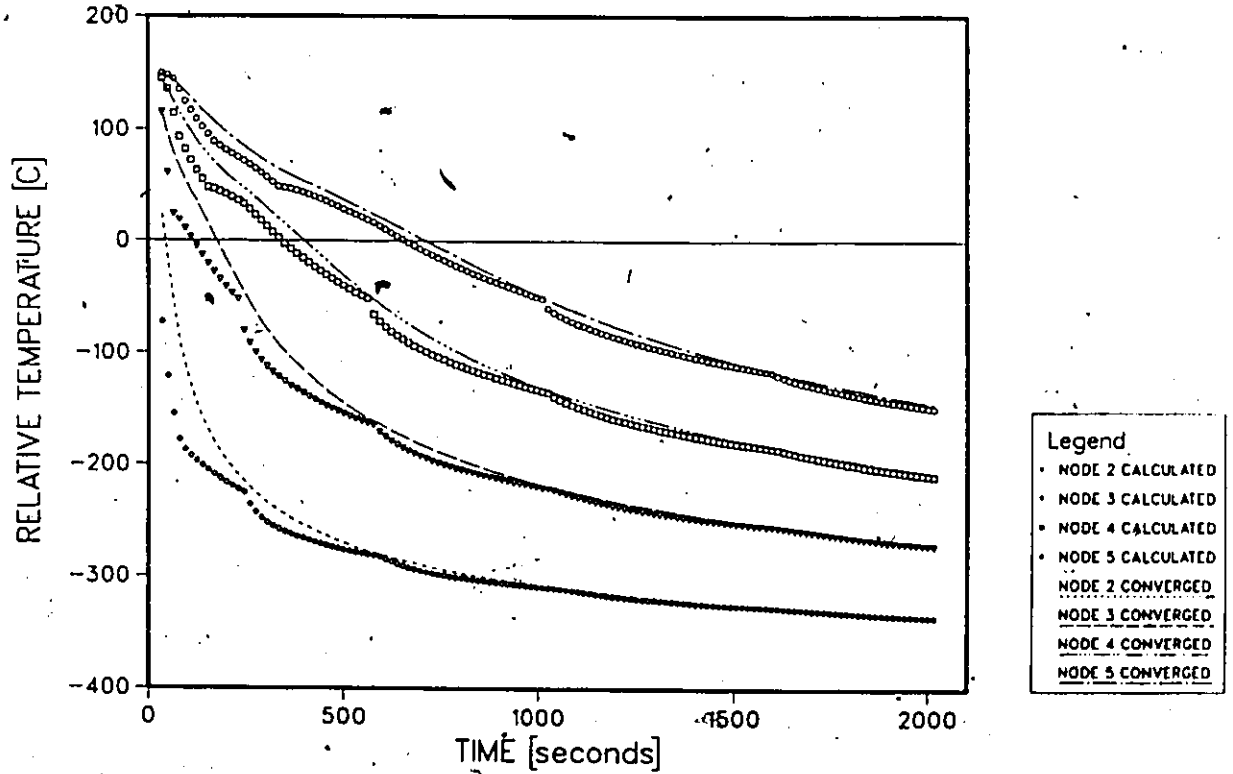

Fig.62 Temperature histories for test case#2 by the apparent capacity method, explicit finite difference. Time step is 15s.

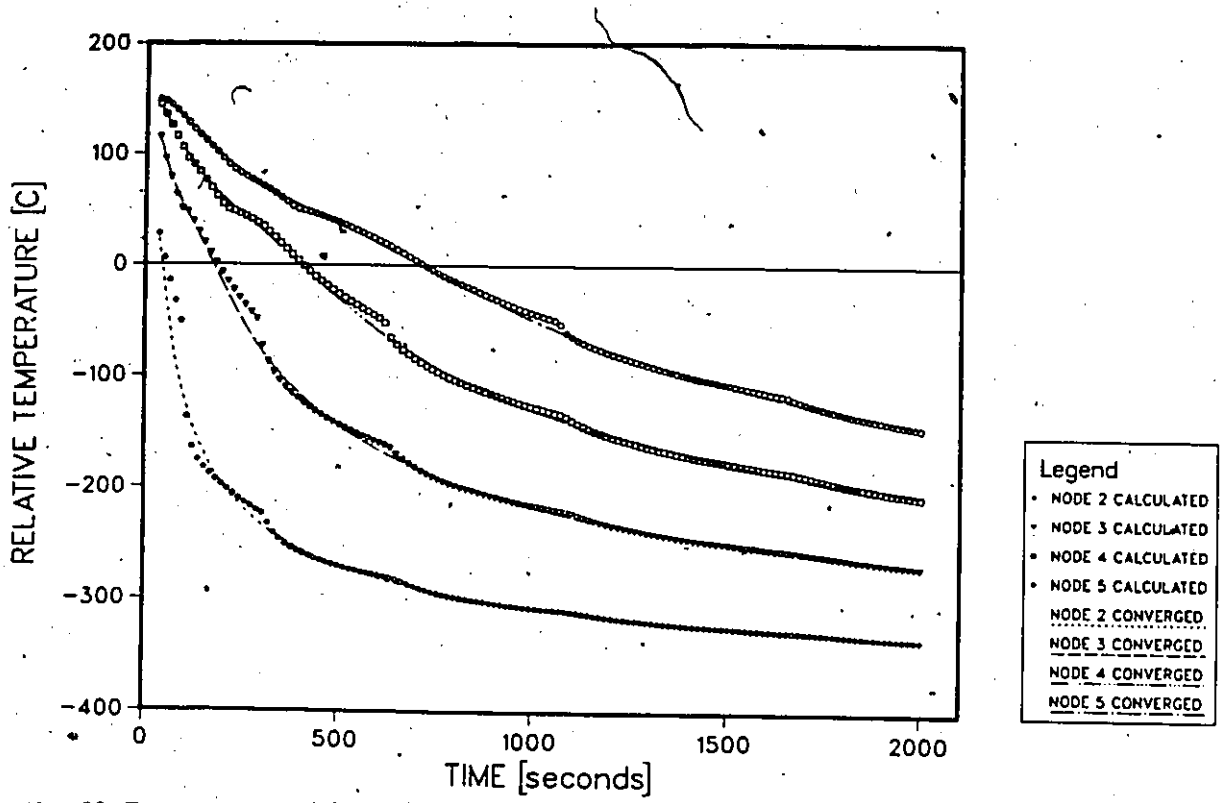

Fig.63 Temperature histories for test case#2 by the enthalpy method, explicit finite difference. Time step is 15s.

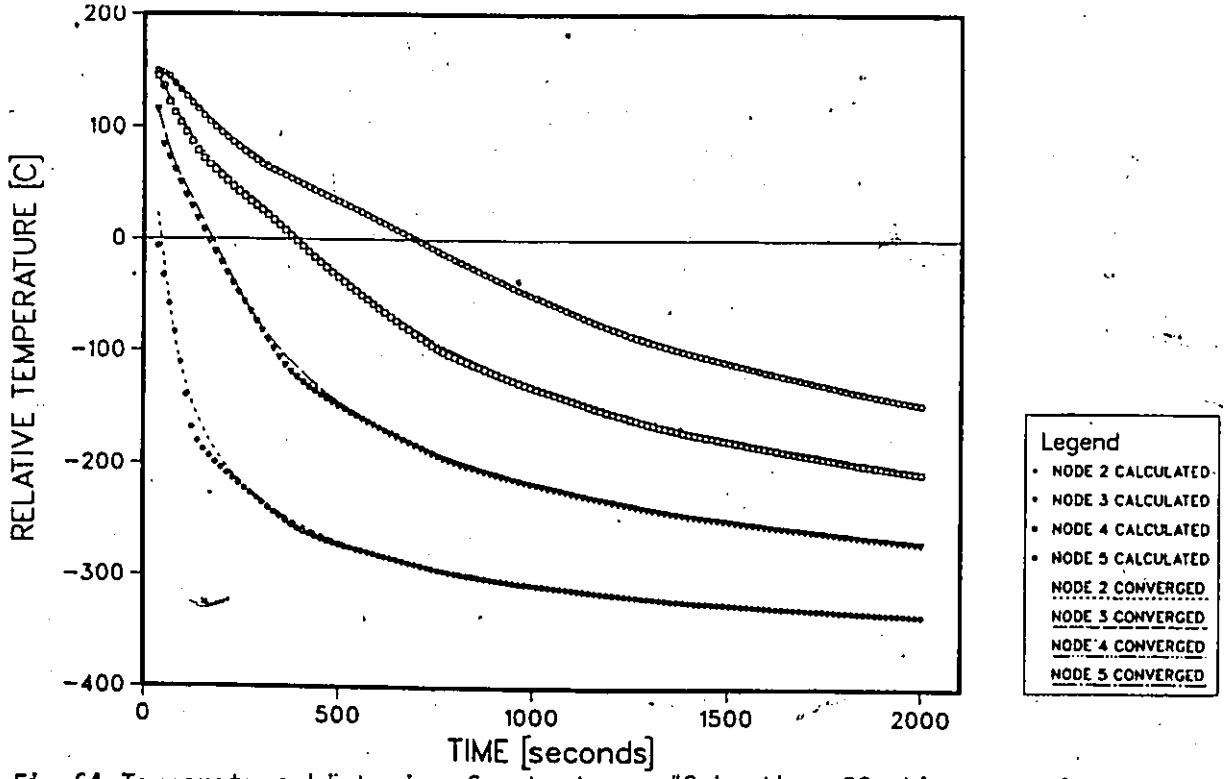

Fig.64 Temperature histories for test case#2 by the effective capacity method, explicit finite difference. Time step is 15s.

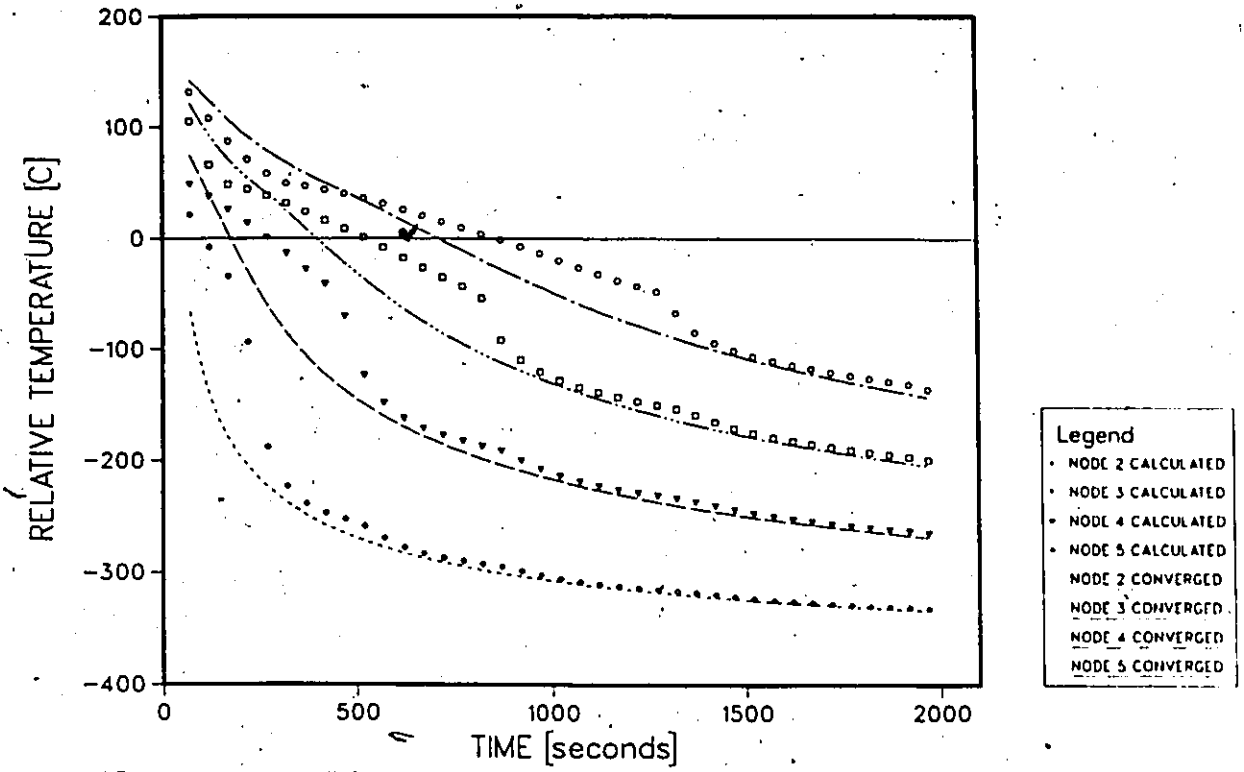

Fig.65 Temperature histories for test case#2 by the post iterative method, implicit finite difference. Time step is 50s.

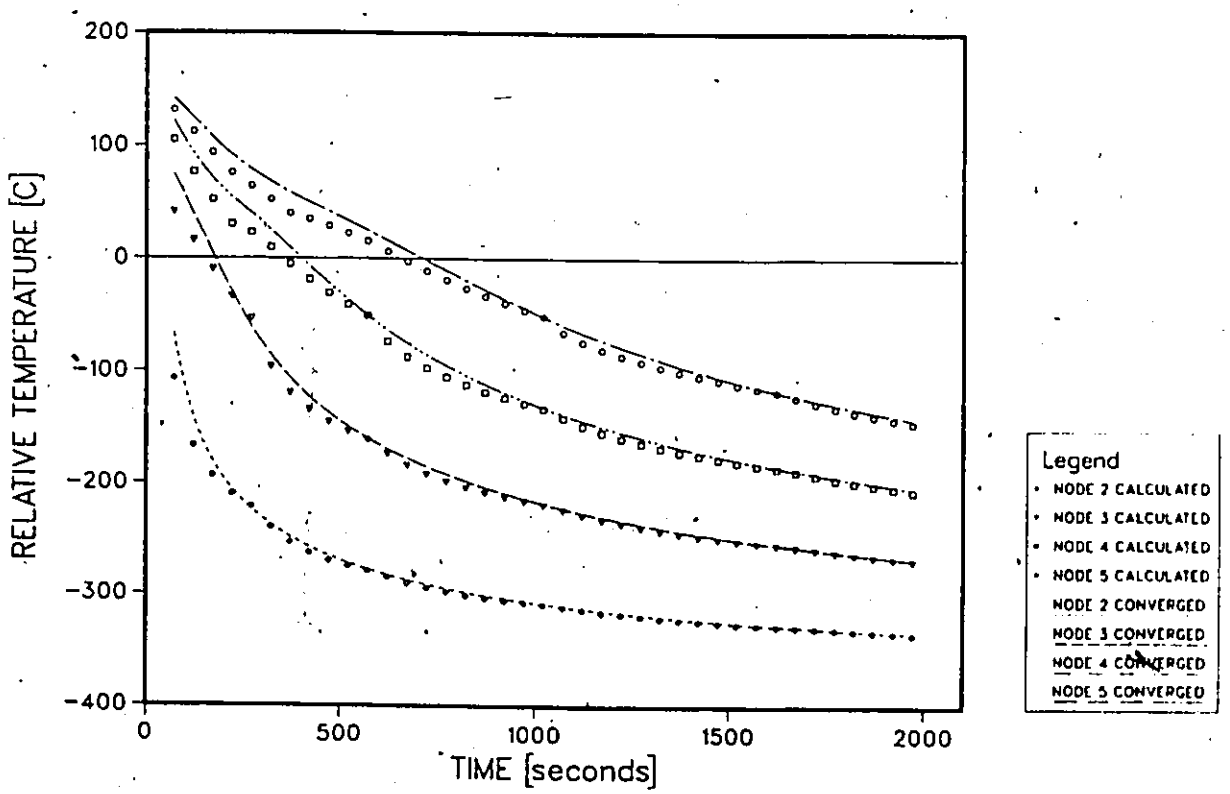

Fig.66 Temperature histories for test case#2 by the apparent capacity method, implicit finite difference. Time step is 50s.

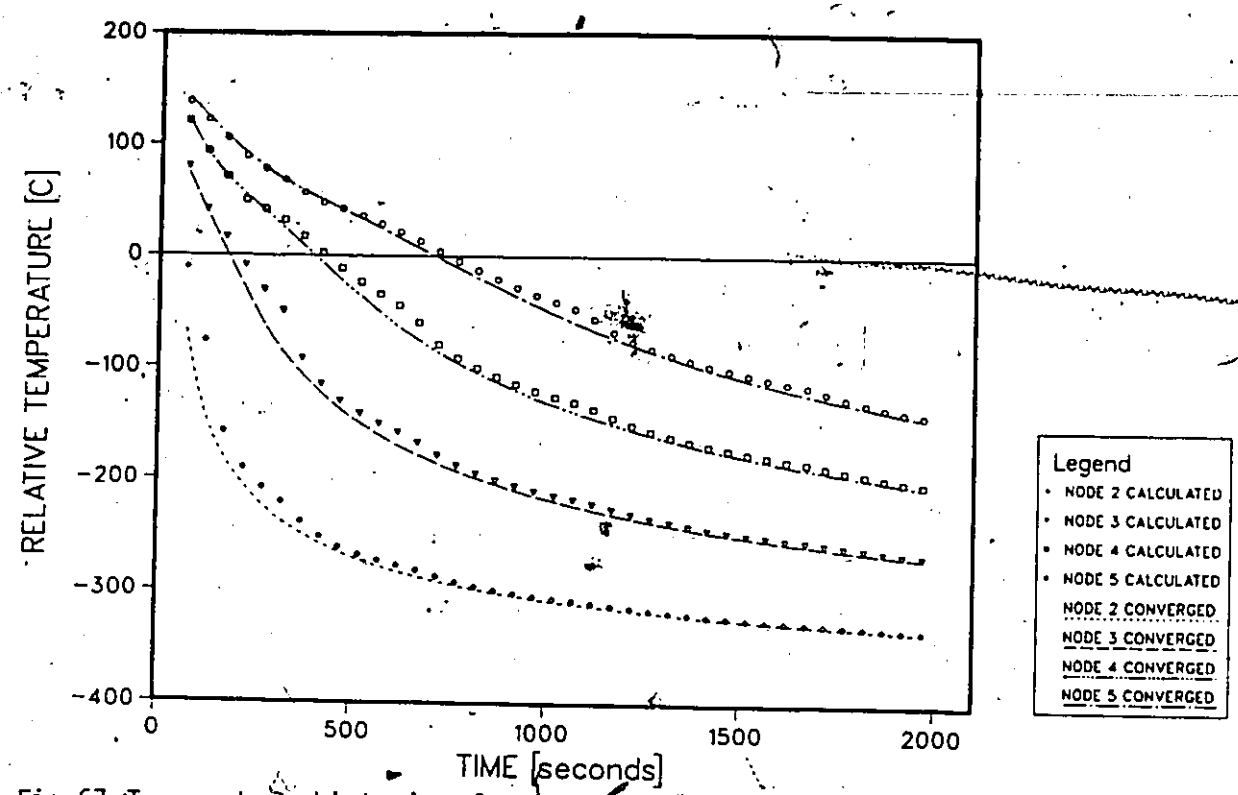

Fig.67 Temperature histories for test case#2 by the enthalpy method, implicit finite difference. Time step is 50s.

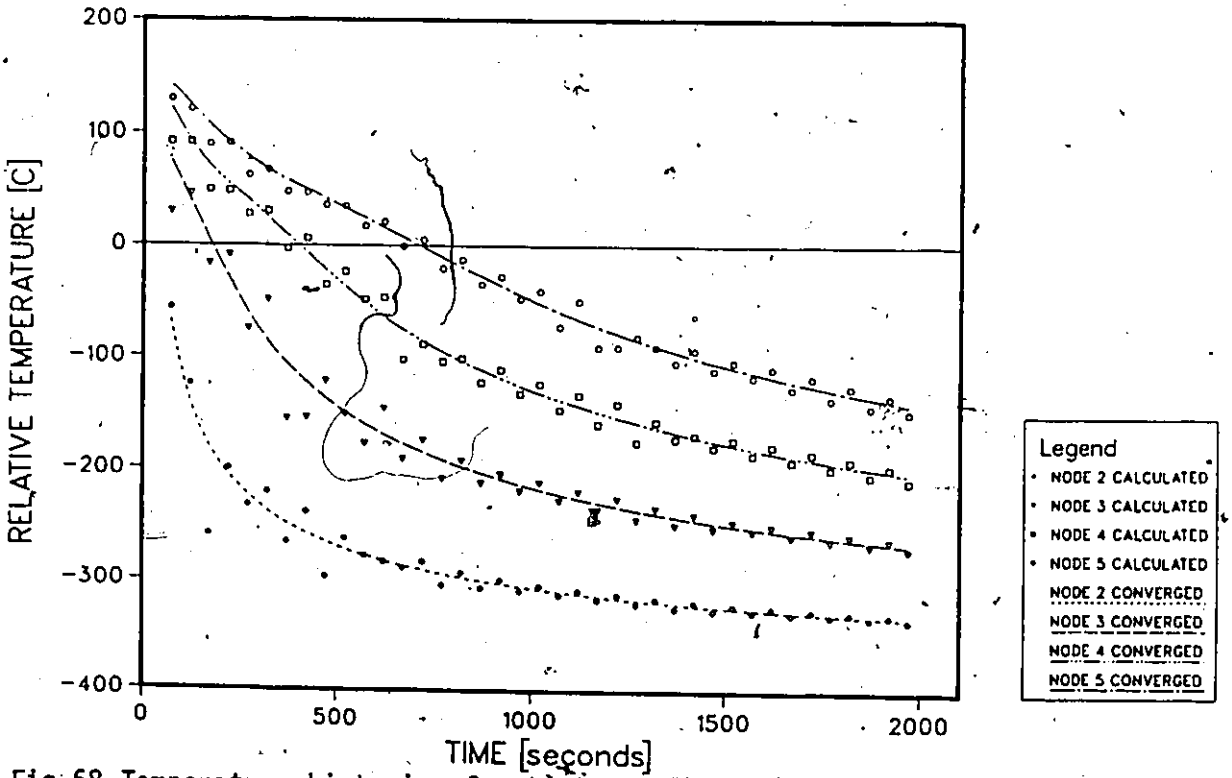

Fig.68 Temperature histories for test case#2 by Pham's method, implicit finite difference. Time step is 50s.

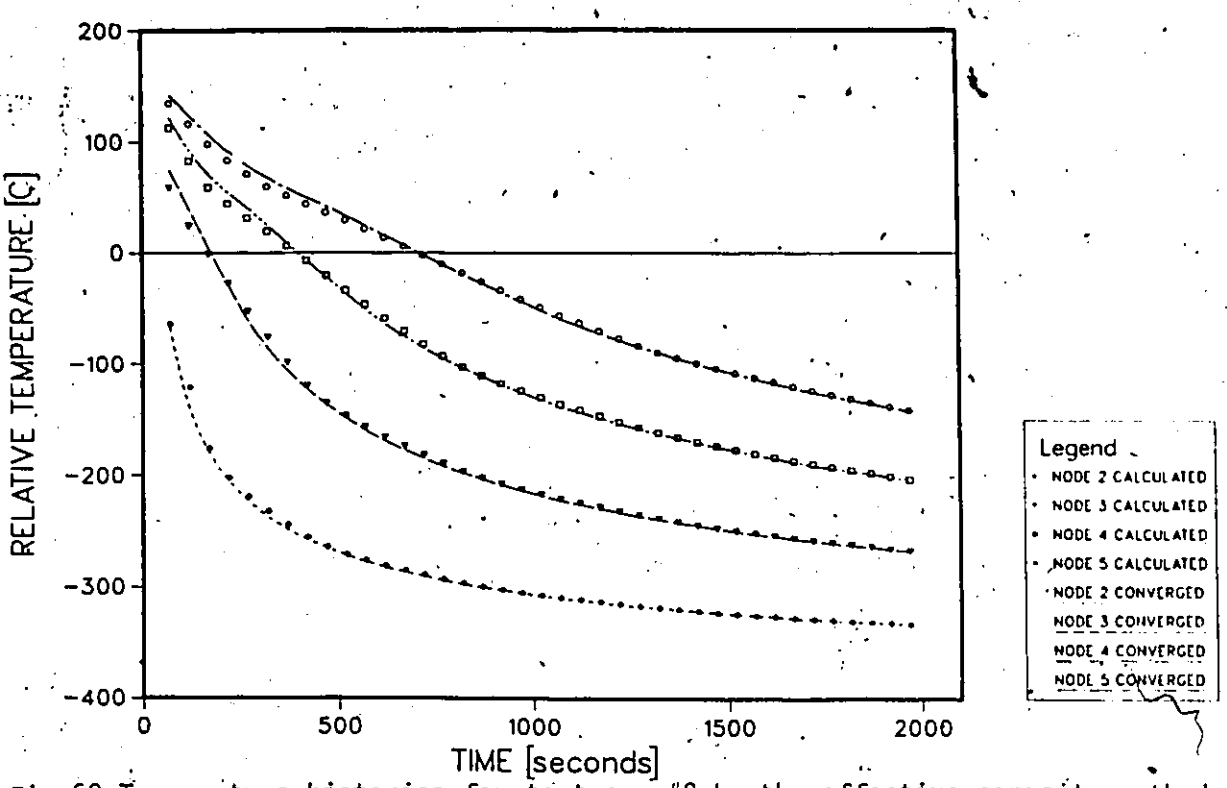

Fig.69 Temperature histories for test case#2 by the effective capacity method, implicit finite difference. Time step is 50s.

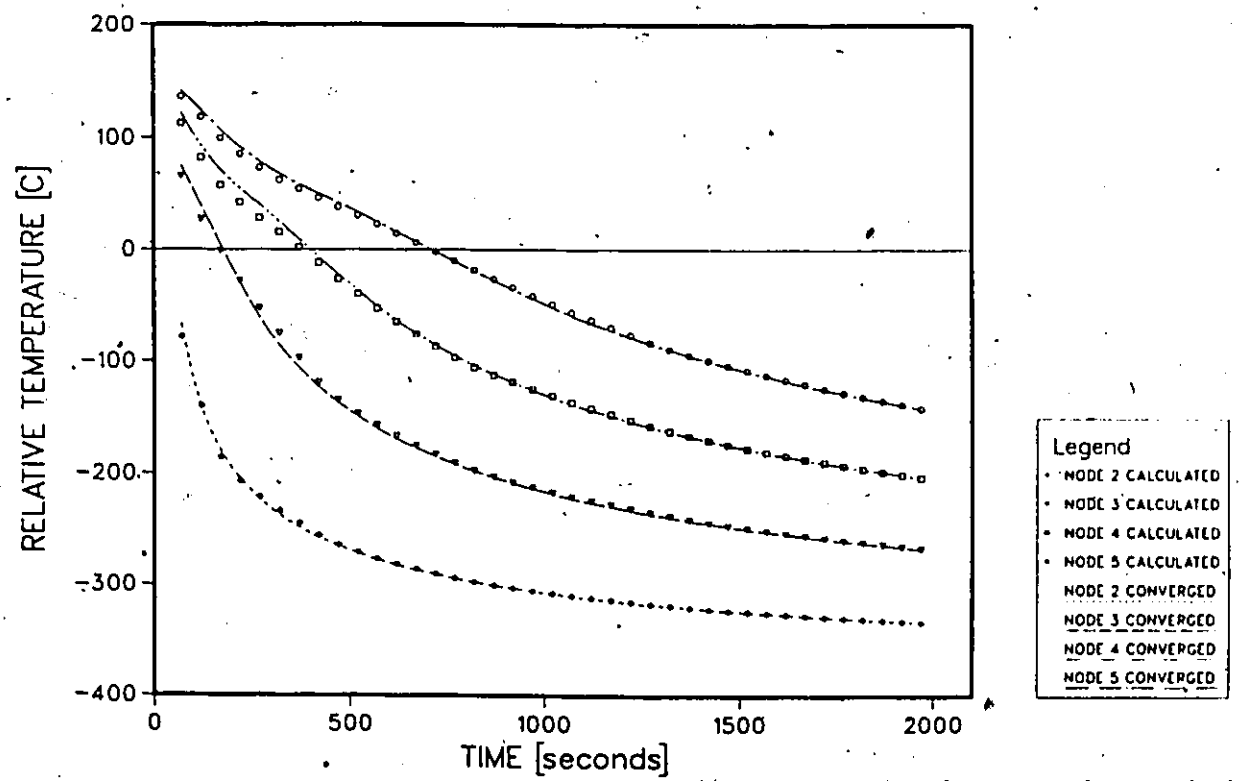

Fig.70 Temperature histories for test case#2 by the effective capacity method, implicit finite element. Time step is 50s.

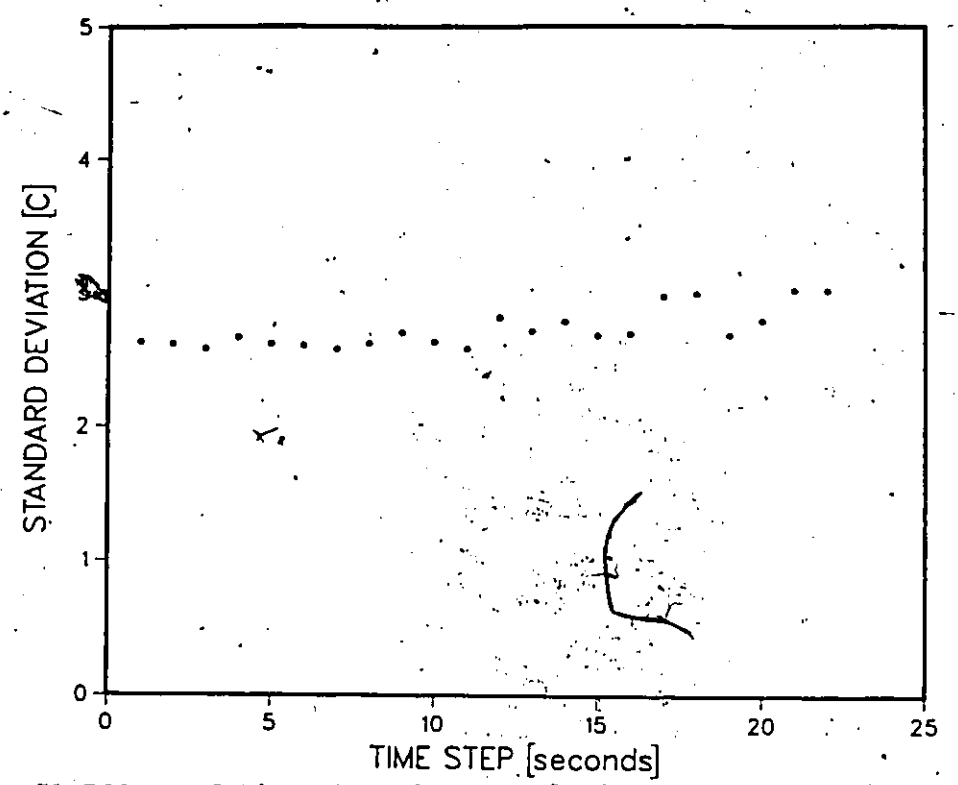

Fig.71 Effect of time step size on solution to test case#2 by the post iterative method, explicit finite difference.

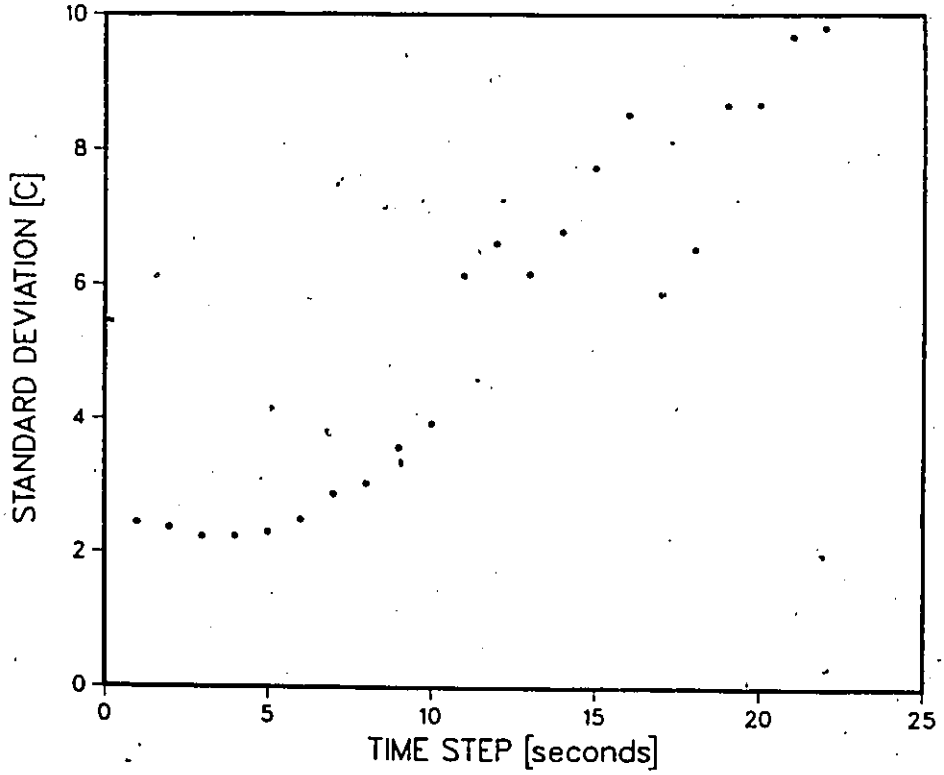

Fig.72 Effect of the time step size on solution to test case#2 by the apparent capacity method, explicit finite difference.

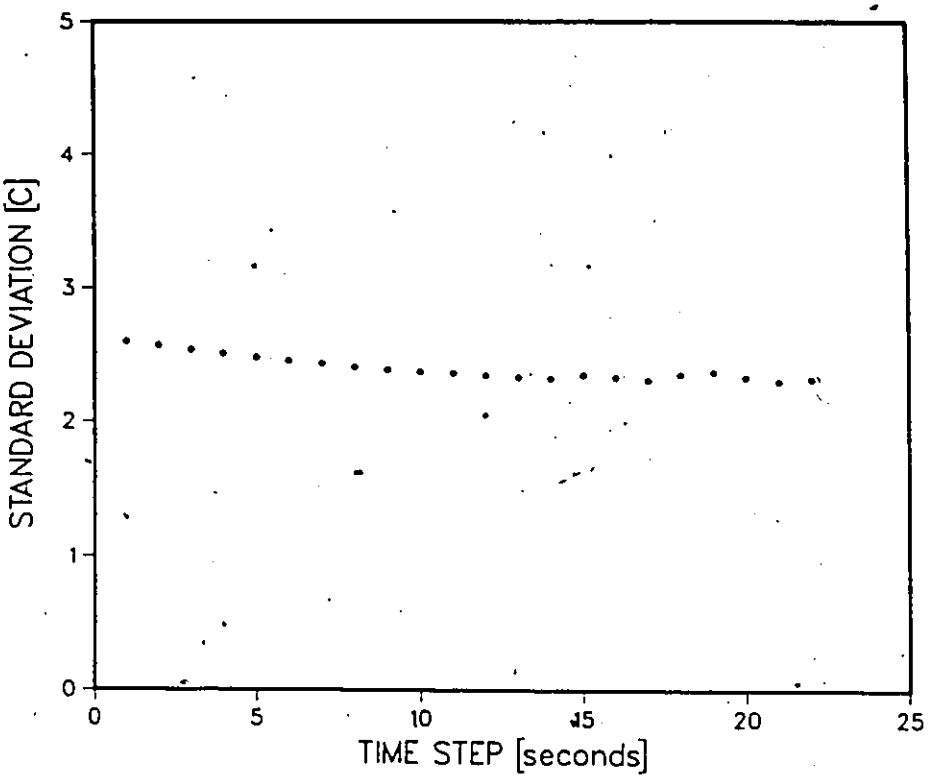

Fig.73 Effect of time step size on solution to test case#2 by the enthalpy method, explicit finite difference.

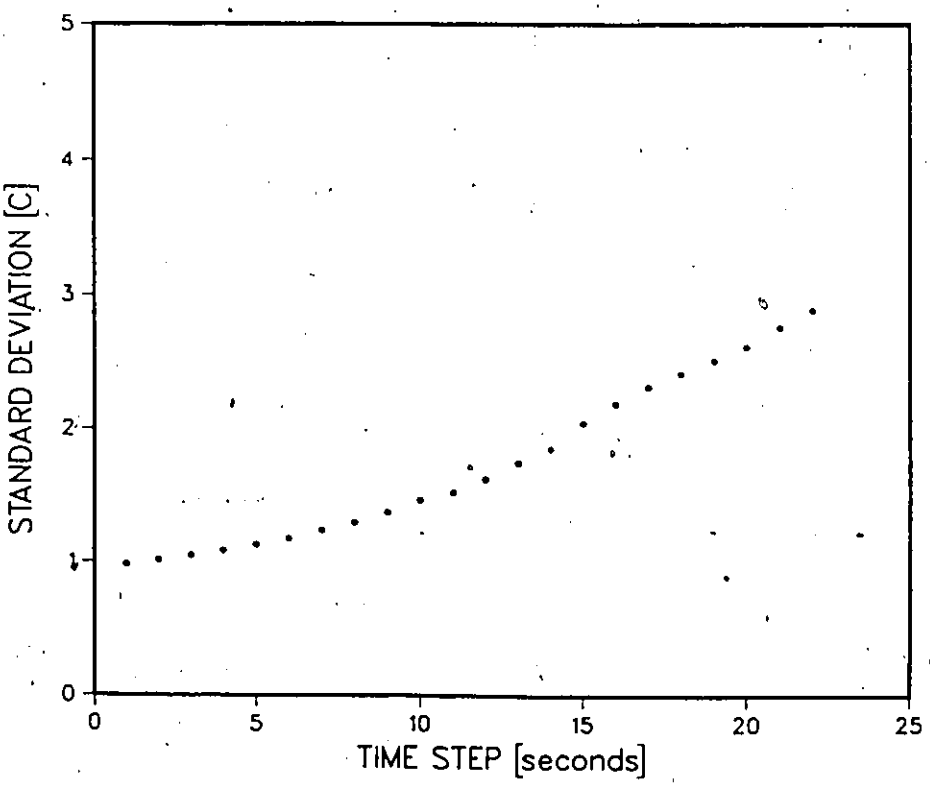

Fig.74 Effect of time step size on solution to test case#2 by the effective capacity method, explicit finite difference.

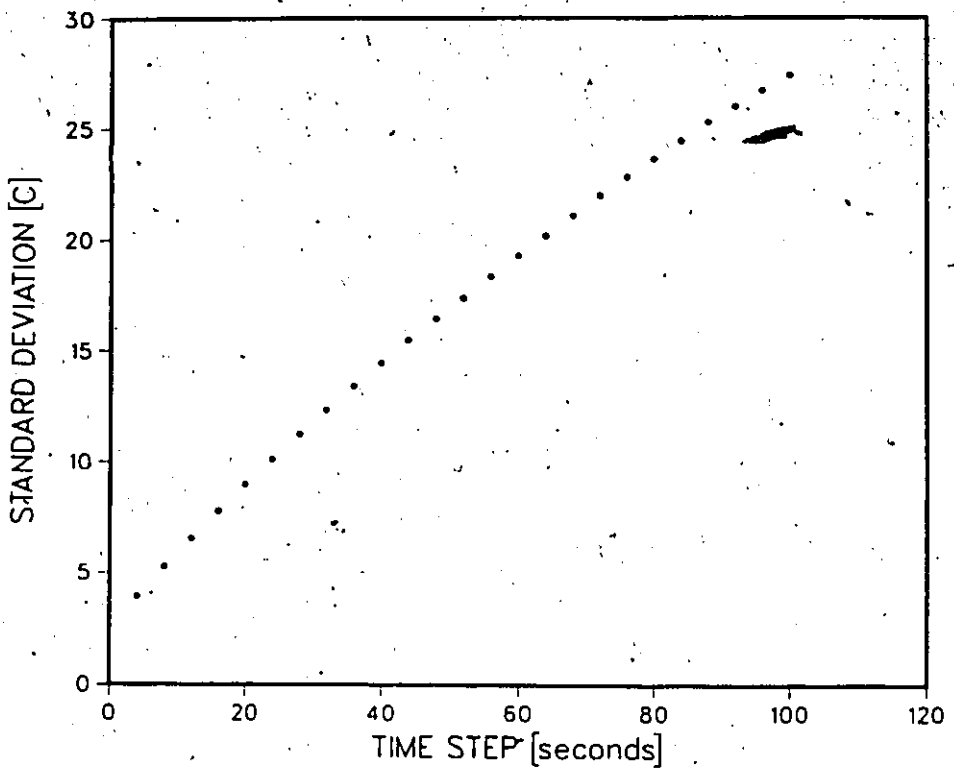

Fig.75 Effect of time step size on solution to test case#2 by the post iterative method, implicit finite difference.

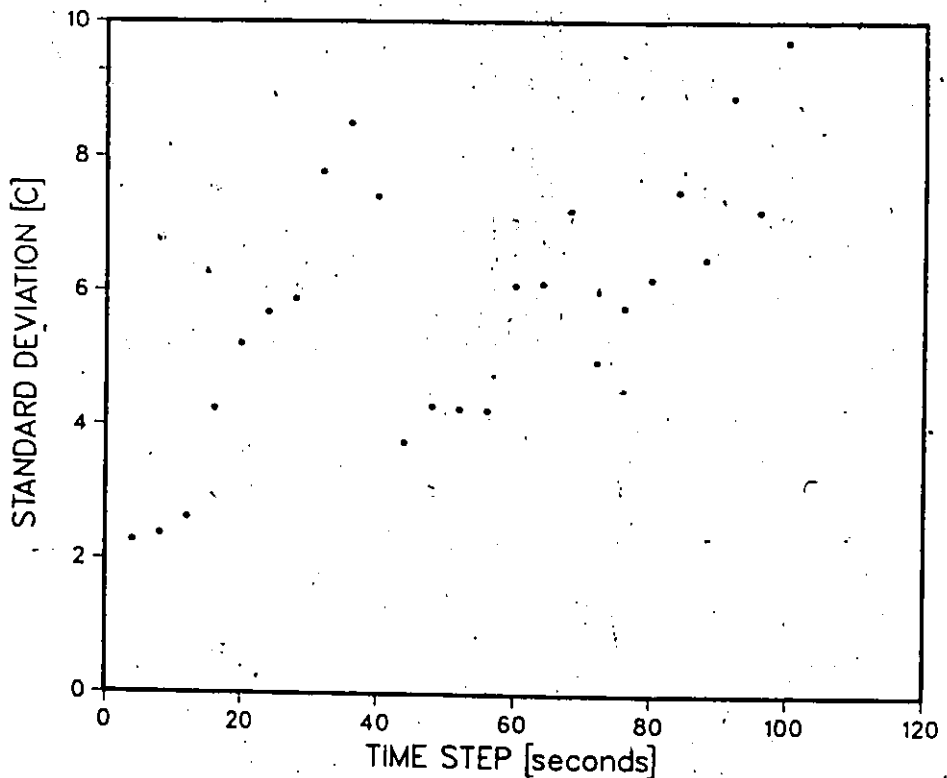

Fig.76 Effect of time step size on solution to test case#2 by the apparent capacity method, implicit finite difference.

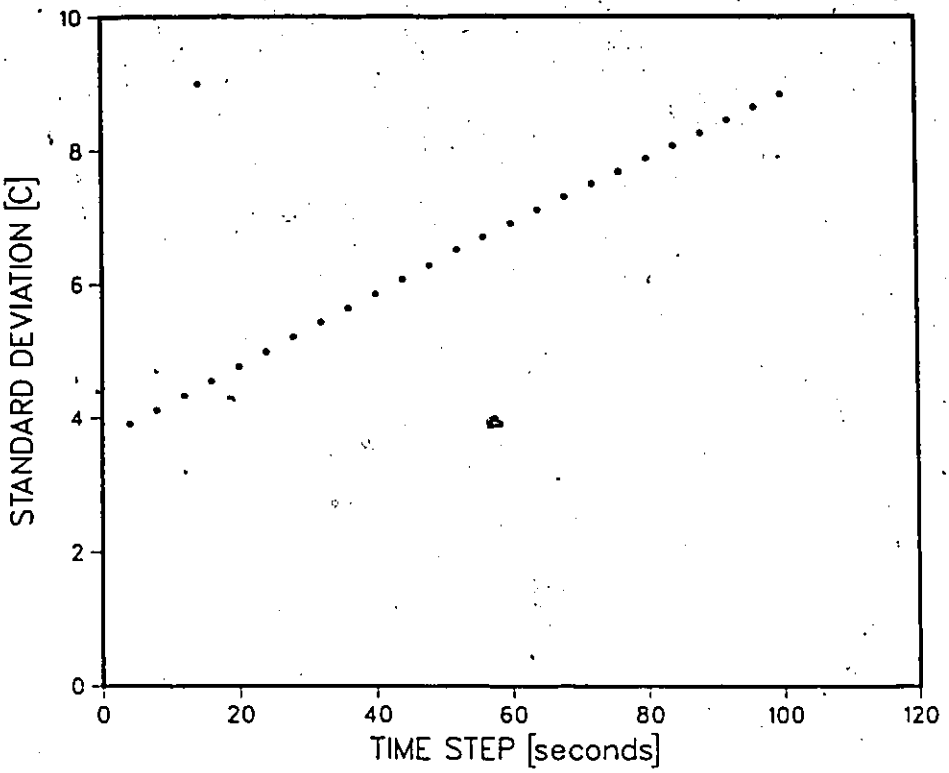

Fig.77 Effect of time step size on solution to test case#2 by the enthalpy method, implicit finite difference.

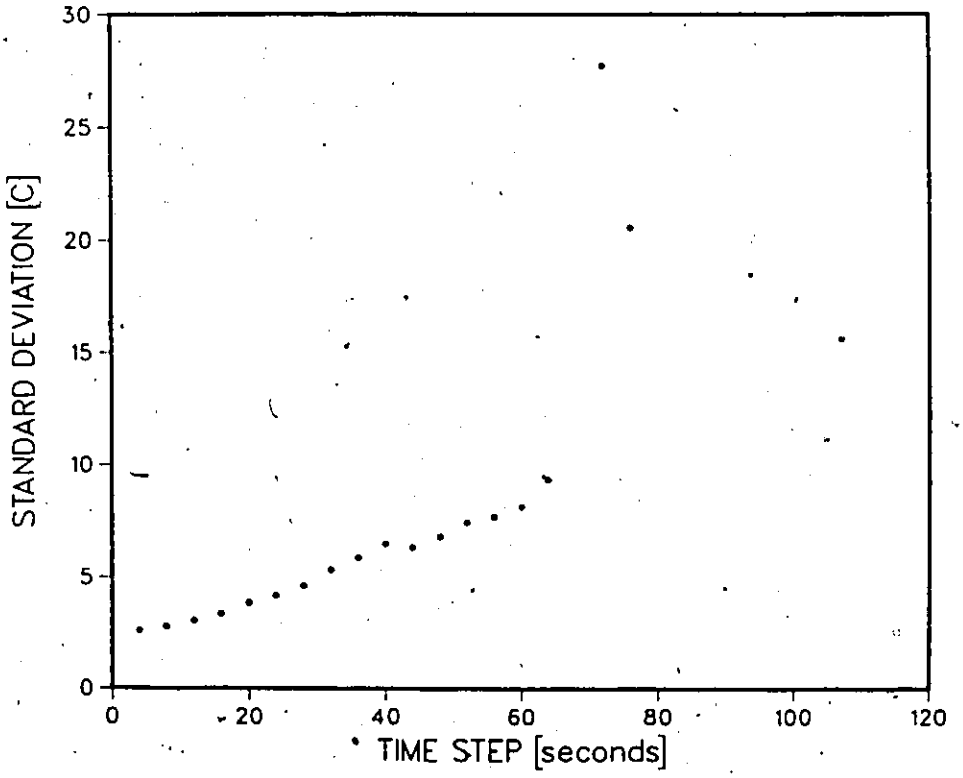

Fig.78 Effect of time step size on solution to test case#2 by Pham's method, implicit finite difference.

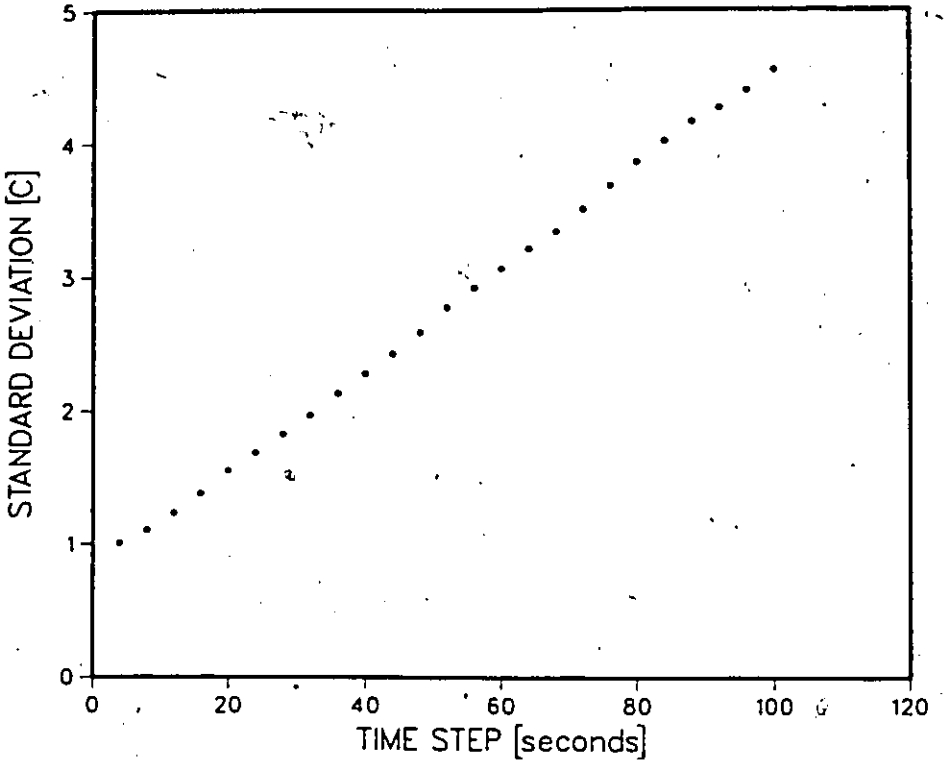

Fig.79 Effect of time step size on solution to test case#2 by the effective capacity method, implicit finite difference.

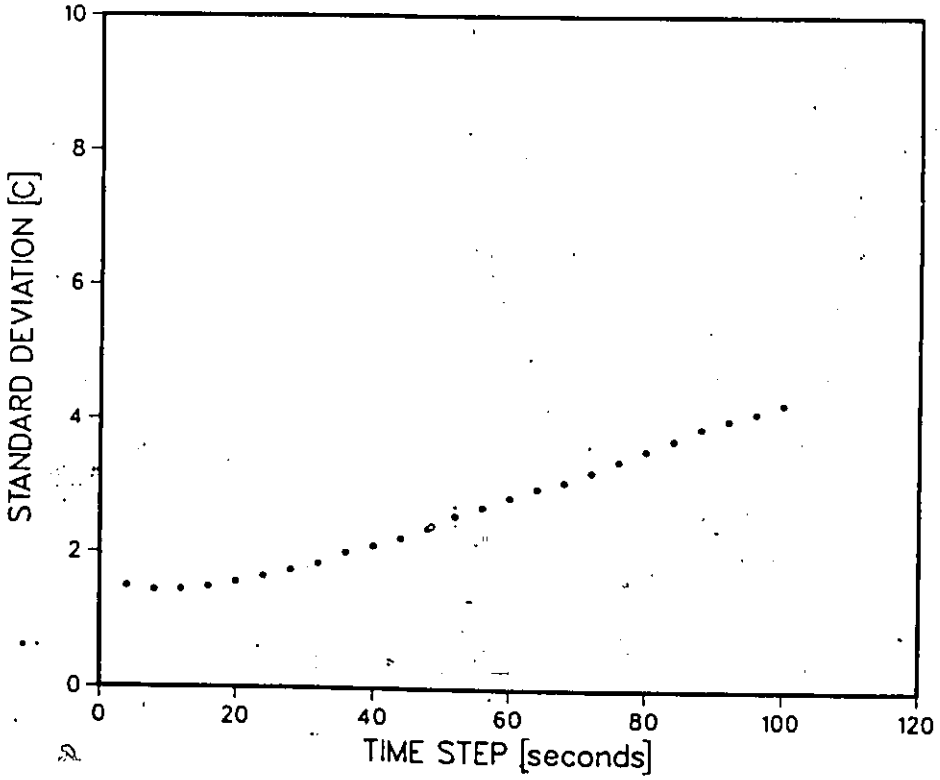

Fig.80 Effect of time step size on solution to test case#2 by the effective capacity method, implicit finite element.

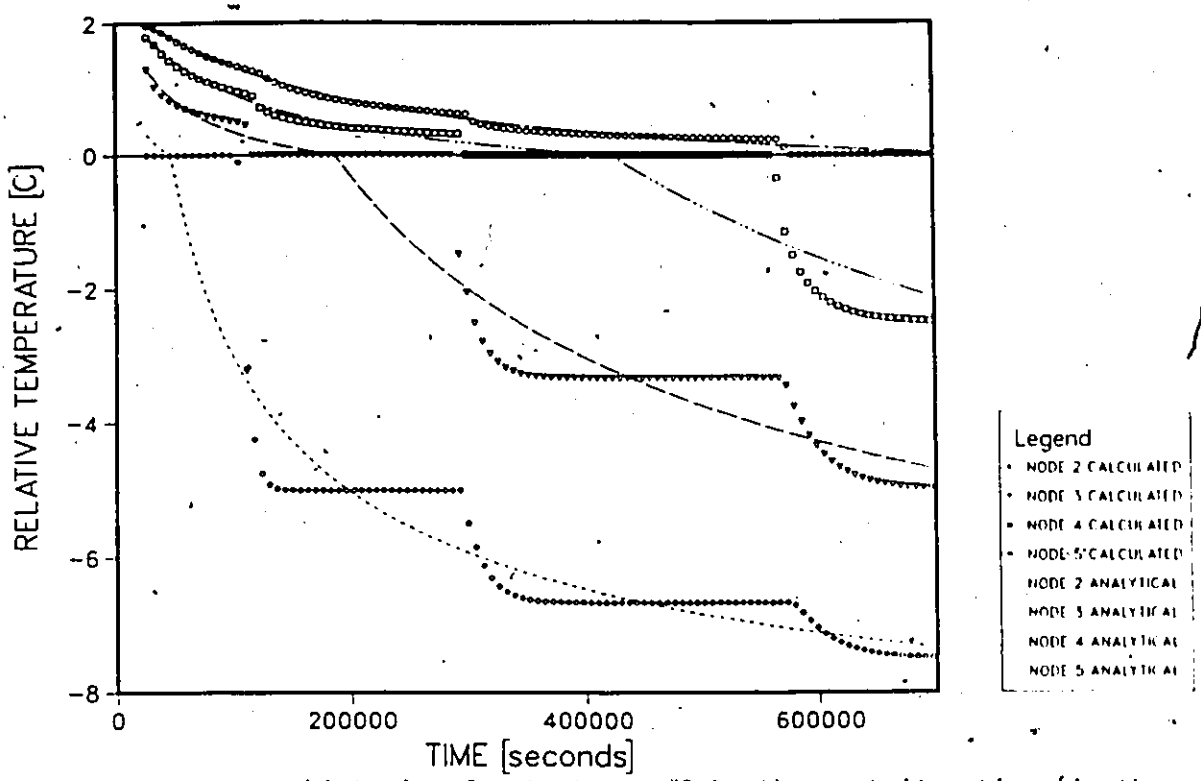

Fig.81 Temperature histories for test case#3 by the post iterative (isothermal) method, explicit finite difference. Time step is 6500s.

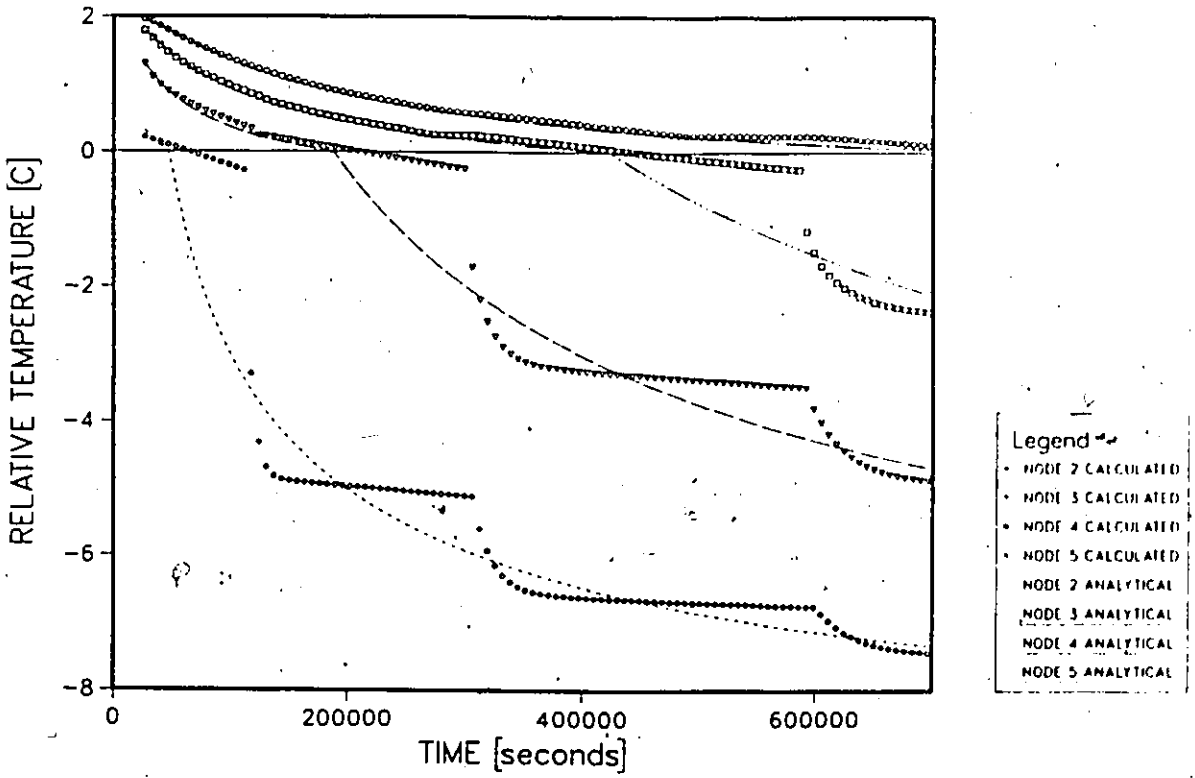

Fig.82 Temperature histories for test case#3 by the post iterative method (mushy=-0.25 to +0.25 C), explicit finite difference. Time step is 6500s.

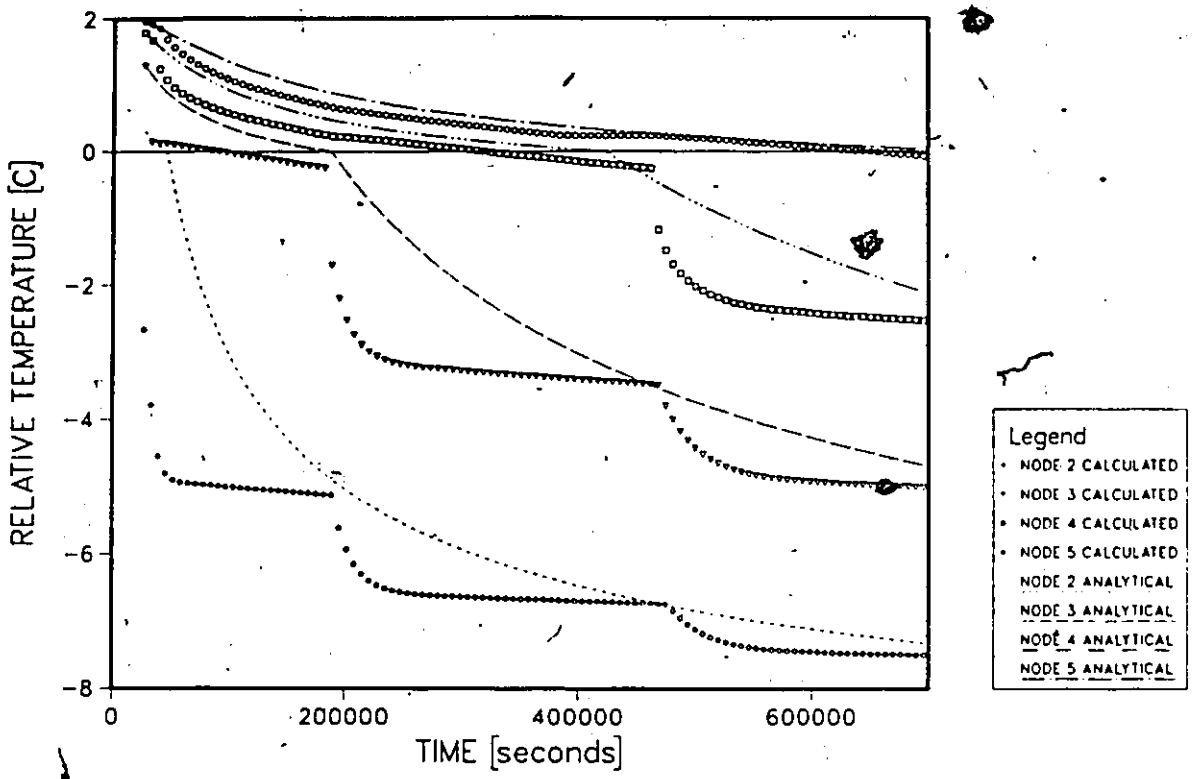

Fig.83 Temperature histories for test case#3 by the apparent capacity method (mushy=-0.25 to +0.25 C), explicit finite difference. Time step is 6500s.

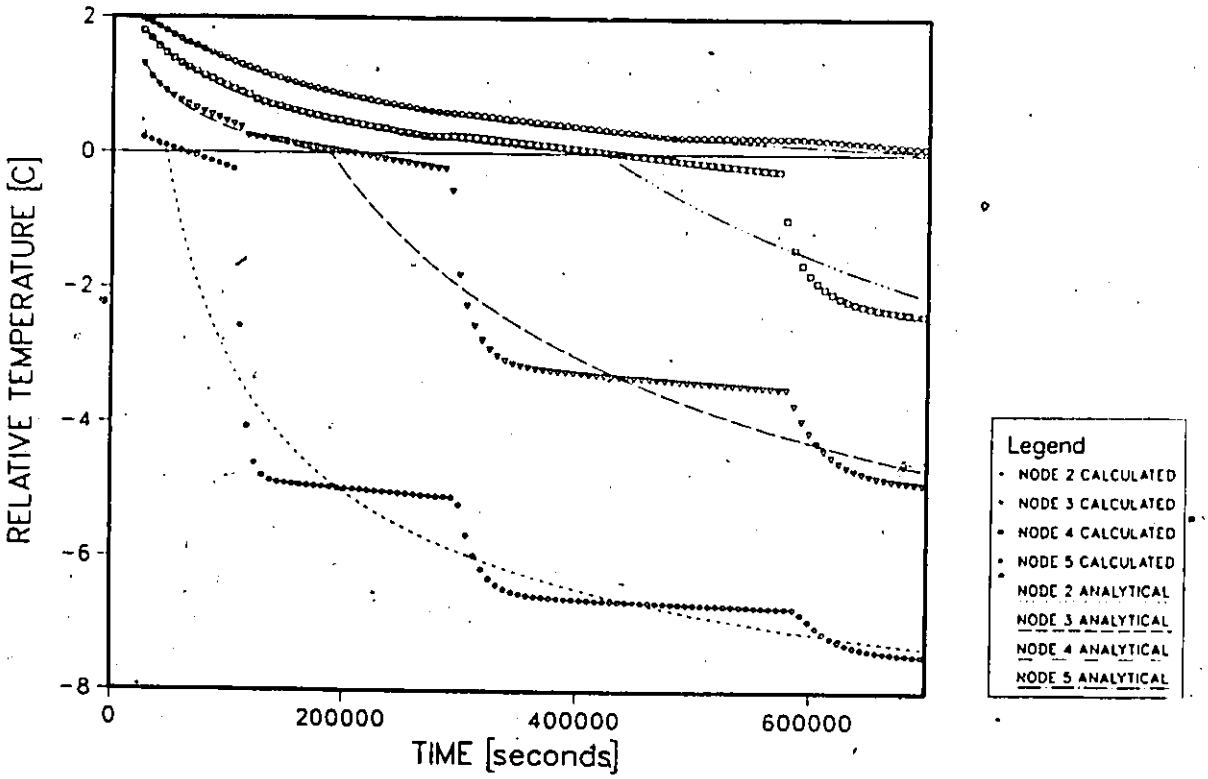

Fig.84 Temperature histories for test case#3 by the enthalpy method (mushy= -0.25 to +0.25 C), explicit finite difference. Time step is 6500s.

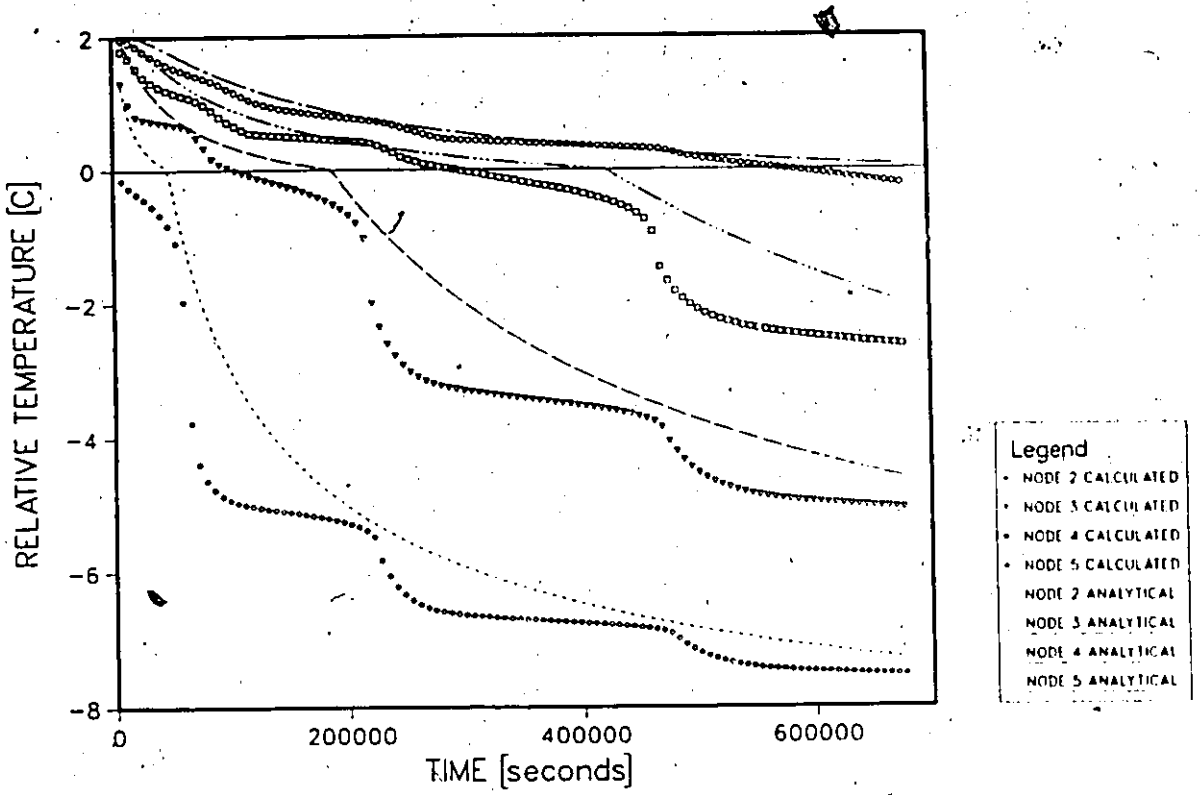

Fig.85 Temperature histories for test case#3 by the effective capacity method (mushy=-0.25 to +0.25 C), explicit finite difference. Time step is 6500s.

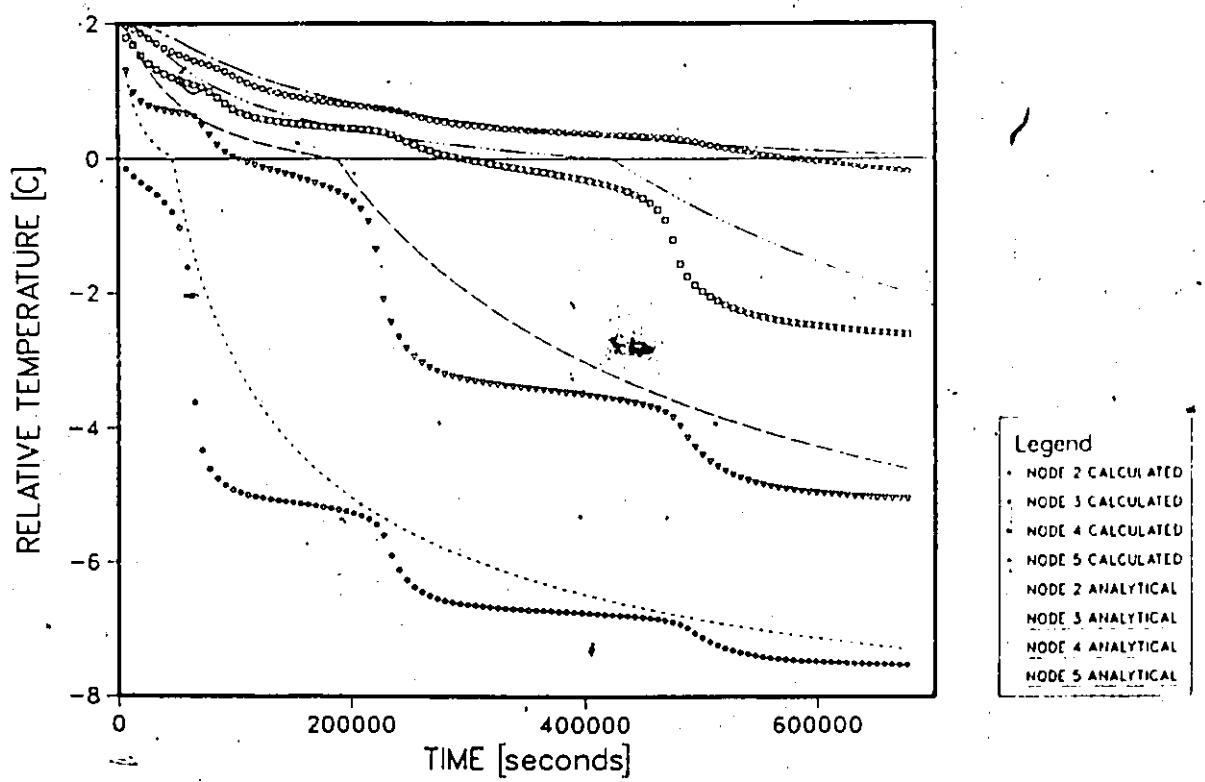

Fig.86 Temperature histories for test case#3 by the effective capacity method (mushy=Gaussian), explicit finite difference. Time step is 6500s.

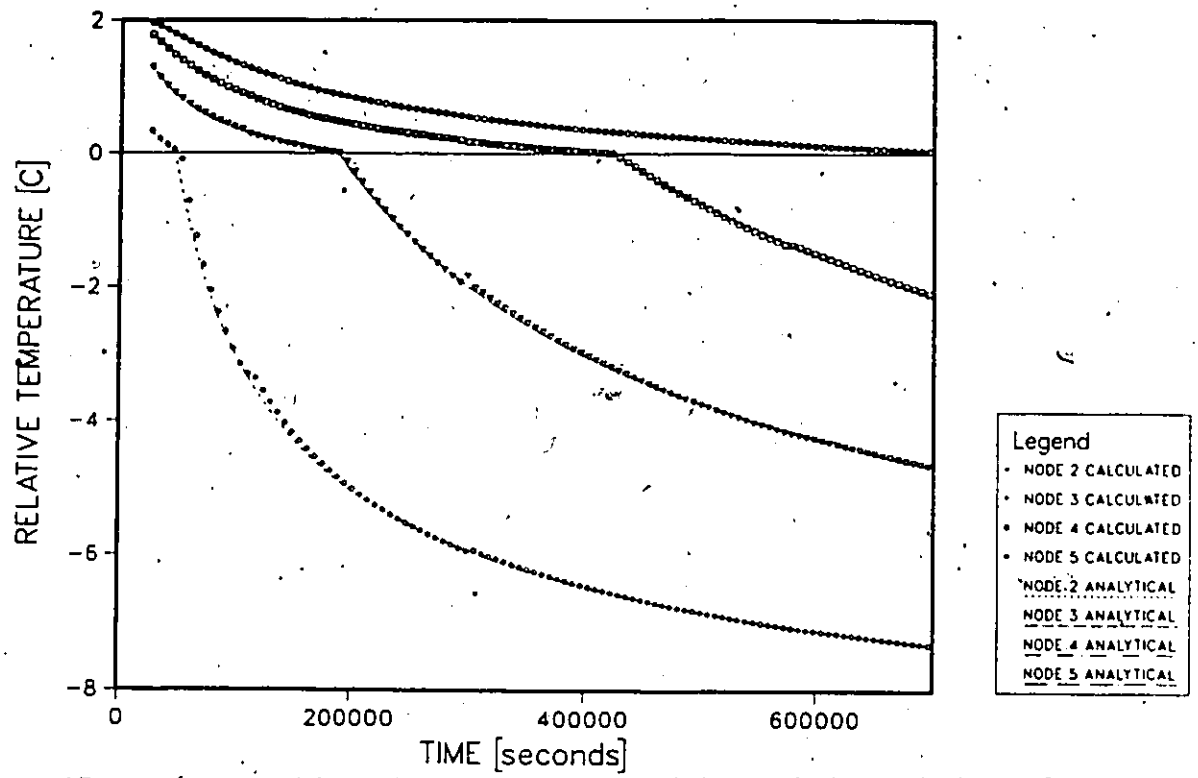

Fig.87 Temperature histories for test case#3 by Tacke's method, explicit finite difference. Time step is 6500s.

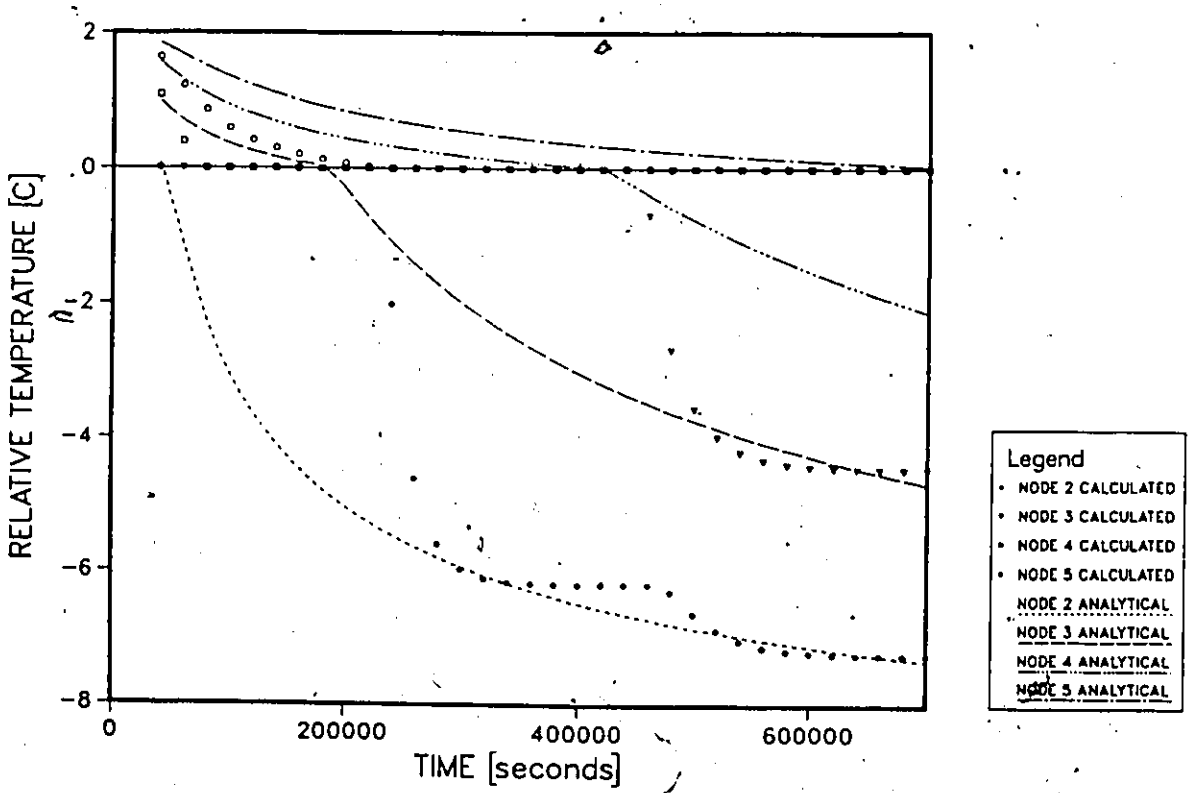

Fig.88 Temperature histories for test case#3 by the post iterative (isothermal) method, implicit finite difference. Time step is 20000s.

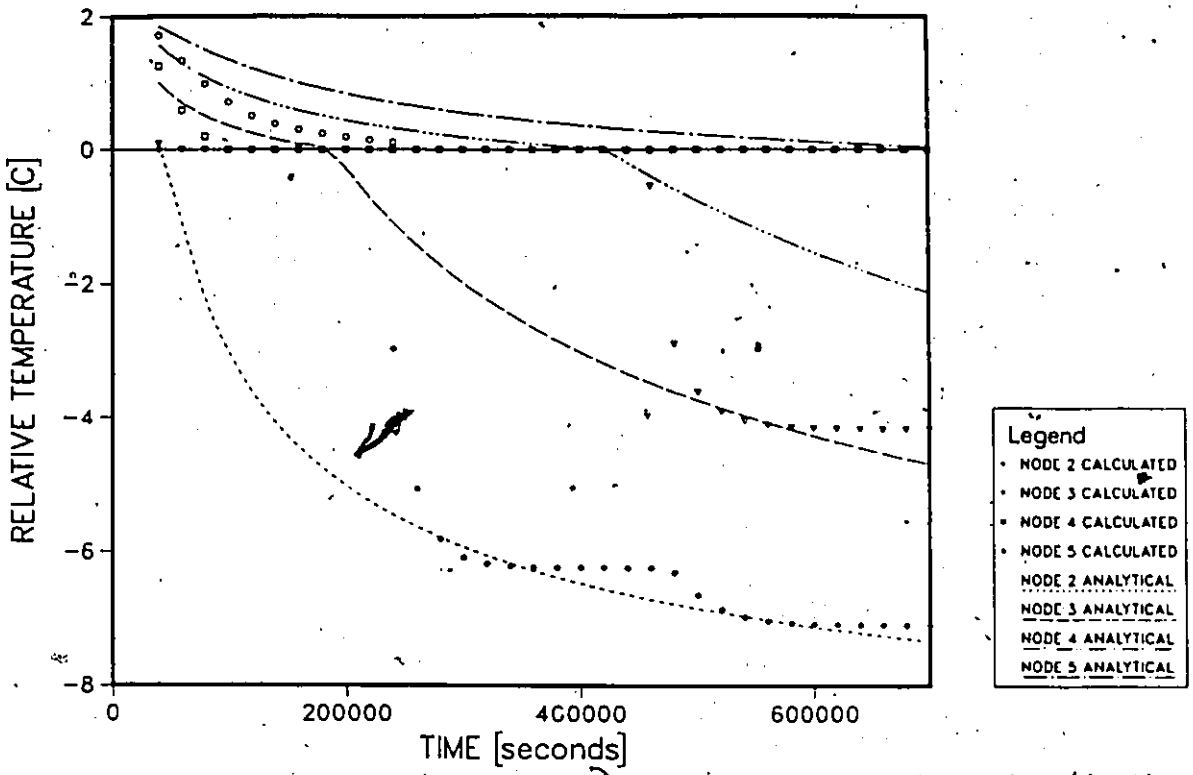

Fig.89 Temperature histories for test case#3 by the post iterative (isothermal) method, implicit finite element. Time step is 20000s.

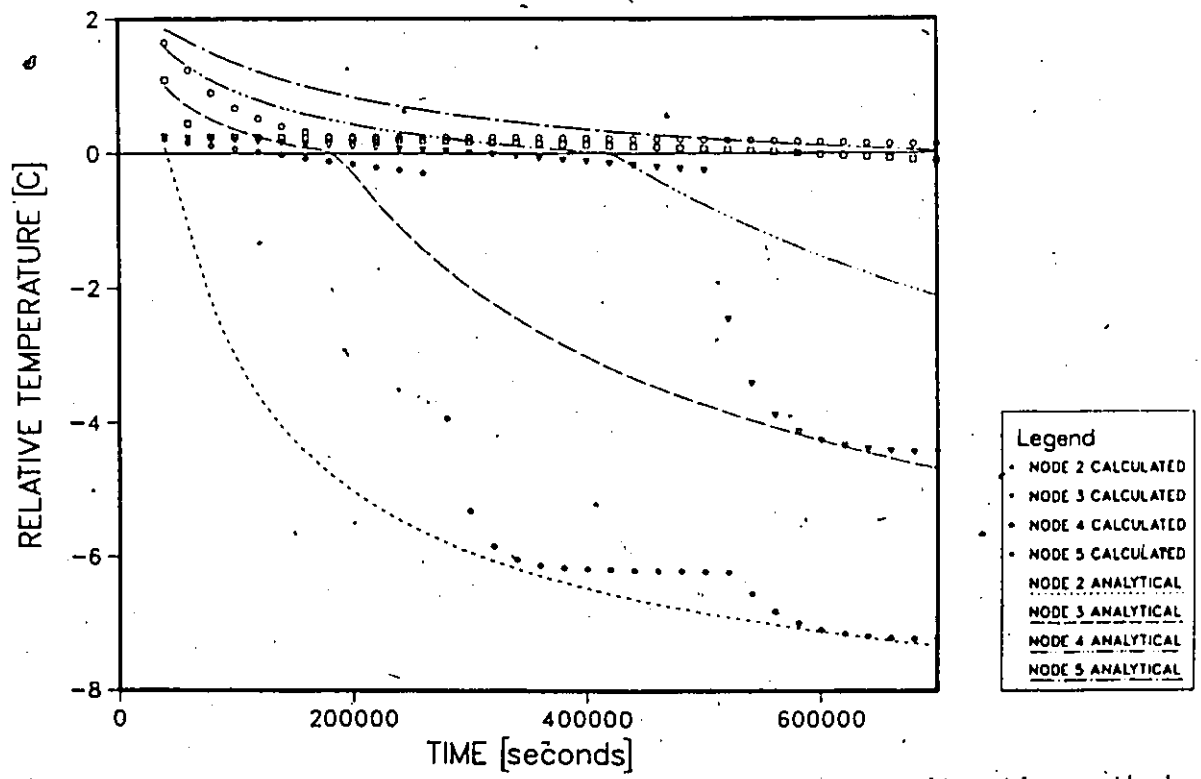

Fig.90 Temperature histories for test case#3 by the post iterative method (mushy=-.25 to +.25 C), implicit finite difference. Time step is 20000s.

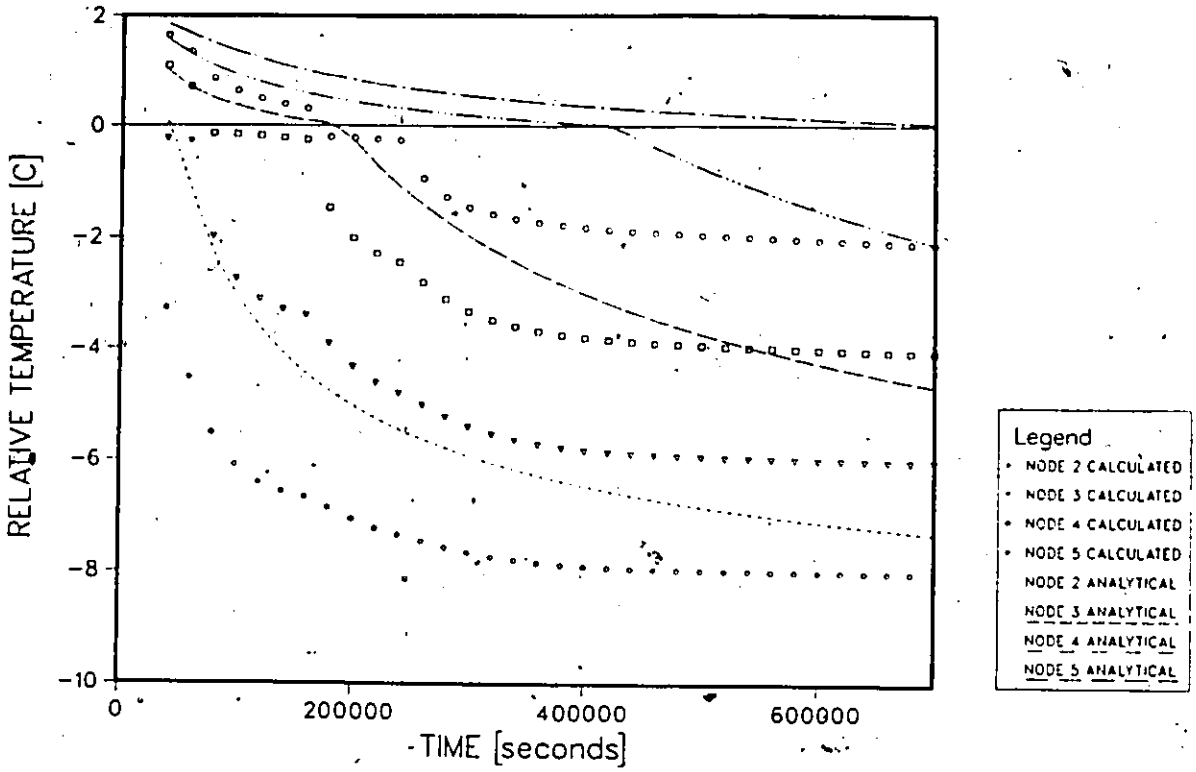

Fig.91 Temperature histories for test case#3 by the apparent capacity method (mushy=-.25 to +.25 C), implicit finite difference. Time step is 20000s.

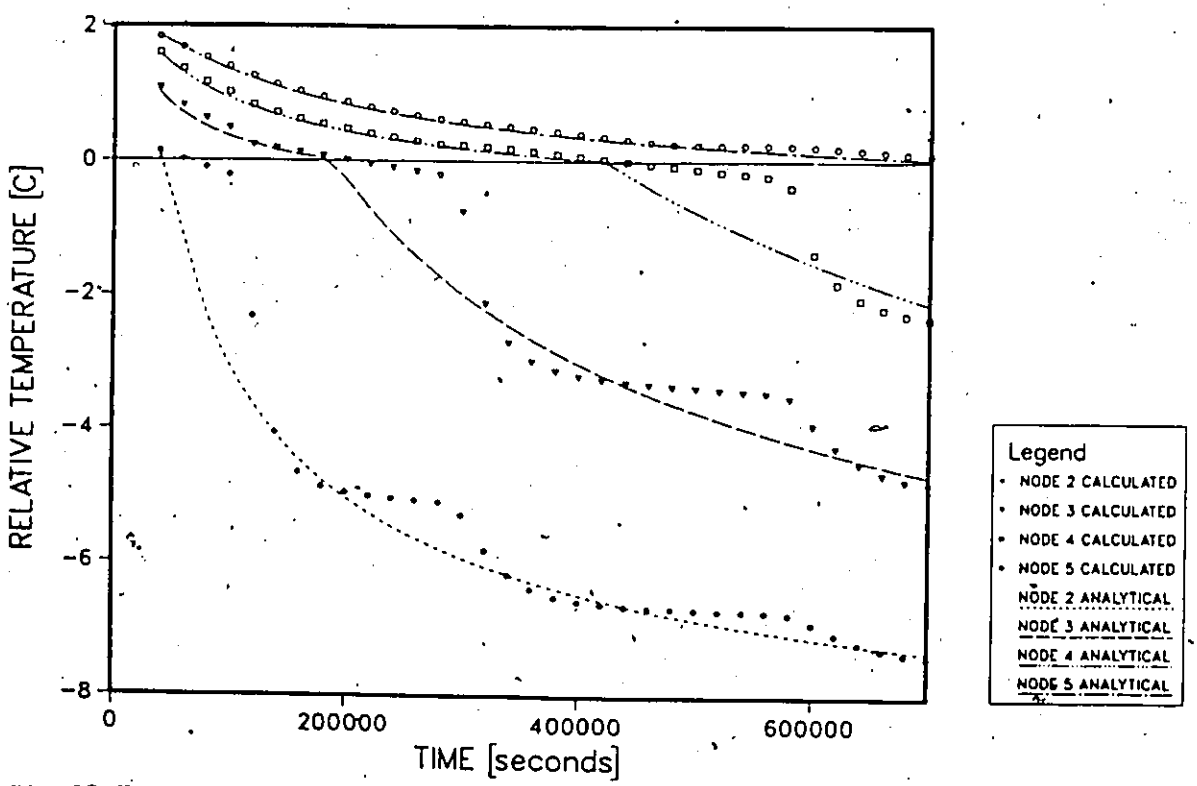

Fig.92 Temperature histories for test case#3 by the enthalpy method (mushy= -0.25 to +0.25 C), implicit finite difference. Time step is 20000s.

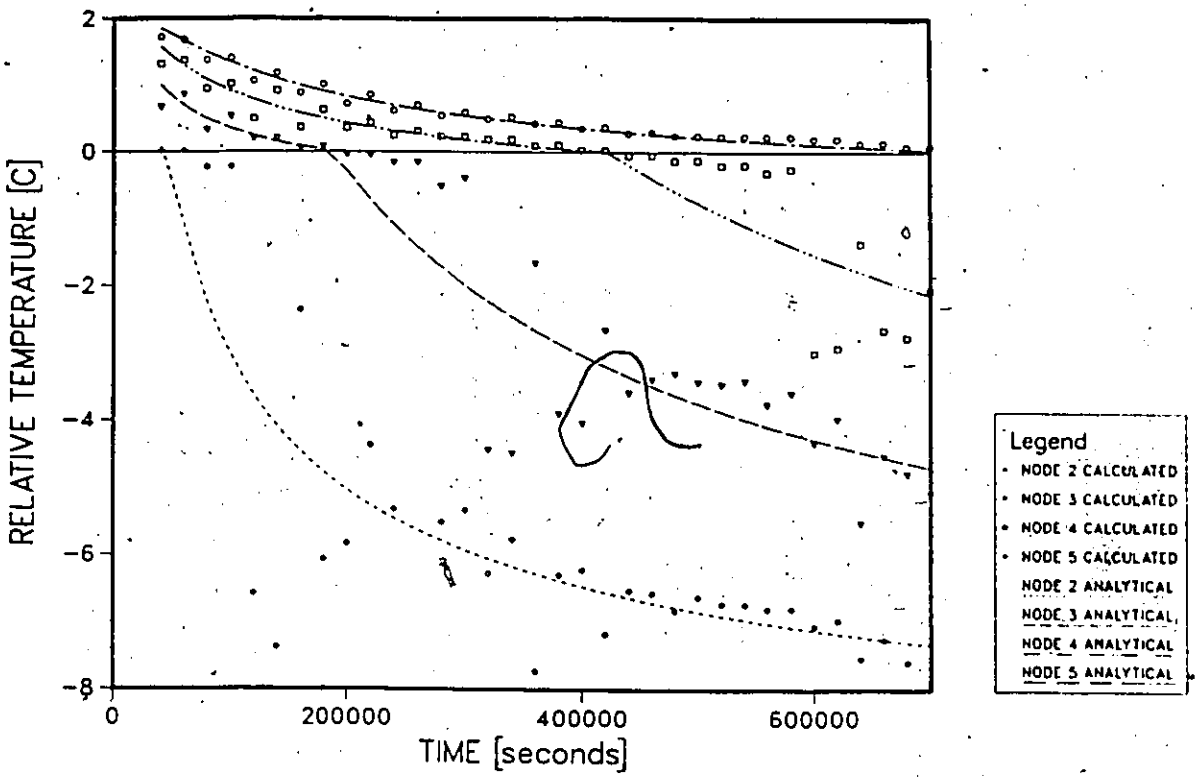

Fig.93 Temperature histories for test case#3 by Pham's method (mushy=-0.25 to +0.25 C), implicit finite difference. Time step is 20000s.

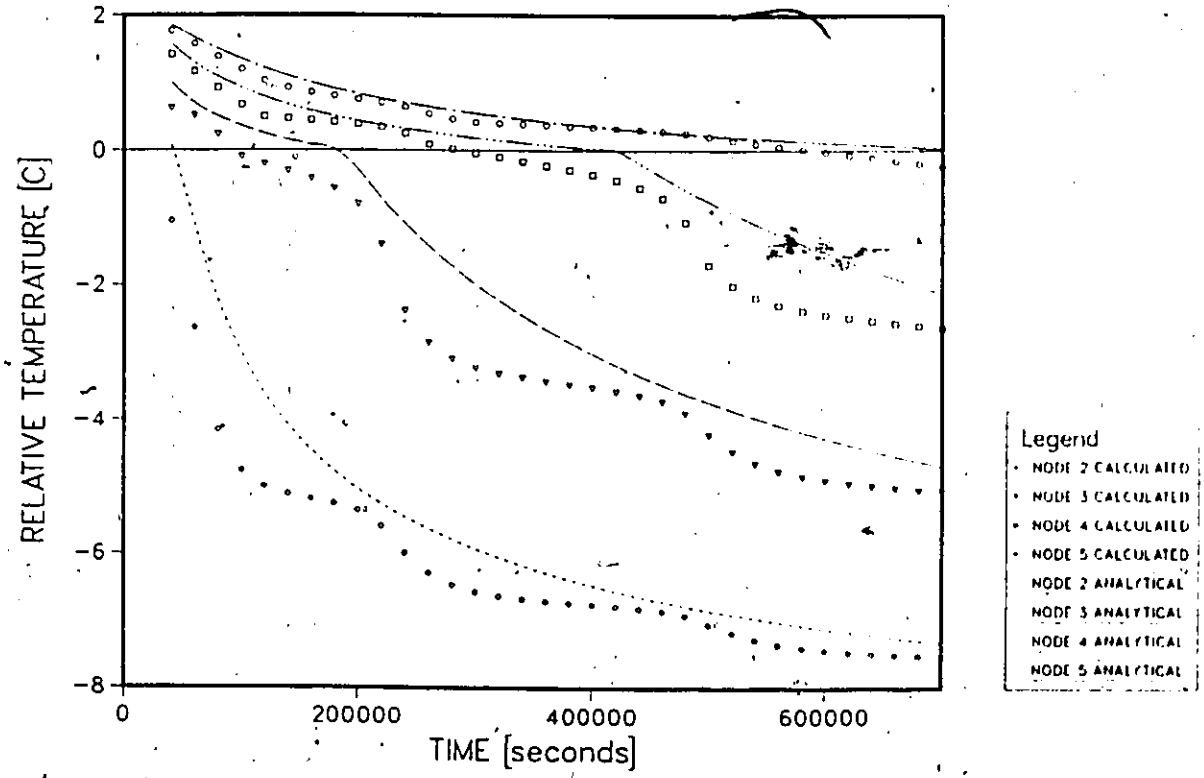

Fig.94 Temperature histories for test case#3 by the effective capacity method (mushy=-.25 to +.25 C), implicit finite difference. Time step is 20000s.

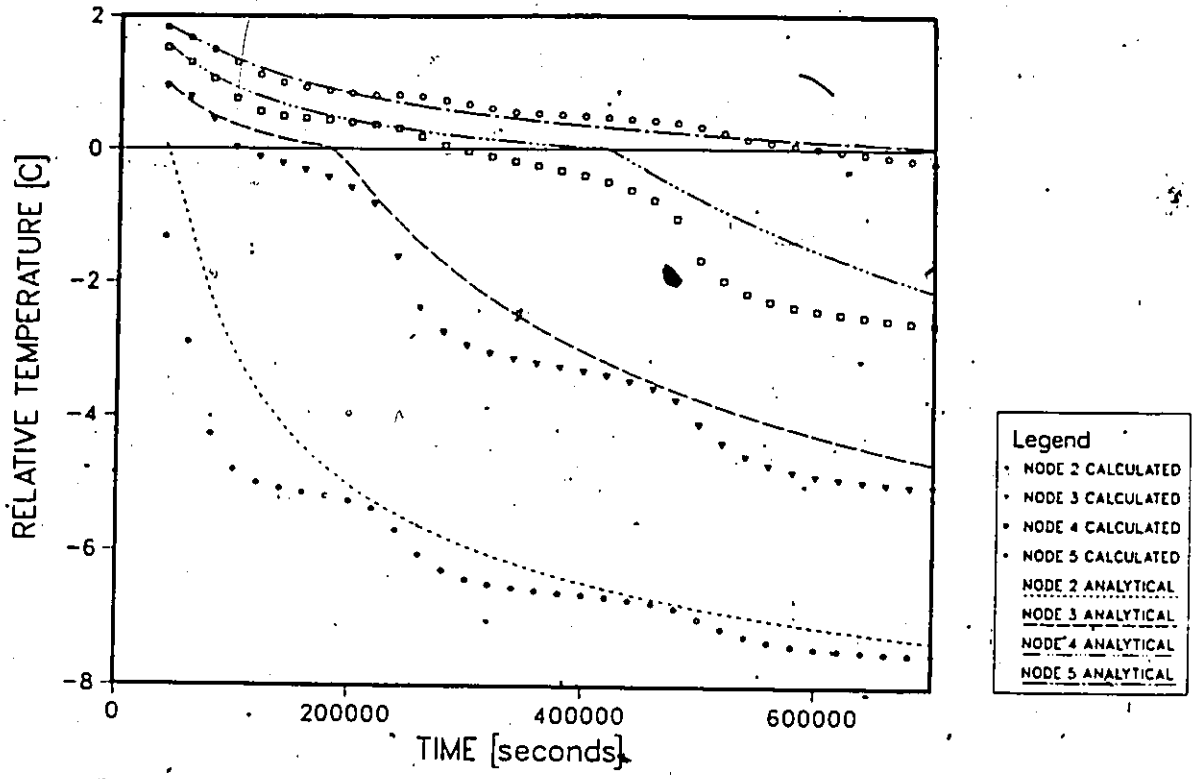

Fig.95 Temperature histories for test case#3 by the effective capacity method (mushy=-.25 to +.25 C), implicit finite element. Time step is 20000s.

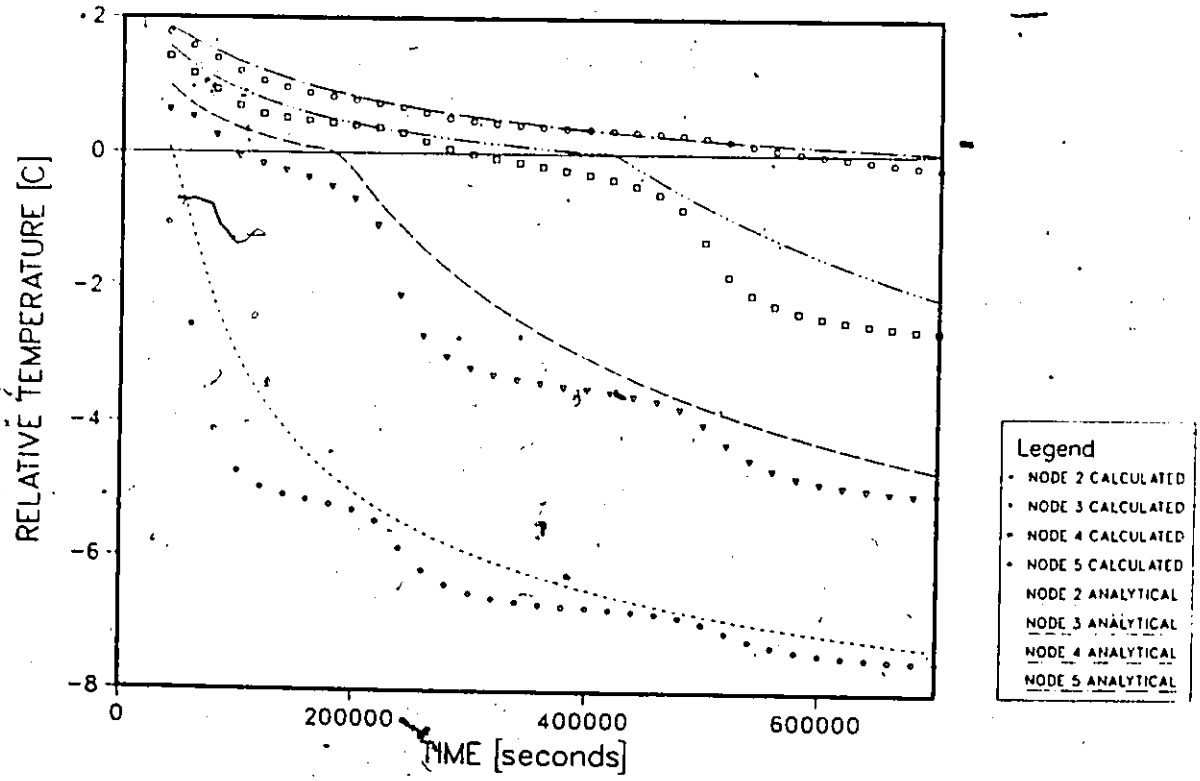

Fig.96 Temperature histories for test case#3 by the effective capacity method (mushy=Gaussian),implicit finite difference. Time step is 20000s.

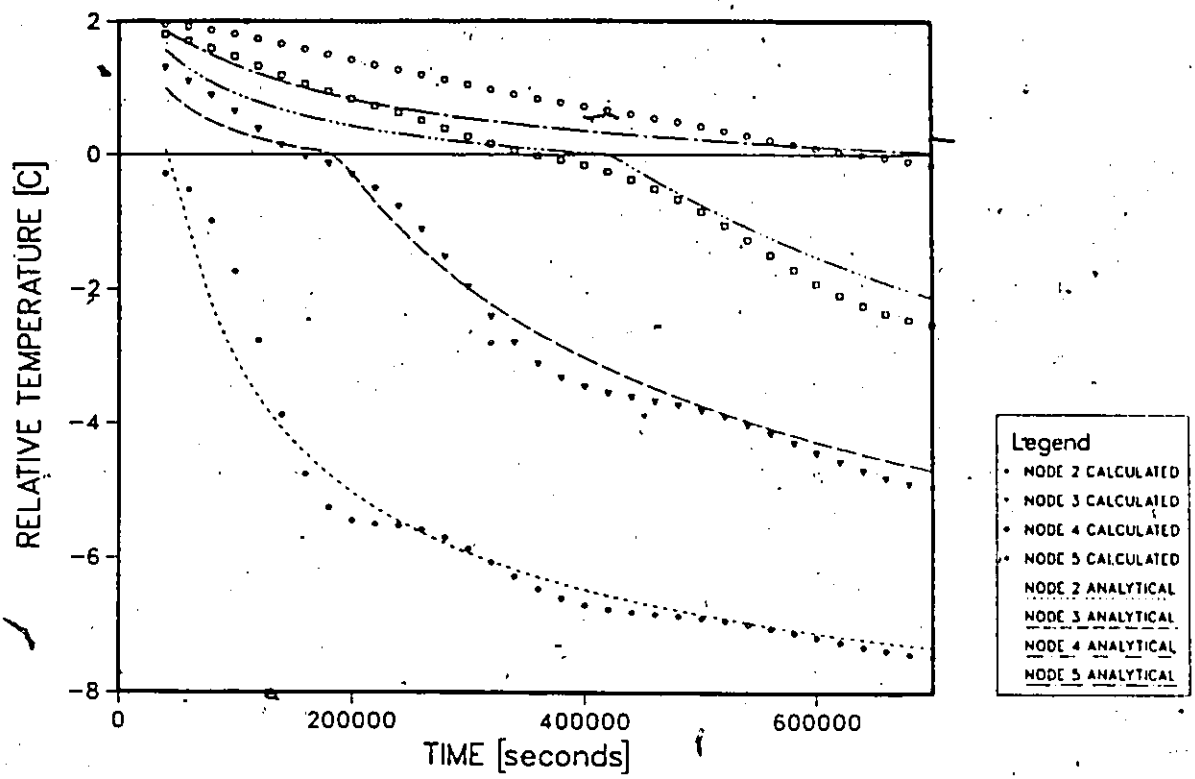

Fig.97 Temperature histories for test case#3 by Blanchard and Fremond's method (parameter=0.5 C), implicit finite difference. Time step is 40000s.

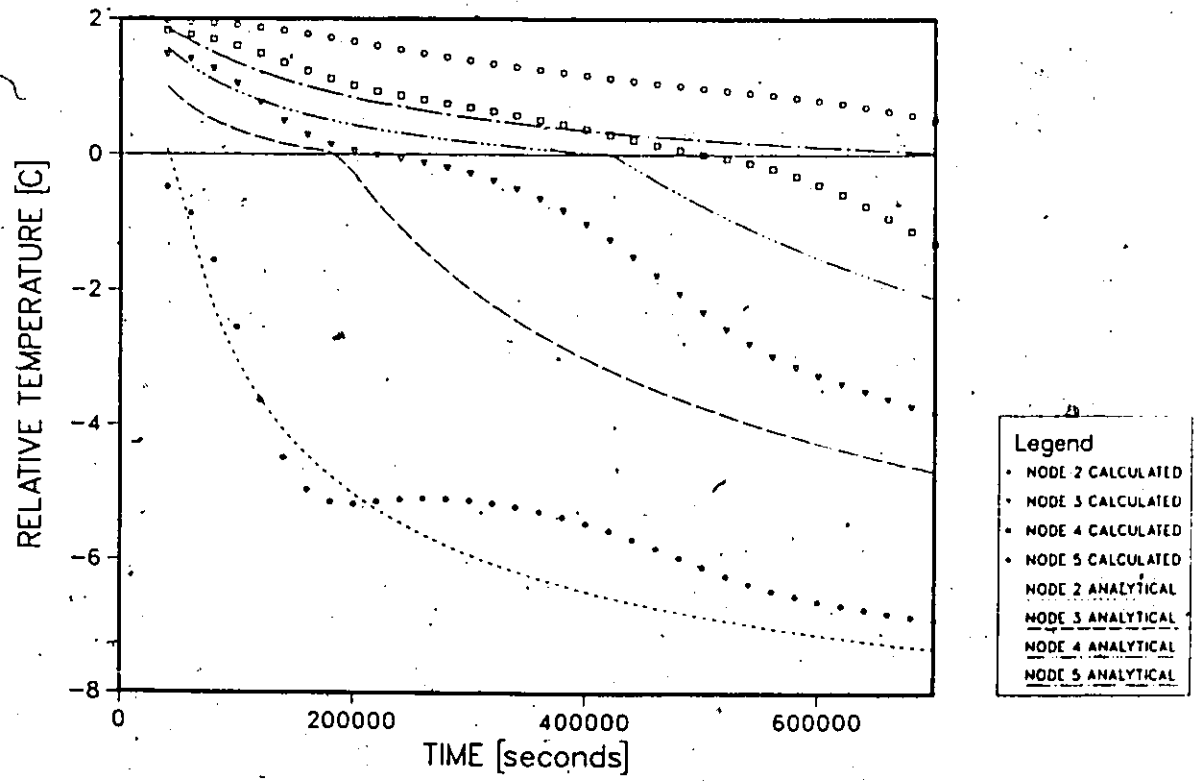

Fig.98 Temperature histories for test case#3 by Blanchard and Fremond's method (parameter=0.5 C), implicit finite element. Time step is 40000s.

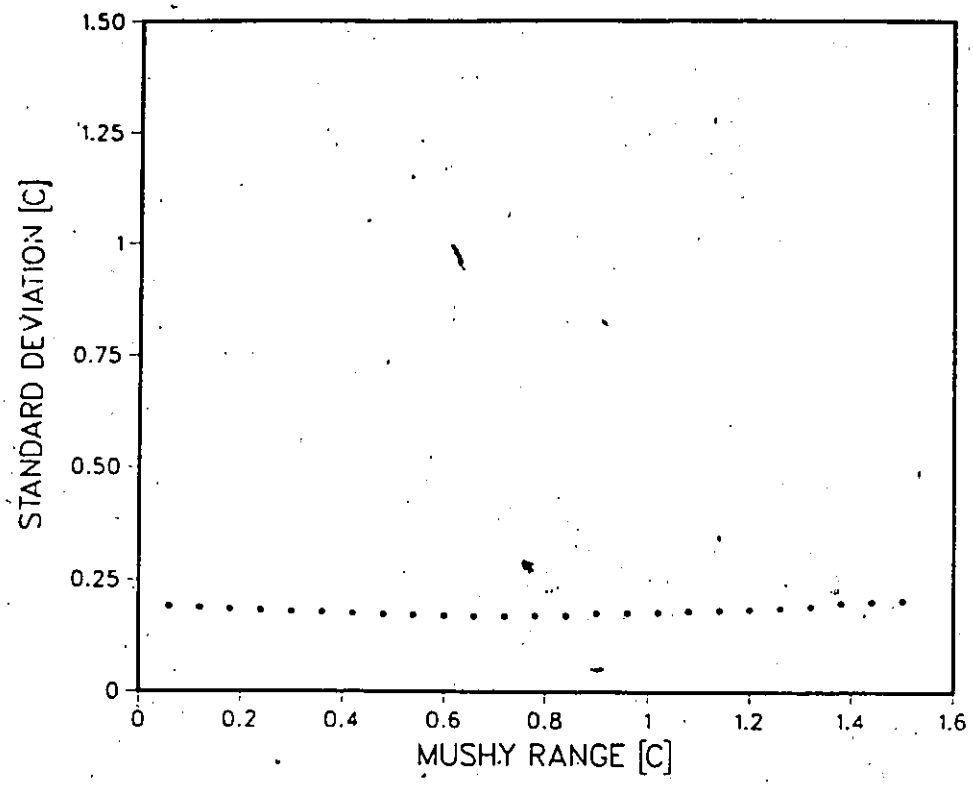

Fig.99 Effect of assumed mushy range on solution to test case#3 by the post iterative method, explicit finite difference. Time step is 6500s.

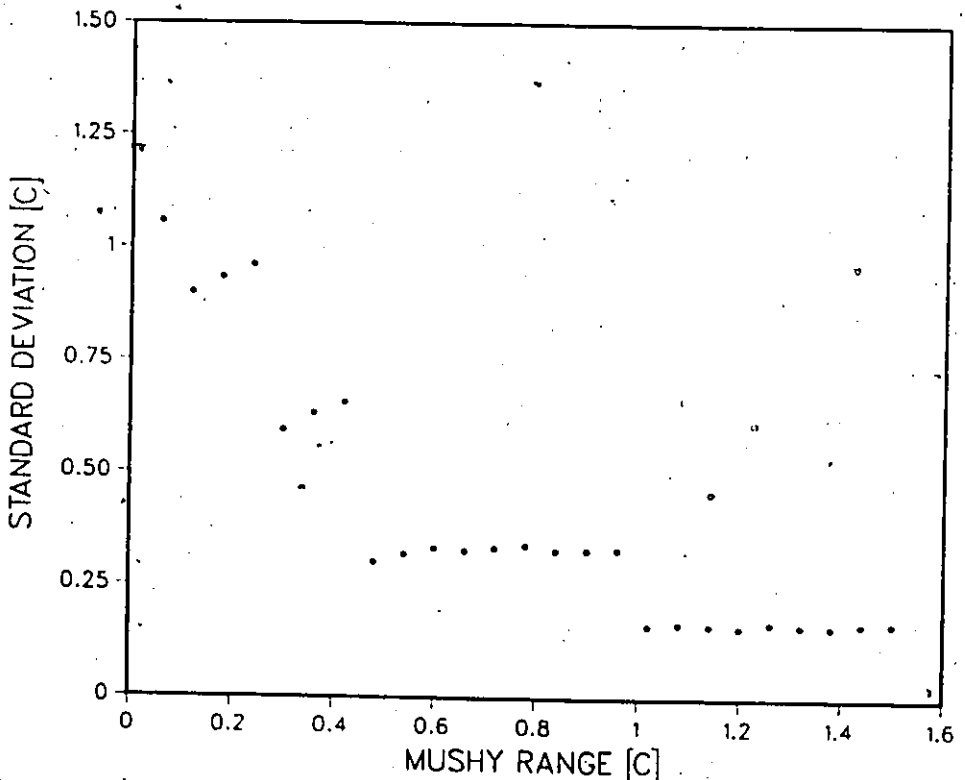

Fig.100 Effect of the assumed mushy range on solution to test case#3 by the apparent capacity method, explicit finite difference. Time step 6500s.

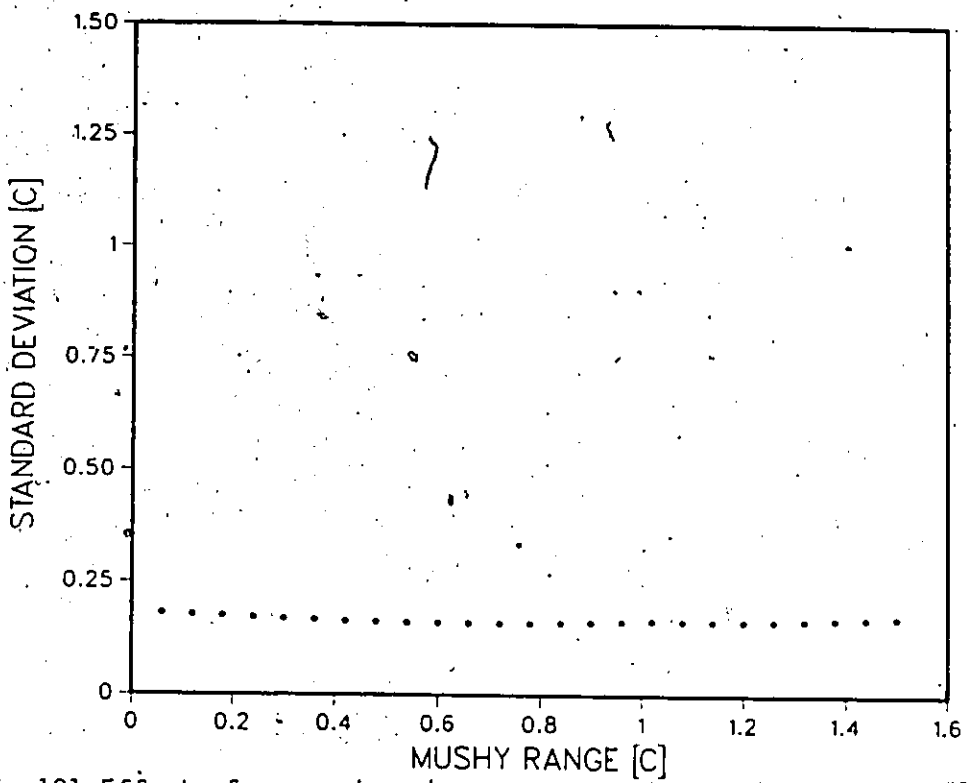

Fig.101 Effect of assumed mushy range on solution to test case#3 by the enthalpy method, explicit finite difference. Time step is 6500s.

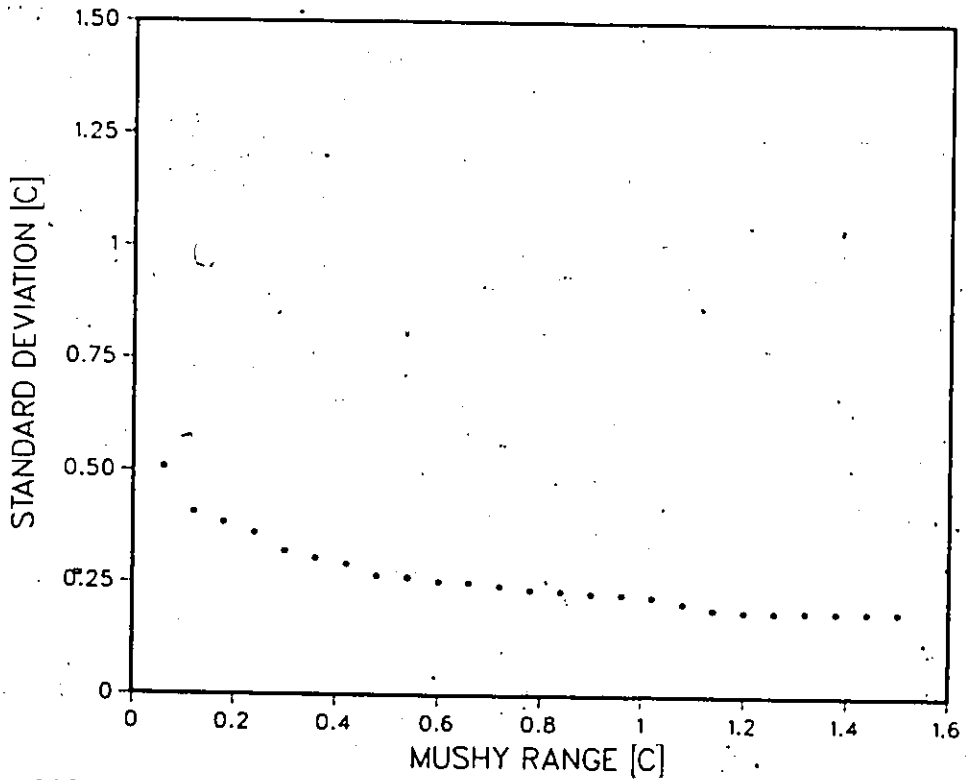

Fig.102 Effect of assumed mushy range on solution to test case#3 by the effective capacity method, explicit finite difference. Time step 6500s.

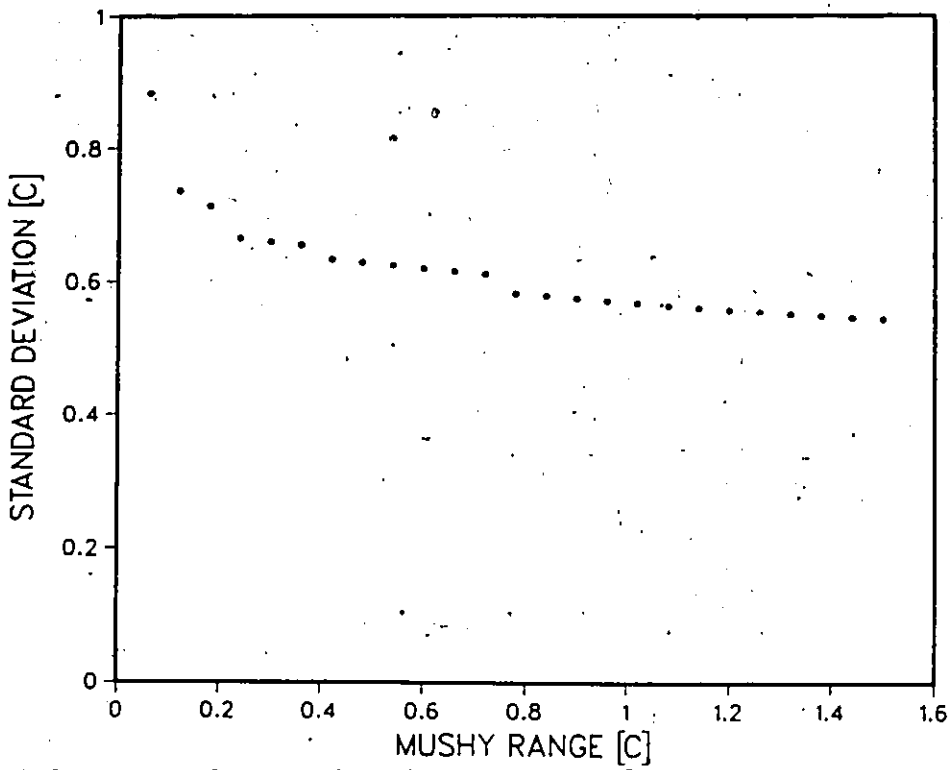

Fig.103 Effect of assumed mushy range on solution to test case#3 by the post iterative method, implicit finite difference. Time step is 20000s.

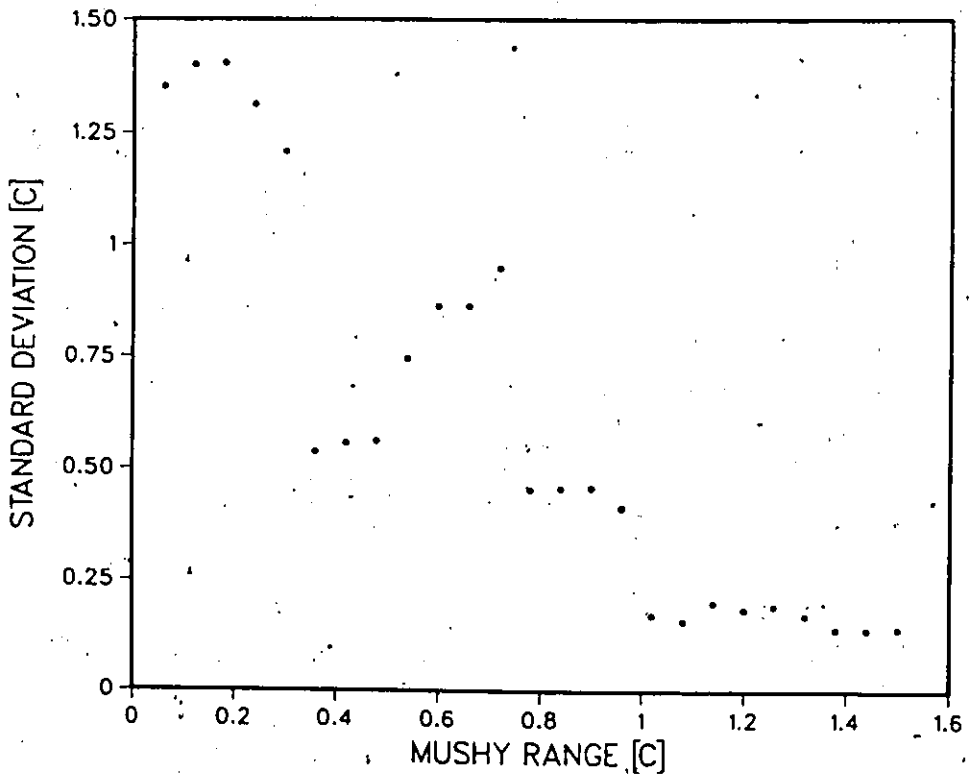

Fig.104 Effect of assumed mushy range on solution to test case#3 by apparent capacity method, implicit finite difference. Time step is 20000s.

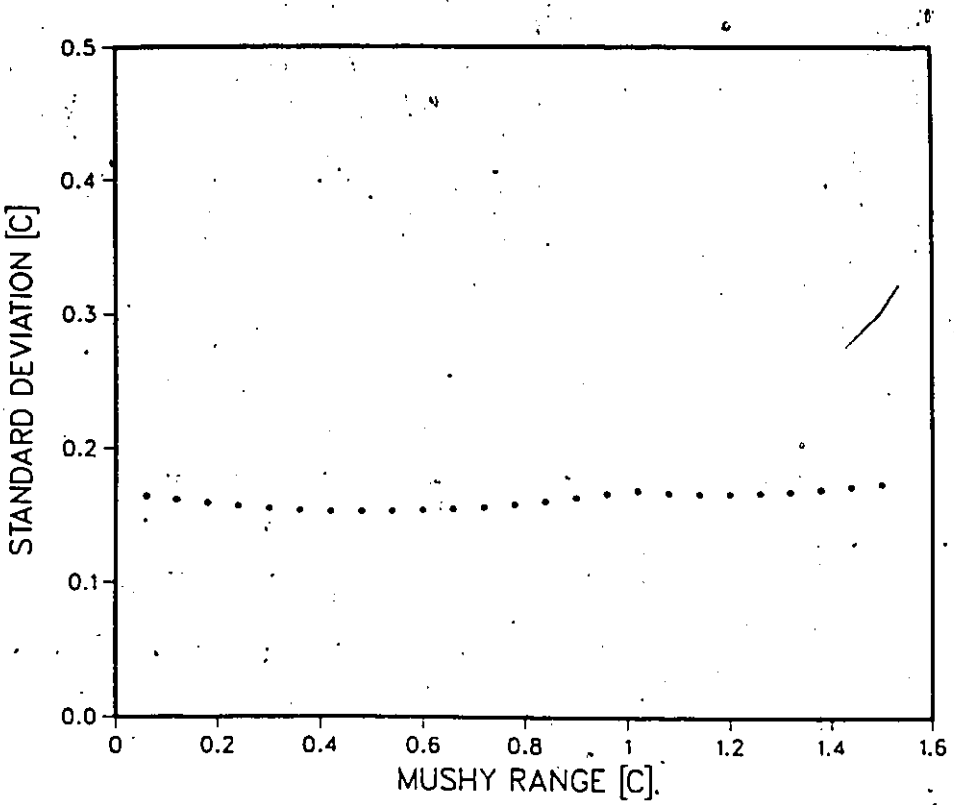

Fig.105 Effect of assumed mushy range on solution to test case#3 by enthalpy method, implicit finite difference. Time step is 20000s.

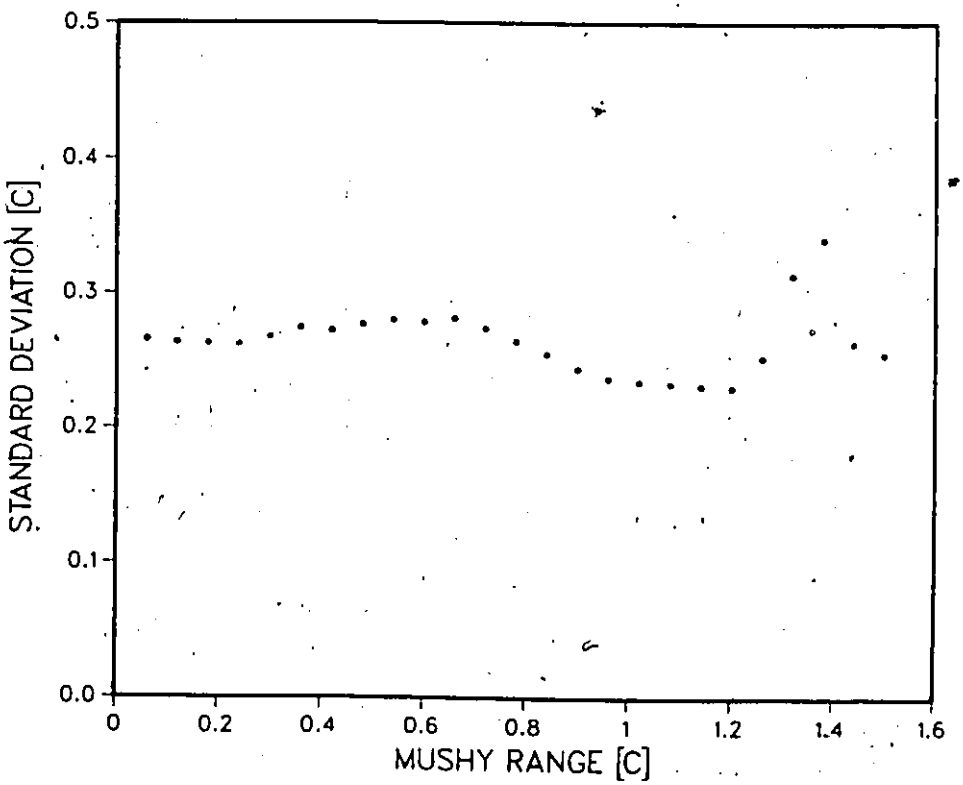

Fig.106. Effect of assumed mushy range on solution to test case#3 by Pham's method, implicit finite difference. Time step is 20000s.

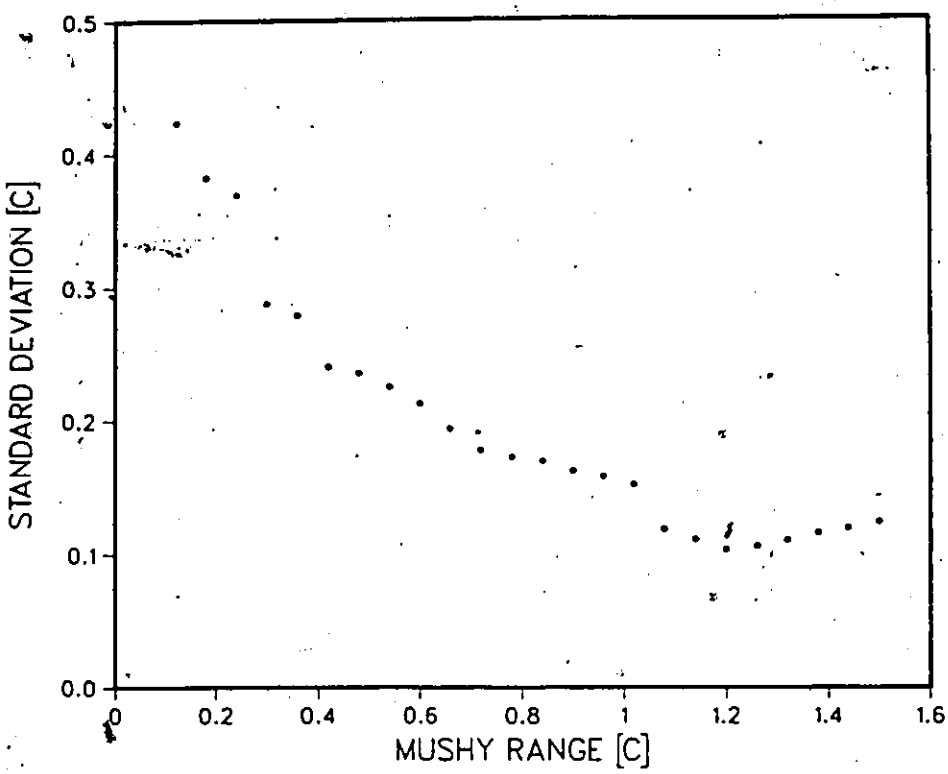

Fig.107 Effect of assumed mushy range on solution to test case#3 by effective capacity method; implicit finite difference. Time step is 20000s.

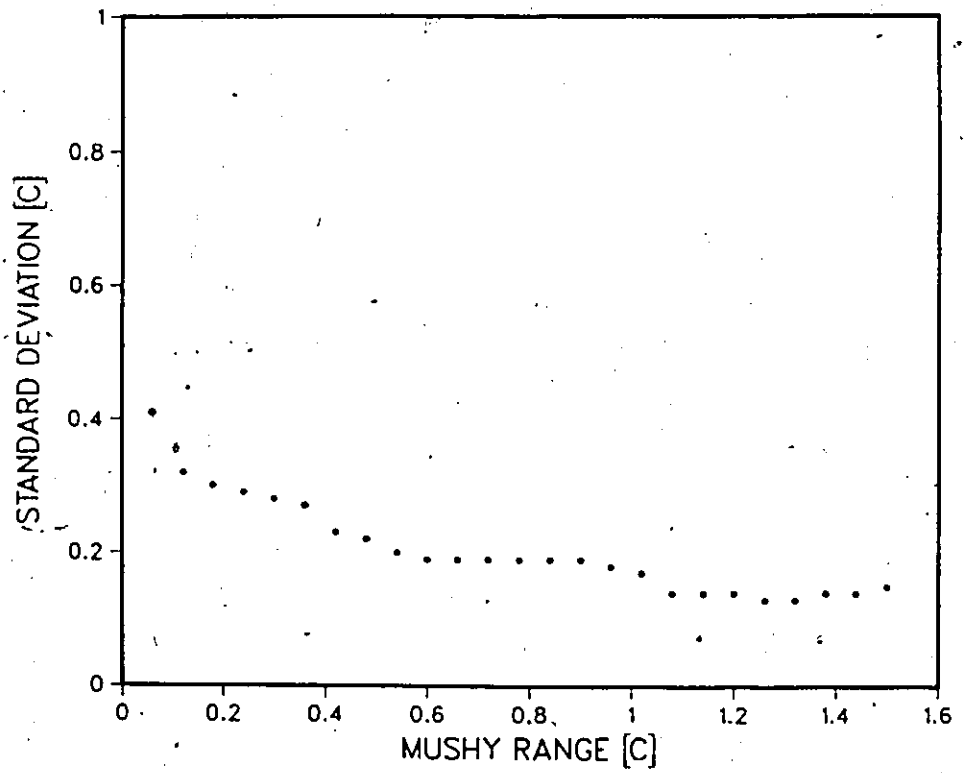

Fig.108 Effect of assumed mushy range on solution to test case#3 by effective capacity method, implicit finite element. Time step is 20000s.

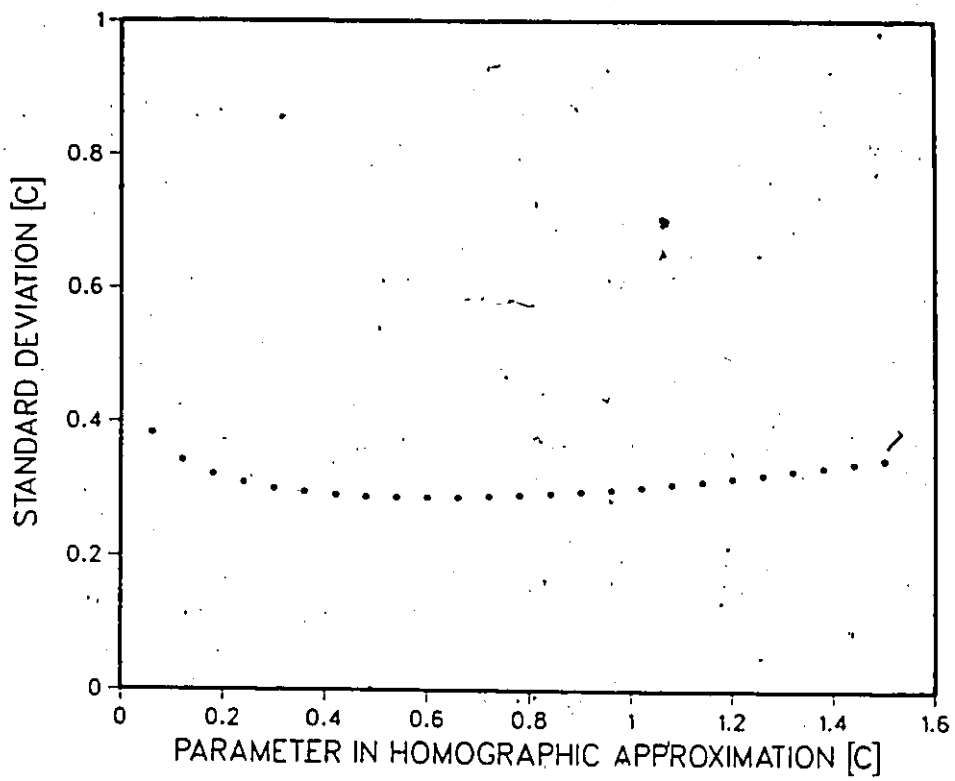

Fig.109 Effect of assumed mushy range on solution to test case#3 by Blanchard and Fremond's method, implicit finite difference. Time step is 40000s.

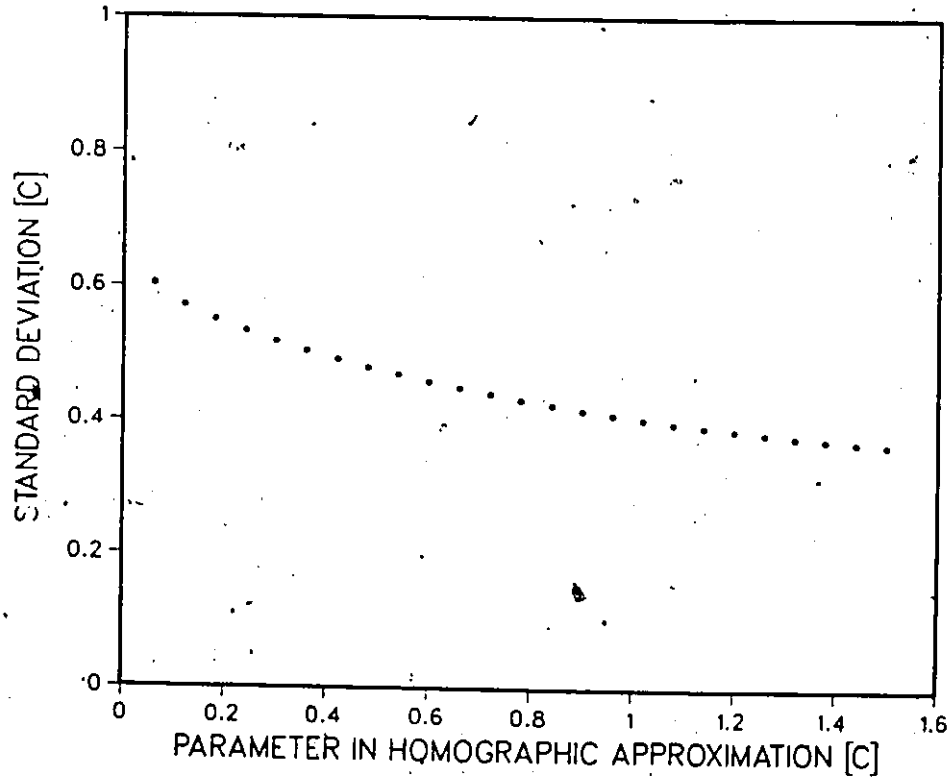

Fig.110 Effect of assumed mushy range on solution to test case#3 by Blanchard and Fremond's method, implicit finite element. Time step is 40000s.

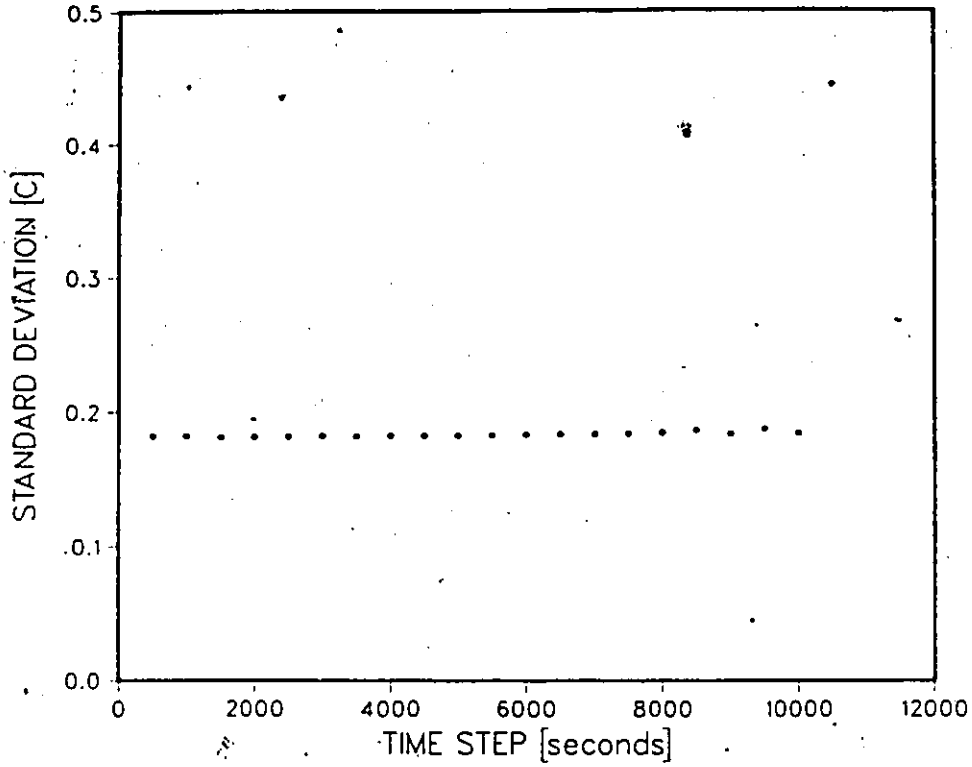

Fig.111 Effect of time step size on solution to test case#3 by post iterative (isothermal) method, explicit finite difference.

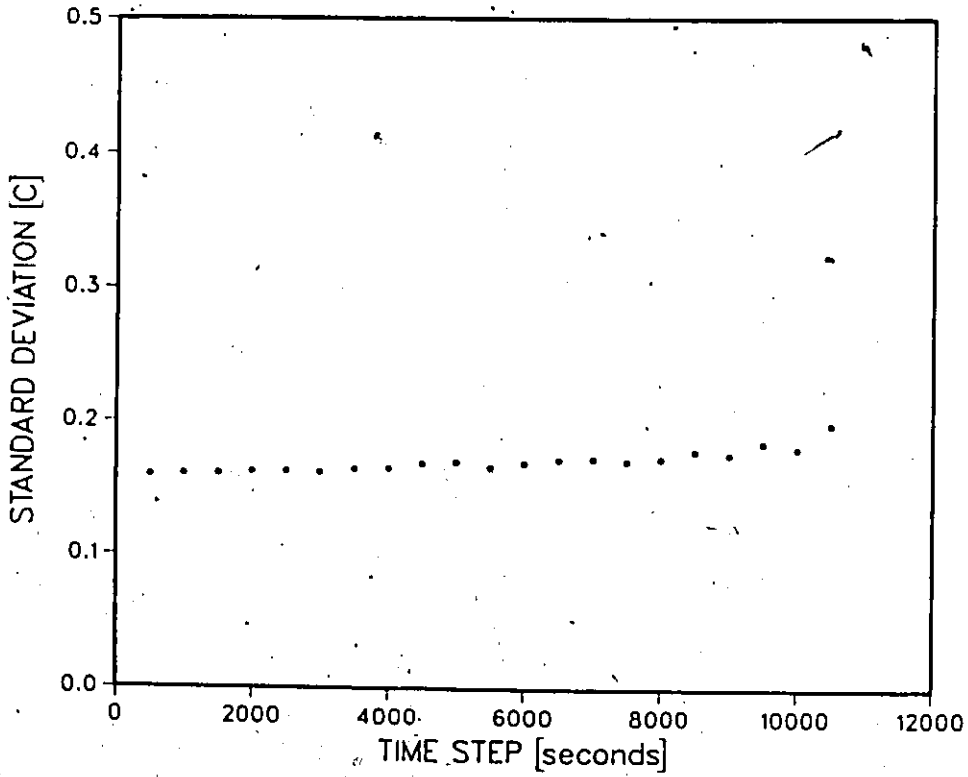

Fig.112 Effect of time step size on solution to test case#3 by post iterative method (mushy=-0.25 to +0.25 C), explicit finite difference.

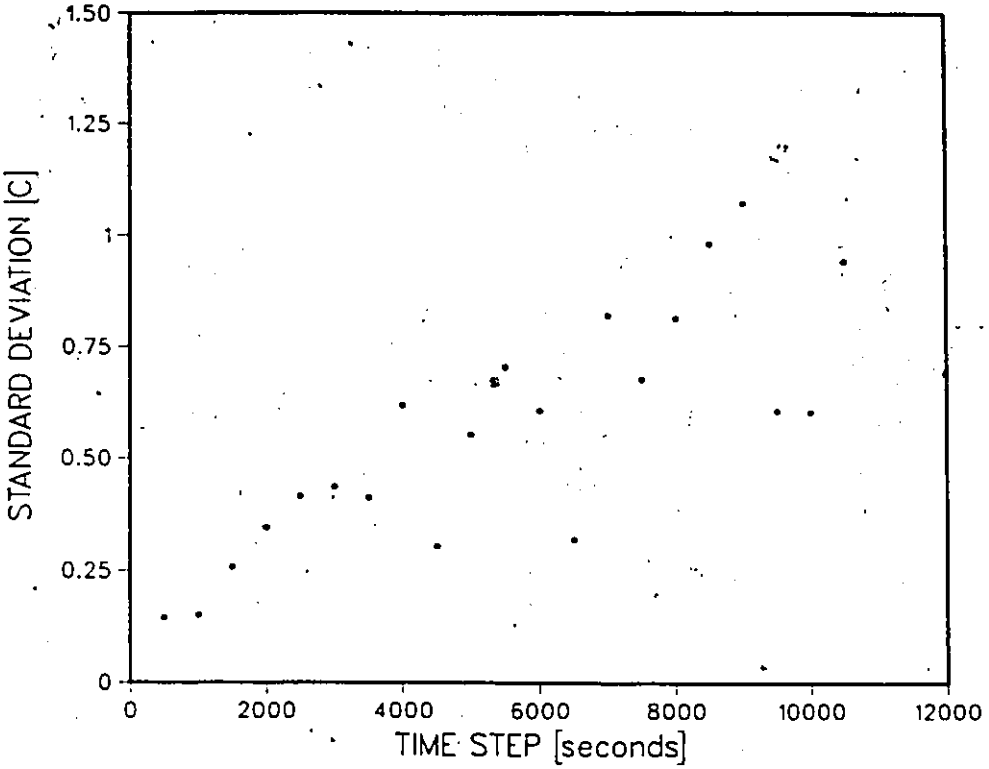

Fig.113 Effect of time step size on solution to test case#3 by apparent capacity method(mushy=-0.25 to +0.25 C), explicit finite difference.

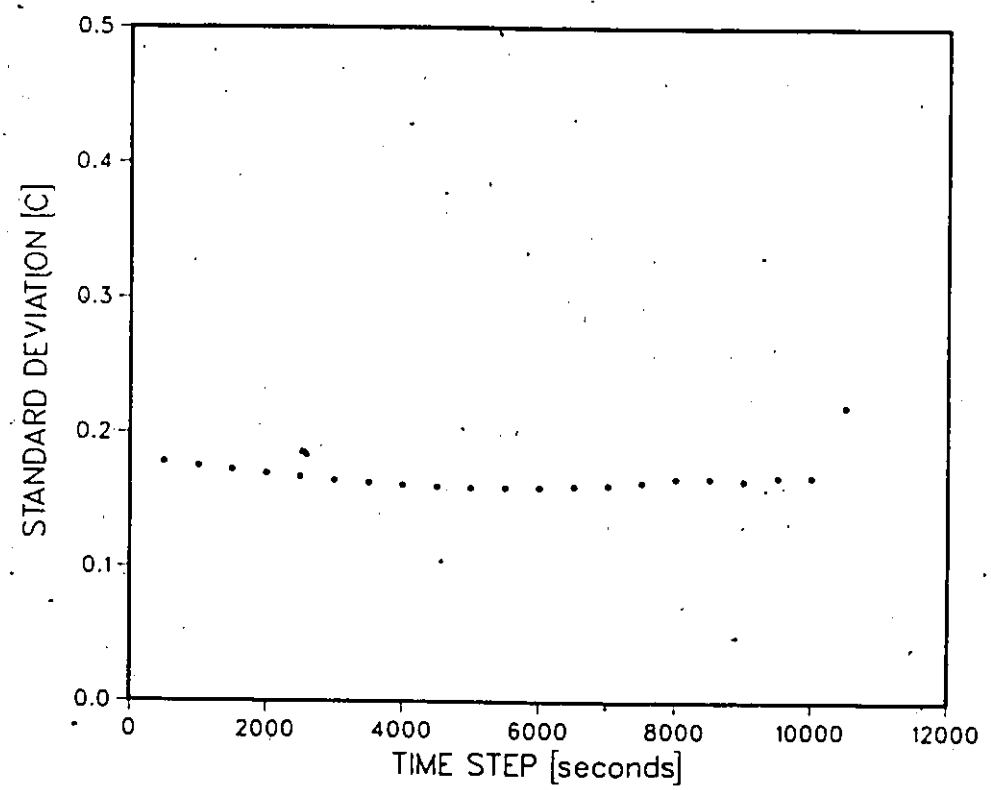

Fig.114 Effect of time step size on solution to test case#3 by enthalpy method (mushy=-0.25 to +0.25 C), explicit finite difference.

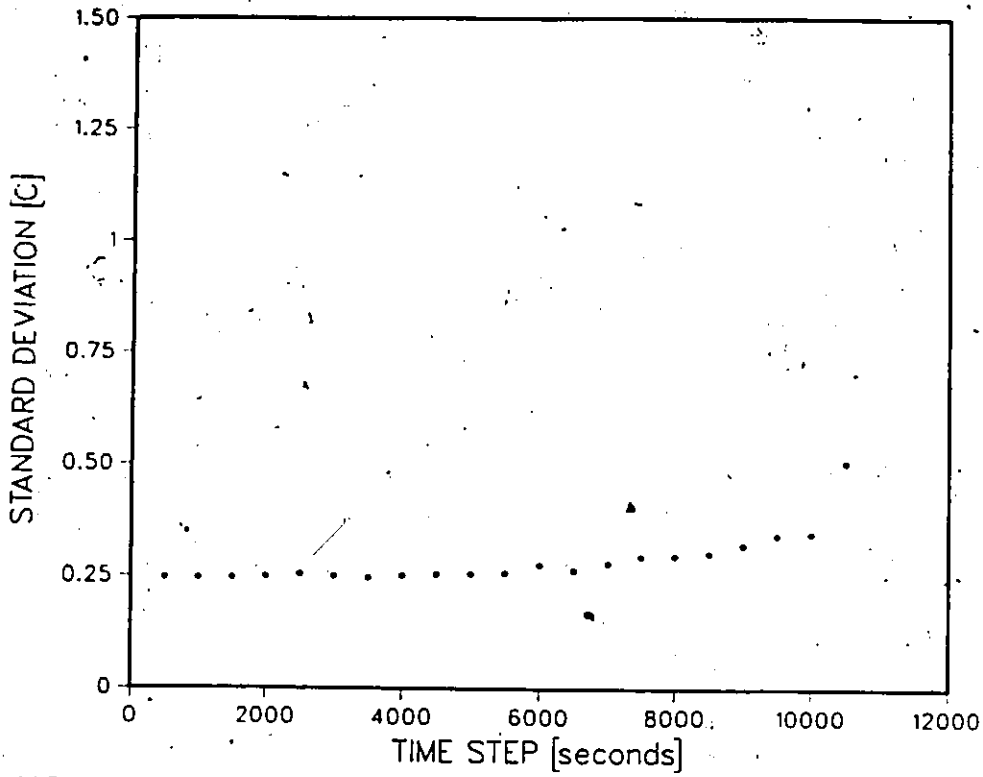

Fig.115 Effect of time step size on solution to test case#3 by effective capacity method(mushy=-0.25 to +0.25 C), explicit finite difference.

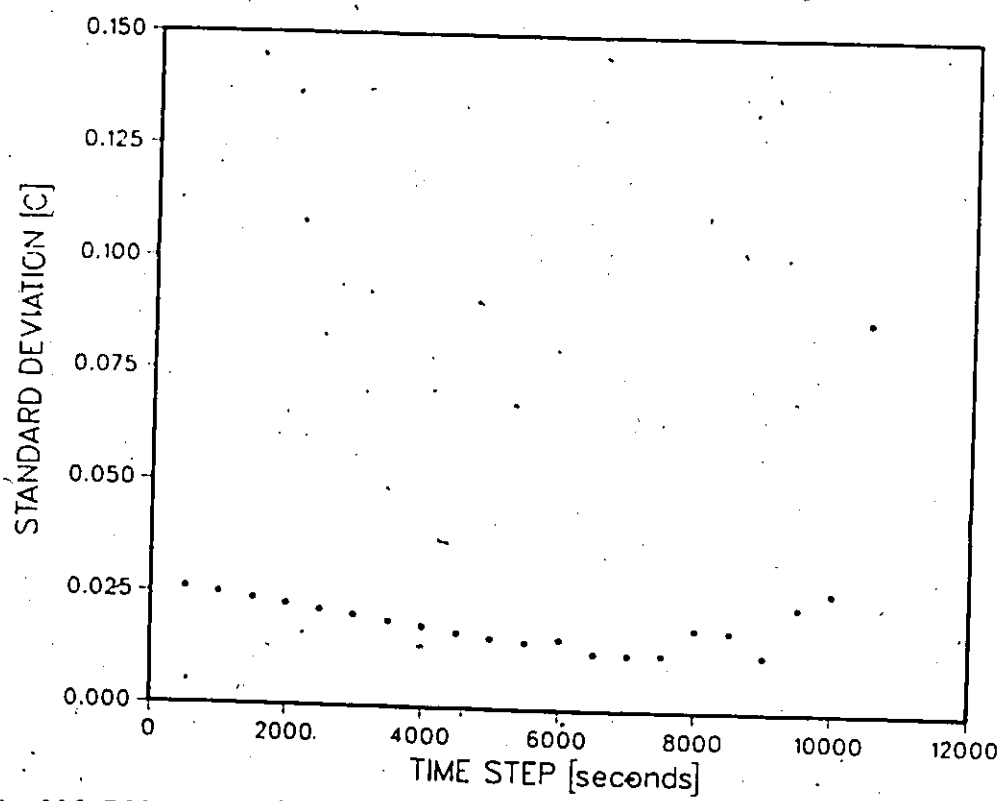

Fig.116 Effect of time step size on solution to test case#3 by Tacke's method, explicit finite difference.

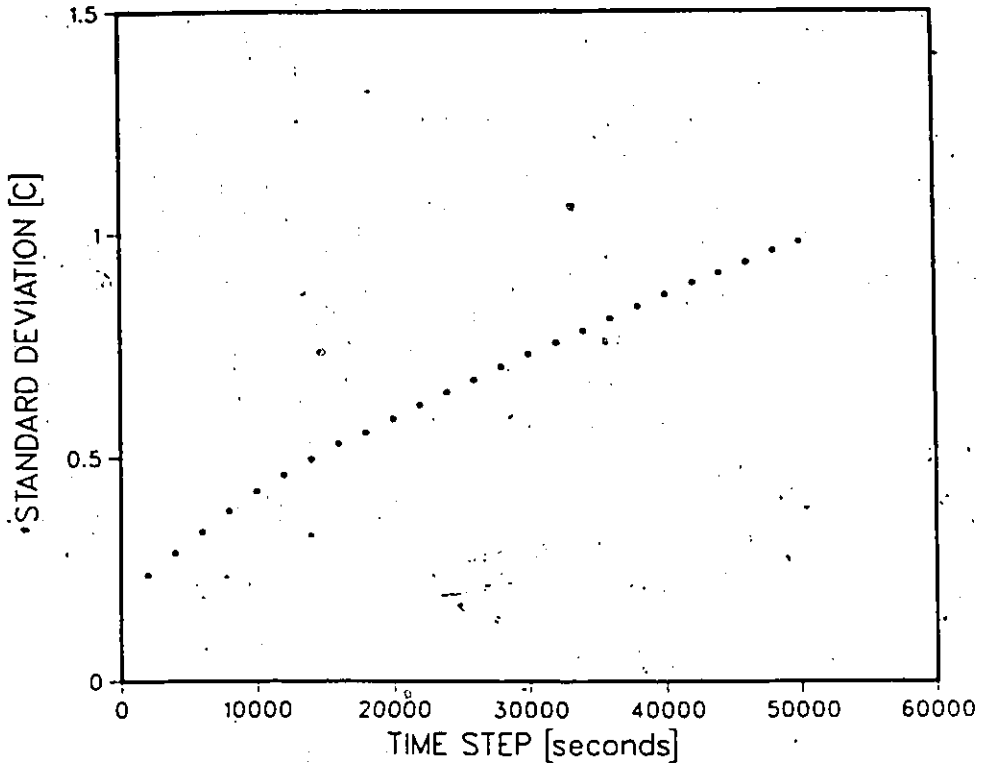

Fig.117 Effect of time step size on solution to test case#3 by post iterative (isothermal) method, implicit finite difference.

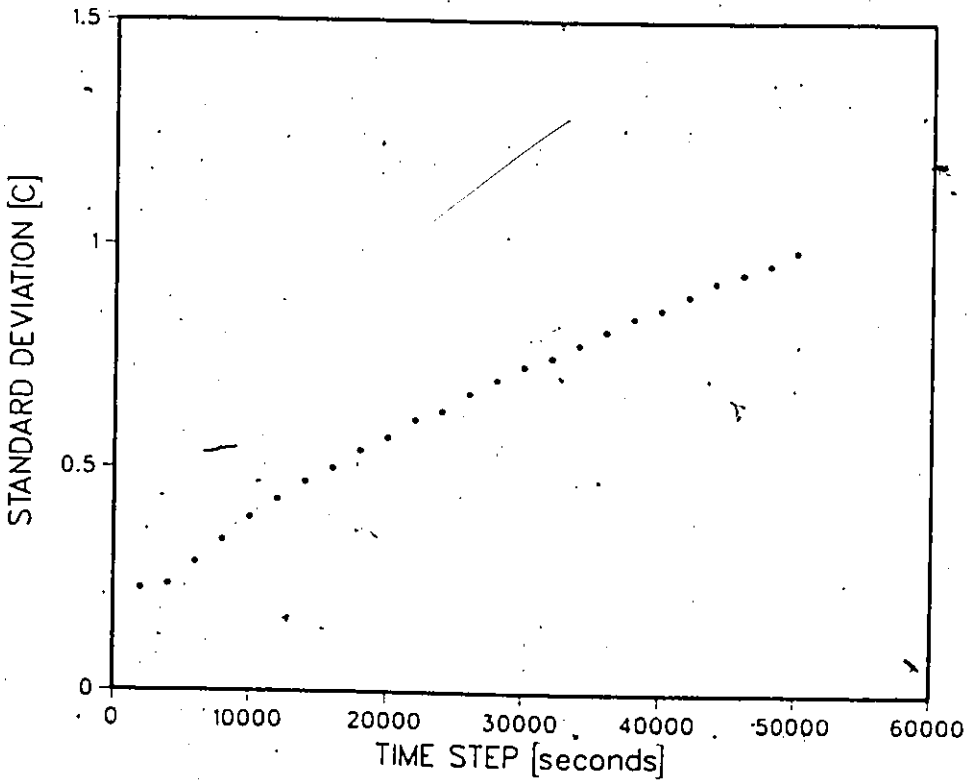

Fig.118 Effect of time step size on solution to test case#3 by post iterative (isothermal) method, implicit finite element.

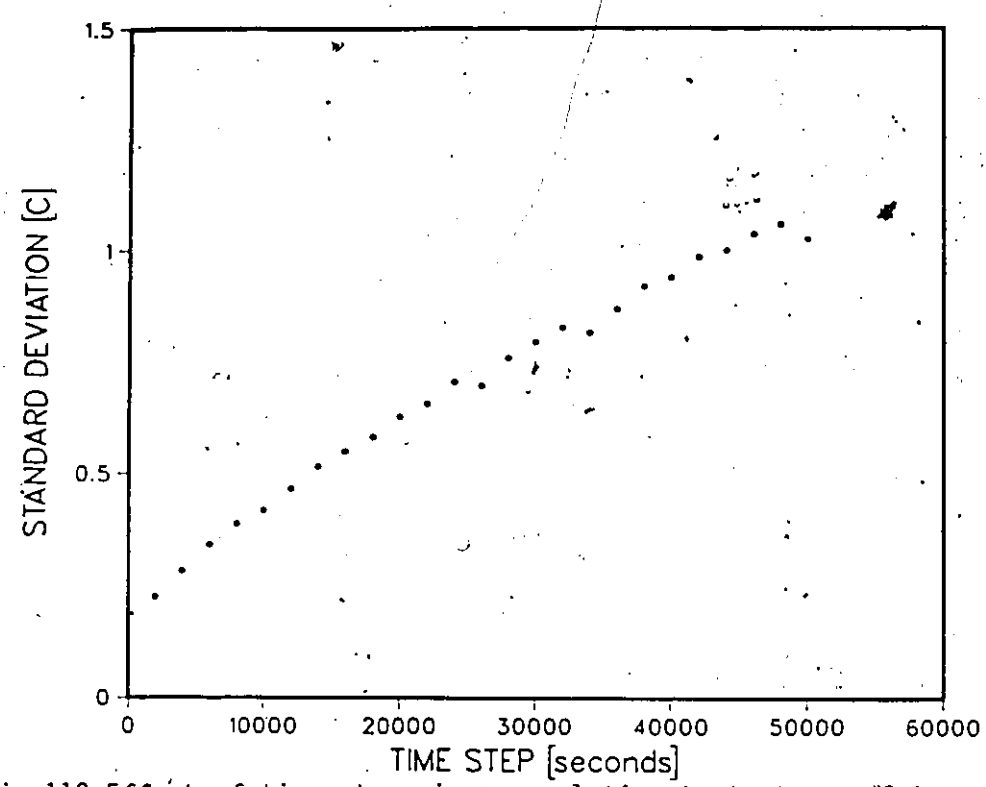

Fig.119 Effect of time step size on solution to test case#3 by post iterative method (mushy=-0.25 to +0.25 C), implicit finite difference.

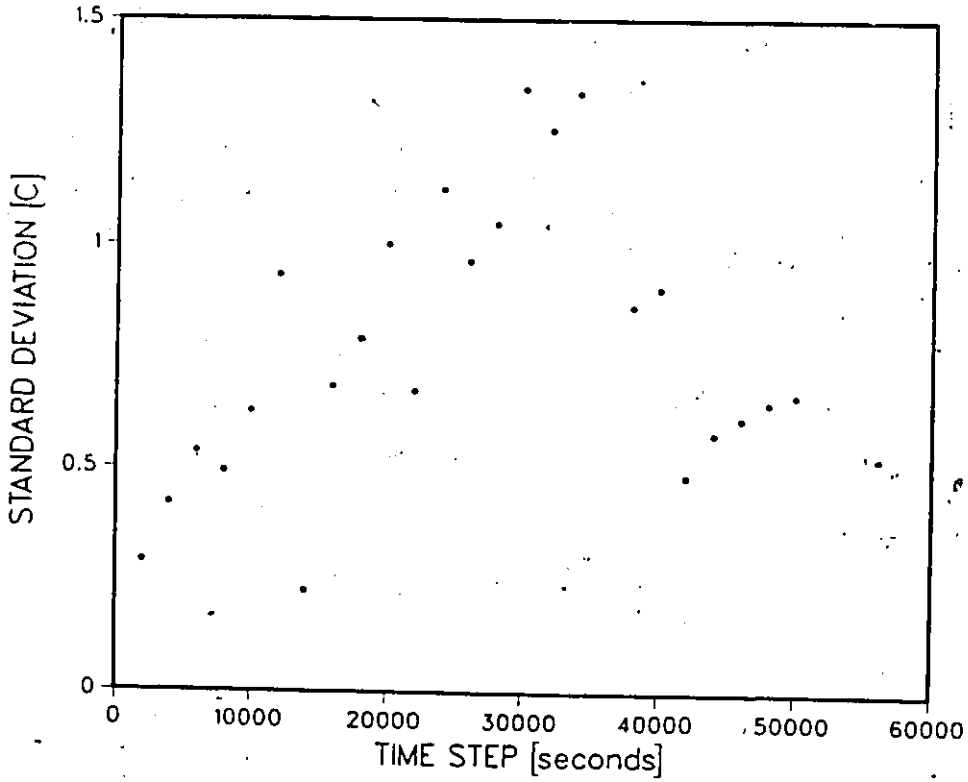

Fig.120 Effect of time step size on solution to test case#3 by apparent capacity method(mushy=-0.25 to +0.25 C), implicit finite difference.

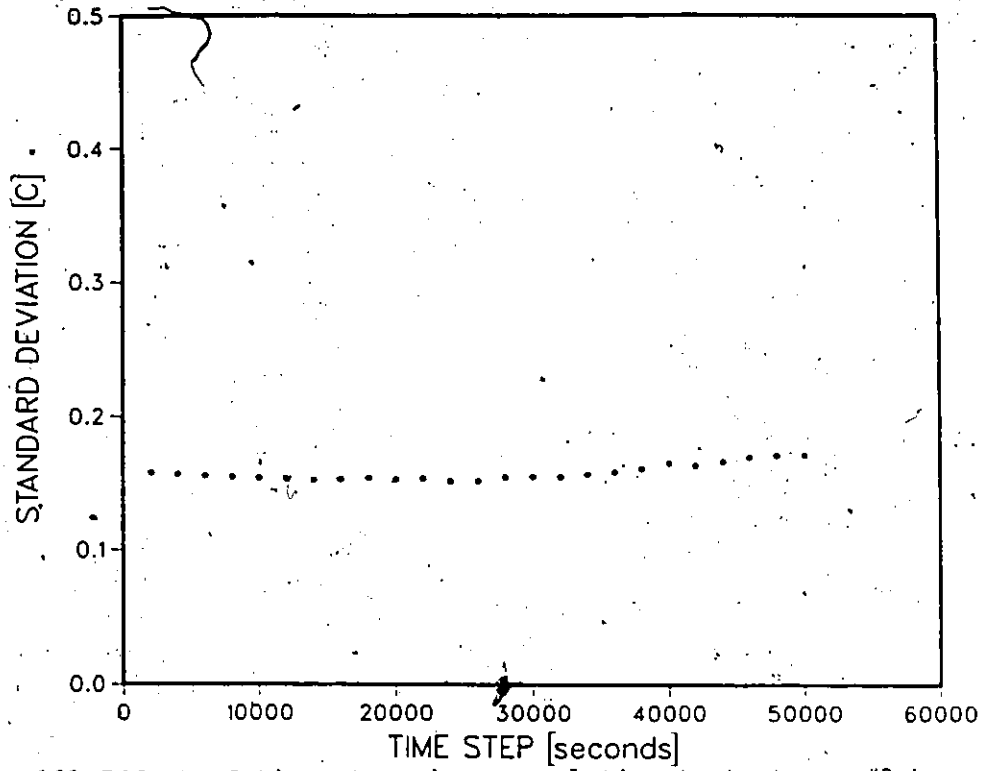

Fig.121 Effect of time step size on solution to test case#3 by enthalpy method (mushy=-0.25 to +0.25 C), implicit finite difference.

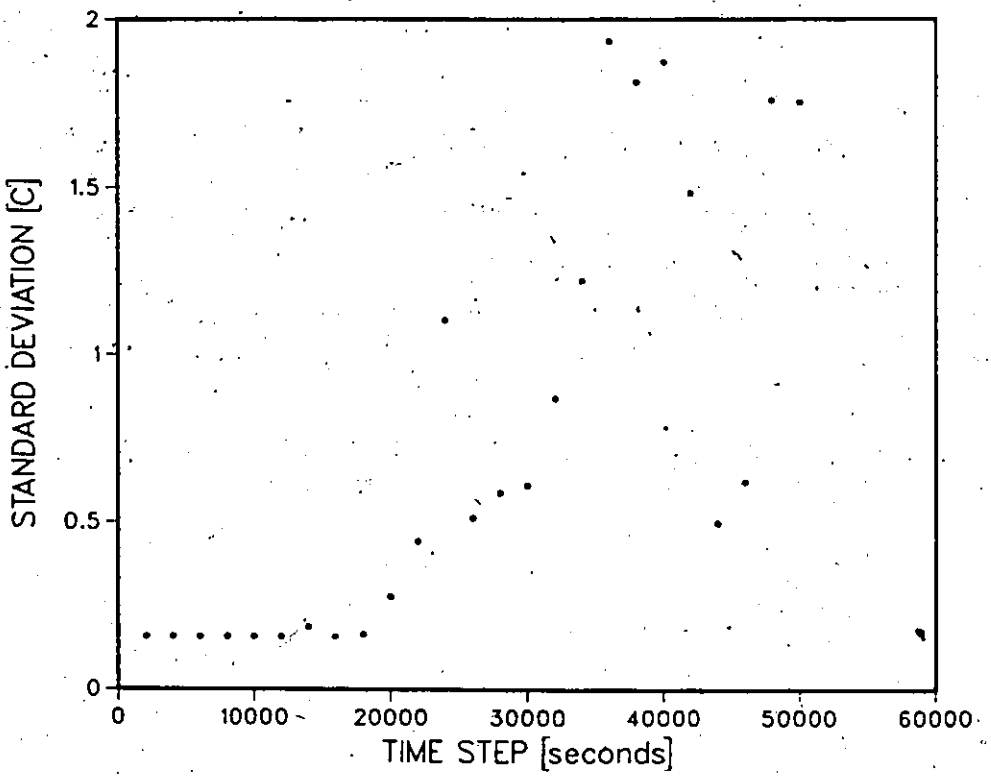

Fig.122 Effect of time step size on solution to test case#3 by Pham's method (mushy=-0.25 to +0.25 C), implicit finite difference.

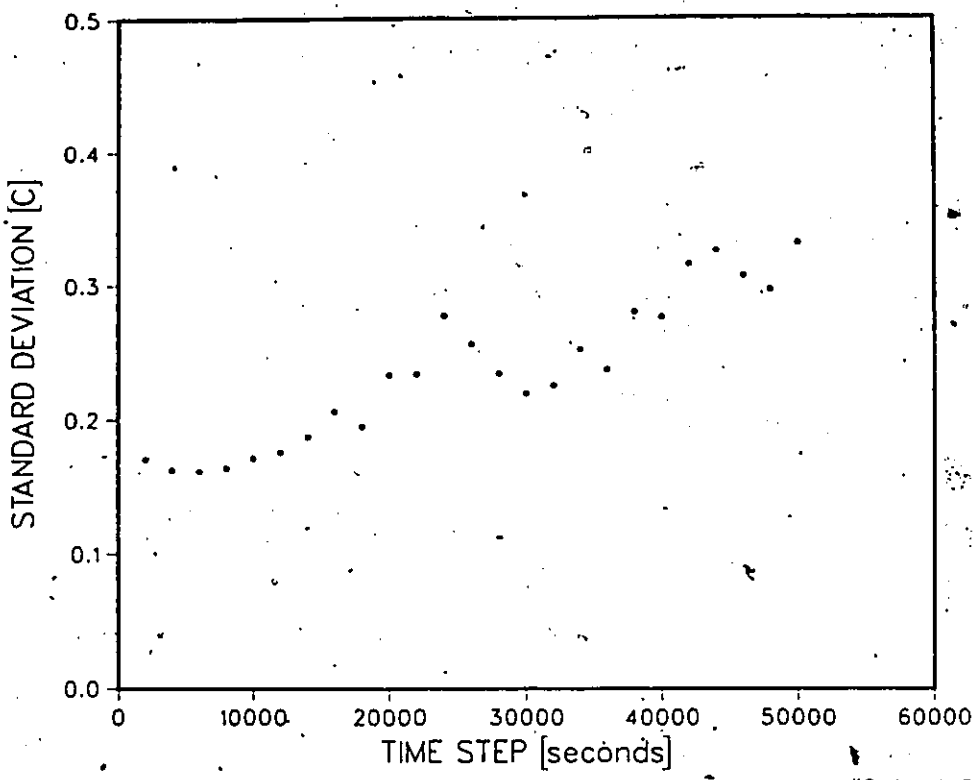

Fig.123 Effect of time step size on solution to test case#3 by effective capacity method(mushy=-0.25 to +0.25 C), implicit finite difference.

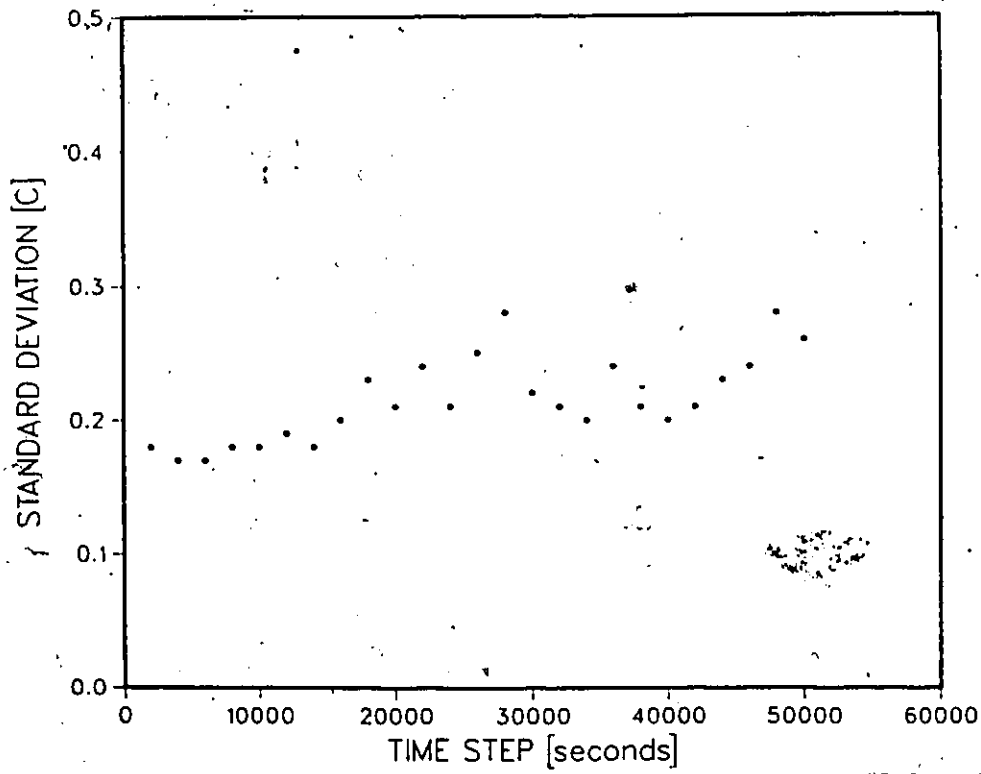

Fig.124 Effect of time step size on solution to test case#3 by effective capacity method(mushy=-0.25 to +0.25 C), implicit finite element.

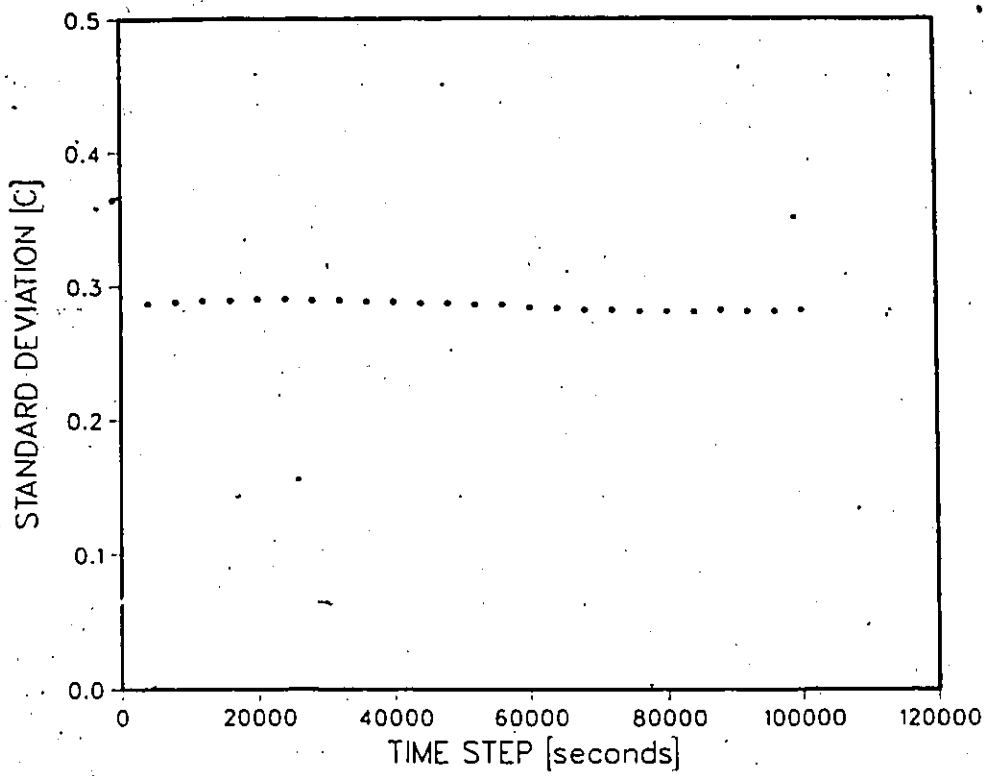

Fig.125 Effect of time step size on solution to test case#3 by Blanchard and Fremond's method (parameter=0.5 C), implicit finite difference.

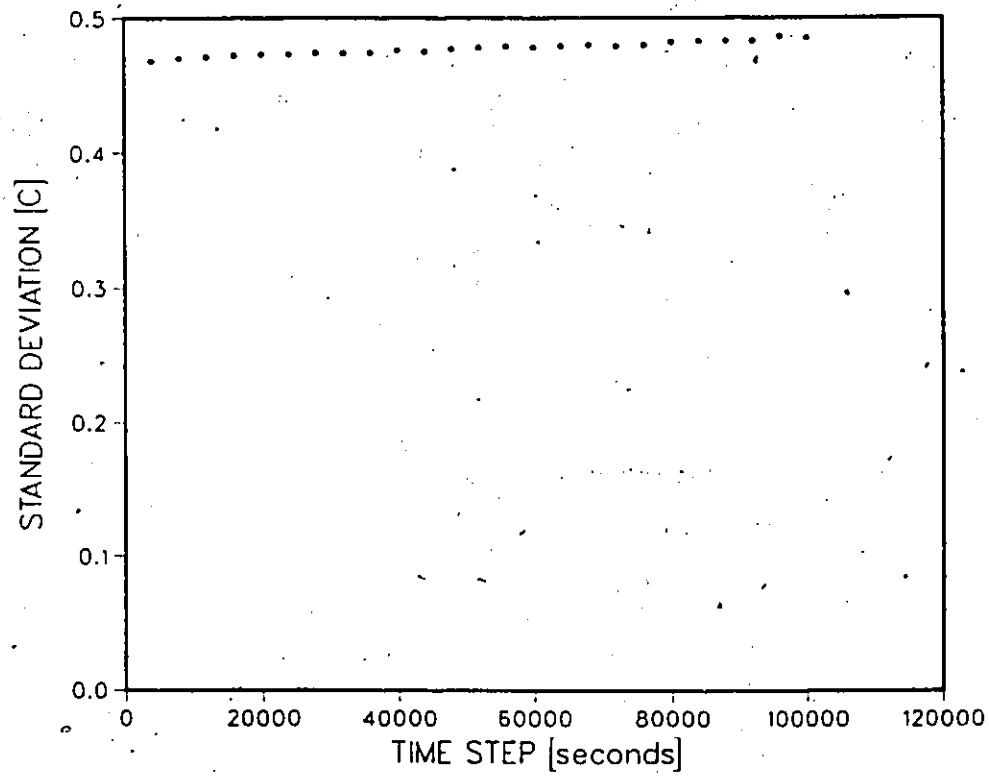

Fig.126 Effect of time step size on solution to test case#3 by Blanchard and Fremond's method (parameter=0.5 C), implicit finite element.

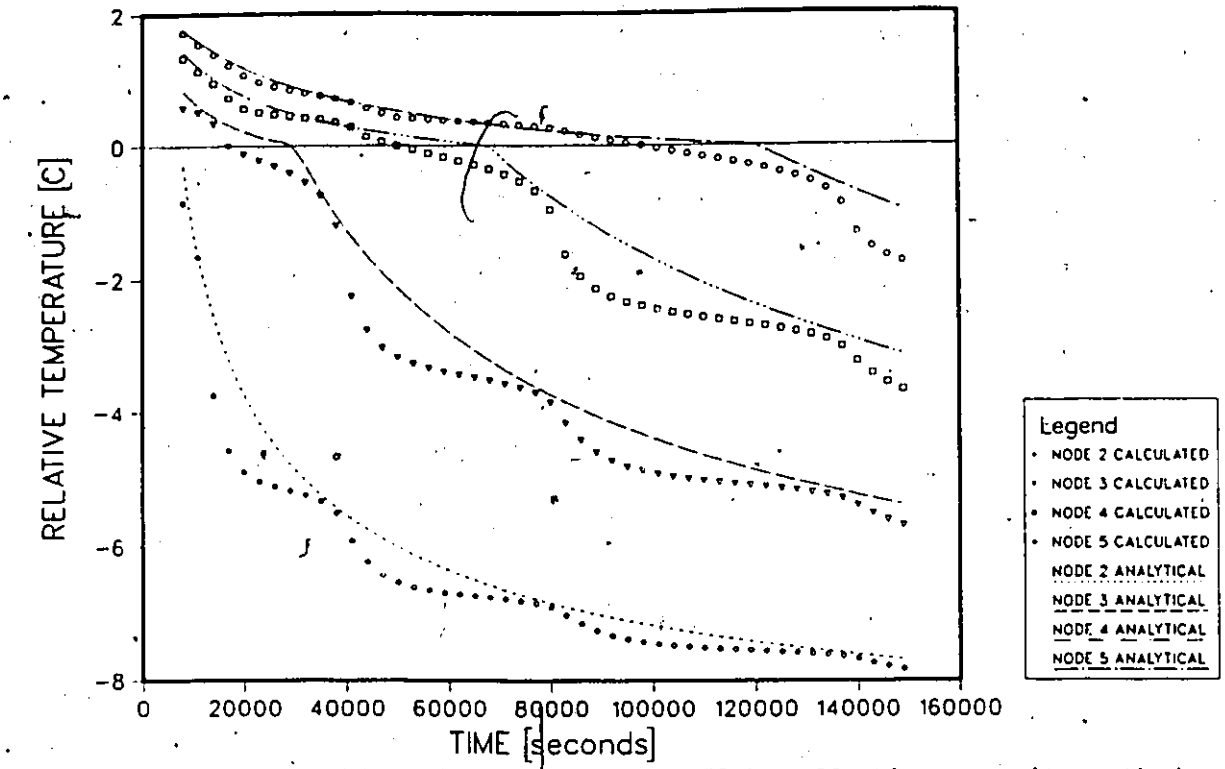

Fig.127 Temperature histories for test case#3 by effective capacity method (mushy=-0.25 to +0.25 C), implicit finite difference. Time step 3000s.

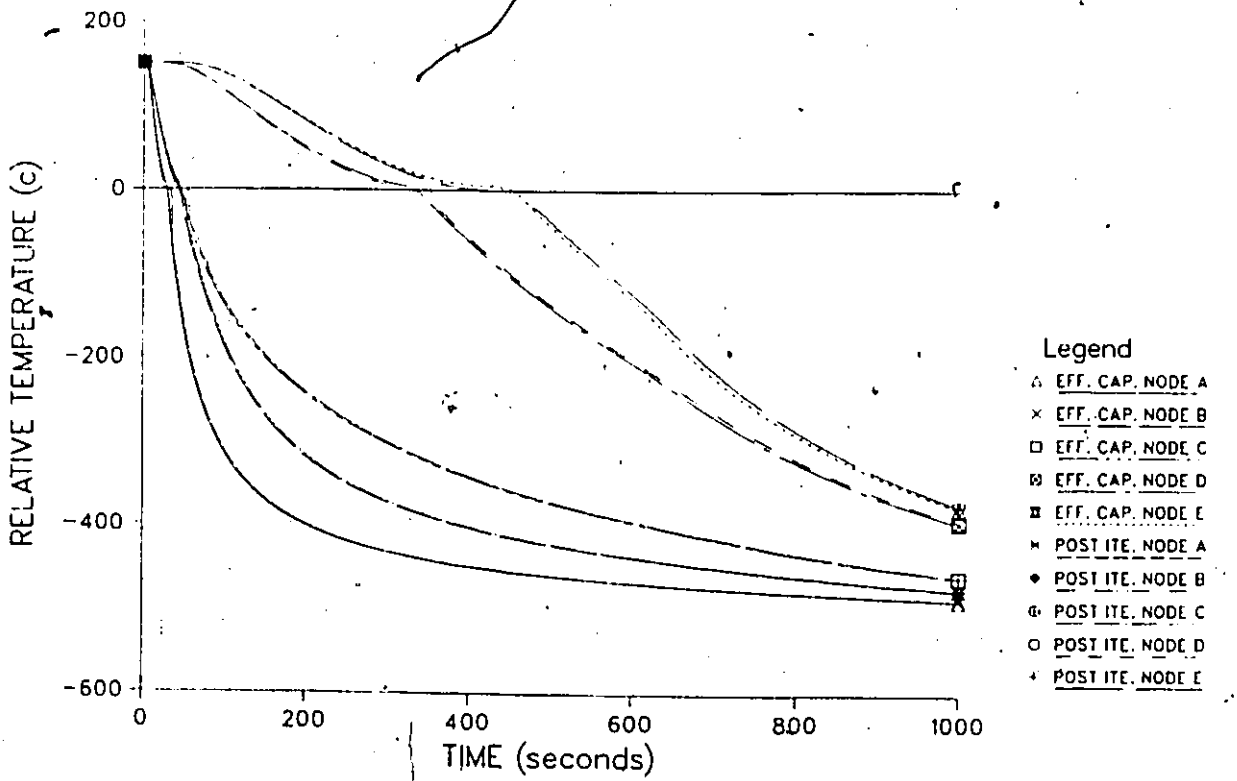

Fig.128 Converged solution for test case#4, time step is 1.0 s, and spatial increment is 0.002 m.

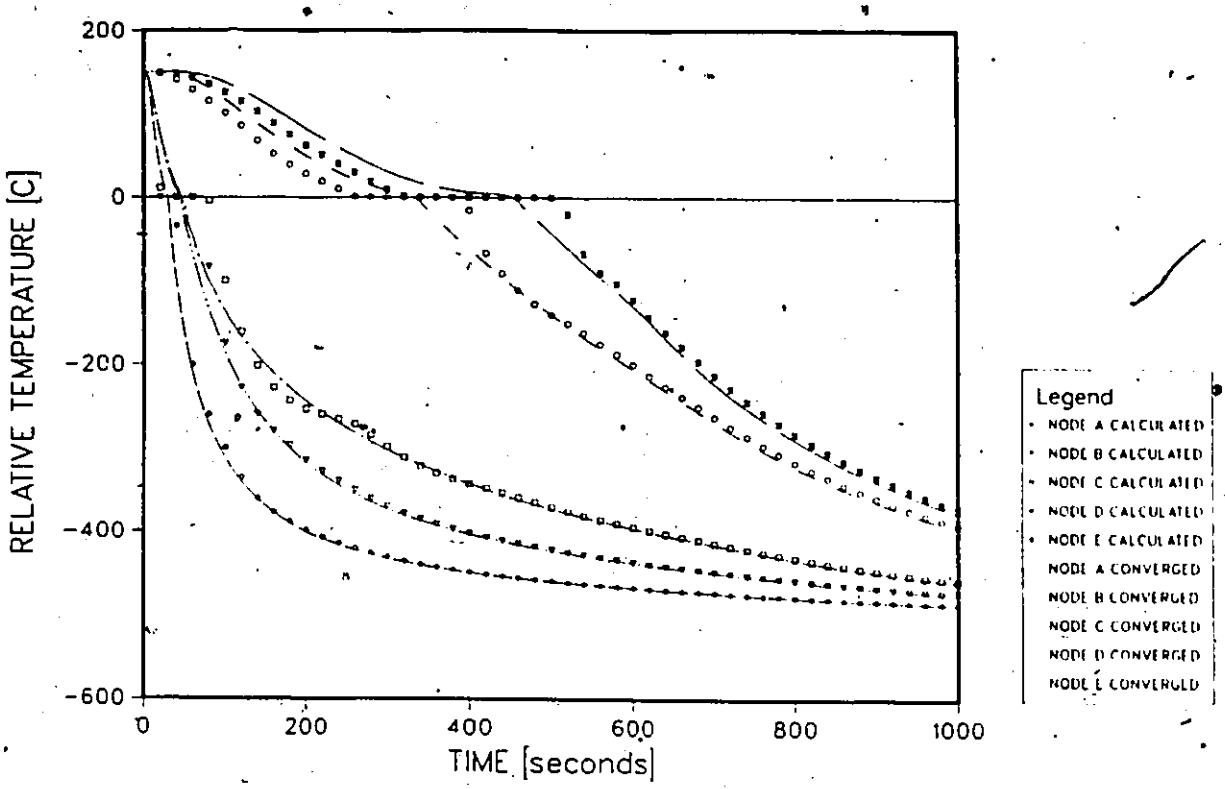

Fig.129 Temperature histories for test case#4 by post iterative (isothermal) method, implicit finite difference. Time step is 20 s.

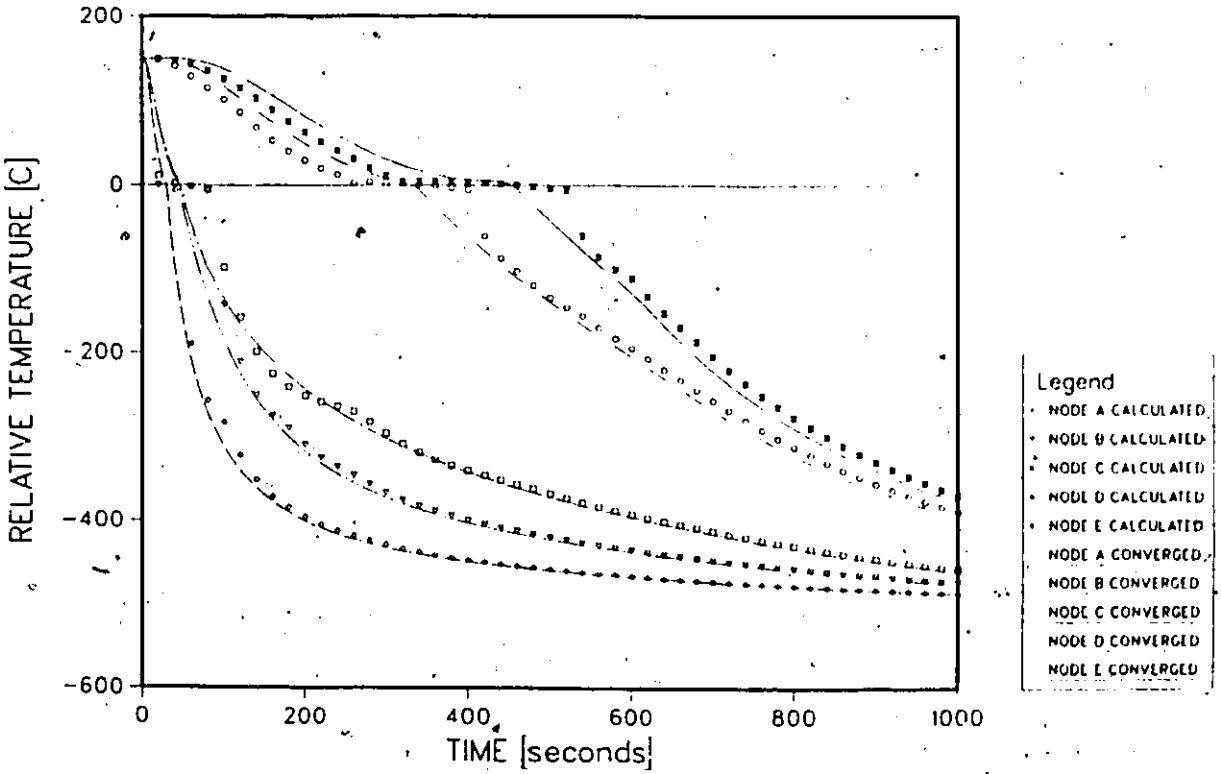

Fig.130 Temperature histories for test case#4 by post iterative method (mushy=-5. to +5. C), implicit finite difference. Time step is 20s.

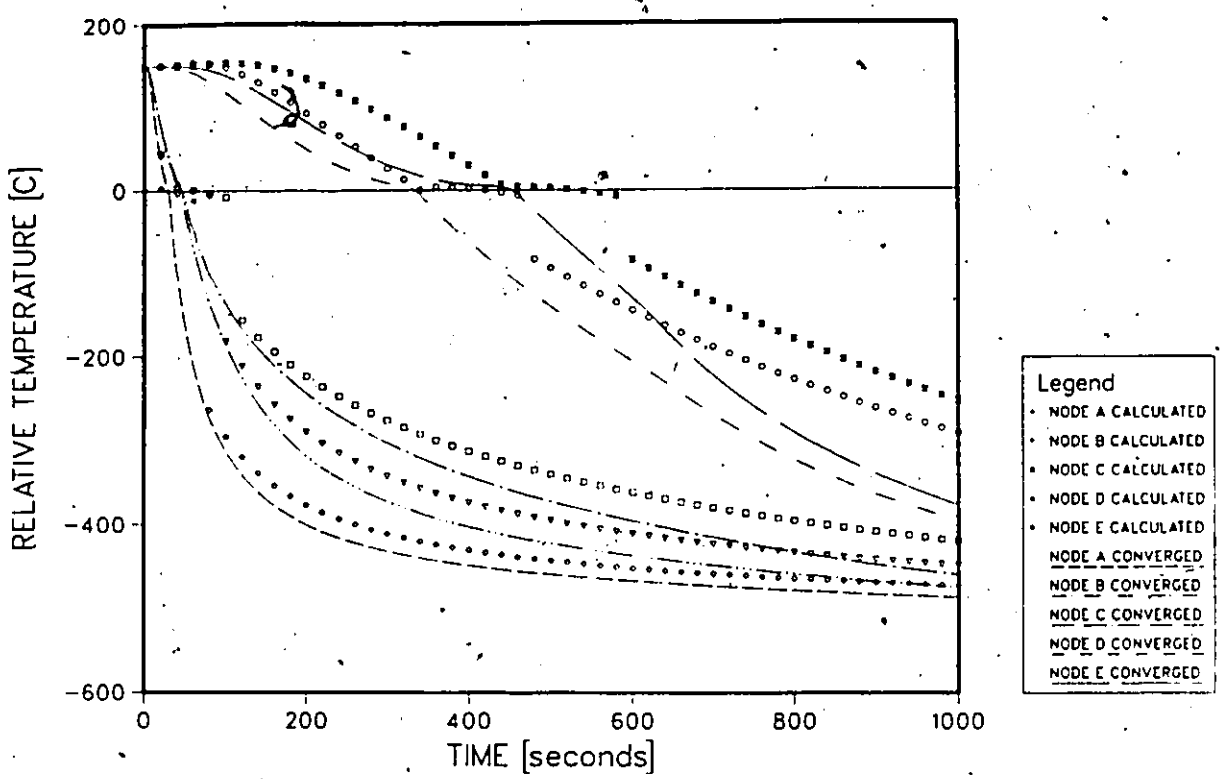

Fig.131 Temperature histories for test case#4 by post iterative method (mushy=-5. to +5. C), implicit finite element. Time step is 20s.

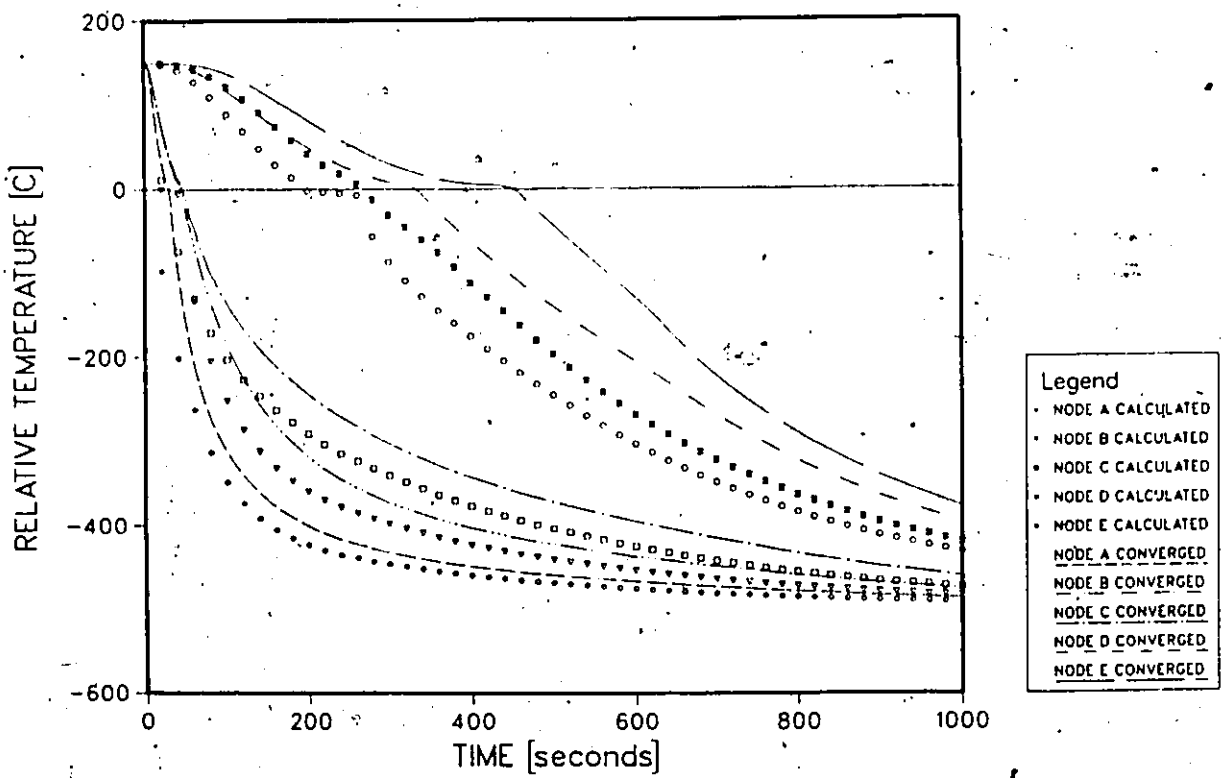

Fig.132 Temperature histories for test case#4 by apparent capacity method (mushy=-5. to +5. C), implicit finite difference. Time step is 20s.

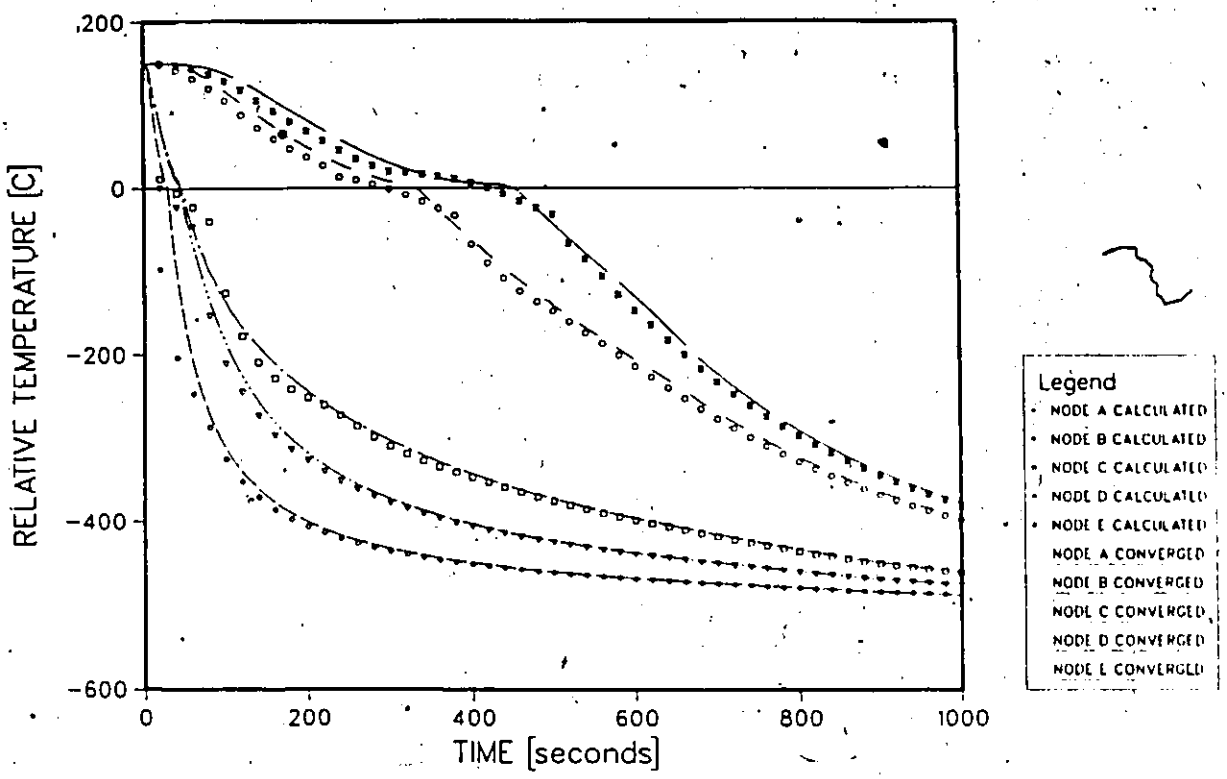

Fig.133 Temperature histories for test case#4 by apparent capacity method (mushy=-25. to +25. C), implicit finite difference. Time step is 20s.

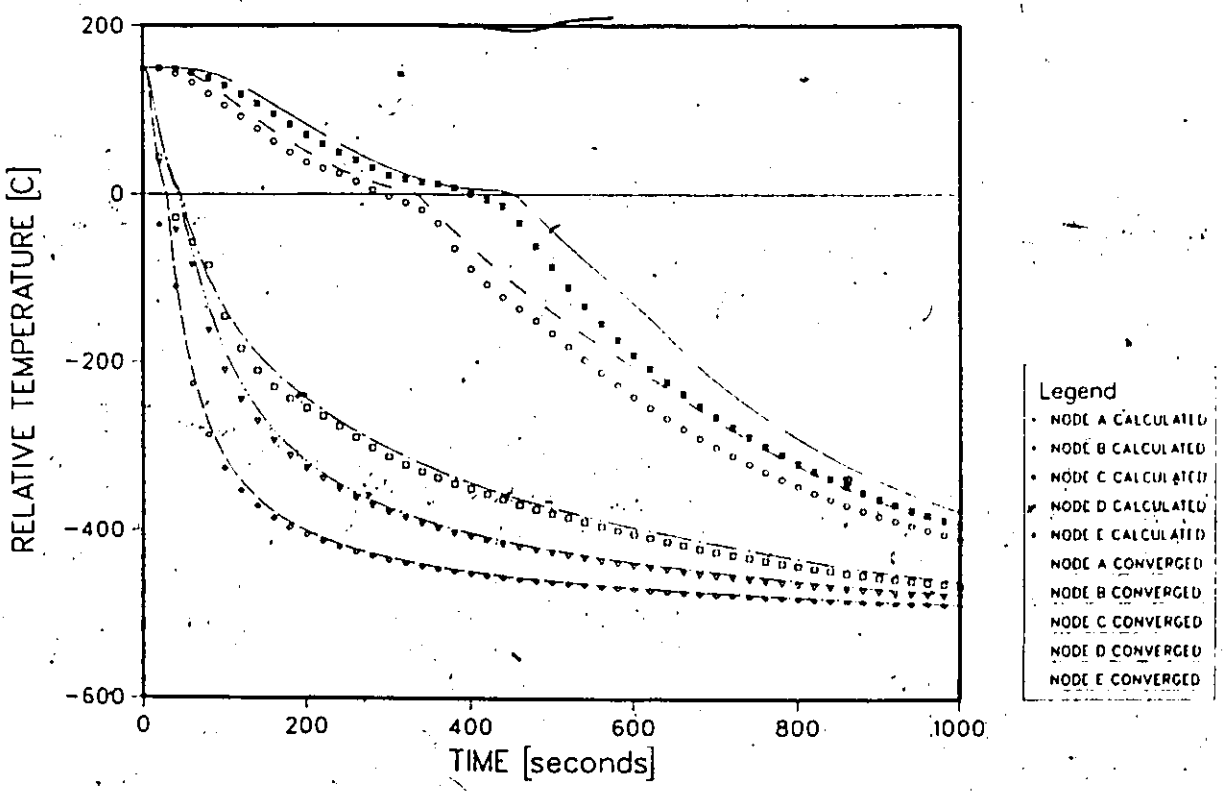

Fig.134 Temperature histories for test case#4 by effective capacity method (mushy=-5. to +5. C), implicit finite difference. Time step is 20s.

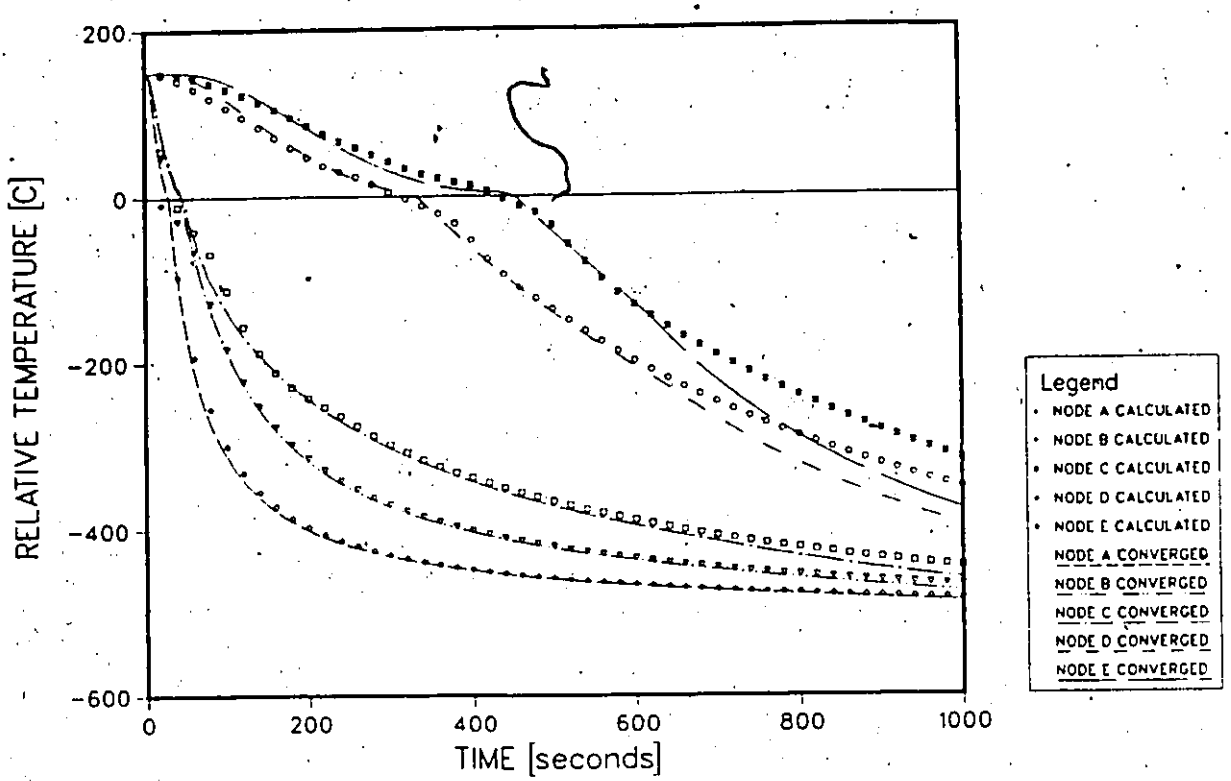

Fig.135 Temperature histories for test case#4 by effective capacity method (mushy=-5. to +5. C), implicit finite element. Time step is 20s.

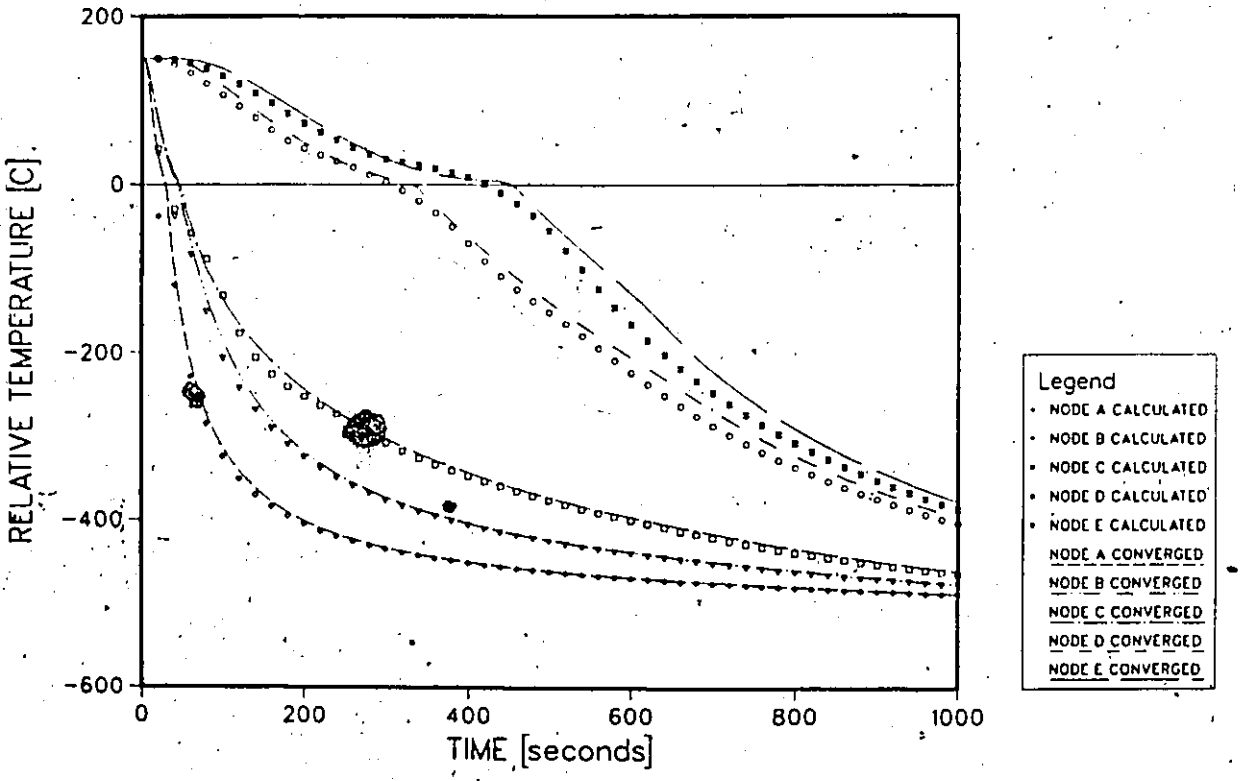

Fig.136 Temperature histories for test case#4 by effective capacity method (mushy=-25. to +25. C), implicit finite difference. Time step is 20s.

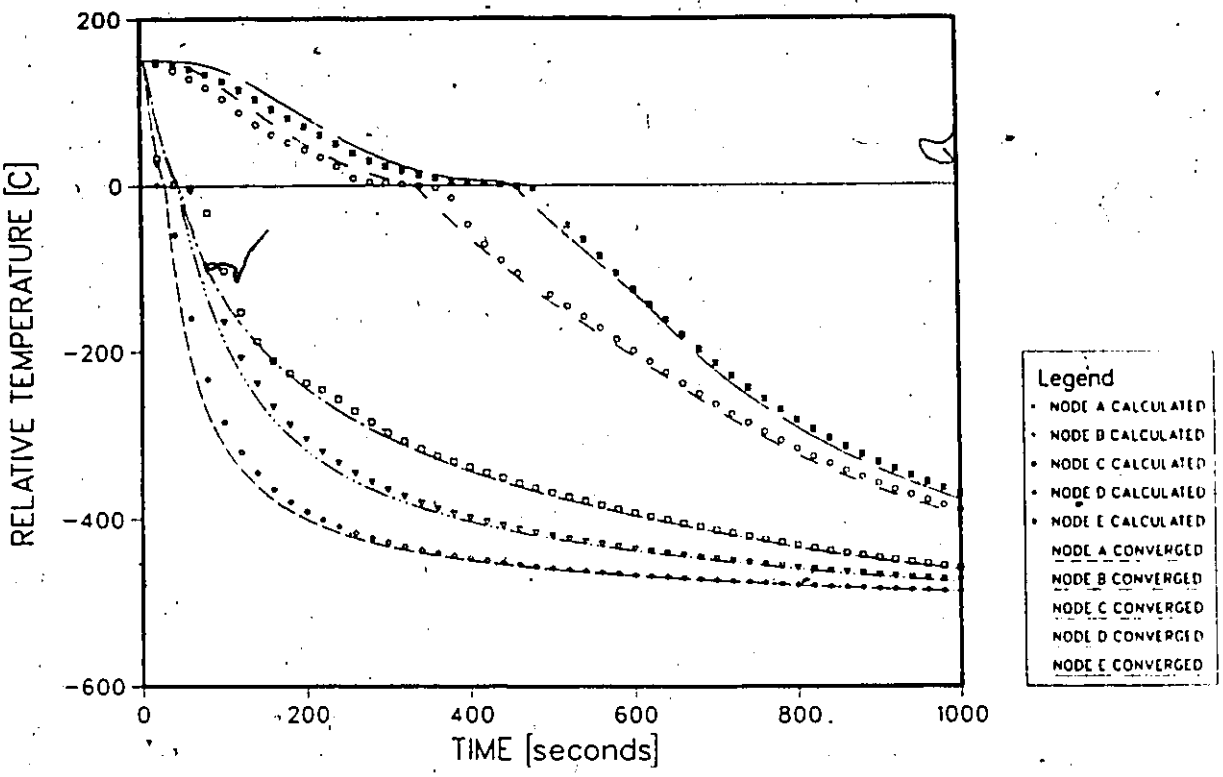

Fig.137 Temperature histories for test case#4 by enthalpy method (mushy= -5. to +5. C), implicit finite difference. Time step is 20s.

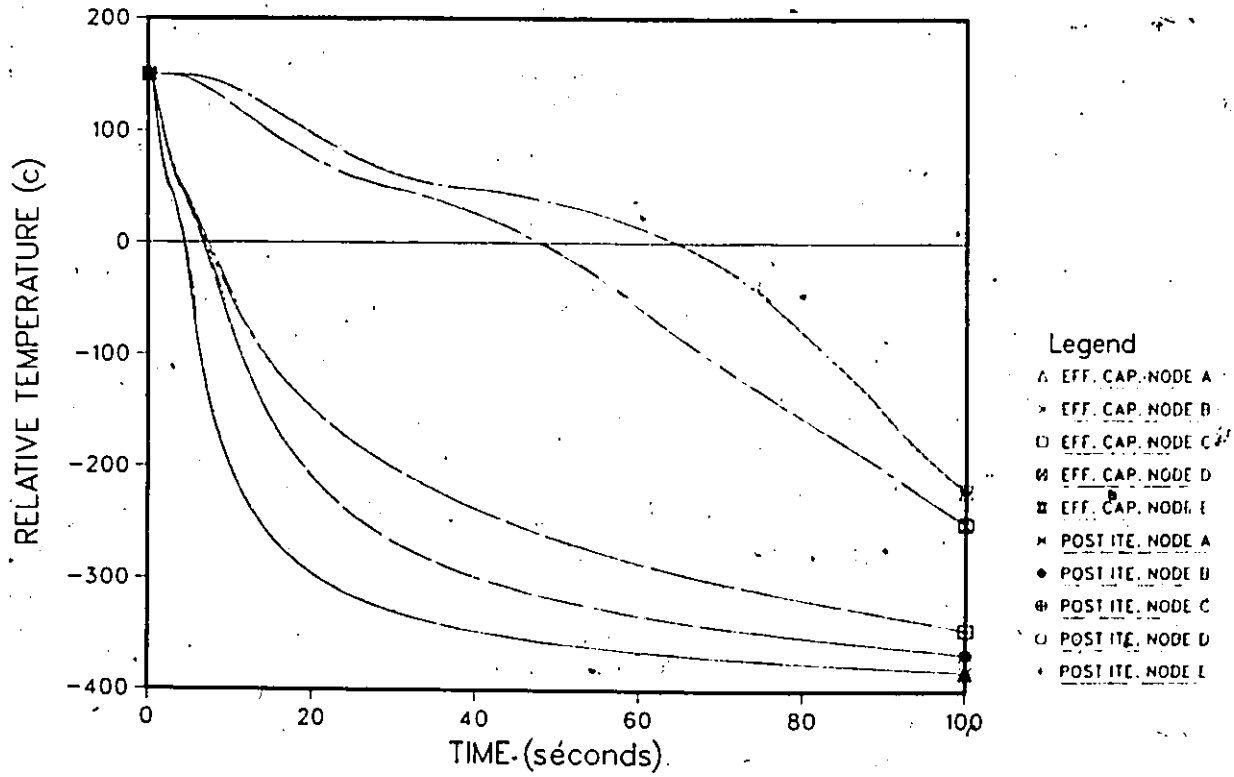

Fig.138 Converged solution to test case#5, time step is 0.1s and spatial increment is 0.005m.

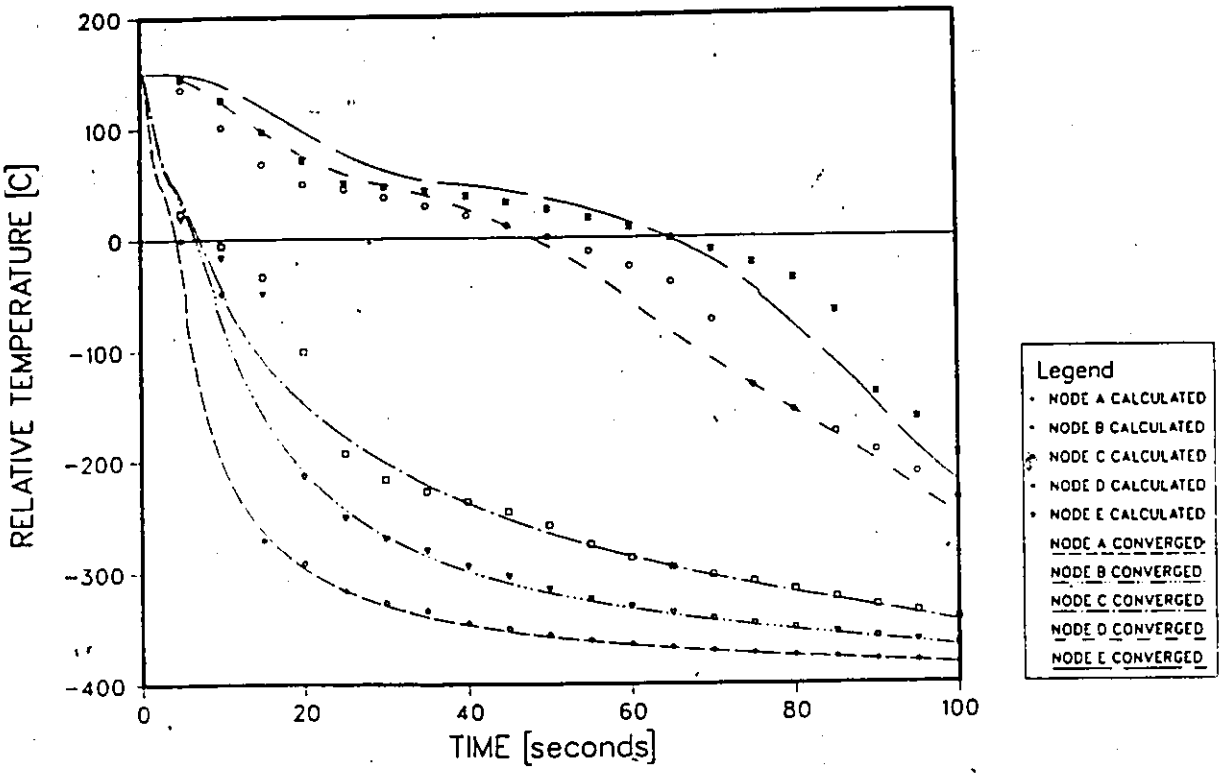

Fig.139 Temperature histories for test case#5 by post iterative method, implicit finite difference. Time step is 5s.

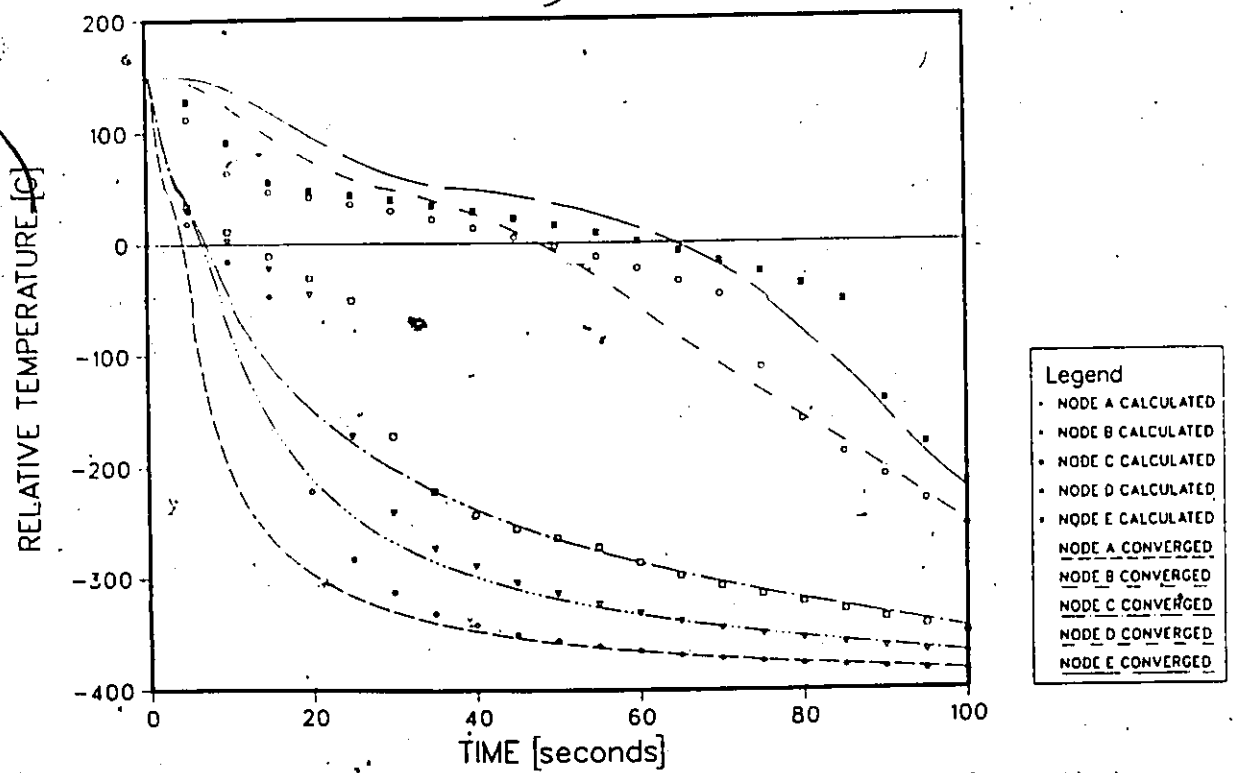

Fig.140 Temperature histories for test case#5 by post iterative method, implicit finite element. Time step is 5s.

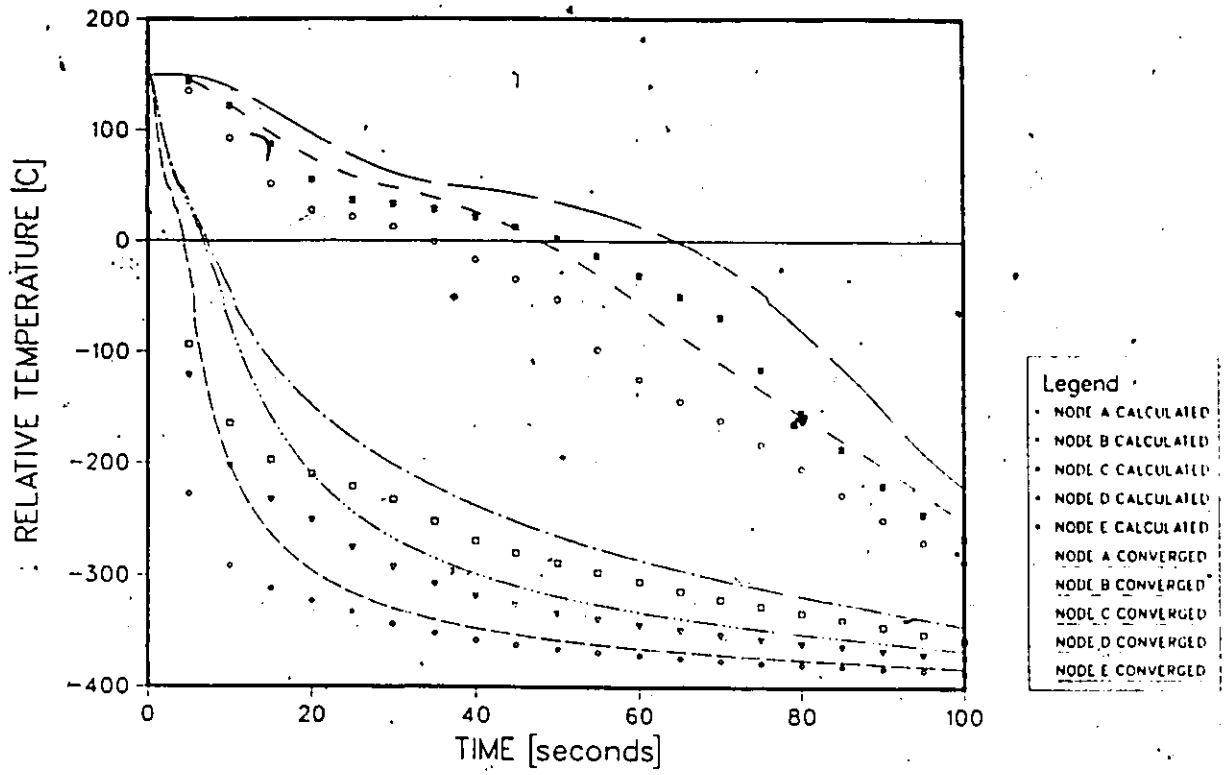

Fig.141 Temperature histories for test case#5 by apparent capacity method, implicit finite difference. Time step is 5s.

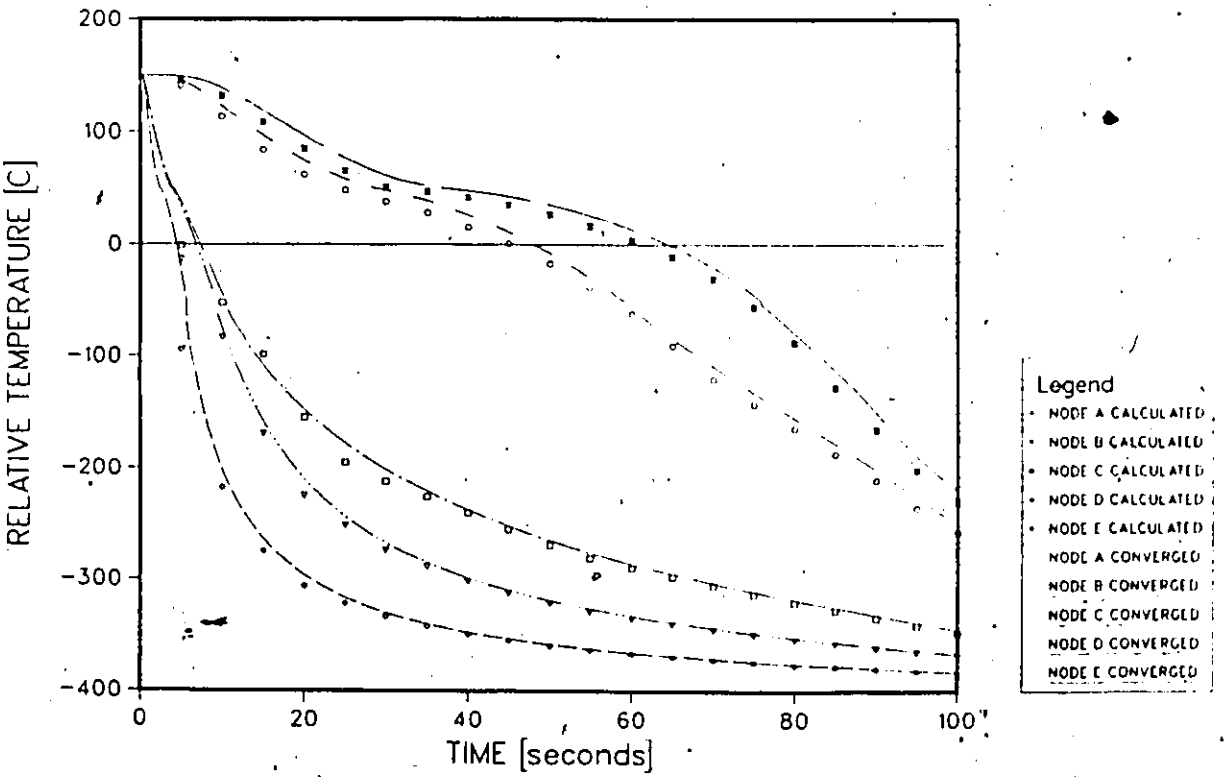

Fig.142 Temperature histories for test case#5 by effective capacity method, implicit finite difference. Time step is 5s.

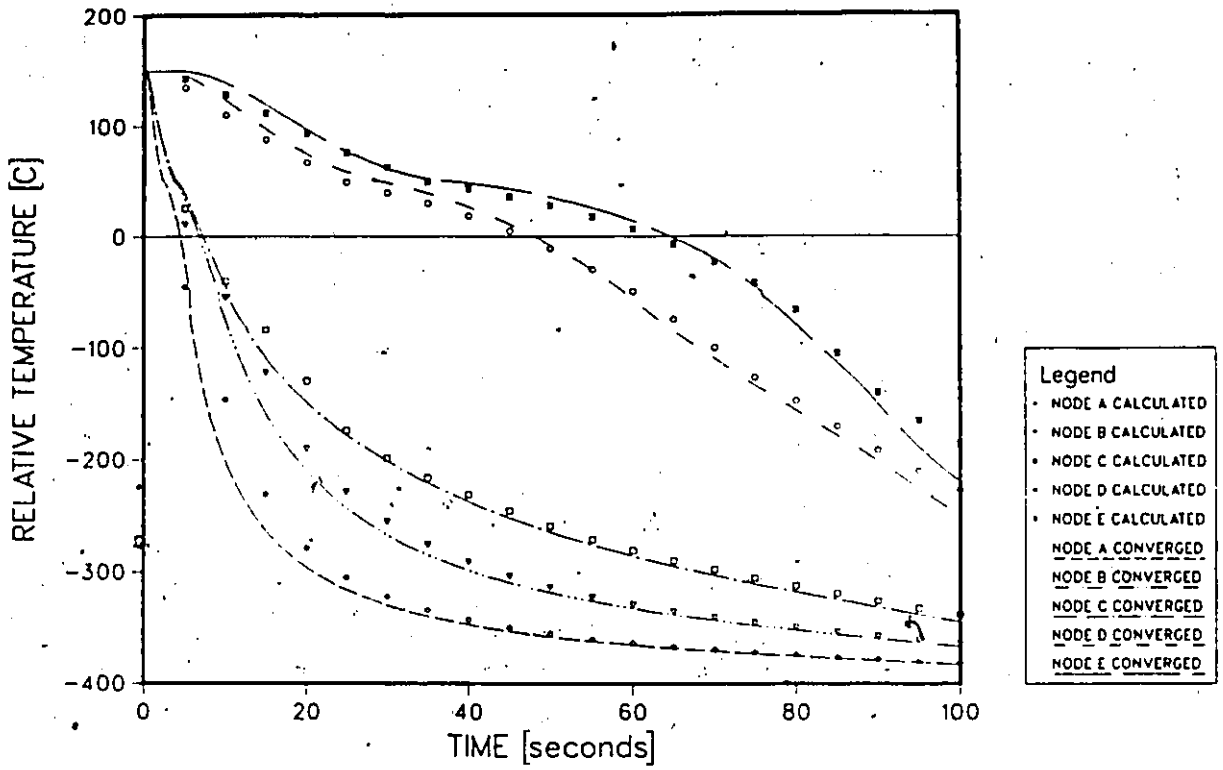

Fig.143 Temperature histories for test case#5 by effective capacity method, implicit finite element. Time step is 5s.

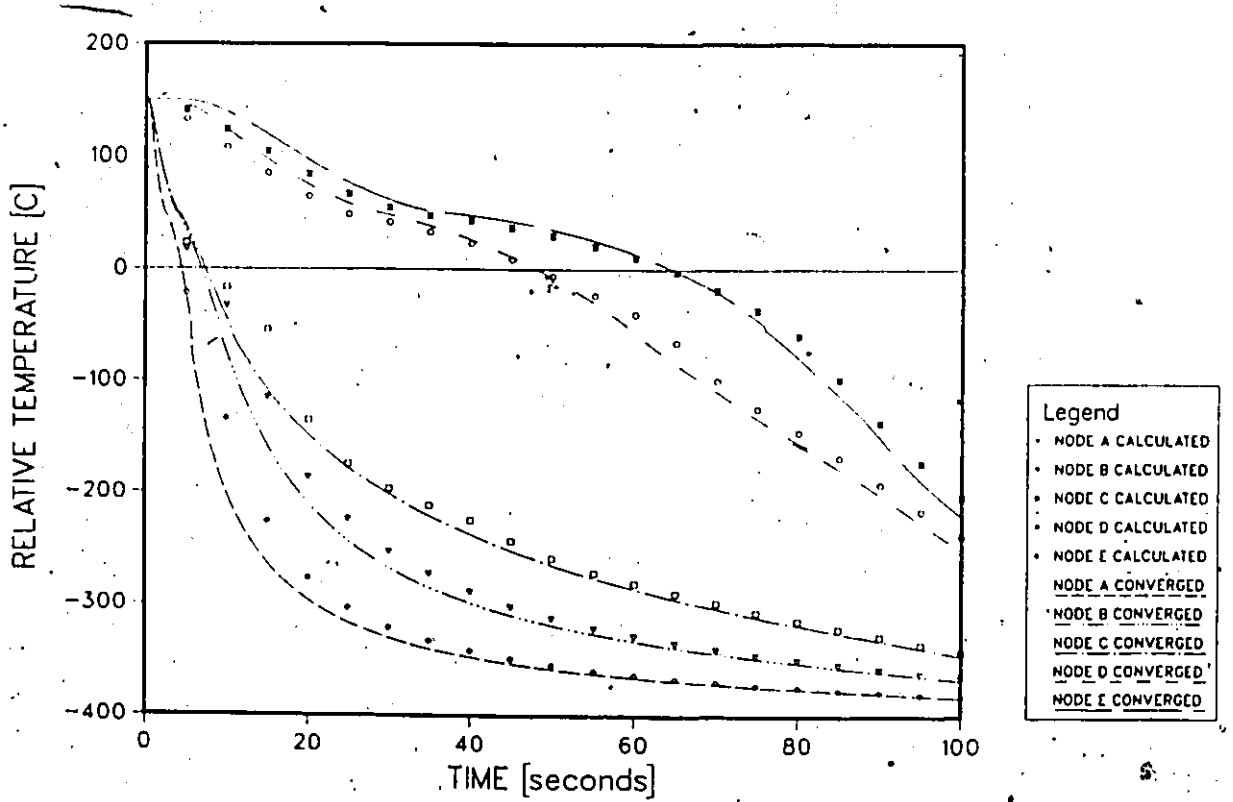

Fig.144 Temperature histories for test case#5 by enthalpy method, implicit finite difference. Time step is 5s.

REFERENCES

1. Salcudean, M., Abdullah, Z., "Numerical Simulation of Casting Processes," to be presented at International Heat Transfer Conference in August, 1986.

2. Erickson, W.C., "Computer Simulation of Solidification," AFS International Cast Metals Journal, pp. 30-41, 1980.

3. Sully, L., "The Thermal Interphase Between Castings and Chill Molds," AFS Transactions, Vol. 84, pp. 735-744, 1976.

4. Srinivasan, M., "Heat Transfer Coefficients at the Casting-Mould Interface During Solidification of Flake Graphite Cast Iron in Metallic Moulds," Indian Journal of Technology, Vol. 20, pp. 123-129, 1982.

5. Fox, L., "What Are the Best Numerical Methods," in Ockendon and Hodgkins, Moving Boundary Problems in Heat Flow and Diffusion, Oxford University Press, pp. 210-241, 1975.

6. Furzeland, R.M., "A Comparative Study of Numerical Methods for Moving Boundary Problems," J. Inst. Maths. Applics., Vol. 26, pp. 411-429, 1980.

7. Vlack, V., "Elements of Materials Science and Engineering," Addison-Wesley Publishing Company, 1980.

8. Stefan, J., Ann. Phys. U. Chem. (Wiedemann) N.F., 42, 269-86, 1891.

9. Neumann, F., "Die Partiellen Differentialgleichungen der Mathematischen Physik," Reimann-Weber, Vol. 2, p. 121, 1912.

10. Dusinberre, G.M., "Numerical Methods for Transient Heat Flows," Trans. ASME 67:703, 1945.

11. Doherty, P.C., "Hot Pipe," U.S. Geological Survey Computer Contribution No. 4, 1970.

12. Rolph, W.D., Bathe, D., "An Efficient Algorithm for Analysis of Nonlinear Heat Transfer with Phase Changes," Int. J. Num. Meth. Engr., Vol. 18, pp. 119-134, 1982.

13. Hashemi, H.T., Sliepcevich, C.M., "A Numerical Method for Solving Two-Dimensional Problems of Heat Conduction with Change of Phase," Chem. Eng. Prog. Symp. Series, No. 79, Vol. 63, pp. 34-41, 1967.

14. Comini, G., Del Giudice, S., Lewis, R.W., Zienkiewicz, O.C., "Finite Element Solution of Nonlinear Heat Conduction Problems with Special Reference to Phase Change," Int. J. Num. Meth. Engr., Vol. 8, pp. 613-624, 1974.

15. Pham, Q.T., "A Fast Unconditionally Stable Finite-Difference Scheme for Heat Conduction with Phase Change," Int. J. Heat Mass Transfer, Vol. 28, No. 11, pp. 2079-2084, 1985.

16. Crowley, A.B., "Numerical Solution of Stefan Problems," Int. J. Heat Mass Transfer, Vol. 21, pp. 215-219, 1978.

17. Bell, G.E., Wood, A.S., "On the Performance of the Enthalpy Method in the Region of a Singularity," Int. J. Num. Meth. Engr., Vol. 19, pp. 1583-1592, 1983.

18. Tacke, K.H., "Discretization of the Explicit Enthalpy Method for Planar Phase Change," Int. J. Num. Meth. Engr., Vol. 21, pp. 543-554, 1985.

19. Meyer, G.H., "Multidimensional Stefan Problems," SIAM J. Numer. Anal., Vol. 10, No. 3, pp. 522-538, 1973.

20. Shamsunder, N., Sparrow, E.M., "Analysis of Multidimensional Conduction Phase Change Via the Enthalpy Model," Journal of Heat Transfer, pp. 333-340, August 1975.

21. Jerome, J.W., "Nonlinear Equations of Evolution and a Generalized Stefan Problem," Journal of Diff. Eqn., Vol. 26, pp. 240-261, 1977.

22. Kikuchi, N., Ichikawa, Y., "Numerical Methods for a Two-Phase Stefan Problem by Variational Inequalities," Int. J. Num. Meth. Engr., Vol. 14, pp. 1221-1239, 1979.

23. Blanchard, D., Fremond, M., "The Stefan Problem: Computing Without the Free Boundary," Int. J. Num. Meth. Engr., Vol. 20, pp. 757-771, 1984.

24. Brauner, C.M., Fremond, M. Nicolaenko, B., "A New Homographic Approximation to Multiphase Stefan Problems, in Free Boundary Problems. Theory and Applications," (A. Fasano and M. Primicerio, Eds.), Elsevier, Amsterdam, 1982.

25. Meyer, G.H., "An Application of the Method of Lines to Multidimensional Free Boundary Problems," J. Inst. Maths. Applics., Vol. 20, pp. 317-329, 1977.

26. Lazaridis, A., "A Numerical Solution of the Multidimensional Solidification (or Melting) Problem," Int. J. Heat Mass Transfer, Vol. 13, pp. 1459-1477, 1970.

27. Duda, J.L., Malone, M.F., Notter, R.H., Vrentas, J.S., "Analysis of Two-Dimensional Diffusion - Controlled Moving Boundary Problems," Int. J. Heat Mass Transfer, Vol. 18, pp. 901-910, 1975.

28. Sparrow, E.M., Ramodhyani, S., Patankar, S., "Effect of Subcooling on Cylindrical Melting," J. Heat Transfer, Vol. 100, pp. 395-402, 1978.

29. Crank, J., Gupta, R.S., "Isotherm Migration Method in Two Dimensions," Int. J. Heat Mass Transfer, Vol. 18, pp. 1101-1107, 1975.

30. Crank, J., Crowley, A.B., "Isotherm Migration Along Orthogonal Flow Lines in Two Dimensions," Int. J. Heat Mass Transfer, Vol. 21, pp. 393-398, 1978.

31. Lynch, D.R., O'Neill, K., "Continuously Deforming Finite Elements for the Solution of Parabolic Problems, With and Without Phase Change," Int. J. Num. Meth. Engr., Vol. 17, pp. 81-96, 1981.

32. Lynch, D.R., "Unified Approach to Simulation on Deforming Elements with Application to Phase Change Problems," Journal of Computational Physics, Vol. 47, No. 3, pp. 387-411, 1982.

33. Goodrich, L.E., "Efficient Numerical Technique for One-Dimensional Thermal Problems with Phase Change," Int. J. Heat Mass Transfer, Vol. 21, pp. 615-621, 1978.

34. Voller, V., Cross, M., "An Explicit Numerical Method to Track a Moving Phase Change Front," Int. J. Heat Mass Transfer, Vol. 26, pp. 147-150, 1983.

35. Lunardini, V.J., "Heat Transfer in Cold Climates," Van Nostrand Reinhold, New York, pp. 471-532, 1981.

36. Holman, J.P., "Heat Transfer," McGraw-Hill Book Company, New York, 1981.

37. Shih, T.M., "Numerical Heat Transfer," Hemisphere Publishing Corporation, U.S.A., 1984.

38. Carnahan, B., Luther, H.A., Wilkes, J.O., "Applied Numerical Methods," Wiley, New York, 1969.

39. Peaceman, D.W., Rachford, H.H., "The Numerical Solution of Parabolic and Elliptic Differential Equations," J. Soc. Indust. Appl. Math., Vol. 3, pp. 28, 1955.

40. Zienkiewicz, A., "The Finite Element Method," McGraw-Hill, 1977.

41. Cook, R.D., "Concepts and Applications of Finite Element Analysis," Wiley, 1981.

42. Sokolnikoff, I.S., "Mathematical Theory of Elasticity," McGraw-Hill, New York, 1956.

43. Segerlind, L.J., "Applied Finite Element Analysis," John Wiley and Sons Inc., New York, 1976.

44. Salcudean, M., Mashaie, A., "Mathematical Modelling of Heat Transfer in Permanent Molds," (Rep. II - Cylindrical - 2D Coordinates), Department of Mechanical Engineering, University of Ottawa, July, 1983.

45. Salcudean, M., Abdullah, Z., "Numerical Simulation of Casting Processes," International Heat Transfer Conference to be held in August, 1986.

46. Metals Handbook; Properties and Selection of Metals, American Society for Metals, Vol. 1, 1961.

47. Thermophysical Properties of Matter, Y.S. Touloukian, Ed., IFI/Plenum, New York, 1970.

48. Angus, H.T., Cast Iron: Physical and Engineering Properties, Butterworths, London, 1976.

49. Patankar, S.V., Numerical Heat Transfer and Fluid Flow, McGraw-Hill Book Co., 1980.

50. Hsu, C.T., Comparison of a Finite Element and a Finite Difference Computer Code in Heat Transfer Calculations, ASME Paper 79-PVP-63.

APPENDIX A

The tridiagonal matrix is of the form:

$$A_j T_{j-1} + B_j T_j + C_j T_{j+1} = D_j, \quad j=1,2,\ldots,J \qquad (A1)$$

with A_1 and D_J equal to zero. The tridiagonal matrix solving algorithm resembles Gaussian elimination. To begin with, values of "β_j" and "α_j" are calculated as:

$$\beta_1 = B_1 \qquad j=1 \qquad (A2)$$

$$\alpha_1 = D_1/B_1 \qquad j=1 \qquad (A3)$$

$$\beta_j = B_j-(A_j C_{j-1})/\beta_{j-1} \qquad j=2,3,\ldots,J \qquad (A4)$$

$$\alpha_j = (D_j-A_j \alpha_{j-1})/\beta_j \qquad j=2,3,\ldots,J \qquad (A5)$$

Since "β_j" and "α_j" are always expressed in terms of coefficients at lower index numbers, they can be calculated without difficulty. Once they have been found, the unknowns "T_j" can be calculated as:

$$T_J = \alpha_J \qquad j=J \qquad (A6)$$

$$T_j = \alpha_j - C_j T_{j+1}/\beta_j \qquad j=J-1,J-2,\ldots,1 \qquad (A7)$$

Since the unknowns "T_j" are always calculated in terms of values with the same or higher index and since they are calculated beginning with the largest index values, they can be found without difficulty.

For further details on the tridiagonal matrix solving algorithm, see Carnahan [38].